

PERSISTENT FIRING AND DEPOLARIZATION BLOCK  
IN RAT CA1 PYRAMIDAL NEURONS

by

Beate Knauer

A thesis submitted in partial fulfilment of the requirements for the degree of

Philosophiae Doctoris (PhD) in Neuroscience

from the International Graduate School of Neuroscience

Ruhr University Bochum



March 31<sup>st</sup> 2015

This research was conducted at the Neural Dynamics Lab within the Faculty of Psychology in association with the Mercator Research Group 1 at the Ruhr University under the supervision of Jun.-Prof. Dr. Motoharu Yoshida

*Printed with the permission of the International Graduate School of Neuroscience,  
Ruhr University Bochum*

*"Die allererste und größte Aufgabe im Leben besteht darin, das Gleichgewicht zu halten."*

Wiesmann (2012) [1]

## **Statement**

I certify herewith that the dissertation included here was completed and written independently by me and without outside assistance. References to the work and theories of others have been cited and acknowledged completely and correctly. The “Guidelines for Good Scientific Practice” according to § 9, Sec. 3 of the PhD regulations of the International Graduate School of Neuroscience were adhered to. This work has never been submitted in this, or a similar form, at this or any other domestic or foreign institution of higher learning as a dissertation.

The abovementioned statement was made as a solemn declaration. I conscientiously believe and state it to be true and declare that it is of the same legal significance and value as if it were made under oath.

Beate Knauer / Signature

Bochum, 14.07.2015

## **PhD Commission**

Chair: Prof. Dr. Stefan Herlitze

1<sup>st</sup> Internal Examiner: Jun.-Prof. Dr. Motoharu Yoshida

2<sup>nd</sup> Internal Examiner: Prof. Dr. Denise Manahan-Vaughan

External Examiner: Prof. Dr. Maxim Volgushev

Non-Specialist: Prof. Dr. med. Dr. rer. nat. habil. Konstanze F. Winklhofer

Date of Final Examination: June 30, 2015

PhD Grade Assigned: magna cum laude

# Contents

<b>I List of figures</b> .....	IV
<b>II List of tables</b> .....	VI
<b>III List of abbreviations</b> .....	VII
<b>IV List of compounds</b> .....	IIIX
<b>V Abstract</b> .....	1
<b>1 Introduction</b> .....	3
<b>1.1 The hippocampus</b> .....	4
1.1.1 Short-term maintenance of information in the hippocampus .....	6
1.1.2 The role of the hippocampus in seizures and epilepsy .....	7
<b>1.2 The hippocampal cholinergic system</b> .....	9
1.2.1 The role of the cholinergic system in short-term maintenance of information .....	10
1.2.2 The role of the cholinergic system in seizures and epilepsy .....	13
<b>1.3 Electrophysiological properties of CA1 pyramidal neurons related to cholinergic signaling</b> .....	14
1.3.1 The role of muscarinic-dependent intracellular processes in short-term maintenance of information .....	19
1.3.2 The role of muscarinic-dependent intracellular processes in seizure-related epileptiform activity.....	22
<b>1.4. Summary and hypotheses</b> .....	24
<b>2 Method</b> .....	25
<b>2.1 Animals</b> .....	26
<b>2.2 Chemicals and solutions</b> .....	27
<b>2.3 Preparation of acute brain slices</b> .....	28
<b>2.4 Recording procedures</b> .....	29
<b>2.5 Selection of neurons for data analysis</b> .....	32
2.5.1 Only pyramidal neurons were analyzed .....	32
2.5.2 Silent RMP was required for the inclusion of cells .....	32
<b>2.6 Identification of the cell's anatomical location</b> .....	34

---

2.6.1 Dorso-ventral axis .....	34
2.6.2 Proximo-distal axis.....	36
<b>2.7 Raw data analysis</b> .....	<b>37</b>
2.7.1 Passive properties.....	38
2.7.2 Hyperpolarization activated current .....	39
2.7.3 Action potential properties .....	40
2.7.4 Post-burst properties.....	43
2.7.5 Excitability .....	44
2.7.6 Persistent activity parameters.....	47
<b>2.8 Statistical comparison of group data</b> .....	<b>50</b>
2.8.1 Comparison with previously reported data .....	51
2.8.2 Comparison of categorical data.....	52
<b>3 Results</b> .....	<b>54</b>
<b>3.1 The effect of carbachol on intrinsic electrophysiological properties and its modulation by intercellular variability</b> .....	<b>55</b>
3.1.1 The effect of carbachol on intrinsic electrophysiological properties .....	55
3.1.2 Modulation of intrinsic properties by intercellular variability .....	67
3.1.3 Summary of the cholinergic effects on CA1 pyramidal neurons .....	79
<b>3.2. Persistent firing</b> .....	<b>81</b>
3.2.1 <i>In vitro</i> CA1 pyramidal neurons engaged in persistent firing .....	81
3.2.2 Persistent firing was intrinsic to individual neurons .....	85
3.2.3 Intrinsic persistent firing may be a physiologically plausible phenomenon .....	91
3.2.4 Mechanism underlying intrinsic persistent firing in CA1 pyramidal neurons .....	95
3.2.5 Sensitivity of persistent firing to the carbachol concentration .....	104
3.2.6 Sensitivity of persistent firing to inter-cellular variability within CA1 .....	105
3.2.7 Summary of persistent firing in CA1 pyramidal neurons .....	106
<b>3.3 Depolarization block</b> .....	<b>108</b>
3.3.1 The mechanism underlying the switch between persistent firing and depolarization block .....	108
3.3.2 Sensitivity of depolarization block to inter-cellular variability.....	122
3.3.3 Aspects of inter-cellular variability modulating the occurrence of persistent firing and depolarization block.....	124
3.3.4 Summary of the interrelation between persistent firing and depolarization block.....	128
<b>4 Discussion</b> .....	<b>129</b>
<b>4.1 Overall summary of the data</b> .....	<b>130</b>
4.1.1 Effects of cholinergic stimulation on CA1 pyramidal neurons .....	130
4.1.2 Cholinergic excitation enabled intrinsic persistent firing in CA1 pyramidal neurons .....	131

---

4.1.3 Interrelation between persistent firing and depolarization block .....	131
<b>4.2 Interpretation and discussion with regard to <i>in vitro</i> data of others .....</b>	<b>132</b>
4.2.1 Heterogeneous responses during potassium channel blockade .....	132
4.2.2 A potential explanation for the late report of persistent firing in CA1 pyramidal neurons .....	133
<b>4.3 Interpretation and discussion with regard to the potential situation <i>in vivo</i> .....</b>	<b>140</b>
4.3.1 Relation between <i>in vitro</i> and <i>in vivo</i> data .....	140
4.3.2 Input specificity .....	145
4.3.3 Interaction with concurrent neurotransmission .....	146
4.3.4 Embedding persistent firing in neuronal networks .....	147
4.3.5 Questioning the interpretation of persistent-firing and depolarization block as either memory- or seizure-related activity .....	151
<b>4.4 Conclusion .....</b>	<b>154</b>
<b>5 References .....</b>	<b>156</b>
<b>6 Appendix .....</b>	<b>177</b>
6.1 Supplemental data .....	178
6.2 Curriculum Vitae .....	203
6.3 List of publications .....	206
6.4 Acknowledgements .....	207

# I List of figures

Figure 1.1:	The hippocampal formation across species and its location in the brain. ....	5
Figure 1.2:	The hippocampal proper and its subfields. ....	6
Figure 1.3:	Cholinergic innervation of the hippocampus ....	9
Figure 1.4:	Impact of the cholinergic tone on potential mechanisms mediating short-term retention of information. ....	12
Figure 1.5:	TRPC channel activation induced by muscarinic stimulation. ....	18
Figure 1.6:	Sustained action potential firing during the delay period. ....	20
Figure 1.7:	Epileptiform activity in CA1 pyramidal neurons. ....	23
Figure 2.1:	Attaining a whole-cell patch configuration. ....	31
Figure 2.2:	Neurons with a non-pyramidal shape were excluded from data analysis. ....	33
Figure 2.3:	Measures from the remainder of the brain allowed an estimation of the cell's dorso-ventral origin. ....	35
Figure 2.4:	Measurement of the cell's location in the proximo-distal axis. ....	37
Figure 2.5:	Quantification of the input resistance by a low amplitude current injection. ....	39
Figure 2.6:	Action potential threshold quantification. ....	41
Figure 2.7:	Validation of the Kaplan-Meier survival analysis. ....	47
Figure 2.8:	Depolarization block occurred at highly variable time points. ....	49
Figure 3.1.1:	The effect of 10 $\mu$ M Cch on passive electrophysiological properties and $I_h$ . ....	57
Figure 3.1.2:	Properties of individual action potentials were altered by carbachol. ....	58
Figure 3.1.3:	The afterhyperpolarization was mostly abolished in carbachol. ....	59
Figure 3.1.4:	Spike frequency accommodation was reduced by carbachol. ....	60
Figure 3.1.5:	Cells were more excitable in the presence of carbachol. ....	61
Figure 3.1.6:	Considerably lower current injections were sufficient to induce depolarization block in the presence of Cch. ....	63
Figure 3.1.7:	$I_h$ , post-burst potentials and firing frequency were modulated by increasing Cch concentrations. ....	65
Figure 3.1.8:	The effect of maturation on intrinsic electrophysiological properties. ....	69
Figure 3.1.9:	In ACSF+SB various measures, but not the AHP, indicated a lower excitability in neurons from aged compared to juvenile animals. ....	71
Figure 3.1.10:	The lower excitability in neurons from aged compared to juvenile animals was preserved in the presence of 10 $\mu$ M carbachol. ....	72
Figure 3.1.11:	The cells' location within the hippocampus. ....	74
Figure 3.1.12:	Neurons in the dorsal compared to the ventral half of the hippocampus were more excitable in the absence of Cch. ....	76
Figure 3.1.13:	The excitability was higher in neurons from the proximal compared to the distal third of CA1. ....	78
Figure 3.2.1:	CA1 pyramidal cells showed persistent firing in the presence of carbachol. ....	83



Figure 3.2.2: Quantitative analysis of carbachol-dependent persistent firing in paired samples superfused with nACSF. ....	85
Figure 3.2.3: Carbachol-dependent persistent firing during the blockade of fast ionotropic synaptic transmission. ....	86
Figure 3.2.4: In the presence of synaptic blockers, the likelihood of excitatory postsynaptic potentials was unaffected by the stimulus. ....	87
Figure 3.2.5: Dye-coupling of CA1 pyramidal neurons occurred rarely. ....	89
Figure 3.2.6: Spikelets could be readily detected. ....	90
Figure 3.2.7: Persistent firing was largely unchanged, despite a shortened stimulus duration. ....	92
Figure 3.2.8: Persistent firing was also observed in aged animals and was similar to that in juvenile animals. ....	94
Figure 3.2.9: Muscarinic acetylcholine receptors were required for intrinsic persistent firing of CA1 pyramidal neurons. ....	96
Figure 3.2.10: Sole potassium channel blockade did not induce persistent firing. ....	97
Figure 3.2.11: Chelating intracellular calcium impeded persistent firing. ....	98
Figure 3.2.12: Elevated ATP concentrations in the intracellular fluid attenuated persistent firing if prolonged dilution times were allowed. ....	100
Figure 3.2.13: Flufenamic acid attenuated carbachol-dependent persistent firing. ....	102
Figure 3.2.14: Persistent firing was attenuated by the bath-application of the TRPC4/5 channel blocker ML204. ....	103
Figure 3.2.15: Modulation of persistent firing by the carbachol concentration. ....	105
Figure 3.3.1: The propensity for depolarization block was higher at higher carbachol concentrations but the characteristics of the depolarization block were unaffected. ....	109
Figure 3.3.2: Individual cells showed both persistent firing and depolarization block depending on the carbachol concentration. ....	111
Figure 3.3.3: Retigabine hyperpolarized the post-burst membrane potential significantly. ....	113
Figure 3.3.4: Retigabine prohibited depolarization block by depressing action potentials. ....	115
Figure 3.3.5: The effect of voltage-gated K <sup>+</sup> channels on the amplitude and duration of the depolarization block. ....	116
Figure 3.3.6: SK channel activity affected the switch between persistent firing and depolarization block. ....	117
Figure 3.3.7: Non-K <sup>+</sup> channel effects of cholinergic stimulation endowed cells with the ability to engage in persistent activity. ....	120
Figure 3.3.8: Depolarization block was suppressed by the bath-application of the TRPC4/5 channel blocker ML204. ....	121
Figure 3.3.9: The sag ratio correlated significantly with the depolarization block duration. ....	123
Figure 3.3.10: Cells exhibiting persistent firing or depolarization block were recorded at disparate locations in the proximo-distal axis. ....	125
Figure 3.3.11: The post-burst membrane potential in cells exhibiting persistent firing or depolarization block. ....	127
Figure 4.1: Previously reported TRPC channel blockade or knock out may have left the induction of depolarization block unaffected. ....	136
Figure 4.2: Low fraction of delay-related errors at delay intervals of six seconds. ....	144
Figure 4.3: Time cells cover a well defined interval during a delay period. ....	149
Figure 4.4: Depolarization block during place field traversal. ....	153

## II List of tables

Table 2.1: 2x2 contingency table for chi square. ....	52
Table 2.2: McNemar-test assessing paired categorical parameters. ....	53
Table 3.2.1: Intracellular dilution times of the cells exposed to 4 and 10 mM ATP. ....	99

## III List of abbreviations

ACh	acetylcholine
AChR	acetylcholine receptor
ACSF	artificial cerebrospinal fluid
ADP	afterdepolarization
AP	action potential
AMPA	2-amino-3-(5-methyl-3-oxo-1,2-oxazol-4-yl)propanoic acid
AHP	afterhyperpolarization
BOLD	blood oxygen level dependent
CA	cornu ammonis
Cch	carbachol
DAG	diacylglycerol
fAHP	fast afterhyperpolarization
FF <sub>fix</sub>	average firing frequency at 10 - 20 s after the stimulus offset
FF <sub>max</sub>	average firing frequency during the most depolarized 500 ms
FFA	flufenamic acid
fMRI	functional magnet resonance imaging
GABA	gamma-aminobutyric acid
HW	action potential half width
ICF	intracellular fluid
I <sub>CAN</sub>	calcium-sensitive non-selective cation current mediated by the TRPC channel
HCN	gene coding the protein of the hyperpolarization activated channel
I <sub>h</sub>	hyperpolarization activated current
IP <sub>3</sub>	inositol trisphosphate
KCNQ7.2/3	gene coding the protein for the voltage-gated channel
M	mean
M <sub>1</sub> - M <sub>5</sub>	muscarinic acetylcholine receptor types 1 - 5
mAChR	muscarinic acetylcholine receptors
nACSF	normal ACSF
mAHP	medium afterhyperpolarization
mGluR	metabotropic glutamate receptor
NMDA	N-methyl D-aspartate
PIP <sub>2</sub>	phosphatidylinositol 4,5-bisphosphate
PLC	phospholipase C
PP <sub>fix</sub>	average membrane potential across 10 - 20 s after the stimulus offset
PP <sub>max</sub>	average membrane potential during the most depolarized 500 ms
R	resistance
RGB	retigabine
RMP	resting membrane potential
R <sub>in</sub>	input resistance
sADP	slow afterdepolarization

SB	synaptic blockers
SD	standard deviation
SEM	standard error of the mean
TRPC channel	canonical transient receptor potential channel
$V_m$	membrane potential

## IV List of compounds

	Supplier	Catalog number	
ABC kit	Vector by biozol	VEC-PK-6100	VECTASTAIN(R) Elite ABC-Peroxidase Kits, Rabbit IgG
Apamin	Alfa Aesar	J60961	H-Cys-Asn-Cys-Lys-Ala-Pro-Glu-Thr-Ala-Leu-Cys-Ala-Arg- Arg-Cys-Gln-Gln-His-NH <sub>2</sub> (Cys1-Cys11, Cys3-Cys15)
Atropine	Sigma	A0132	10,10-bis(4-pyridinylmethyl)-9(10H)-anthracenone
BAPTA	Sigma	A4926	1,2-Bis(2-Aminophenoxy)ethane-N,N,N',N'-tetraacetic acid
Biocytin	Sigma	B4261	N <sub>ε</sub> -(+)-Biotinyl-L-lysine
CaCl	Sigma	223506	CaCl
CaCl	J.T.Baker	0504	CaCl
Carbachol	Acros	10824	H <sub>2</sub> NCO <sub>2</sub> CH <sub>2</sub> CH <sub>2</sub> N(CH <sub>3</sub> ) <sub>3</sub> Cl
Carbachol	Alfa Aesar	L06674	H <sub>2</sub> NCO <sub>2</sub> CH <sub>2</sub> CH <sub>2</sub> N(CH <sub>3</sub> ) <sub>3</sub> Cl
Choline Chloride	Sigma	C1879	(CH <sub>3</sub> ) <sub>3</sub> N(Cl)CH <sub>2</sub> CH <sub>2</sub> OH
D(+)-Glucose -	AppliChem	A1349	C <sub>6</sub> H <sub>12</sub> O <sub>6</sub> ·
DAB kit	Vector by biozol	VEC-SK-4100	ImmPACT(TM) DAB Peroxidase Substrate, CE
DMSO	Sigma	D2650	Dimethyl sulfoxide
EGTA	Roth	3054.1	Ethylene glycol bis(β-aminoethyl)-ether)N,N,N',N' tetraacetic acid
Flufenamic acid	Alfa Aesar	B23583	N-(3-Trifluoromethylphenyl)anthranilic acid
Gelatine (Porcine skin Type A)	Sigma	G8150	
GTP	Sigma	G9002	Guanosine 5'-triphosphate tris salt
HEPES	AppliChem	1069	4-(2-Hydroxyethyl)-peperazin-1-ethansulfonsäure
Hydrochloric Acid	J.T. Baker	6081	HCl
Hydrogen Peroxide	J.T. Baker	7047	H <sub>2</sub> O <sub>2</sub>
Ketamine	cp-pharma	401650	ketamine hydrochloride (100 mg/ml), chlorocresol
Kynurenic acid	Sigma	K3375	4-Hydroxyquinoline-2-carboxylic acid
L-Ascorbic acid	Sigma	A5960	L-Threoascorbic acid, Antiscorbutic factor
NaATP	Sigma	A6419	Adenosine 5'-triphosphate disodium salt hydrate

	Supplier	Catalog number	
Magnesium chloride	Roth	2189.2	MgCl <sub>2</sub>
Magnesium sulfate	AppliChem	1037	MgSO <sub>4</sub>
ML204	Vanderbilt University	donation	4-Methyl-2-(1-piperidinyl)quinoline
Mowiol 4-88	Sigma	81381	[-CH <sub>2</sub> CHOH-] <sub>n</sub>
Paraformaldehyde	Sigma	441244	HO(CH <sub>2</sub> O) <sub>n</sub> H
Phosphocreatine di(tris) salt	Sigma	P1937	N-(Imino[phosphonoamino]methyl)-N-methylglycine
Picrotoxin	TCI Europe	C0375	C <sub>30</sub> H <sub>34</sub> O <sub>13</sub>
Potassium chloride	VWR	26764.298	KCl
Potassium hydroxide	J.T.Baker	0385	KOH
Potassium D-gluconate	Sigma	G4500	2,3,4,5,6-Pentahydroxycaproic acid potassium salt
Retigabine	Axon	1525	ethyl N-[2-amino-4-[(4-fluorophenyl)methylamino]phenyl]carbamate
Sodium bicarbonate	J.T.Baker	0263	NaHCO <sub>3</sub>
Sodium chloride	J.T.Baker	0278	NaCl
Sodium dihydrogen phosphate	J.T.Baker	0303	NaH <sub>2</sub> PO <sub>4</sub>
Sodium phosphate, dibasic	J.T.Baker	0326	Na <sub>2</sub> HPO <sub>4</sub>
Sodium pyruvate	Sigma	P2256	α-Ketopropionic acid sodium salt, or 2-Oxopropanoic acid sodium salt
Trizma hydrochloride	Sigma	T3252	NH <sub>2</sub> C(CH <sub>2</sub> OH) <sub>3</sub> · HCl
Triton X-100 (for electrophoresis)	Sigma	T8532	4-(1,1,3,3-Tetramethylbutyl)phenyl-polyethylene glycol
Trizma base	Sigma	T1503	2-Amino-2-(hydroxymethyl)-1,3-propanediol
XE991	Sigma	X2254	10,10-bis(4-pyridinylmethyl)-9(10 H)-anthracenone
Xylazine	cp - pharma	401510	xylazine hydrochloride (20 mg/ml), methyl-4-hydroxybenzoate

# V Abstract

The balance between functional excitation and detrimental hyperexcitation appears to be a particularly fragile one in the hippocampus. The hippocampus is a subcortical brain region widely acknowledged for its involvement in long-term memory and navigation. However, the hippocampus and, more broadly, the medial temporal lobe are also recognized for playing a crucial role in epilepsy and particularly in pharmacoresistant courses of the disease.

Lately, evidence accumulates indicating that the hippocampus is not only involved in long-term memory but may also take part in the short-term retention of information. In detail, it appears as if the hippocampus is required for retaining a representation of information that is no longer available to sensory organs. Whereas the neuronal underpinnings of long-term memory (synaptic long-term potentiation and depression) were intensely investigated, the cellular mechanisms underlying the neuronal activity supporting the short-term retention of information are yet poorly understood.

One potential mechanism for short-term retention of information in the hippocampus is the modulation of neuronal activity by acetylcholine. Acetylcholine is a neurotransmitter that is involved in muscular activation in the peripheral nervous system and neuronal excitation in the central nervous system. The latter was repeatedly demonstrated to be necessary for hippocampus-dependent short-term retention of information. However, a sensitive balance of central cholinergic excitation appears to be crucial for adaptive functioning. On the one hand, excessive cholinergic stimulation is linked to seizures. On the other hand, an impaired transmission of cholinergic signaling may for example underlie the cognitive decline in Alzheimer's disease. Accordingly, blockers and enhancers of cholinergic signal transduction are successfully used in clinical settings.

Supporting the role of cholinergic-mediated enhancement of neuronal excitation in hippocampus-dependent short-term retention of information, numerous studies reported elevated action potential firing rates while animals retained a piece of information.

Accordingly, increased blood flow, suggesting elevated neuronal activity, in the temporal lobe was reported in humans who performed a memory task which depended on intact cholinergic signaling. Nonetheless, the neuronal mechanisms underlying the increased excitability remained undetermined.

To elucidate which cellular processes may allow the retention of information in the hippocampus, I conducted an *in vitro* electrophysiology study using neurons in acutely sliced brain tissue of rats. Access to individual neurons was obtained by the whole cell patch clamp method with which I recorded and controlled the neuronal activity of excitatory pyramidal cells in the hippocampus.

The results outlined in this dissertation first characterize properties of these neurons and explicate the excitatory effects of cholinergic stimulation. Subsequently, I present that this neuronal modulation by cholinergic activation endowed the cells with the ability to engage in a phenomenon called persistent firing. Persistent firing is action potential spiking that is initiated by a stimulus but outlasts the cessation of the stimulus. In contrast, during the absence of neuromodulation cells did not sustain activity but quickly returned to their pre-stimulus state. Hence, I propose these findings as a potential mechanism for the short-term retention of information in the hippocampus. Additionally, I elaborate on trans-membrane conductances which may mediate persistent firing in hippocampal pyramidal cells. The involvement of canonical transient receptor potential (TRPC) channels in persistent firing is shared with a previously shown phenomenon called depolarization block. During depolarization block the generation of action potentials is prevented by a highly elevated and sustained membrane potential. This form of activity was associated with seizures which may constitute epilepsy in case of recurrent and widespread occurrence. Finally, I relate the newly discovered to the previously well described neuronal activity and highlight potential mechanisms controlling whether cells tended to engage in the memory-related persistent firing or the epilepsy-related depolarization block.

The findings will be placed in the context of previous reports on cholinergic effects in CA1 pyramidal neurons. Thereafter, I will discuss the physiological relevance of persistent firing in the light of multifaceted neurotransmission and the embedding in neuronal networks. Finally, I will question the interpretation of persistent firing and depolarization block as unambiguously memory- and seizure-related activity, respectively.



# 1 Introduction

## 1.1 The hippocampus

1.1.1 Short-term maintenance of information in the hippocampus

1.1.2 The role of the hippocampus in seizures and epilepsy

## 1.2 The hippocampal cholinergic system

1.2.1 The role of the cholinergic system in short-term maintenance of information

1.2.2 The role of the cholinergic system in seizures and epilepsy

## 1.3 Electrophysiological properties of CA1 pyramidal neurons related to cholinergic signaling

1.3.1 The role of muscarinic-dependent intracellular processes in short-term maintenance of information

1.3.2 The role of muscarinic-dependent intracellular processes in seizure-related epileptiform activity

## 1.4. Summary and hypotheses

The aims of the project summarized by the dissertation at hand were twofold. On the one hand, I will cover potential mechanisms underlying mnemonic aspects of hippocampal function. On the other hand, I will set these adaptive mechanisms in relation to neuronal activity in the hippocampus which may underlie electrographic seizures.

Noteworthy, this dissertation sets a spotlight on intrinsic neuronal mechanisms. Therefore, I will, in the most part, disregard network related data. Importantly, this selectiveness shall not reflect the significance of either experimental level. Instead, it serves to support the relevance of intrinsic cellular properties as complementary mechanisms.

Firstly, I will introduce the hippocampus and its involvement in the short-term retention of information as well as its role in epilepsy. Secondly, I will introduce a neurotransmitter system that provides the hippocampus with cholinergic activation. Therein, I will outline the effects of acetylcholine receptor stimulation on memory and its participation in epileptic activity. Lastly, I will introduce different electrophysiological characteristics of hippocampal neurons, which may relate to mnemonic-processes and to epileptiform activity.

## 1.1 The hippocampus

The hippocampal formation is an extensively studied area of the brain located in the medial portion of the temporal lobe. It is classified as archicortex displaying a 3-layered structure and representing a phylogenetically old part of the brain [2]. The hippocampal formation comprises the dentate gyrus, the cornu ammonis subfields 1-3 (CA1 - CA3) and the subiculum. It has a highly similar anatomical structure across different mammalian species (Fig. 1.1) where it appears to fulfill comparable functions [2]. These functions revolve around spatial navigation and memory (reviewed in Eichenbaum et al. (1999) [3]).

As depicted in figure 1.1, the hippocampal formation extends considerably along the caudal-rostral axis in humans and along the dorso-ventral axis in rats. Anatomical peculiarities of the dorsal in contrast to the ventral portion of the rat hippocampal formation have long been established [4–7]. These differences in the basic layout appear to be mirrored in a functional segregation along the dorso-ventral axis of the hippocampal formation [8–11], and particularly the CA1 area [12]. Furthermore, the dorsal and ventral portions of the hippocampus were shown to be differentially susceptible to epileptiform activity [13–16] and its detrimental neuronal consequences. To unravel the mechanisms underlying the dorso-ventral differences, much attention was recently focused on the modulation of trans-

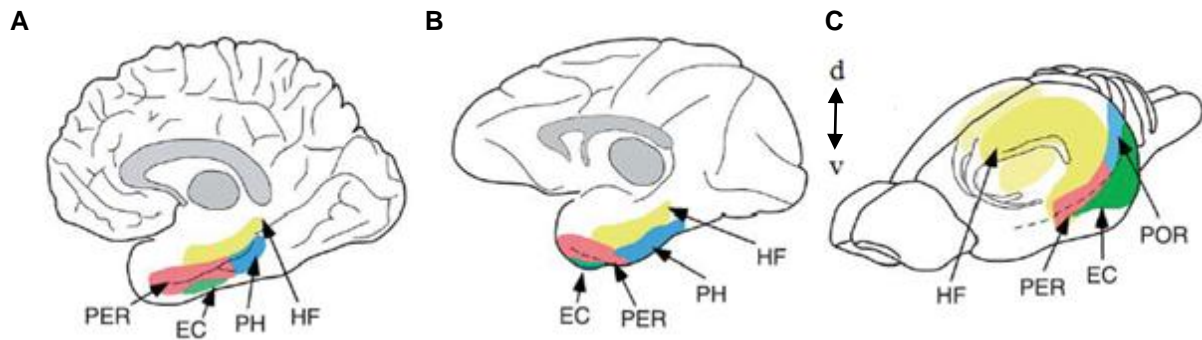


**Figure 1.1: The hippocampal formation across species and its location in the brain.**

The image shows the hippocampal formation (HF, yellow) and adjacent cortices at a medial view on the right hemisphere of a human (A) and monkey (B) brain and a lateral view on the left hemisphere of a rat brain (C). Abbreviations: PER: perirhinal cortex; EC: entorhinal cortex; PH: parahippocampal cortex; HF: hippocampal formation; d: dorsal; v: ventral; POR: postrhinal cortex (homologous to parahippocampal cortex). Fig. 1 in Burwell and Agster (2008); modified.

membrane protein expression [17–20], their pharmacological characteristics [21], and their differential contribution to epileptiform activity [22]. Furthermore, intrinsic [23,24] and integrative [23,25,18] electrophysiological properties of neurons along the dorso-ventral axis were investigated. Following this wealth of evidence suggesting a dorso-ventral disparity, I assessed whether alike can be detected in my sample as well.

As stated before, the subfields CA1 to CA3 constitute the hippocampal proper [2] (Fig. 1.2). The cells of interest throughout this dissertation are pyramidal neurons in the CA1 area. Pyramidal neurons represent the most abundant neuronal type in the brain [4]. In contrast to CA3 [26,27], the pyramidal neurons in CA1 lack excitatory recurrent connections [28,29]. However, prevalent models on information retention in the hippocampus involve the reverberation of information via recurrent excitatory loops [30–34]. This status quo leaves it unclear which alternative mechanism may support short-term retention of information mediated by the CA1 subfield.

The pyramidal layer of the CA1 area extends along a proximo-distal axis spanning from the border of CA2/CA1 to CA1/subiculum (Fig. 1.2). Within the hippocampal formation, the proximal and distal portions of CA1 predominantly receive input from the distal and proximal CA3 area [4]. Regarding extra-hippocampal afferents, the medial and lateral entorhinal cortex project to the proximal and distal fields of CA1, respectively [4]. Furthermore, the output of proximal and distal CA1 projects dominantly to the distal and proximal subfield of the subiculum, respectively [4,35]. However, to the best of my

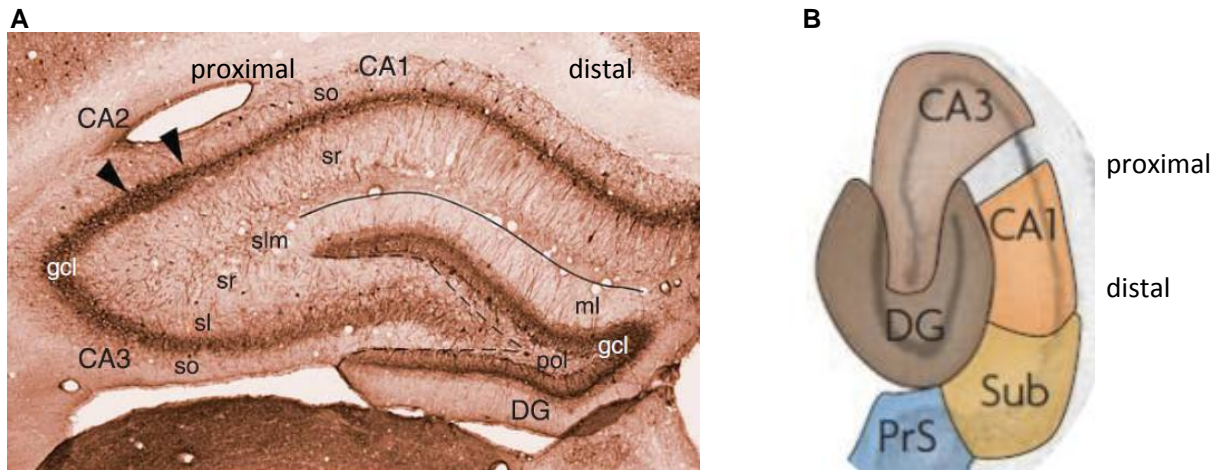


**Figure 1.2: The hippocampal proper and its subfields.**

(A) The image displays the hippocampal proper with its subfields CA1, CA2 and CA3 in a parvalbumin-stained coronal section. The CA1 stratum pyramidale can be seen as the densely stained layer between stratum oriens (so) and stratum radiatum (sr). Figure 10 (c) in Burwell and Agster (2008); modified.

(B) The graph displays a horizontal section overlaid by a color-code demarcating the subfields. Color-coding for CA2 located between CA3 and CA1 is omitted. Fig. 1Ba in van Strien et al. (2009); modified.

Abbreviations: DG: dentate gyrus; gcl: granule cell layer; ml: outer molecular layer; pol: polymorphous layer; PrS: presubiculum; sl: stratum lacunosum; slm: stratum lacunosum-moleculare; so: stratum oriens; sr: stratum radiatum; Sub: subiculum. Stratum pyramidale is not depicted by letters.

knowledge, studies on electrophysiological properties [36], navigation [37], memory, or epilepsy [38–40] that differentiate along the proximo-distal axis are scarce, compared to the extensive literature available regarding potential dorso-ventral segregation [41]. Therefore, I assessed cellular properties along the proximo-distal axis and studied whether these affect persistent firing and depolarization block.

### 1.1.1 Short-term maintenance of information in the hippocampus

The first topic of this dissertation concerns the mnemonic aspect of hippocampal functioning. Traditionally, the hippocampus is thought to be crucial for long-term memory following the pioneering studies with Henry Gustav Molaison (H.M.). H.M. suffered from a severe form of pharmaco-resistant epilepsy which was successfully treated via the bilateral excision of extensive parts of his medial temporal lobe in 1953 [42,43]. The observation of H.M. paying for his remedy from epilepsy with the loss of most of his mnemonic abilities [44] illustrates the involvement of the medial temporal lobe in both memory and epilepsy. The latter will be the second topic of this dissertation.

Besides the well established requirement of the hippocampus for long-term memory [45,46], evidence accumulates indicating that the hippocampus is also involved in the short-term retention of information [47,48]. Studies with patients that have a severed hippocampus support the relevance of the hippocampus for short-term retention of information [49,48,50]. Moreover, elevated neuronal activity in the hippocampus of healthy participants was detected throughout the short-term retention of information, particularly if it was novel [51,52]. In addition, numerous animal studies showed that the hippocampus was required for forming associations if the pieces of information were disconnected by a temporal gap [53–59]. Importantly, the integrity of the hippocampus was dispensable for the acquisition of association tasks as soon as the events, which had to be brought together, were no longer separated in time [60,59].

Based on lesion studies in animals performing a task that required information retention across a short period of time, the hippocampal area CA1 appears to be at least equally important, if not even superior to the area CA3 [56,57,61], despite the abundant excitatory recurrent connections in CA3 [26,27] which are thought to support short-term retention of information [30–34]. Interestingly, CA1 seems not to be crucially dependent on synaptic input from CA3 [62] in a task involving the retention of information across a temporal gap.

In summary, it is conceivable that the hippocampus is involved in short-term retention of information as evident by both human and animal studies. The latter suggest an accentuated role for CA1 compared to CA3. Particularly in light of the lacking recurrent connectivity in CA1, the cellular activity that may allow the CA1 area to support short-term retention of information is yet poorly understood. However, the project underlying this dissertation lead to the proposal of a potential neuronal mechanism for short-term information retention supported by CA1 pyramidal neurons - namely intrinsic persistent firing [63].

### **1.1.2 The role of the hippocampus in seizures and epilepsy**

Besides its adaptive functions, the hippocampus — and more broadly the medial temporal lobe — is involved in epilepsy [64,65]. Epilepsy is a neurological disease characterized by hyper-excitation and hyper-synchrony which affects ~1% of the general population [66]. Electro-encephalic seizures mark an epileptic attack. The worldwide lifetime prevalence of experiencing a seizure is ~10% [67]. However, the occurrence of at least two

spontaneous seizures is required for the diagnosis of epilepsy [67]. Epilepsy involving the medial temporal lobe (i.e. mesial temporal lobe epilepsy), is the most common form of epilepsy [64] and is often poorly manageable with current pharmacotherapy [68].

In mesial temporal lobe epilepsy, the hippocampus is often the seizures onset zone and its electrical stimulation is considered for therapeutic purposes [69]. However, the hippocampus may not be homogeneously affected by epilepsy. Several studies suggest a higher vulnerability of the ventral compared to the dorsal portion of the hippocampus to epileptiform activity [13–15], to the induction of epilepsy by repeated electric stimulation (kindling) [15], and to neuronal lesions following status epilepticus [16]. Furthermore, contrasting the subfields of the hippocampus, the CA1 area displayed more neuronal loss than the CA3 area in a histological study on hippocampal tissue from patients having suffered from mesial temporal lobe epilepsy [38]. A similar study investigating a more heterogeneous population of patients with epilepsy still found a subtle elevation of lesions in CA1 compared to the other hippocampal subfields [40]. To the best of my knowledge, evidence suggesting a differential involvement of discrete areas within CA1 are scarce. However, mid-proximal CA1 was reported to be more vulnerable than distal CA1 with regard to mesial temporal lobe epilepsy associated neuronal loss [38]. Noteworthy, the marker for neuronal loss (sclerosis) used in the aforementioned study was presumably associated with elevated neuronal excitability or with neurons initiating epileptic seizures [70]. This suggestion is supported by a voltage-imaging study reporting highly excitable characteristics of the proximal CA1 area [39].

In summary, the hippocampus is known to be one of the central brain regions involved in epilepsy, whereas the ventral portion is repeatedly shown to be more vulnerable than the dorsal portion. Additionally, CA1 may be more involved than CA3 and mid-proximal CA1 was reported to be more affected than distal CA1.

To recapitulate, the hippocampus is involved in both short-term retention of information and epilepsy. The former was associated with elevated neuronal activity throughout the retention interval and found particularly when the information was novel. The latter is a cerebral disease characterized by hyper-excitation.

## 1.2 The hippocampal cholinergic system

The hippocampus contains local cholinergic neurons [71–74] that may provide cholinergic stimulation of the hippocampus. However, these neurons are yet incompletely understood [73,75] and it was only a recent report that characterized their electrophysiological properties [76].

In contrast, the extensively studied and dominant source of hippocampal acetylcholine are nerve endings that originate in the medial septum and vertical diagonal band of Broca [71,77–81] (Fig. 1.3). The axons of these basal forebrain nuclei enter the hippocampus mainly through the fimbria and fornix [71,80,82] and the ventral portion of the hippocampus appears to be innervated more densely than the dorsal portion [82].

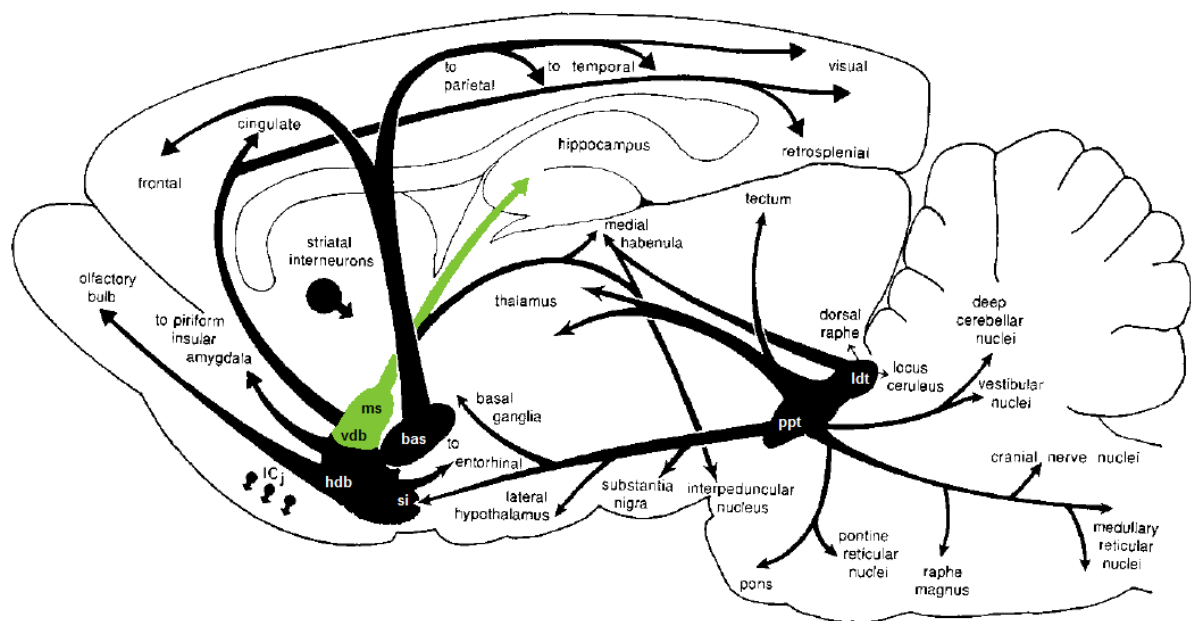


**Figure 1.3: Cholinergic innervation of the hippocampus**

The graph shows a sagittal section of a rat brain and depicts the predominant cholinergic input of the hippocampus originating in the basal forebrain nuclei medial septum (ms) and the vertical diagonal band of Broca (vdb). Fig. 1 in Woolf (1997) [83]; modified.

Abbreviations: bas: nucleus basalis. hdb: horizontal diagonal band nucleus. ICI: island of Calleja. Idt: laterodorsal tegmental nucleus. ms: medial septal nucleus. ppt: pedunculo-pontine nucleus. si: substantia innominata. vdb: vertical diagonal band nucleus.

The cholinergic signal transduction within the hippocampus occurs predominantly via volume transmission [84–87]. Hence, the cholinergic signal may be viewed as setting a tone rather than transmitting discrete informational content [88]. Nonetheless, cholinergic signaling may operate at time intervals of less than a second [89]. However, to the best of my knowledge, the assessment of cholinergic signaling with *in vivo* amperometric techniques currently focuses on the prefrontal cortex [89,90]. Hence, studies on the hippocampus that show an elevated cholinergic tone during active waking and rapid eye movement (REM) sleep by using the microdialysis technique [91] are yet to be refined by adopting novel techniques [92] which provide a higher temporal resolution.

Despite the aforementioned limitations, different levels of cholinergic tone were reported to exert disparate effects in humans and animals. Both the memory- and epilepsy-related evidence will be highlighted in the following.

### **1.2.1 The role of the cholinergic system in short-term maintenance of information**

The previously outlined septo-hippocampal cholinergic signaling was required for learning memory tasks that involved a temporal gap as shown by animal studies that corroborated the functioning of the medial septum [93–95]. In detail, these investigations placed lesions in the medial septum [93], selectively degraded cholinergic neurons in the medial septum [94] or applied the muscarinic acetylcholine receptor (mAChR) antagonist scopolamine acutely and directly to the medial septum [95].

To the best of my knowledge, studies elaborating the role of the cholinergic system in short-term retention of information employing healthy humans are rare. However, in healthy adults the systemic application of scopolamine, which blocks mAChRs, was reported to reduce sustained neuronal activity in the parahippocampal gyrus during short-term retention of information [96]. Thus, the elevated neuronal activity during short-term retention of information in the hippocampus [51] may potentially be mediated by muscarinic cholinergic mechanisms as well [47]. In particular, the assumed cholinergic stimulation of the temporal lobe appears to be crucial for novel, but not for familiar content [97].

In contrast to the scarce evidence derived from healthy adults, the association between alterations in the cholinergic system and the cognitive deterioration early in Alzheimer's disease is broadly acknowledged [98–100]. In detail, muscarinic acetylcholine receptors



appear to be particularly involved [101]. In line with this, cholinergic enhancers are routinely used for therapy, especially at mild to moderate stages of the disease [102]. Furthermore, the cholinergic system is also thought to play a role in the cognitive decline accompanying normal aging [103–105]. Accordingly, aged animals showed an impaired performance in tasks requiring the short-term retention of information which could be improved by mAChR stimulation [106]. One mechanism underlying these behavioral data appears to be an altered neuronal excitability [107–110]. Interestingly, the ventral portion of the hippocampus was reported to be more susceptible to age-related anatomical and functional decline [105].

In light of the aforementioned and further extensive evidence, the cholinergic system is proposed to play an important role in higher cognition [111] and particularly in memory [47,112,113] (Fig. 1.4A).

In short, the cholinergic model of memory, which was brought forward particularly by the Hasselmo lab [112], states that high levels of acetylcholine suppress reverberation within previously established networks [114] (Fig. 1.4B), including CA3 [115]. Furthermore, the functional connectivity between CA1 and CA3 appears to be suppressed during a high cholinergic tone [116–118]. These results are in line with a potentially superior role of CA1 compared to CA3 [56,57,61] and the potentially subordinate role of information transfer from CA3 to CA1 via the Schaffer collaterals [62] during the short-term maintenance of information. In addition to the enhancement of afferent input and the suppression of reverberatory networks (Fig. 1.4B), cholinergic stimulation enhances the excitability of individual neurons [119] (Fig. 1.4C). The latter enables sustained activity without recurrent excitation (Fig. 1.4C) and may potentially be a mechanism mediating the role of CA1 in short-term retention of information [63]. In contrast, during low levels of acetylcholine, retrieval [112] and consolidation [114] are thought to be the predominant operations. However, an elaboration thereon is beyond the scope of this dissertation.

In summary, the cholinergic innervation of the hippocampus via the septo-hippocampal pathway was shown to be required for short-term retention of information. Elevated hippocampal activity during short-term retention of information in healthy adults may be mediated by muscarinic mechanisms, and compromised cognitive functions in the elderly were shown to be related to alterations in the cholinergic system. These and further data are aggregated in the cholinergic model of memory which, amongst other statements, proposes that short-term retention of novel information in the temporal lobe derives from changes in intrinsic cellular properties resulting from a high cholinergic tone.

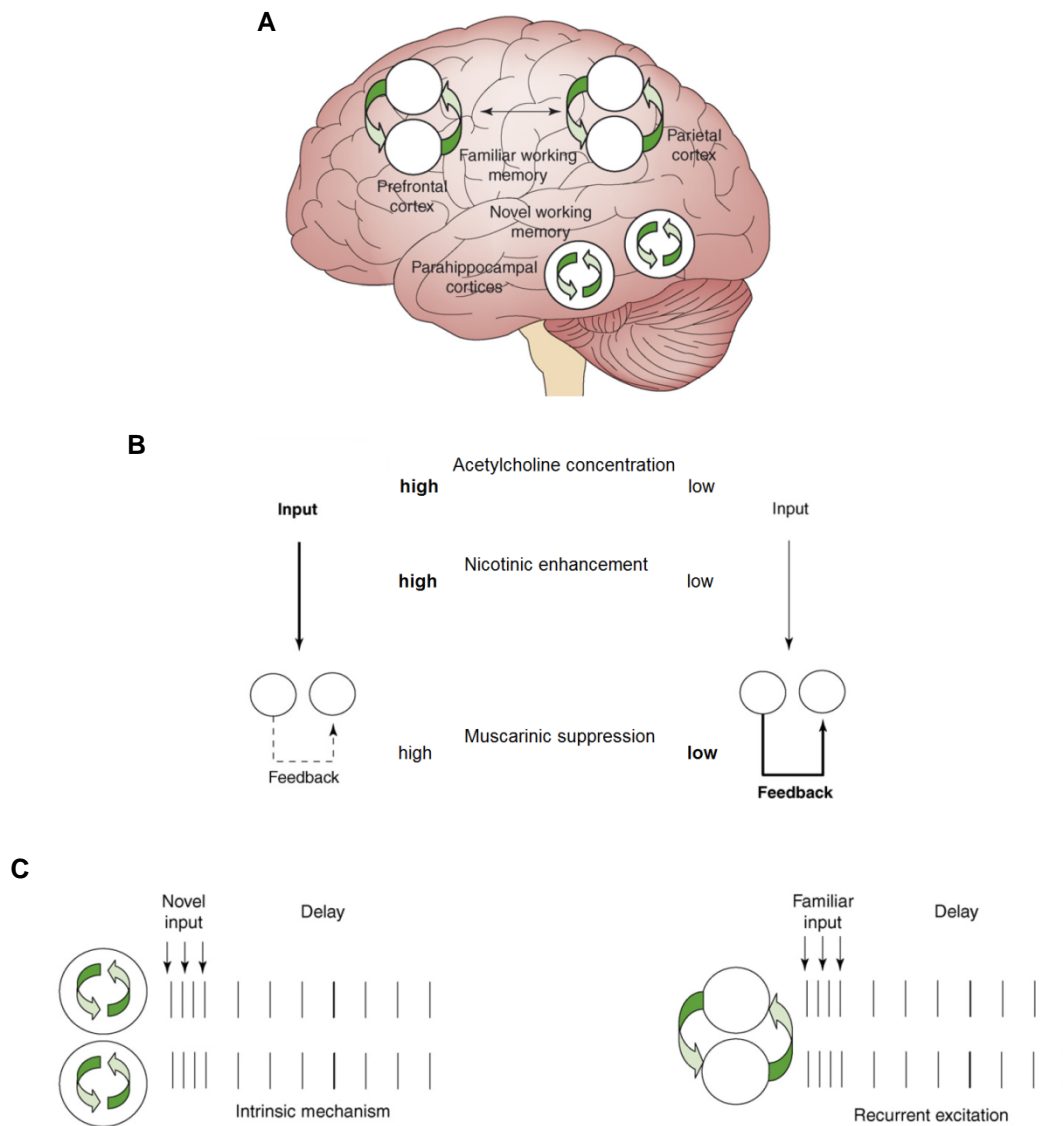


**Figure 1.4: Impact of the cholinergic tone on potential mechanisms mediating short-term retention of information.**

(A) Short-term retention of information (working memory) for familiar content is proposed to be mediated by fronto-parietal networks. In contrast, short-term retention of information for novel content is thought to be mediated by the temporal lobe (parahippocampal cortices).

Figure 1 in Hasselmo and Stern (2006) [47]; modified.

(B) During an elevated cholinergic tone (left), nicotinic signals enhance afferent input (top) and muscarinic signals suppress reverberation within recurrent networks (bottom). In contrast, during reduced cholinergic tone (right), the nicotinic enhancement of afferent input is ameliorated (top) and the muscarinic suppression of recurrent excitation is released (bottom).

Figure 1 in Hasselmo (2006) [112]; modified.

(C) During a high cholinergic tone (left), single cell mechanisms enable intrinsic persistent firing. In contrast, during a low cholinergic tone (right) sustained spiking is permitted by recurrent excitation between cells.

Box 1, Figure 1 a and b in Hasselmo and Stern (2006) [47]; modified.

## 1.2.2 The role of the cholinergic system in seizures and epilepsy

In the early 20th century, the cerebral vasculature was discussed as a potential mediator of epilepsy (reviewed in McLaughlin (1993) [120]) and acetylcholine was considered as anti-epilepticum [121,120]. However, subsequent investigations discovered epileptogenic effects of acetylcholine [122,123] and culminated in the establishment of the pilocarpine animal model of pharmacoresistant temporal lobe epilepsy [124,125]. Pilocarpine is a mAChR agonist and the pilocarpine model is still widely used today [126,127]. In this model, animals are exposed to a single systemic dose of pilocarpine which induces status epilepticus that affects the limbic system. Thereafter, the electroencephalic signature appears to return to normal. However, within four to 44 days, a chronic state commences. The chronic phase is characterized by reoccurring spontaneous seizures at a rate of two to three times per week and it resembles peculiarities observed in human temporal lobe epilepsy [126].

A variety of alterations in the cholinergic system are associated with epilepsy (reviewed in Friedman et al. (2007) [128]). However, the causal relationships and the functional relevance (facilitatory or compensatory) appear to be complex and not yet fully understood. Furthermore, an *in depth* discussion is beyond the scope of the introduction to this dissertation, because the research work of this dissertation focused on acute cholinergic mechanisms. To this end, it is noteworthy that the relationship between the initiation of temporal lobe seizures and acetylcholine is thoroughly established [127] and a potential role of muscarinic receptors in temporal lobe epilepsy starts to emerge [105,129,130].

Common anti-epileptic drugs target sodium and calcium channels or GABA<sub>A</sub> receptors [131,132]. At least some of these drugs seem to also modulate the cholinergic system [133]. Nevertheless, about 30% of patients with epilepsy do not adequately respond to current medication [134] and patients with temporal lobe epilepsy are particularly prone to this disadvantageous course of the disease [68]. For these patients the excision of affected tissue is currently state of the art therapy [135,136]. However, in ca. 30% of the patients with pharmacoresistant epilepsy, surgery is not applicable [135,136]. Therefore, potential new drug targets are extensively investigated for their role in epilepsy [137–143]. These potential targets are canonical transient receptor potential (TRPC) channels which may be activated by cholinergic stimulation [144,145]. Furthermore, new drugs that are in line with the intracellular effects of mAChR stimulation, i.e. K<sup>+</sup> channel modulation, are already tested for

their applicability as anti-epileptic medication [146–149]. Moreover, electrical stimulation of the medial septum is considered for therapy because it may potentially interrupt aberrant activity and may re-set physiological discharges [150].

In summary, excessive cholinergic stimulation of the hippocampus is broadly recognized for being associated with seizures. Furthermore, alterations in the cholinergic system were reported to be associated with epilepsy. However, anti-epileptic treatments which target cholinergic mechanisms are just about to be refined by focusing on the effectors of the intracellular signaling cascades that are induced by mAChR stimulation.

To recapitulate, the cholinergic tone in the hippocampus is predominantly controlled by fibers originating in the basal forebrain. Moderate cholinergic activation of the hippocampus was demonstrated to be involved in the short-term retention of information in healthy as well as aged animals and humans. Furthermore, boundless cholinergic stimulation of the hippocampus is implied in the initiation of seizures. Potentially novel advances in the development of antiepileptic drugs seem to be inspired by the intracellular cascades that are induced by cholinergic stimulation. These intracellular effects of cholinergic stimulation will be described in the following.

## **1.3 Electrophysiological properties of CA1 pyramidal neurons related to cholinergic signaling**

The previous two sections highlighted the role of the hippocampus and the cholinergic system in memory and epilepsy. In the following, I will sketch the intracellular mechanisms that may underlie both phenomena. Therefore, I will first summarize the effects of mAChR stimulation on pyramidal neurons. Thereafter, I will address how these effects may permit the disparate neuronal activities persistent firing and depolarization block that may potentially mediate short-term retention of information and seizures, respectively.

To the best of my knowledge, after a first report about the effects of acetylcholine on intrinsic properties of cortical neurons [151], seminal studies in the early 1980s thoroughly described the effects of cholinergic stimulation on CA1 pyramidal neurons [151–154].

Subsequently, the kinetics [155] and pharmacological properties [156–158] of the cholinergic effects were delineated. These studies and further refinements [159] in the hitherto prevalent techniques for electrophysiological recordings [160] stimulated numerous successive elaborations on the topic. Even subtle effects of cholinergic stimulation on CA1 pyramidal neurons [161–163] were uncovered. The receptors [164] and the intracellular signal transduction cascades [165] mediating these effects were specified. Evidently, the effects of cholinergic stimulation on CA1 pyramidal neurons have been investigated extensively. Subsequently, I will outline these intracellular effects.

Acetylcholine (ACh) is an organic molecule that is released by cholinergic neurons and that binds to acetylcholine receptors (AChRs). These receptors may be ionotropic or metabotropic.

The former gate ions directly once conformational changes were induced by ACh. These ligand-gated channels are comprised by the nicotinic AChRs (nAChRs) and seem to predominantly affect interneurons but not pyramidal neurons in CA1 [166–168]. Nicotinic AChRs play an important role for the signaling within CA1 [169] and for the facilitation of afferent input to CA1 which is implicated in memory processes [112] (Fig. 1.4). However, neither interneurons nor nAChRs are subject of the dissertation at hand and will not be considered further.

The latter metabotropic AChRs do not gate ions themselves. These muscarinic acetylcholine receptors (mAChRs) induce intracellular signaling cascades which modulate ion channels via second messengers [170]. Five muscarinic acetylcholine receptors ( $M_1$ - $M_5$ ) were identified [171,172]. They are expressed on both interneurons and pyramidal neurons at post- and pre-synaptic loci [170,171,173]. Intracellularly, mAChRs couple to guanine nucleotide binding proteins (G-proteins) [174]. On the one hand,  $M_1$ ,  $M_3$  and  $M_5$  were found to couple mainly to  $G_{q/11}$  G-proteins, stimulate phospholipase C (PLC) activity [175] and lead to neuronal excitatory effects. On the other hand,  $M_2$  and  $M_4$  couple mainly to  $G_{i/o}$  G-proteins, thereby block adenylyl cyclase and exert inhibitory neuronal effects [176,177]. Within this dissertation I focus on the excitatory effects mediated by the mAChRs  $M_1$ ,  $M_3$  and  $M_5$ . The intracellular mechanisms that are initiated by the stimulation of  $M_1$ ,  $M_3$  and  $M_5$  affect potassium channels and canonical transient receptor potential (TRPC) channels. In the following; I will first address potassium channels and subsequently turn to TRPC channels.

## Potassium channels

Potassium ( $K^+$ ) channels in CA1 pyramidal neurons were extensively studied [175,178,179] and they are generally accepted for mediating the repolarization of action potentials as well as various forms of afterhyperpolarization (AHP). The afterhyperpolarizing currents are induced by one or multiple action potentials. They are trans-membrane conductances which are carried by the flow of  $K^+$  ions from the cytosol to the extracellular space and may result in a shift of the membrane potential towards more negative values. The fast, medium and slow components of the AHP are differentiated based on their time course and their sensitivity to pharmacological agents [179]. In the following, I will focus on the medium and slow AHP only.

In their perisomatic region [180], CA1 pyramidal neurons express the voltage-gated  $K^+$  channels  $K_{v7.2}$  and  $K_{v7.3}$  which are encoded by the genes *KCNQ2* and *KCNQ3*, respectively.  $K_{v7.2}$  and  $K_{v7.3}$  channels mediate the so called M current ( $I_M$ ) [181] that underlies the medium AHP (mAHP) [182]. The blockade of  $I_M$  by mAChR stimulation was thoroughly investigated [152,175,182,183]. Here, I will briefly allude to the blocking mechanism, as comprehensively reviewed by Brown and Passmore (2009) [175] and Caulfield (1993) [171]. The stimulation of mAChRs activates PLC which then hydrolyses the membrane-bound phosphatidylinositol 4,5 bisphosphonate ( $PIP_2$ ) in the two metabolic products inositol trisphosphate ( $IP_3$ ) and diacylglycerol (DAG). This process leads to a rapid and excessive drop of membrane-bound  $PIP_2$  levels. However,  $PIP_2$  is essential for allowing the ionic conductance of voltage-gated potassium ( $K^+$ ) channels. Hence, upon muscarinic acetylcholine receptor stimulation, voltage-gated  $K^+$  channels are blocked. This dependence on membrane-bound  $PIP_2$  levels is thought to be involved in several potassium conductances [184].

An additional current that may underlie the mAHP is mediated by calcium-sensitive  $K^+$  channels [178,185]. A calcium-sensitive  $K^+$  current was shown to be sensitive to apamin and mediated by SK2 and SK3 channels [186,187]. CA1 pyramidal neurons express both SK2 and SK3 channels in their somatodendritic region [188]. However, the role of SK channels in the mAHP of CA1 pyramidal neurons is controversial. Some groups find them to be involved in the mAHP [186,188] and others find them not to contribute to the mAHP [189,182]. A recent study may have brought the issue forward by having shown that SK channels played a subordinate role compared to KCNQ channels but were crucial in case of KCNQ failure [188]. Furthermore, the modulation of SK channels by acetylcholine is controversial as well. Transient stimulation of CA1 pyramidal cells activates SK2 and SK3 channels [190].

However, recent evidence suggest that not only synaptic but also somatic SK channels may be blocked by mAChR stimulation [191–193].

Notably, the calcium-sensitive sAHP is also blocked by mAChR stimulation [194,195]. However, to the best of my knowledge, the identity of the channels mediating the sAHP are not clarified by today [184]. In the dissertation at hand, the sAHP will not be addressed explicitly. In accordance with the prevailing evidence, I assume to affect the mAHP by modulating channels thought to underlie the mAHP. However, an effect on the sAHP cannot be excluded because not only calcium-sensitive  $K^+$  channels [184], but potentially also the voltage-gated channels  $K_{v7.2}$  and  $K_{v7.3}$  may contribute to the sAHP [196,197].

In summary, the activation of mAChRs blocks  $K^+$  channels which are thought to underlie the mAHP via intracellular signal transduction pathways. This blockade may result in a depolarization of the cell's membrane potential.

### **TRPC channels**

A second class of channels affected by cholinergic modulation are TRPC channels which are thought to mediate the calcium-sensitive non-selective cationic current  $I_{CAN}$  [144,198]. Because  $I_{CAN}$  gates the influx of positively charged ions into the cytosol its activation may lead a calcium-dependent depolarization of the neuron ([199]; but see [200]). Seven members of the TRPC protein family were identified [201]. According to their amino acid sequences and their function, they subgroup into TRPC1, TRPC4/5 and TRPC3/6/7 (TRPC2 is a pseudo gene in humans) [201]. Each TRPC channel is comprised by four subunits and can be either homomeric or heteromeric [202]. The heteromeric channels are assembled by TRPC proteins within their subgroup (TRPC1 may form channels with TRPC3/4/5 or TRPC7) [203]. The isoforms TRPC1/3/4/5 are highly expressed in pyramidal neurons of the CA1 area [204–206].

In contrast to the  $K^+$  channels, the gating mechanisms of TRPC channels appear more heterogeneous and are not yet fully understood [144] (Fig. 1.5). The findings according to Reboresda et al. (2011) [144], are presented here in a concentrated and simplified way. TRPC channels and G-proteins may be tightly linked in space because they were shown to aggregate in lipid rafts. This may allow a direct gating of TRPC channels by conformational changes in the G-protein. Other, more indirect routes of activation were found as well. For example, TRPC4 and TRPC5 are blocked by  $PIP_2$ . This blockade is released upon the stimulation of the cell's mAChRs because  $PIP_2$  is then hydrolyzed by  $PLC\beta$ . The previously mentioned product of the  $PIP_2$  hydrolysis,  $IP_3$ , is well recognized for binding to  $IP_3$  receptors at the endoplasmic

reticulum and thereby releasing calcium ( $\text{Ca}^{2+}$ ) from the internal stores. In CA1 neurons,  $\text{Ca}^{2+}$  from internal stores may then directly or indirectly gate TRPC channels. Neurons in other brain regions appear to possess alternative  $\text{Ca}^{2+}$  sources which may potentially co-exist in CA1 pyramidal neurons as well. Even though not yet well established,  $\text{IP}_3$  may interact with TRPC channels more directly for example via  $\text{IP}_3$  receptors potentially bound to TRPC channels. The second product of  $\text{PIP}_2$  hydrolysis, DAG, may activate protein kinase C (PKC) which is thought to inhibit TRPC4 and TRPC5. In contrast TRPC2/3/6/7 seem to be directly activated by DAG. Hence, the net effects of mAChR stimulation on TRPC channels may depend on the composition of subtypes expressed by the cell.

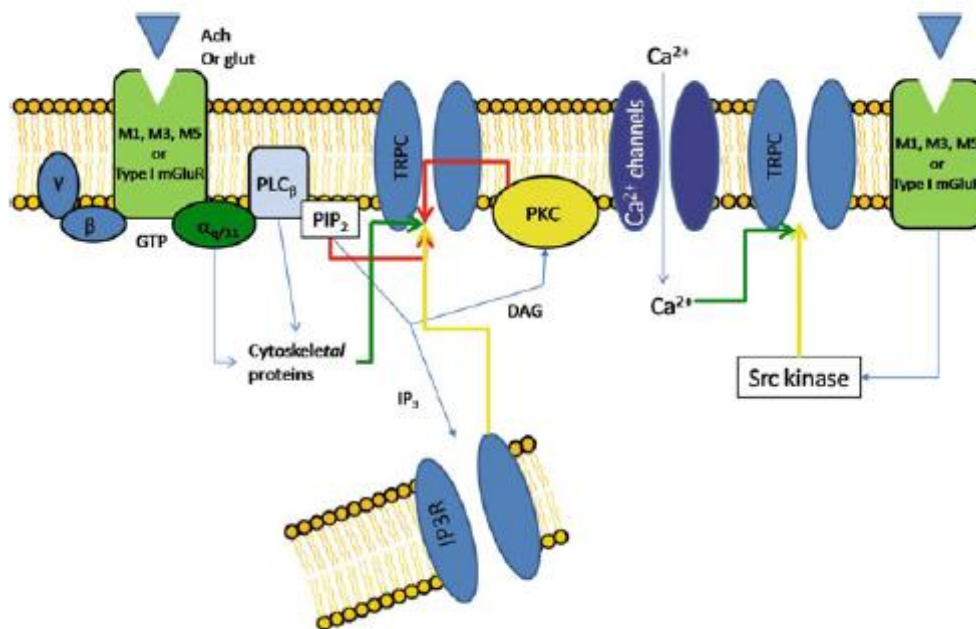


**Figure 1.5: TRPC channel activation induced by muscarinic stimulation.**

The activation mechanism of TRPC channels appears to be complex and is not yet fully understood. Besides muscarinic acetylcholine receptors (M1, M3, M5), type I metabotropic glutamate receptors (mGluRs) may also modulate TRPC channels. Green lines: positive modulation. Red lines: negative modulation. Yellow lines: more data needed. Blue lines: intermediate steps potentially leading to a modulation of TRPC channels

Figure 32.2 in Reboresda et al. (2011) [144].

The aforementioned mechanisms are not exclusive for the mAChRs  $M_1$ ,  $M_3$  and  $M_5$  but may also be induced by type I metabotropic glutamate receptors. In addition, TRPC receptors may also be gated by mechanisms following the activation of receptor tyrosine kinases and the subsequent stimulation of  $\text{PLC}\gamma$ . Furthermore, TRPC channels may also be



gated by store-operated mechanisms related to a tight interaction between TRPC channels and proteins of the endoplasmic membrane [145,203,207].

In summary, the stimulation of mAChRs was shown to activate TRPC channels via G-protein coupled mechanisms and may induce a depolarization of CA1 pyramidal neurons.

In addition to the  $K^+$  channels and the TRPC channels, the excitability of CA1 pyramidal neurons is also controlled by hyperpolarization activated currents ( $I_h$ ) [189]. These non-selective cationic currents are thought to be mediated by nucleotide gated channels that are encoded by the HCN gene [208]. However, these channels may also be modulated by PLC and  $PIP_2$  [209]. Hence, mAChR stimulation may potentially also affect  $I_h$ .

To recapitulate, mAChR stimulation on CA1 pyramidal neurons may induce a variety of effects, e.g.  $K^+$  channel blockade and TRPC channel stimulation, that result in an elevated neuronal excitability.

After the introduction of the intracellular mechanisms and membrane potential effects of mAChR stimulation, I will highlight their relation to short-term retention of information and to epilepsy-related neuronal activity.

### **1.3.1 The role of muscarinic-dependent intracellular processes in short-term maintenance of information**

As outlined before (section 1.2.1), persistent action potential spiking is thought to mediate short-term retention of information [47]. Persistent spiking is a state of elevated neuronal excitability during which action potential firing outlasts the stimulus interval that induced the firing [210].

Electrophysiological recordings from CA1 neurons in animals were sampled while they performed a task that requires short-term retention of information. The data obtained from monkeys [211–213], rabbits [214,215] and rats [216,217] showed sustained spiking activity in a subset of cells during the delay period (Fig. 1.6). Interestingly the firing during the delay period was more pronounced in cells from the dorsal compared to the ventral portion of the hippocampus [218]. However, the mechanism that may potentially underlie these observations was not clear.

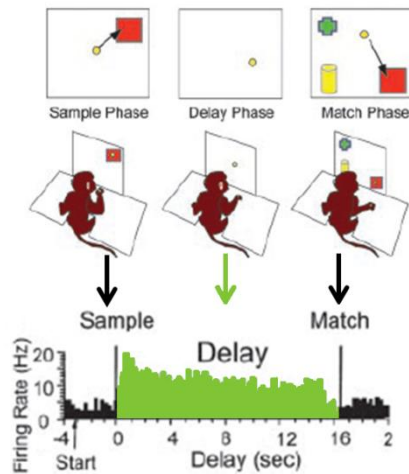


**Figure 1.6: Sustained action potential firing during the delay period.**

The image shows a monkey that was first presented with a sample stimulus (left) which had to be retained throughout a delay (middle) in order to be recognized and identified thereafter (right). During the delay period, when the sample had to be retained throughout a short time interval (10 s), the hippocampal neurons displayed an elevated firing frequency. Figure 1A in Hampson et al. (2004) [213]; modified.

As highlighted earlier in this chapter (section 1.2.1), short-term retention of information requires cholinergic stimulation of the hippocampus. Hence, the mechanism of the aforementioned sustained spiking in CA1 may involve cholinergic modulation as well. In the following I will revisit the cholinergic effects on both  $K^+$  and TRPC channels in the light of short-term retention of information.

### Potassium channels

As previously shown, the performance of aged animals in tasks requiring short-term retention of information was lower than that of young animals, but could be rescued by systemically enhancing the cholinergic tone [106]. A potential underlying mediator of this cholinergic-dependent impairment could be a more pronounced AHP in aged animals compared to young animals [219]. More specifically, a group of aged animals that successfully learned the task exhibited cells with a significantly attenuated AHP, compared to the AHP of neurons from aged animals that did not learn the task [107,219]. The augmented AHP in cells of aged animals was selective for the medium and slow component [219] and was associated with a reduced neuronal excitability [107]. Changes in the expression, the properties or the gating prerequisites of the aforementioned SK channels may underlie these changes because the enhancement of SK channel conductance impairs the performance on a task that involved short-term retention of information [220]

In summary, SK channels may modulate the cellular activity of CA1 pyramidal neurons that is required for short-term retention of information and could mediate the elevated firing frequency recorded *in vivo*.

### **TRPC channels**

In the entorhinal cortex [119] and other areas of the brain [221–225], a cholinergic-dependent persistent firing was previously reported and proposed as a mechanism to allow the short-term maintenance of information [112,226]. Importantly, this persistent firing was mediated by intrinsic properties of individual cells [227]. The centerpiece of this intrinsic mechanism is thought to be the muscarinic (or metabotropic [228,229]) activation of  $I_{CAN}$  via TRPC channels [230]. Such an intrinsic mechanism would be particularly suitable for CA1 pyramidal neurons because they lack excitatory recurrent connections [28,29].

About 15% of CA1 interneurons were previously shown to exhibit mAChR-dependent persistent firing [167]. However, to the best of my knowledge, it was not clear whether CA1 pyramidal neurons may have the propensity to exhibit persistent firing that was induced by a somatic current stimulus which mimics afferent input. The resting membrane potential of CA1 pyramidal neurons was previously shown to be depolarized during tonic cholinergic stimulation [153,162]. This depolarization may lead to sustained action potential generation independent of stimulation by current injection [153]. Yet, persistent activity induced by a discrete current stimulus would be a more appropriate mechanism for the retention of information.

In summary, it was unclear whether TRPC channel activation by mAChR stimulation may allow intrinsic persistent firing in CA1 pyramidal neurons that could underlie the stimulus-related elevated firing frequencies reported *in vivo*.

As previously noted, the  $I_h$  mediating HCN channels are pivotally involved in CA1 pyramidal neuron excitability [189] and may be affected by cholinergic activation [209]. Hence,  $I_h$  could play a role in the cholinergic mediated persistent firing that is thought to underlie short-term retention of information [47]. Accordingly, HCN channels were shown to support persistent firing in neurons of the prefrontal cortex [231,232].

### 1.3.2 The role of muscarinic-dependent intracellular processes in seizure-related epileptiform activity

As previously elucidated, cholinergic signaling in the hippocampus is strongly implicated in the initiation of seizures (section 1.1.2 and section 1.2.2). In the following, I consider the potential involvement of  $K^+$  channels and TRPC channels therein.

#### Potassium channels

Various forms of epilepsy are associated with mutations in  $K^+$  channels [233], including  $K_{v7.2}$  and  $K_{v7.3}$  [234]. Consequently,  $K^+$  channel modulators are considered as new therapeutic approaches for patients with epilepsy [146–149,235].

*In vitro*, both voltage-gated and calcium-sensitive  $K^+$  channels were found to be insufficient for the induction of seizure-related epileptiform activity [236]. However, in the presence of a cholinergic agonist, which permitted epileptiform activity, the blockade of  $I_M$  was found to significantly enhance the duration and amplitude of this epileptiform activity [236]. Accordingly,  $I_M$  was reported to be involved in the cessation of *in vitro* interictal events [237]. Hence, in case of aberrant activity, additional blockade of  $I_M$  may facilitate the switch to epileptiform activity

SK channels were found to be down-regulated in response to pilocarpine induced status epilepticus [238]. Despite a subordinate role of SK channels when in concert with KCNQ channels, they were reported to be fundamentally important in case the functionality of KCNQ channels was hampered *in vitro* [188]. A computational model supports the substantial role of SK channels on a network level [239].

#### TRPC channels

*In vitro*, both interneurons [167] and CA1 pyramidal neurons [236] were shown to exhibit a cholinergic-dependent epileptiform activity that was characterized by a depolarization block (Fig. 1.7). Detailed investigations of the epileptiform activity in CA1 pyramidal neurons first indicated that it was mediated by a calcium-sensitive non-selective cationic current ( $I_{CAN}$ ) [236] and later demonstrated to be mediated by TRPC channels [141].

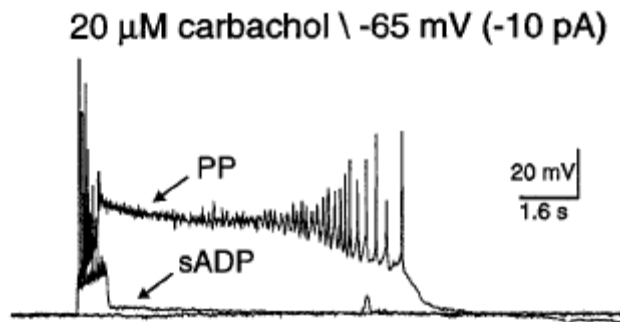


**Figure 1.7: Epileptiform activity in CA1 pyramidal neurons.**

The graph depicts the membrane potential of a CA1 pyramidal neuron maintained at -65 mV with -10 pA direct current injection which is exposed to a 800 ms current injection of incrementing amplitude. The first depolarizing current injection induced a slow afterdepolarization (sADP). The second depolarizing current injection induced a plateau potential (PP) that was characterized by a depolarization block during which no action potentials were generated (arrow). Fig. 4C in Fraser and MacVicar (1996) [236]; modified.

Note: The MacVicar group uses the term 'plateau potential' for epileptiform activity that comprises a depolarization block. In contrast, the Hasselmo group uses the term 'plateau potential' to refer to the membrane potential during persistent firing. Throughout this dissertation I will use 'plateau potential' as descriptive term for the post-stimulus membrane potential relative to the pre-stimulus baseline membrane potential and additionally indicate the type of activity (either persistent firing or depolarization block).

Furthermore, an extensive body of evidence implies TRPC channels in epileptiform activity and epilepsy [137,138,140]. However, the findings [138,140] appear somewhat inconsistent regarding the relation between epileptiform activity *in vitro* and seizure severity *in vivo*. The deviation may potentially be attributed to the induction of seizures *in vivo* via mAChR stimulation in contrast to the induction of epileptiform activity *in vitro* via metabotropic glutamate receptor stimulation. Yet, the gating mechanism is still incompletely understood and therefore, treatment for patients with epilepsy that targets TRPC channels appears to be still out of sight.

Additionally, HCN channels were shown to be involved in epilepsy (reviewed in Reid et al. (2012) [240]). Accordingly, HCN channels played a role in the epileptiform activity of *in vitro* CA1 pyramidal neurons reported by the MacVicar group [241].

In summary, both  $K^+$  channels and TRPC channels appear to be involved in memory-related persistent firing in brain areas other than CA1. Furthermore,  $K^+$  channels and TRPC channels were reported to affect epilepsy and epileptiform activity comprising depolarization block in CA1 pyramidal neurons.

## 1.4. Summary and hypotheses

In this chapter I elucidated that the hippocampus and the cholinergic system are involved in short-term retention of information and seizures. Neuronal activity that is associated with short-term retention of novel information and seizures are persistent firing and epileptiform activity, respectively. I lined out that persistent firing may be a property intrinsic to individual neurons and that epileptiform activity is comprised by depolarization block. Moreover, I showed that both  $K^+$  channels and TRPC channels were reported to be involved in either of these phenomena.

Intrinsic persistent firing was observed in the principal neurons of various cortical areas and in interneurons of the hippocampal CA1 region. However, it was unclear whether CA1 pyramidal neurons may have the ability to exhibit intrinsic persistent firing as well. If so, it would be of interest whether the same neurons may also display depolarization block because this would replicate the findings of the MacVicar group in a different strain of rats and with slightly different methods. Furthermore, the aim would then be to investigate which properties determine whether a cell exhibits the memory-related persistent firing or the seizure-related depolarization block.

Hence, the central research questions of the dissertation at hand are as follows:

- 1) Do CA1 pyramidal neurons display cholinergic-dependent persistent firing *in vitro*?
  - 1a) Is the cholinergic-dependent persistent firing of CA1 pyramidal neurons *in vitro* an intrinsic property of individual cells?
  - 1b) Are the characteristics of the intrinsic persistent firing of *in vitro* CA1 pyramidal neurons a physiologically plausible mechanism for short-term retention of information?
  - 1c) Is the mechanism underlying intrinsic persistent firing in CA1 pyramidal neurons in line with previous reports from intrinsic persistent firing in other areas of the brain
- 2) Do CA1 pyramidal neurons, that were processed in the same way as those that exhibit persistent firing, also engage in depolarization block?
  - 2a) What intrinsic cellular properties control whether intrinsic persistent firing or depolarization block is displayed by CA1 pyramidal neurons?

# 2 Method

## 2.1 Animals

## 2.2 Chemicals and solutions

## 2.3 Preparation of acute brain slices

## 2.4 Recording procedures

## 2.5 Selection of neurons for data analysis

2.5.1 Only pyramidal neurons were analyzed

2.5.2 Silent RMP was required for the inclusion of cells into data analysis

## 2.6 Identification of the cell's anatomical location

2.6.1 Dorso-ventral axis

2.6.2 Proximo-distal axis

## 2.7 Raw data analysis

2.7.1 Passive properties

2.7.2 Hyperpolarization activated current

2.7.3 Action potential properties

2.7.4 Post-burst properties

2.7.5 Excitability

2.7.6 Persistent activity parameters

## 2.8 Statistical comparison of group data

In short, I performed ruptured whole cell patch clamp recordings in the current clamp mode under the usage of a potassium gluconate based intracellular fluid from somata of pyramidal neurons in the CA1 pyramidal layer of acutely sliced hippocampal sections after transcardiac perfusion of 14-24 days old Long Evans rats with a choline chloride based solution.

The method described in the following refers to the vast majority of the recordings (~90%). For a subset of recordings, that were previously reported, some details differed as specified in the publication [63].

## 2.1 Animals

I used Long-Evans rats bred by animals that were mostly (>90%) obtained from Charles River, but sporadically also from Harlan and Janvier. Animals were kept at the central animal facility of the medical faculty (ZVM) at Ruhr University Bochum (RUB) where an open cage system with standard cage dimensions (inner measures, b x h x d, 32.8 cm x 19.0 cm x 55 cm) was used. The animals were maintained at a temperature of 20-22°C, a humidity of 45-55%, a 12:12 h light:dark cycle with lights-on at 6 a.m. (CET; 7 a.m. CEST). They were provided with food (V1534-000, Ssniff, Soest, Germany) and water ad libitum.

A small subset of cells (n = 18) was obtained from animals (n = 9) kept in the Mercator Research Group 1 (MRG 1) at Ruhr University Bochum. They were housed in the same cages as in the ZVM, provided with food (V1534-000, Ssniff, Soest, Germany) and water ad libitum, housed in an air flow cabinet (Uni Protect, Bioscape, Castrop-Rauxel, Germany) maintained at 23.5-24.5°C, with a pressure of 25 Pa, and on a 12:12 h light:dark cycle with lights-on at ~7 p.m. (CEST).

At a postnatal age of 14 to 24 days (P14-24), experimental animals of either sex were separated from their mother during the lights-on period and sacrificed within ~30 min.

For a subset of experiments I used aged animals (n = 7) that comprised males from the same parental stock as the juvenile animals but were kept until an age of 24 to 27 months before they were sacrificed. At the day of sacrifice, the aged rats weighed 572-744 g with an average of 662 g (SD: 59 g). These data did not include an eighth animal, and two cells obtained from it, because I rejected it due to a brain tumor in the left hemisphere (for details see supplemental data, p. 178).



## 2.2 Chemicals and solutions

In the majority of the experiments, I used a choline chloride based cutting solution for the preparation of the slices, a normal artificial cerebrospinal fluid (nACSF) for maintaining the slices before recording, a nACSF with compounds blocking fast ionotropic synaptic transmission (ACSF+SB), and a potassium gluconate based intracellular fluid (ICF).

The choline chloride based cutting solution (~308 mOsm) contained (in mM) 110 CholineCl, 1.25 NaH<sub>2</sub>PO<sub>4</sub>, 7 MgCl<sub>2</sub>, 2.5 KCl, 7 D-Glucose, 3 pyruvic acid, 1 ascorbic acid, 26 NaHCO<sub>3</sub>, 0.5 CaCl<sub>2</sub>. The pH was adjusted by saturation with 95% O<sub>2</sub> - 5% CO<sub>2</sub> for at least 20 minutes after mixing and during usage. At maximum, I stored the solution for 4 days at 4°C. An artificial cerebrospinal fluid containing choline chloride is reported to be particularly suitable for preparing slice from the brains of aged animals [242]. Because, a subproject involved the investigation of neurons from aged animals, I used the choline chloride cutting solution for all animals including the juvenile ones.

The nACSF (~325 mOsm) contained (in mM) 124 NaCl, 1.25 NaH<sub>2</sub>PO<sub>4</sub>, 1.8 MgSO<sub>4</sub>, 3 KCl, 10 D-Glucose, 26 NaHCO<sub>3</sub>, 1.6 CaCl<sub>2</sub>. The pH was adjusted by saturation with 95% O<sub>2</sub> - 5% CO<sub>2</sub> for at least 20 minutes after mixing and during usage. At maximum, I stored the solution for 5 days at 4°C.

The ACSF+SB was nACSF with an additional 2 mM kynurenic acid and 0.1 mM picrotoxin to simultaneously block ionotropic glutamatergic and GABA<sub>A</sub> receptors, respectively. Kynurenic acid and picrotoxin were added daily to the nACSF and mixed for  $\geq 45$  min before recording.

Normally, I kept the nACSF and the ACSF+SB at a recording temperature of  $35 \pm 1^\circ\text{C}$ . However, in my hands, the bath applied TRPC4/5 channel antagonist ML204 [243,244] was neither functional at a concentration of 10  $\mu\text{M}$  ( $n = 9$ ) nor 20  $\mu\text{M}$  ( $n = 6$ ) when used with my standard procedures. In my standard approach, the ACSF was pre-heated to 43-48°C by an in-line heater in order to achieve  $35 \pm 1^\circ\text{C}$  in the recording chamber. Limited stability of ML204 [244] when exposed to such high temperatures may have been the reason for the derogated functionality. Setting the temperature of the in-line heater to 35.0°C, slightly increasing the speed of flow and reducing the ACSF volume in the recording chamber allowed me to maintain ML204 stable and test for its effect on persistent firing and depolarization block at a recording temperature of  $30 \pm 1^\circ\text{C}$ . Cells that were exposed to

ML204 were maintained at  $30 \pm 1^\circ\text{C}$  throughout the entire recording interval, i.e. also in the absence of ML204.

The standard ICF (~320 mOsm) contained (in mM) 120 K-gluconate, 10 HEPES, 0.2 EGTA, 20 KCl, 2 MgCl<sub>2</sub>, 7 Phosphocreatine di(tris) salt, 4 Na<sub>2</sub>ATP, 0.3 GTP, and 0.1% (w/v) biocytin. The pH was adjusted to 7.3 with KOH (5 M/L). Biocytin was added to allow for histological staining of patched neurons (see p. 179 and 180 for details of the procedures).

An ICF additionally containing 10 mM BAPTA (~355 mOsm) was used to test for the effect of the intracellular calcium concentration because BAPTA is a fast and highly selective chelator of intracellular calcium [245].

An ICF containing a total of 10 mM Na<sub>2</sub>ATP (~344 mOsm) was used to test for the effect of intracellular ATP because intracellular ATP was shown to block TRPC5 channels in a heterologous expression system [246].

Before the histological staining, slices with the patched neuron were maintained at  $4^\circ\text{C}$  in 4% PFA in 0.1 M Sodium Phosphate buffer (NaPB) which contained (in mM) 19 NaH<sub>2</sub>PO<sub>4</sub> and 81 Na<sub>2</sub>HPO<sub>4</sub>.

## 2.3 Preparation of acute brain slices

The majority of cells (~90%) were obtained from animals that were transcardially perfused before decapitation. The remaining neurons were obtained from animals whose brains were immediately excised following decapitation upon the achievement of deep anesthesia.

All experimental protocols were in accordance with the guidelines of the local animal ethics commission. In detail, the preparation proceeded as follows.

An intraperitoneal injection of a ketamine:xylazine mixture at a concentration of 100:4 mg/kg induced general anesthesia. Whether animals were in the tolerance stage of general anesthesia [247] was checked by trying to elicit the toe-pinch reflex after righting, postural and eyelid closure reflexes were abolished. If necessary, additive doses of the same ketamine:xylazine mixture was applied. Surgery was only commenced upon the loss of the toe-pinch reflex. Firstly, the chest was opened to obtain access to the heart. The rib cage was not removed but flipped up to avoid excessive premature blood loss. While holding the right ventricle, the right atrium or the superior vena cava were severed, the left ventricle was

impaled with a 21 gauge needle and 15-20 ml ice-cold pre-oxygenated (95% O<sub>2</sub> - 5% CO<sub>2</sub>) cutting solution was injected. Once the blood was replaced with cutting solution, animals were decapitated. While immersed in ice-cold cutting solution, the brain was extracted from the skull and subsequently submerged in fresh, oxygenated ice-cold cutting solution. After ~1 min, the brain was retrieved, placed upside-down on filter paper and the cerebellum was removed. Cyanoacrylate glue was quickly spread on the specimen disc in the pre-cooled slicing chamber of a vibratome (Leica VT 1000S, Leica Instruments, Wetzlar, Germany), the brain was promptly placed right-side up onto the glue and the slicing chamber was immediately flooded with oxygenated ice-cold cutting solution. After dissecting the brain by one coronal cut at ~5-6 mm from the frontal pole and one sagittal cut at the central fissure, slices of 350 µm thickness were cut horizontally at a frequency of 80 Hz, 0.2 mm/s and an amplitude of 1 mm. Throughout the slicing procedure, the cutting solution was constantly oxygenated and cooled. Following the dissection of tissue medial to the hippocampus, slices were individually transferred to compartmentalized holding chambers with nACSF at 30°C. Records of both the hemisphere as well as the consecutive numbering were kept for each slice. After incubating the slices for ~30 min at 30°C, the holding chambers were transferred to room temperature (~21-22°C) until the commencement of recordings, but for at least 30 min. Upon completion of the slicing procedure, a commercially available digital meter (Milomex Ltd, UK) was used to measure various dimensions from the remainder of the brain. These data allowed *post-hoc* calculation of the cell's origin in the dorso-ventral axis, relative to the top of the brain.

## 2.4 Recording procedures

After completion of the incubation as described above, slices were transferred onto a submerged Polyamid/Elasthan net in a recording chamber fixed to a vibration isolation table (Microplan, Saarbrücken, Germany). The recording chamber was superfused with pre-oxygenated (95% O<sub>2</sub> - 5% CO<sub>2</sub>) ACSF. Unless stated otherwise, the temperature of the ACSF during recording was maintained at 34 to 36°C. Therefore, an inline solution heater (N<sup>o</sup> 640102; Warner Instruments, Hamden, CT, USA) was set to ~43 to 48°C by a TCU-2 temperature controller (Fine Science Tools, North Vancouver, BC, Canada). Influx of the ACSF to the recording chamber was provided by gravity at a rate of ~1.5 ml per minute. Efflux of the ACSF was provided by a pump (Minipuls 3, Gilson, France). To stabilize the slice, strings of dental floss (attached to a ~13.5 x 13.5 mm metal frame) were placed

orthogonal to the proximo-distal axis of CA1. A string spacing of ~2.5 mm was chosen to spare the CA1 area from the mechanical impact of the strings. The slice was visualized using an upright microscope (Axioskop, Zeiss, Thornwood, USA), equipped with a Sony CCD camera (Japan). The region of interest was identified by using a low magnification objective lens (EC EPIPLAN, 5x, Zeiss, Thornwood, USA). After the region of interest was centered within the optic field, the objective lens was changed to a 40x, 0.8 numerical aperture, water-immersion objective (LUMPlanFIIR, Olympus, Tokyo, Japan). Cells were visualized by Debut Video Capture (NCH Software) on a Dell computer and a 27" Fujitsu screen.

Patch pipettes with a resistance of 3 to 8 M $\Omega$  were pulled from glass capillaries (GB150F-8P, World Precision Instruments, Hofheim, Germany) using a P-87 (Sutter Instruments; Navato, CA, USA) puller. Pipettes were backfilled through a 0.2  $\mu$ m cellulose acetate syringe filter (Titan 3 Spritzenfilter, msscientific Chromatographie-Handel GmbH, Berlin, Germany) with the K-gluconate based ICF specified above.

First, a cell was identified and centered to the optic field by moving the microscope using a micro manipulator (Luigs & Neumann GmbH, Ratingen, Germany). Following this, the objective lens was slightly raised to create space for inserting the recording pipette between the slice and the objective lens. Subsequently the pipette was immersed in to the ACSF using the same kind of micro manipulator as for the microscope. The pipette resistance was registered and compensated for promptly. While applying weak positive air pressure inside the pipette, the objective and the pipette were lowered to just above the slice. Before lowering the pipette into the tissue the air pressure was released and the junction potentials were compensated by adjusting the pipette offset function built in the amplifier (Axoclamp 2-B, Axon Instruments). Afterwards, the positive air pressure was applied again. To monitor the resistance, the seal test function in the clampex software (Clampex 9.2, Axon Instruments, Sunnyvale, USA) was used. The pipette was lowered into the tissue and moved until just above the cell as verified by an apparent dip on the surface of the cell (Fig. 2.1A) and an increase in resistance. After this, the positive air pressure was increased until the development of a relatively large scale "bubble" (Fig. 2.1B). Following this presumed clearance of extracellular matrix, the pipette was repositioned and the exposed membrane was approached. Instantaneously, the positive pressure was released and a well-dosed, cell-specific suction was applied (Fig. 2.1C) to increase the interconnection between cell membrane and pipette. A resistance beyond 1 G $\Omega$  and a membrane potential of <-60 mV and zero current flow were indicators for a stable patch. Once a stable patch was obtained, only a light negative pressure

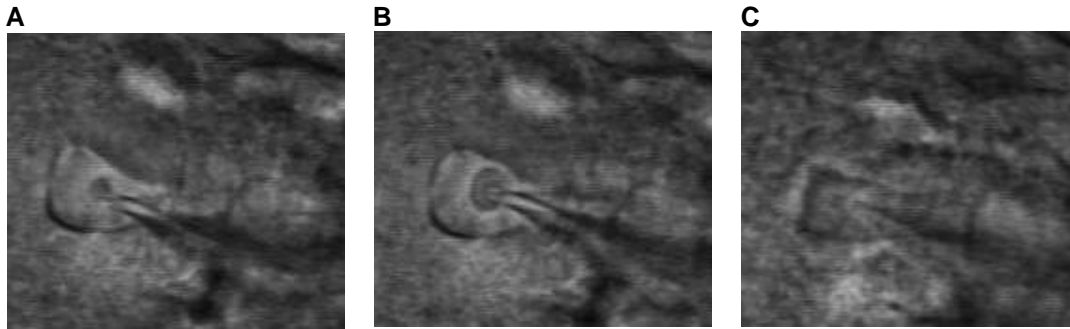


**Figure 2.1: Attaining a whole-cell patch configuration.**

(A-C) The same cell viewed through a 40x object lens is displayed.

(A) Upon approaching the cell with low positive air pressure, a small initial dip indicates close proximity to the cell. (B) Once the positive pressure is increased, a larger scale "bubble" appears and presumably indicates the clearance of extracellular matrix. (C) When clear access to the cell's membrane was obtained, as shown in (B), negative pressure was applied to form a G $\Omega$  seal.

was maintained and the membrane was ruptured by trains of short but strong negative air pressure. The air pressure in the pipette was supervised by a pressure monitor (BP1-B, World Precision Instruments, Sarasota, FL, USA). Immediately after the rupture of the membrane and frequently throughout the recording, the series resistance was compensated and read out.

Recordings were obtained in current clamp mode using the bridge balance circuit with an Axoclamp 2-B amplifier (Axon Instruments, Sunnyvale, USA), digitized at a rate of 20 kHz using Digidata 1322A (Axon Instruments, Sunnyvale, USA) applying a low pass-filter of 10 kHz. Digitized signals were visualized and saved to a hard drive using a data acquisition software pClamp 9 (Clampex 9.2, Axon Instruments, Sunnyvale, USA).

The liquid junction potential has previously been measured to be  $\sim 10$  mV and I calculated it (Clampex 9.2, Axon Instruments, Sunnyvale, USA) to be  $\sim 13$  mV. The liquid junction potential was not compensated.

After experimental procedures were completed, the pipette was slowly (within 5-10 min) retracted from the cell to preserve the membrane for maintaining the morphology and for allowing *post-hoc* staining. After the retraction, the pipette was raised just above the slice, moved back to its recording position and pictures were taken using Debut Video Capture (HCH Software). These saved pictures provided an estimate of the recording position in case the cell staining failed. Following the extraction of the pipette from the ACSF and the removal of the retaining device, the slice was transferred to 4% PFA in NaPB (specified above). Within  $\leq 10$  weeks (usually 2 days - 4 weeks) the staining was revealed by an immunohistochemical protocol (supplemental material, p. 179).

## 2.5 Selection of neurons for data analysis

Unless otherwise stated, the selection criteria were established on the cells in slices superfused with ACSF+SB and obtained from trans-cardially perfused animals.

### 2.5.1 Only pyramidal neurons were analyzed

Upon the impalement of the neuron, I judged whether I was confronted with a pyramidal cell or an interneuron. Interneurons presented themselves with a more hyperpolarized RMP, a marked fast afterhyperpolarization, they exhibited so called chattering action potential (AP) trains whereby several APs were grouped together and then followed by a pause, and no apparent  $I_h$ . Varying combinations of a subset of these electrophysiological characteristics appeared in conjunction. *Post-hoc* analysis showed that neurons which I classified as interneurons had a full width at half height ( $AP_{FW1/2H}$ ) of  $\sim 0.5$  ms ( $n = 6$ ) whereas the presumed pyramidal neurons had an average  $AP_{FW1/2H}$  of 1.2 ms (SD: 0.3 ms,  $n = 137$ ). However, three cells had a half width more than 2 standard deviations above the mean. Detailed inspection verified that these cells showed unusual responses that indicated a compromised health status and were thus excluded from further analysis. Following the biocytin staining, neurons that exhibited a non-pyramidal shape were also excluded (Fig. 2.2).

### 2.5.2 Silent RMP was required for the inclusion of cells

Only neurons with a non-spiking resting membrane potential (RMP) in nACSF or ACSF+SB were included in the analysis. In a minority of cells ( $n < 20$ ), the superfusate contained Cch during the impalement. Most neurons ( $\sim 61\%$  [41/67] in ACSF+SB +10  $\mu$ M Cch) no longer had a silent RMP upon the superfusion of Cch. Consequently, I could not judge whether the neurons impaled in the presence of Cch would have had a silent RMP without Cch. However, I compared whether these neurons behaved similarly to those that had a silent RMP without Cch. In particular, I compared the current injection needed to maintain the cells just below their action potential threshold. In affirmed healthy cells, this current ranged from  $\sim 10$ -100 pA. If I needed a comparable current injection to hold the neurons, that were impaled in the presence of Cch, just below their action potential threshold, I classified them as being at good health and included them in the analysis.

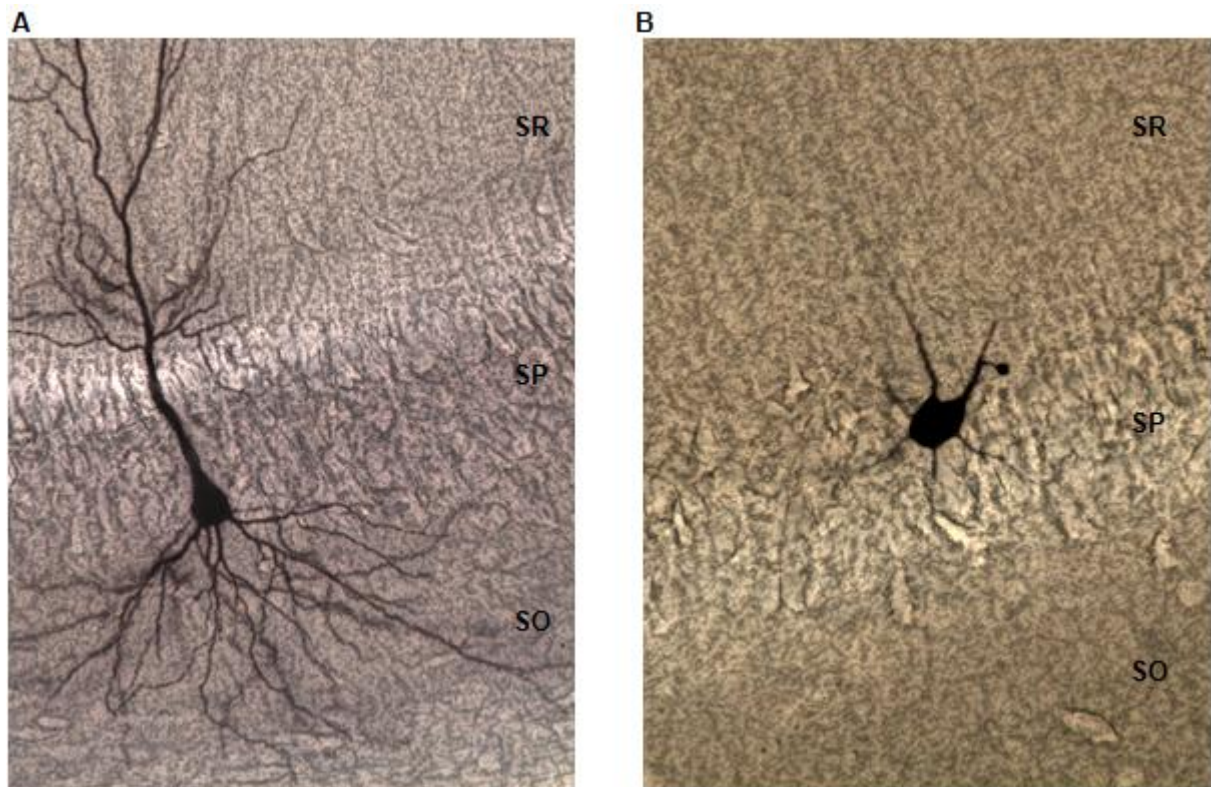


**Figure 2.2: Neurons with a non-pyramidal shape were excluded from data analysis.**

The images show neurons within the hippocampal CA1 area. For comparability, strata follow the same sequence in both images, with stratum oriens (SO) at the bottom, followed by the stratum pyramidale (SP) and the stratum radiatum (SR) at the top.

(A) The cell exhibits a prototypical pyramidal shape with one apical dendrite extending into stratum radiatum and basal dendrites extending into stratum oriens (ID: 140103/R5).

(B) The image shows an examples of a neuron with a non-pyramidal shape that was excluded because it was a presumed interneuron. (ID: 121216/L2).

Frequently, an apparently arbitrary RMP of -50 mV [248], -55 mV [249], -58 mV [219], or -60 mV [250] is reported as cut-off criterion for the inclusion of cells into data analysis. The RMP of pyramidal neurons in my sample was usually between -70 and -58 mV with an average of -63.5 mV (SD: 3.5 mV,  $n = 159$ ). Six cells had a silent RMP more depolarized than two standard deviations above the mean. One cell had a RMP more hyperpolarized than two standard deviations below the mean.

The RMP of neurons in the medial entorhinal cortex were reported to adopt more hyperpolarized RMPs as animals aged [251]. Importantly, the shift occurred throughout the age range across which I also used my experimental animals. The RMP of CA1 pyramidal neurons also hyperpolarized as animals matured [252–254]. In these studies, the age range at which I used my experimental animals was collided into one group. However, the overall

picture indicates that the RMP of CA1 pyramidal neurons may change across P14-24. Developmental changes in channel expression and conductance that affect the RMP support this suggestion. Amongst other currents, the RMP is influenced by a hyperpolarization activated cyclic nucleotide-gated cationic current ( $I_h$ ) [18,24,255]. The channels mediating  $I_h$  [256] and  $I_h$  itself (mouse data: [257]) were shown to achieve maturity by the end of the third postnatal week or to gradually mature until the end of the fourth postnatal week [258].

These data indicate that throughout the age range of my experimental animals, developmental changes may still have occurred. Accordingly, the neurons with the outlier depolarized and hyperpolarized RMP originated from particularly young (P14-16) and old (P24) animals, respectively. Despite the evidence indicating a developmental aspect of RMP values observed in my sample, the electrophysiological properties of neurons with a RMP more depolarized than 2 SD above the mean were thoroughly investigated for signs of an inadequate health status, e.g. paroxysmal depolarization shifts in the absence of Cch. Cells were only selected for further data analysis if no signs of a compromised health status could be detected.

## 2.6 Identification of the cell's anatomical location

### 2.6.1 Dorso-ventral axis

To approximate the anatomical origin of each cell, the hemisphere and the identification number of each slice (sequentially from dorsal to ventral) was documented. After slicing was completed, multiple measures were taken from the remainder of the brain (Fig. 2.3) using a commercially available digital meter (Milomex Ltd, UK). Using the identification number of the slice and the measures from the remainder of the brain, the distance from the top of the brain was determined for both surfaces of each slice. Based on the hemisphere from which the slice was obtained, the cell's location was determined to be either on the top or the bottom the a slice. This definition of the cell's location at the top or the bottom appears appropriate with respect to the thickness of the slice (0.35 mm), as well as the optical and mechanical limits of visually guided patch clamp. If no record of the slice's hemispheric origin was available, the middle of the slice was assumed as an approximation of the cell's location within the slice. Consolidating both measures (distance of the slice's surface



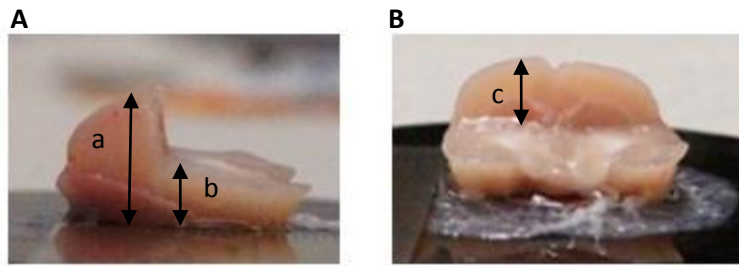


**Figure 2.3: Measures from the remainder of the brain allowed an estimation of the cell's dorso-ventral origin.**

(A) A view from the left onto a not trans-cardially perfused brain is shown. The total height is indicated by (a). The ventral height is indicated by (b).

(B) A view from caudal onto the coronal plane of a not trans-cardially perfused brain. The dorsal height is indicated by (c).

from the top of the brain and the location of the cell on either side of the slice) yielded the distance of the cell from the top of the brain in mm. Measures of  $\leq 1\text{mm}$  and  $\geq 5\text{mm}$  were rare and thus thoroughly checked for plausibility. Based on this plausibility-check, the location's quantification from three neurons were rejected due to an apparent mismeasurement.

The quantification of the cells' location in the dorso-ventral axis of the hippocampi from my experimental animals could not be set into direct relation to the bregma location reported in a stereotactic atlas [259]. Firstly, bregma is a location on the top of the skull [260] and consequently the measures are in relation to the top of the skull. In contrast, my measures were relative to the top of the brain. Secondly, the brain's volume of juvenile animals was reported to be lower than that of adult animals [261].

Nonetheless, I attempted to obtain an anatomy-based (as opposed to a sample based) classification of the dorso-ventral location of cells. The aim was to quantify the outermost dorsal and ventral points of the hippocampus in P14-24 animals based on the aforementioned method. Hence, I analyzed the slices of all neurons I ever recorded in the hippocampus (including pyramidal neurons, interneurons, and subicular, CA1 and CA2 neurons) and for which the dorso-ventral measures were obtained as described above ( $n = 417$ ).

The slices of the most dorsally and most ventrally recorded hippocampal neurons had morphological characteristics corresponding to an approximate bregma location of  $-3.4\text{mm}$  and  $-7.8\text{mm}$  in the adult rat brain [259], respectively. The horizontal plates at  $-3.1$  and  $-8.42\text{mm}$  in Paxinos and Watson (2007) [259] were the most dorsal and the most ventral ones containing discernible hippocampal specifications. Taking developmental [261] and potential

inter-strain differences (Paxinos and Watson rat brain atlas [259] was based on adult male Wistar rats) into account, this comparison indicated that I potentially spanned the full extent of the hippocampus in P14-P24 Long-Evans rats.

However, my sampling may have been biased towards a dorsal or ventral subpopulation. Hence, determining cut-off lines by using the average or the median (despite its advanced outlier insensitivity) of the entire sample could have resulted a classification of dorsal and ventral locations specific to my sample and poorly comparable to other reports. Therefore, I used the arithmetic middle only between the most extreme dorsal and most extreme ventral location to obtain a half-split cut off line. To account for potential measuring inaccuracies, I averaged the locations of the neurons obtained from the five most dorsal and the five most ventral slices, which did not introduce an unduly sampling bias. The five most dorsally and most ventrally obtained neurons were on average located at 0.82 mm (SD: 0.21 mm) and -4.97 mm (SD: 0.03 mm) below the top of the brain, respectively.

Based on these anatomical estimates of the hippocampal proper's dimension in P14-24 Long-Evans rats, I defined that neurons located in the dorsal half of the hippocampus had to be obtained from  $\leq 3.015$  mm below the top of the brain. Likewise, cells located in the ventral half of the hippocampus had to be obtained from  $> 3.015$  mm below the top of the brain. To assess more disparate populations, neurons in the most dorsal ( $\leq 2.283$  mm below the top of the brain) and most ventral ( $\geq 3.747$  mm below the top of the brain) third of the hippocampus were also analyzed.

## 2.6.2 Proximo-distal axis

In slices with successful biocytin staining, I quantified the proximo-distal location of the cell. In case of failed biocytin staining, the location in the proximo-distal axis was not quantified. However, pictures taken right after the recording were used to verify the location within CA1.

Pictures of the slices containing the recorded neuron were usually obtained during the first and second day after the completion of the staining procedure (supplemental material, p. 179). The pictures were captured in the bright field mode of a fluorescence microscope (BZ-9000, Keyence Deutschland GmbH, Neu-Isenburg, Deutschland) with the *light stopping* set to 10% or 15% to increase the contrast. Under close guidance of a stereotactic atlas [259], I determined the borders of CA1 to the adjacent areas CA2 and subiculum on merged images of the slice, the hippocampus and the CA1 area at a 4x, 10x and 20x magnification,

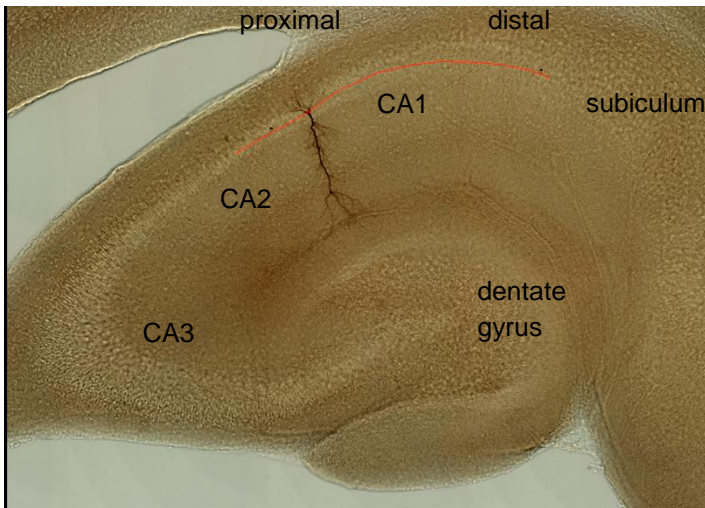


**Figure 2.4: Measurement of the cell's location in the proximo-distal axis.**

The figure shows the merged image of a horizontal slice containing the hippocampal formation taken at a 10x magnification. The red line indicates the measures taken from the border of CA1 with CA2 to the soma and from the soma to the border of CA1 with the subiculum. The neuron is the dark structure in CA1 that extends towards the dentate gyrus. The proximo-distal location of the cell was determined to be 24.5%. ID: 130718/L3.

respectively. The diverse sections at the specified magnifications were chosen because different aspects defining the borders of CA1 could be seen well in different magnifications. If available, I quantified the distance of the soma to each border in all three images. The measured distances followed the curved outline of the CA1 pyramidal layer at the superficial to deep height of the recorded neuron's soma (Fig. 2.4). The *multi-point line* option of the aforementioned fluorescence microscope allowed the quantification of a curvilinear distances in  $\mu\text{m}$ . The cell's proximo-distal location was the distance of the soma from the CA2-border relative to the full length of the CA1 field, multiplied by 100 to obtain a percentage. The cell's relative location in the proximo-distal axis was averaged across the three magnifications (4x, 10x, 20x) and the obtained value was used for analysis.

## 2.7 Raw data analysis

Here and henceforth, scale bars apply to all traces of the same signal type (i.e. either current or voltage), unless stated otherwise. Several protocols involve repetition of either exactly the same command or a slightly altered command. These repetitions will be called 'sweeps' throughout this dissertation. One individual sweep will be termed 'trace'.

## 2.7.1 Passive properties

### Resting membrane potential

The resting membrane potential was the average membrane potential during a 10 s interval without current injection. The interval was sampled as soon as possible after gaining stable access to the cell. If the superfusate was changed, the interval was sampled at the earliest 5 min after the switch and at the latest when a stable response was observed, which was in general no later than 15 min after the switch.

### Input resistance

The input resistance was assessed at -70, -65 and at -60 mV. A hyperpolarizing voltage deflection was induced by a -5 pA square pulse that lasted 500 ms. The input resistance was calculated according to Ohm's law (Formula 1).

$$R = \frac{V_{pre} - V_{inter}}{I_{pre} - I_{inter}} \quad \text{Formula 1}$$

V and I were the membrane potential and the current, respectively. Pre and inter indicated an interval prior to and during the square pulse, respectively.

The current step was chosen to have such a small amplitude because it was not permitted to induce the activation of voltage-dependent currents. In 143 cells which were superfused with ACSF+SB and held at -70 mV, the -5 pA current step induced an average hyperpolarizing voltage deflection of 0.55 mV (SD: 0.17 mV).

Due to the low amplitude of the current pulse and the induced voltage deflection, the quantification of the input resistance was highly sensitive to noise in the membrane potential. Several procedures were employed to reduce the influence of noise. First, the square pulse was repeated seven times. Second, within the 500 ms before and during the square pulse, three partially overlapping 200 ms intervals were investigated to maximize the number of included runs. Third, individual runs were excluded if either prior or during the square pulse no 200 ms interval existed with membrane fluctuations below 1 mV. Fourth, if a run was included in the analysis, only the 200 ms interval with the lowest standard deviation was chosen from before and during the square pulse, respectively. Fifth, across all valid runs, the 200 ms intervals before and during the square pulse were each averaged to one correspondent membrane potential trace. Sixth, the mean membrane potential across the 200 ms interval was

determined from both average membrane potential traces. Finally, the resultant output (Fig. 2.5) was visually inspected. In the last step, some protocols had to be excluded because too few runs were valid and could therefore not average fluctuations below 1 mV out.

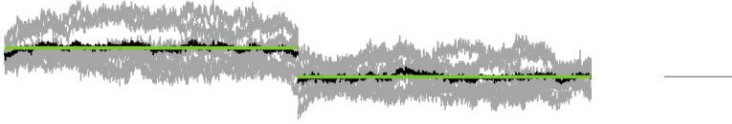


**Figure 2.5: Quantification of the input resistance by a low amplitude current injection.**

The left traces represent intervals from seven sweeps prior to the current injection. The right traces represent intervals from seven sweeps during the current injection. Individual 200 ms intervals are shown in grey. The average membrane potential traces are shown in black. The mean membrane potential across interval is indicated by the green lines. In the displayed example the membrane potential before and during the square pulse was -69.79 and -70.20 mV, respectively and the resultant input resistance was 84.2 M $\Omega$ . Vertical scale bar: 1 mV. Horizontal scale bar: 50 ms. ID: 111113/L7/f18

## 2.7.2 Hyperpolarization activated current

I induced the hyperpolarization activated non-selective cationic current ( $I_h$ ) from a baseline membrane potential of -70 mV by applying hyperpolarizing current steps with a duration of 1 s and varying amplitudes from -300 pA to -50 pA (descending increments of 50 pA). For each current command I determined the following three parameters. First, the average baseline membrane potential ( $V_{BL}$ ) across the 200 ms preceding the current injection. Second, the membrane potential at the negative peak ( $V_{peak}$ ) within 150 ms after the stimulus onset. Third, the average steady state membrane potential ( $V_{SS}$ ) across the 200 ms preceding offset of the current injection. In addition, I determined the amount of membrane fluctuation during the baseline and the steady state membrane potential by the absolute difference of the maximum and minimum membrane potential within the interval. A given sweep was excluded if the membrane fluctuation exceeded 2 mV. All traces were visually inspected for slow distortions of the membrane potential and individual sweeps were excluded if either of the aforementioned measure was corroborated

The sag ratio was determined as the magnitude of the depolarization following the negative peak, relative to peak amplitude of the direct current induced hyperpolarization normalized to the baseline (Formula 2).

$$\text{sag ratio} = \frac{V_{\text{peak}} - V_{\text{ss}}}{V_{\text{peak}} - V_{\text{BL}}}$$

**Formula 2**

For data analysis I used the sweeps that induced a peak membrane potential of -80, -85 and -90 mV. Higher values of the sag ratio indicated a more pronounced underlying  $I_h$ .

### 2.7.3 Action potential properties

To assess properties of action potentials (APs), I examined isolated APs only. I considered an AP to be isolated when it occurred more than 5 seconds after a previous AP.

#### Action potential threshold

To date, there is no consensus on the automated determination of the action potential (AP) threshold [262]. The judgment based on visual inspection by an experienced researcher is considered to be the gold standard [262]. The most commonly used operationalization of the automated AP threshold ( $AP_{\text{thresh}}$ ) detection is the passing of an *ad-hoc* defined value of the voltage trace's first derivative (e.g. 10 mV/ms; [263]). However, Sekerli et al. (2004) [262] highlighted that the performance of this method is notably sensitive to deviations of any well educated guess from the actual rising slope at the  $AP_{\text{thresh}}$ . Therefore, I refrained from applying the most commonly used method for determining the  $AP_{\text{thresh}}$  to my recordings.

Henze and Buzsáki (2001) [264] advocated the maximum of the voltage trace's third derivative as the  $AP_{\text{thresh}}$ . However, an extensive study on seven methods for quantifying the  $AP_{\text{thresh}}$  assessed this third derivative method as performing comparably poor [262]. The inconsistency in the evaluation of the third derivative method may be explained by the different neuronal populations used in both studies. Sekerli et al. (2004) [262] did not investigate AP traces from mammalian cortex, whereas Henze and Buzsáki (2001) [264] performed their study on recordings from *in vivo* CA1 pyramidal neurons.

Sekerli et al. (2004) [262] recommended their methods number II and number VI. In method II, the  $AP_{\text{thresh}}$  was determined to be at the maximum of the second derivative relative to the membrane potential. In method VI, the  $AP_{\text{thresh}}$  was defined as the minimum value of the first derivative during the rising phase of the action potential.

I decided to compare the third derivative method used by Henze and Buzsáki (2001) [264] with method VI [262] because both determined the  $AP_{\text{thresh}}$  relative to time. In contrast, method II [262] determined the  $AP_{\text{thresh}}$  relative to the membrane potential (phase space).

In line with the concordant neuronal type used by Henze and Buzsáki (2001) [264] and by me, the maximum of the third derivative (method V) was superior to method VI [262] in determining the  $AP_{\text{thresh}}$  in the majority of my recordings (Fig. 2.6A). However, visual inspection revealed that the maximum of the third derivative (method V) overestimated the action potential threshold in the case of a smooth AP onset or in the presence of a shoulder (Fig. 2.6B). The overestimation of the action potential threshold by method V was previously reported [262]. In those cases, method VI provided a more acceptable approximation of the action potential threshold. In relation to a  $AP_{\text{thresh}}$  identified by visual inspection, method VI still underestimated the  $AP_{\text{thresh}}$ . However, this underestimation was negligible in comparison to the overestimation by method V (Fig. 2.6B). In ACSF+SB without Cch 87.3% of my recordings (117 of 134 recordings) were evaluated with method V. In the remaining 12.7% the  $AP_{\text{thresh}}$  was approximated with method VI.

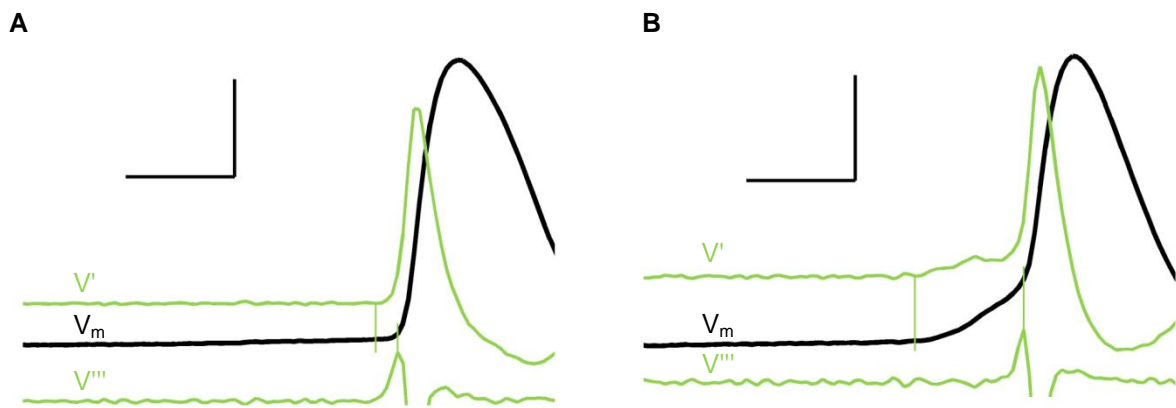


**Figure 2.6: Action potential threshold quantification.**

(A and B) The black traces show the membrane potential ( $V_m$ ) during an action potential of two distinct CA1 pyramidal neurons. The top and the bottom green traces show the first ( $V'$ ) and third ( $V'''$ ) derivative of the membrane potential, respectively. For indicating the action potential threshold of the membrane potential, the vertical green lines extend the minimum of the first derivative at the leading edge and the maximum of the third derivative.

(A) In the majority of my recordings, the maximum of the third derivative could appropriately capture the action potential threshold. In contrast, the minimum of the first derivative at the leading edge underestimated the action potential threshold. Vertical scale bar:  $V$ : 25 mV;  $V'$ : 500 mV/ms;  $V'''$ : 5295 mV/ms<sup>3</sup>. Horizontal scale bar: 1 ms. ID: 130111/R2/f25.

(B) In the presented case of an action potential with a shoulder, the maximum of the third derivative overestimated the action potential threshold. Despite a remaining slight underestimation, the maximum of the first derivative provided a more appropriate approximation of the action potential threshold under those circumstances. Vertical scale bar:  $V$ : 26 mV;  $V'$ : 417 mV/ms;  $V'''$ : 4852 mV/ms<sup>3</sup>. Horizontal scale bar: 1 ms. ID: 140825/L6/f24.

In summary, I rejected the most commonly used  $AP_{\text{thresh}}$  operationalization because of its sensitivity to the appropriateness of an *ad-hoc* determined value. In general, I rejected one of the superior methods from a study on non-cortical neurons [262] for the  $AP_{\text{thresh}}$  analysis of my recordings from *in vitro* CA1 pyramidal neurons. Instead, I mostly used the maximum of the third derivative to quantify the  $AP_{\text{thresh}}$ , which was advocated in a study of *in vivo* CA1 pyramidal neurons [264].

Regarding the implementation of an approximation to the derivative with Matlab, it is important to note that I did not use  $\text{diff}(V)/\text{diff}(t)$  but instead  $\text{gradient}(V)/\text{gradient}(t)$ . The former is a one-sided approximation method and thereby more susceptible to deviate from the genuine derivative as a result of the limited sampling frequency. Furthermore, noise accumulates with repeated derivations. Consequently, the latter central approximation method allows a considerably more reliable detection of the maximum in the third derivative.

### **Action potential amplitude**

The AP amplitude (in mV) was the difference in the  $V_m$  between the  $AP_{\text{thresh}}$  and the AP peak. I quantified the AP peak as the global maximum of  $V_m$  within 2 ms following the  $AP_{\text{thresh}}$ .

### **Action potential peak slopes**

The AP peak rising slope (in mV/ms) was the maximum in the first derivative of the  $V_m$  between the  $AP_{\text{thresh}}$  and the AP peak.

The AP peak falling slope (in mV/ms) was the minimum in the first derivative of the  $V_m$  within 3 ms following the AP peak.

### **Action potential widths**

The full width at half height of the AP was the difference between the time points at which the  $V_m$  was equal to one half of the AP amplitude during its falling and rising phase.

The full width at one third of the AP's height was the difference between the time points at which the  $V_m$  was equal to one third of the AP amplitude during its falling and rising phase.

### **Fast afterhyperpolarization**

The fast afterhyperpolarization (fAHP) was the most hyperpolarized  $V_m$  within the AP peak and the 5 ms following the AP peak. In the majority of recordings the fAHP was not followed by an apparent repolarization.



### **Firing type**

The firing type was classified in bursting and non-bursting. For the assessment, I held cells at a baseline  $V_m$  of -70 mV and exposed them to incrementing (50 pA) current square pulses of 50 to 400 pA for 1 s. For analysis, I chose the first sweep that contained at least two events. In line with other groups [265,266], I defined burst-firing as the occurrence of action potentials with an instantaneous firing frequency  $> 100$  Hz. The instantaneous firing frequency was the inverse of the inter-spike interval in seconds.

### **2.7.4 Post-burst properties**

To assess the post-burst properties, I stimulated cells at a baseline membrane potential of -60 to -65 mV with a burst of five square pulses at a frequency of 47 Hz. Each stimulus lasted 1 ms. The amplitude had to be sufficient to induce action potentials at all five stimulations (determined by increments of 100 pA). The inter-stimulus interval was 25 ms. The stimulation was repeated every ten seconds. Ten sweeps were usually sampled. The fluctuation during the baseline membrane potential was determined as the absolute difference between the maximum and minimum  $V_m$  in the interval from 500 ms before the stimulus onset until the stimulus onset. Sweeps with a fluctuation exceeding 2 mV were excluded. The five sweeps with the lowest fluctuation were averaged to one trace. This average trace was used for data analysis.

To account for the potential sampling rate errors one-point  $V_m$  measures (i.e. peak and  $\tau$ ) was the average from 1 ms before until 1 ms after the detected value.

The assessment of afterhyperpolarization (AHP) parameters was undertaken relative to the time at which the  $V_m$  crossed the baseline after the cessation of the last stimulus. The rationale behind that was to reduce the influence of fast components of the AHP. If the  $V_m$  did not cross below baseline, the cell was rated as not having an AHP in that condition. In those cases I assessed the post-burst  $V_m$  at 0.2, 0.5 and 1 s after the stimulus offset as well as the  $V_m$  at the negative peak following the stimulus offset.

### **Post-burst afterhyperpolarization**

Measures of the post-burst AHP comprised both the medium and the slow component.

The duration of the post-burst AHP was the time difference between crossing the average baseline  $V_m$  value after the stimulus offset until 95% return to the baseline from the negative peak; or at maximum 3 s.

The area of the post-burst AHP was quantified within the interval of the aforementioned AHP duration.

The AHP decay time constant was the difference between the time at the negative peak  $V_m$  and the time at which the  $V_m$  returned to 63.2% of the average baseline value and remained there (or above) for at least ten ms.

### **Medium afterhyperpolarization**

The cardinal quantification of the medium AHP (mAHP) was the negative peak of the  $V_m$  within 300 ms after the stimulus offset. To account for the potential sampling rate errors the peak membrane potential was the average from 1 ms before until 1 ms after the detected peak.

The mAHP latency was the difference between the time at which the post-stimulus  $V_m$  crossed the average baseline  $V_m$  value and the time at the negative peak  $V_m$ .

### **Slow afterhyperpolarization**

The slow AHP (sAHP) was determined at 0.2, 0.5 and 1 s after the post-stimulus  $V_m$  crossed the average baseline  $V_m$ .

## **2.7.5 Excitability**

### **Adaptation ratio**

The spike frequency accommodation (a.k.a. adaptation) was determined in regular spiking (i.e. non-bursting) neurons only. For the assessment, I held cells at a baseline  $V_m$  of -70 mV and exposed them to incrementing (50 pA) current square pulses of 50 to 400 pA for 1 s. For analysis, I chose the first sweep that contained at least eight action potentials. The adaptation ratio was the last inter-spike interval over the first inter-spike interval. Therewith, higher values indicated stronger adaptation and furthermore specified the fold increase in the inter-spike interval across time.

### Current-frequency relationship

To determine the current-frequency relationship, I held cells at a baseline  $V_m$  of -70 mV and exposed them to incrementing (50 pA) current square pulses of 50 to 400 pA for 1 s with an inter-stimulus interval of 10 or 14 s. For analysis, I determined the number of action potentials elicited by each of the current pulses and plotted them against the direct current command. In nACSF, I manually terminated the protocol in a small subset of cells ( $n = 10$ ) because five successive sweeps that contained action potentials were recorded. However, for the remaining cells all current injections up to 400 pA were applied, if feasible.

The current injection often induced persistent firing or depolarization block in the presence of carbachol. The sweep with which persistent firing was elicited was still analyzed because the number of action potentials during the stimulus was not affected by the subsequent persistent firing. However, none of the sweeps thereafter were considered for analysis because persistent firing had to be terminated with manual direct current injection. By the onset of the next sweep the persistent firing was either not yet terminated or the membrane potential was still considerably hyperpolarized. Even if the membrane potential returned back to the baseline of -70 mV, a considerably stronger current injection was needed to maintain that baseline. This indicated that the sweeps following the persistent firing were not comparable to previous sweeps. In some cases this was apparent in a reduced firing frequency at stronger current amplitudes whereas the frequency should have increased. The sweep in which depolarization block occurred for the first time was not considered for data analysis. Despite the high excitability, as evident by the depolarization block, the firing frequency was diminished because action potential generation was prohibited during the depolarization block. Therefore, the relationship between excitability and firing frequency was no longer linear. Any following sweeps were not assessed due to the same reasons as explained for the persistent firing.

Inter-stimulus intervals of up to 1 min would have been needed to allow the cell to return to its properties as before the persistent firing or depolarization block. Due to the need of conducting the other stimulation protocols such long inter-stimulus intervals were not feasible.

These aforementioned peculiarities in the presence of carbachol introduced a selection bias towards less excitable cells at stronger current injections. This is because the highly excitable cells engaged either in persistent firing or in depolarization block and had to be excluded from the analysis thereafter (or from that sweep on in case of depolarization block). Hence, the more excitable cells were, the sooner they engaged in persistent firing or

depolarization block and the sooner they dropped out of the sample that was available for the assessment of excitability according to the current-frequency relationship. Thus, particularly less excitable cells comprised the sample at higher current amplitudes.

### **Discontinuation rate and drop out reasons in the presence of Cch**

To allow an assessment of the excitability in the presence of carbachol, I adopted an analysis that took the previously described drop out (discontinuation) of highly excitable cells into consideration.

Kaplan-Meier survival analysis is commonly used in clinical studies assessing whether the time until the occurrence of a certain event differed between experimental groups (e.g. [148,267]). Here, I adopted this method to judge the excitability of CA1 pyramidal neurons because the widely used current-frequency relationship was corroborated by a selection bias for less excitable neurons at higher current (for details, see previous section). The selective drop out of highly excitable neurons could be used for assessing the excitability. The rate at which cells were discontinued from the assessment of the current-frequency relationship could be compared between groups by using the Kaplan-Meier survival analysis. Therefore, the last current amplitude with which cells could be assessed was analogue to the survival time.

To validate the Kaplan-Meier survival analysis for assessing the excitability in CA1 pyramidal neurons, I chose two populations of cells that, by definition, differed in their excitability. Namely, I compared cells that showed persistent firing against cells that showed depolarization block in response to a 2 s, 100 pA square pulse from a baseline  $V_m$  just below threshold. Persistent firing is associated with memory processes, i.e. a function within the physiological range [119]. Depolarization block is associated with seizures, i.e. a response that is related to a disease which is characterized by hyperexcitation [236].

The rate at which cells had to be omitted from the analysis of the current-frequency relationship was significantly more pronounced in cells that exhibited depolarization block compared to cells that exhibited persistent firing (Kaplan-Meier survival analysis,  $\chi_1^2 = 27.015$ ,  $p < 0.001$ , Fig. 2.7). This cross-validation may support the use of the Kaplan-Meier survival analysis for assessing the excitability of cells in the presence of carbachol.

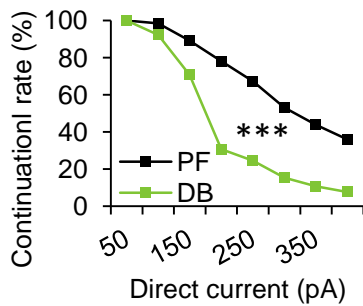


**Figure 2.7: Validation of the Kaplan-Meier survival analysis.**

The graph shows the rate at which cells were transferred to subsequent increases of the current amplitude (50 to 400 pA, 50 pA increments) of a 1s square pulse that was applied to a baseline membrane potential of -70 mV. The cumulative continuation rate was significantly different between the cells that either engaged in depolarization block (DB) or in persistent firing (PF) in response to a 2s, 100 pA square pulse at a baseline membrane potential just below firing threshold. \*\*\*  $p < 0.001$

Furthermore, the average current amplitude during the last unperturbed current injection could be compared between groups. Higher current amplitudes indicated lower excitability because cells needed stronger current injections to engage in persistent firing or depolarization block.

## 2.7.6 Persistent activity parameters

To assess persistent activity I applied a 2 s, 100 pA square pulse to cells at a baseline membrane potential just below the firing threshold.

Parameters of persistent activity refer to the cell's response within 30 s following the stimulus offset. Thirty seconds are feasible because *in vivo* electrophysiological recordings of behaving animals reported persistent activity for up to 30 s [217,213]. Thirty seconds are sufficient, because in behavioral experiments, a retention period of 30 s is repeatedly reported as the most challenging condition for both rats [217] and monkeys [213]. These data render a further prolongation futile.

### Overall response categories

#### *No PF*

Cells were categorized as showing no persistent firing when their membrane potential returned to baseline in unison with the cessation of the current injection.

#### *PF*

Cells were categorized as showing persistent firing when they continued to generate action potentials despite the cessation of the stimulus. ST PF: Cells were categorized as self-terminating persistent firing when the action potential firing ceased within 30 s after the

stimulus offset. LL PF: Cells were categorized as long-lasting persistent firing when the action potential generation lasted for at least 30 s.

### *DB*

Cells were categorized as showing depolarization block when at any point in time either during the stimulation or during the post-stimulus interval a depolarization block occurred. The depolarization block was defined as membrane potential more depolarized than the cells action potential threshold but nonetheless devoid of action potentials.

### **Post-stimulus plateau potential**

For the analysis of persistent firing, the post-stimulus plateau potential was the average membrane potential across the fixed interval of 10- 20 s following the stimulus offset and was termed  $PP_{\text{fix}}$ . Membrane potential values more positive than -30 mV were excluded to eliminate the majority of the action potentials. The rationale for choosing the interval from 10 to 20 ms following the stimulus offset was that by this time (a) persistent firing reached a stable state after a more pronounced response immediately following the stimulus offset, and (b) self-terminating persistent firing responses would most likely decline in their response intensity if they it did not yet cease firing.

For the analysis of the post-stimulus plateau potential in recordings that contained episodes of depolarization block the most depolarized 500 ms interval was evaluated and was termed  $PP_{\text{max}}$ . The most depolarized 500 ms were determined by using a sliding window analysis. In the sliding window analysis, a 500 ms interval was advanced by 100 ms steps until 30 s after the stimulus offset. The most depolarized interval was chosen for further analysis. For the comparison of recordings containing depolarization block to recordings without depolarization block,  $PP_{\text{max}}$  was quantified in both. The rationale for quantifying the plateau potential during the most depolarized 500 ms was that a fixed interval often omitted the episode of depolarization block because the depolarization block could occur at any time within the recording and could be short-lasting (Fig. 2.8). Hence, a long duration, fixed analysis window could not capture the characteristics of the depolarization block.

According to its quantification,  $PP_{\text{max}}$  represented the most intense response achieved within a recording and had a positive linear relationship with the response intensity.

### **Post-stimulus firing frequency**

For the analysis of persistent firing, the post-stimulus firing frequency was the average action potential firing rate across the fixed interval of 10-20 s following the stimulus offset, and was termed  $FF_{\text{fix}}$ .

In recordings that contained episodes of depolarization block or that were compared to such, the post-stimulus firing frequency was the average of action potential firing across the 500 ms interval of most depolarized membrane potential and was termed  $FF_{\max}$ . The interval of most depolarized membrane potential was determined as described for  $PP_{\max}$ . During the transition from action potential firing to depolarization block (or vice versa), only the membrane potential "fluctuations" that clearly overshoot zero mV were classified as action potentials. Notably,  $FF_{\max}$  followed an inverse U-shape relationship with the response intensity, i.e. in the case of absent/faint persistent activity  $FF_{\max}$  is zero/low; in the case of

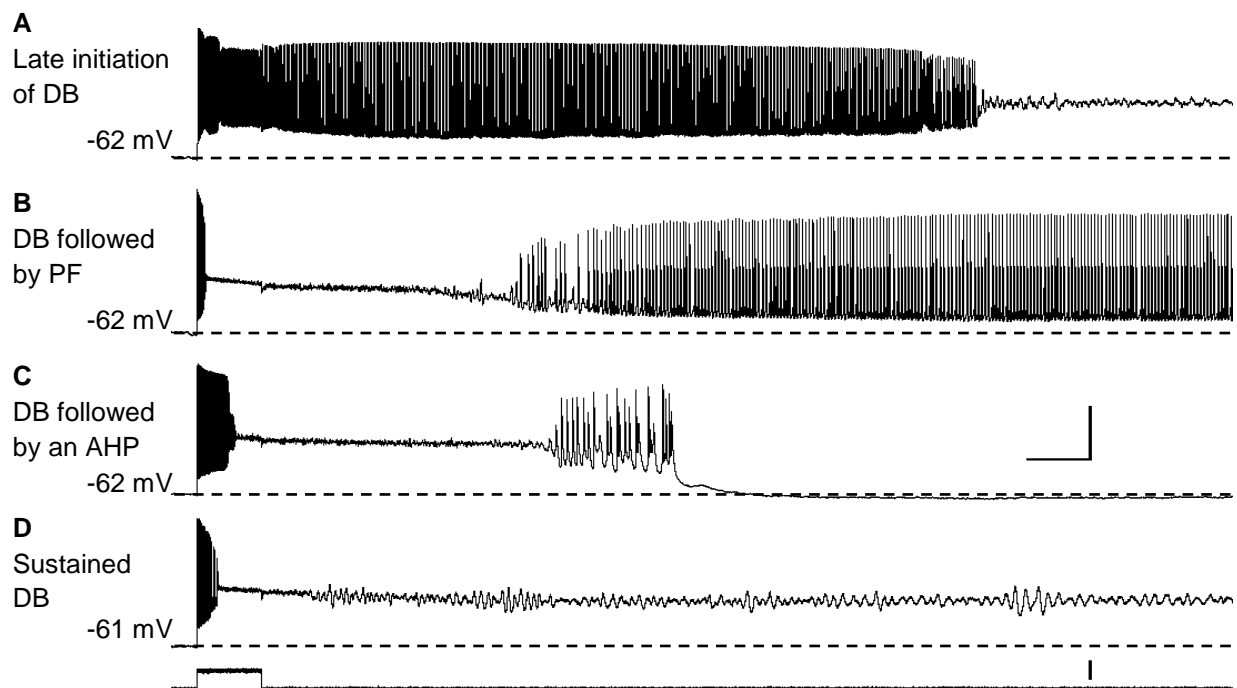


**Figure 2.8: Depolarization block occurred at highly variable time points.**

(A-D) The graphs depict the membrane potential of different cells in response to a 2 s, 100 pA square pulse (bottom of D). Dotted lines represent the baseline membrane potential which is indicated before the stimulus onset. Horizontal scale bar: 2 s. Vertical voltage scale bar: 40 mV. Vertical current scale bar: 100 pA.

(A) Depolarization block (DB) could occur within 30 s after the stimulus offset following an extended period of persistent firing. ID: 1410/24/R6/f39. ACSF+SB +20  $\mu$ M carbachol (Cch).

(B) After an initial depolarization block, the membrane potential could transition to persistent firing (PF). ID: 141017/L6/f33. ACSF+SB +20  $\mu$ M Cch.

(C) Depolarization block could be followed by a hyperpolarization (AHP) that circumvented further action potential generation. ID: 130602/R2/f101. ACSF+SB +10  $\mu$ M Cch.

(D) Depolarization block could be sustained throughout 30 s following the stimulus offset. ID: 130722/R8/f59. ACSF+SB +5  $\mu$ M Cch.

substantial persistent activity  $FF_{\max}$  is high; and in the case of depolarization block  $FF_{\max}$  is zero or low. This inverted U-shape relationship is noteworthy because it affects the interpretation of  $FF_{\max}$ .

### Duration of depolarization block

Depolarization block was defined at a membrane potential more depolarized than -40 mV and with an amplitude of membrane fluctuation below 40 mV. The duration of depolarization block was the summation of time that neurons spent in that state during the 30 s interval after the stimulus offset.

## 2.8 Statistical comparison of group data

I expressed group data as average and standard deviation (SD), when I illustrated the variability within my sample (e.g. age of the experimental animals, superfusion times, etc.), without implying an extrapolation to a population level. In contrast, I express group data as mean  $\pm$  standard error of the mean ( $M \pm SEM$ ) when I illustrated the extent of the error made while estimating a population level with the mean of the investigated sample. Numbers in bars graphs represent the sample size.

All statistical comparisons were conducted as two-tailed tests with a significance level of  $\alpha = 0.050$  and a threshold for trends at  $\alpha = 0.100$ . P values were reported according to the common nomenclature: n.s.  $p \geq 0.1$  (not significant), †  $p < 0.1$  (trend), \*  $p < 0.05$ , \*\*  $p < 0.01$ , and \*\*\*  $p < 0.001$ .

For assessing the excitability of cells via the current-frequency relationship  $T$ -test were conducted for each current amplitude. Hence, eight individual comparisons were undertaken. A repeated measures ANOVA was not feasible due to the change in sample size as the current amplitude increased. A selection of only cells that were transferred to the highest current amplitude would have introduced a bias towards less excitable cells (for details see 2.7.5 Excitability), even at low current amplitudes. The consequential  $\alpha$ -error accumulation due to multiple comparisons was corrected by adjusting the significance threshold. The adjustment of the significance threshold was conducted by using bonferroni's method. According to the eight comparisons, the adjusted  $p$  values were the following: n.s.  $p \geq 0.0125$  (not significant), §  $p < 0.0125$  (trend), #  $p < 0.00625$ , ##  $p < 0.00125$ , and ###  $p < 0.000125$ .

Paired and two-sample  $T$ -tests, as well as one-way analysis of variance (ANOVA) and linear regressions were conducted with Matlab R2009b (Math Works). If the assumption of



variance homogeneity for the two sample  $T$ -test was violated (as assessed with Levene's test) I used the unequal variance  $T$ -test to assess statistical significance [268] and indicated this by reporting the corrected degrees of freedom including three decimal places (even if they were zero). Normality of the data was inspected with Lillifors test. In case of non-normality, the alternative non-parameteric tests were assessed. However, due to the robustness of the  $T$ -test against violations of the normality assumption in general [269] and little to no effect on the outcome of my comparisons in particular, I consistently reported parametric test statistics, as long as permitted by the levels of measurement.

One-way and two-way repeated measures ANOVA, binomial logistic regressions and Kaplan-Meier survival analysis (log rank test) were conducted with SPSS22 (IBM). Therefore, I extracted the sample's raw data with Matlab. For the repeated measures ANOVA, I assess the assumption of Sphericity with Mauchly's test and, if violated, I used the Greenhouse-Geisser correction. *Post-hoc* tests were Bonferroni corrected.

If the sample size for any group in the aforementioned comparisons fell below five ( $T$ -test, ANOVA) or 20 (regression), I did not consider the results conclusive and only reported descriptive statistics.

## 2.8.1 Comparison with previously reported data

To compare my data against the data obtained by Fraser and MacVicar (1996) [236], I generated a normally distributed random sample of the reported size ( $n = 50$ ), mean (9.9 s) and standard deviation (SD: 4.2; according to the reported standard error of the mean (0.6) divided by the square root of  $n-1$ ). To assess the goodness of fit between this target distribution ( $t$ ) and the randomly generated distribution ( $r$ ), I calculated the absolute difference between these two distributions for the mean ( $|M_t - M_r|$ ) and the standard deviation ( $|SD_t - SD_r|$ ). A sample size of 50 is rather limited for a random process. Consequentially, the difference between the target distribution and the randomly generated distribution could be substantial. Therefore, I repeated the procedure 100 times. Thereafter, I chose the iteration for which the product of the difference of the mean and the difference of the standard deviation ( $|M_t - M_r| * |SD_t - SD_r|$ ) was minimal. The randomly generated data set captured the average and variance of the data set reported by Fraser and MacVicar (1996) [236]. It was then used for a comparison with my experimentally obtained data set via a two-sample  $T$ -test as mentioned before.

## 2.8.2 Comparison of categorical data

The significance of unpaired categorical parameters (e.g. the presence or absence of a silent RMP) was determined according to the 2x2 contingency table specified in Table 2.1. Via custom-designed Matlab scripts, I determined Chi square values ( $\chi^2$ ) according to Formula 3. The degrees of freedom (df) were the number of groups - 1 multiplied with the number of outcomes - 1. The  $p$  value was determined by subtracting the probability of the cumulative chi square distribution (built in Matlab) for the aforementioned  $\chi^2$  and df from one.

**Table 2.1: 2x2 contingency table for chi square.**

	outcome 1	outcome 2	
group 1	a	b	Sum group 1: SG1 = (a+b)
group 2	c	d	Sum group 2: SG2 = (c+d)
	Sum outcome 1	Sum outcome 2	Grand sum:
	SO1 = (a+c)	SO2 = (b+d)	GS = (a+b+c+d)

$$\frac{(ad-bc)^2 * GS}{SG1 * SG2 * SO2 * SO1} = \chi^2$$

**Formula 3**

Due to its robustness to small ( $n < 5$ ) samples in individual cells as long as a sufficient ( $n \geq 50$ ) overall sample size was provided [270]  $\chi^2$  was also applied if these requirements were fulfilled. However, if the grand sum was  $\geq 50$  but one of the contingency table's cells contained no observation, I computed the  $p$  value according to Fisher-Yates-test with the equation specified in Formula 4 [271]. If the grand sum was  $< 50$  and one of the contingency table's cells contained  $< 5$  observation, I refrained from a statistical assessment [270].

$$\frac{SG1! * SG2! * SO1! * SO2!}{GS! * a! * b! * c! * d!} = p$$

**Formula 4**

The significance of paired categorical parameters was assessed by determining  $\chi^2$  with a custom-written Matlab script that implemented the McNemar-test [271,270] as specified in Table 2.2 and Formula 5. The  $p$  value was then determined as previously described for  $\chi^2$ .

**Table 2.2: McNemar-test assessing paired categorical parameters.**

		Second superfusate	
		+	-
first superfusate	+	a	b
	-	c	d

$$\frac{(b-c)^2}{b+c} = \chi^2$$

**Formula 5**

# 3 Results

3.1 The effect of carbachol on intrinsic electrophysiological properties and its modulation by intercellular variability

3.1.1 The effect of carbachol on intrinsic electrophysiological properties

3.1.2 Modulation of intrinsic properties by intercellular variability

3.1.3 Summary of the cholinergic effects on CA1 pyramidal neurons

3.2 Persistent firing

3.2.1 *In vitro* CA1 pyramidal neurons engaged in persistent firing

3.2.2 Persistent firing was intrinsic to individual neurons

3.2.3 Intrinsic persistent firing may be a physiologically plausible phenomenon

3.2.4 Mechanism underlying intrinsic persistent firing in CA1 pyramidal neurons

3.2.5 Sensitivity of persistent firing to the carbachol concentration

3.2.6 Sensitivity of persistent firing to inter-cellular variability within CA1

3.2.7 Summary of persistent firing in CA1 pyramidal neurons

3.3 Depolarization block

3.3.1 The mechanism underlying the switch between persistent firing and depolarization block

3.3.2 Sensitivity of depolarization block to inter-cellular variability

3.3.3 Aspects of inter-cellular variability modulating the occurrence of persistent firing and depolarization block

3.3.4 Summary of the interrelation between persistent firing and depolarization block

Firstly, I will characterize the electrophysiological properties of CA1 pyramidal neurons and the effect of cholinergic activation thereon. Subsequently, I will focus on cholinergic-mediated intrinsic persistent firing which may potentially have a role in short-term retention of information. Finally, I will elucidate the interrelation between persistent firing and the seizure-related depolarization block.

## **3.1 The effect of carbachol on intrinsic electrophysiological properties and its modulation by intercellular variability**

The majority of neurons in my sample were obtained from trans-cardially perfused animals at P14-24 whose hippocampal slices were superfused with artificial cerebrospinal fluid (ACSF) in the presence of agents that blocked fast ionotropic synaptic transmission (ACSF+SB, 2 mM kynurenic acid and 0.1 mM picrotoxin). Due to the large sample size ( $n = 69$ ), I used this group to characterize the effect of 10  $\mu$ M carbachol (Cch) on intrinsic electrophysiological properties and its modulation by intercellular variability of CA1 pyramidal neurons.

The sample size varied between parameters because not all protocols were executed in all cells and because individual protocols had to fulfill inclusion criteria (see methods section 2.5) which may allowed the analysis of one but not another property from one and the same neuron.

For readability and comprehensibility, the results will be reported in an aggregated format. For details on the test statistics the interested reader is referred to the supplementary material.

### **3.1.1 The effect of carbachol on intrinsic electrophysiological properties**

As outlined in the introduction (chapter 3), the effects of cholinergic stimulation on CA1 pyramidal neurons have been profoundly investigated. In the following, I briefly assess the effect of Cch on intrinsic electrophysiological properties on my sample of CA1 pyramidal neurons (supplementary table 6.1.1). Therefore, I compared cells that were first superfused

with ACSF+SB and subsequently exposed 10  $\mu\text{M}$  bath applied Cch. Unless otherwise stated, I will report paired *T*-test results throughout this section because the independent variable (ACSF+SB vs. ACSF+SB+10  $\mu\text{M}$  Cch) consisted of two groups which were successively established within the same cell and because the dependent variables had a metric scale of measurement (e.g. membrane potential or duration). In the case of dependent variables that accommodated a non-metric scale of measurement (e.g. dichotomous response types like silent vs. non-silent RMP) I assessed significance with an appropriate test out of the Chi-square test family (for details see section 2.8.2). In the case of having tested the difference between ACSF+SB and ACSF+SB+10  $\mu\text{M}$  Cch at different states of the same cell (i.e. different holding potential during  $R_{\text{in}}$  measurement or different induction amplitudes for  $I_{\text{h}}$ ), I used a two-way repeated measures ANOVA and subsequent Bonferroni-corrected *post-hoc* tests to account for the increased complexity of the acquired data and to avoid  $\alpha$ -error accumulation. I will explicitly indicate these deviations from the otherwise consistently used paired *T*-test statistics in the following section.

In line with previous reports [272], the bath application of Cch induced a depolarization which resulted in a significant shift from a silent resting membrane potential (RMP) in ACSF+SB to a non-silent RMP in the presence of 10  $\mu\text{M}$  Cch (McNemar-test,  $p < 0.001$ , Fig. 3.1.1A). Even the 26 out of 69 neurons which still displayed a silent RMP in the presence of 10  $\mu\text{M}$  Cch had a significantly more depolarized RMP than the same cells previously recorded in ACSF+SB only ( $p = 0.022$ , Fig. 3.1.1B).

To assess the effect of Cch on  $R_{\text{in}}$ , I analyzed 33 cells from which  $R_{\text{in}}$  measures were obtained at the three holding potentials -70, -65, and -60 mV and both in the absence and presence of 10  $\mu\text{M}$  Cch (Fig. 3.1.1C). To remain within the scope of this dissertation, I briefly summarize the rather complex effects of Cch on  $R_{\text{in}}$  (Tab. 6.1.1). In ACSF+SB,  $R_{\text{in}}$  was significantly voltage-dependent as it was elevated at more depolarized membrane potential (3x2 two-way repeated measures ANOVA, independent variables: three holding potentials (-70, -65, and -60 mV) two conditions (ACSF+SB only vs. ACSF+SB+10  $\mu\text{M}$  Cch), dependent variable:  $R_{\text{in}}$ ,  $p < 0.001$ ). During the bath application of Cch, this voltage dependence of  $R_{\text{in}}$  appeared to be blocked at hyperpolarized membrane potentials (-70 to -65 mV) but unaffected at more depolarized membrane potentials (-65 to -60 mV). This interpretation followed reports about the voltage dependence of  $R_{\text{in}}$  in CA1 pyramidal neurons [273]. These results indicated that  $I_{\text{h}}$  was blocked by the superfusion of Cch. Besides blocking the voltage dependence of  $R_{\text{in}}$ , the superfusion of Cch may have left  $R_{\text{in}}$  unaffected because

the significant difference at -60 mV (Bonferroni-corrected *post-hoc* test,  $p < 0.01$ ) may have been a residue of the voltage-dependent blockade at lower membrane potentials. Hence, the Cch-induced blockade and facilitation of other currents (e.g.  $I_M$  and  $I_{CAN}$ , respectively) may have balanced out such that no apparent net change in  $R_{in}$  was detected. If anything,  $R_{in}$  may have been reduced at more depolarized membrane potentials during the superfusion of Cch (Fig. 3.1.1C), suggesting the relative dominance of a newly introduced or facilitated current at more depolarized membrane potentials in my sample.

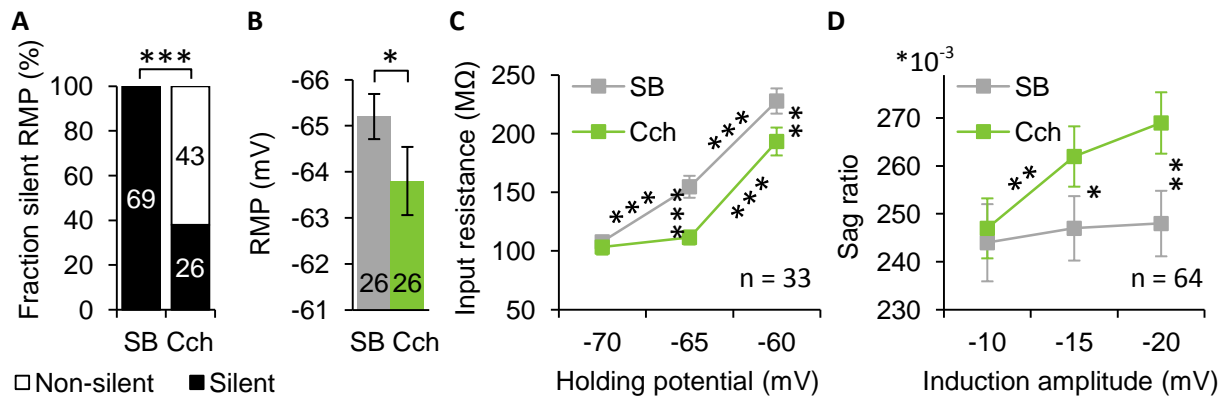


**Figure 3.1.1: The effect of 10  $\mu$ M Cch on passive electrophysiological properties and  $I_h$ .**

(A) The fraction of cells exhibiting a silent resting membrane potential (RMP) in ACSF+SB (SB) significantly decreased upon the bath application of 10  $\mu$ M carbachol (Cch).

(B) Even in the neurons which still exhibited a silent RMP in the presence of Cch, the RMP was significantly more depolarized than in the same cells before the application of Cch (SB).

(C&D) Significant differences within one solution are indicated by diagonal stars on top or below the lines connecting the compared groups. Significant differences between solutions are indicated by vertical stars right next to the compared groups.

(C) The input resistance of cells bathed in SB exhibited a significant voltage dependence. During the superfusion with 10  $\mu$ M Cch, the voltage dependence of  $R_{in}$  was blocked at hyperpolarized membrane potentials, but unaffected at depolarized membrane potentials. The blockade of the voltage dependence of  $R_{in}$  at hyperpolarized membrane potentials may have resulted in a significantly lower  $R_{in}$  at -65 mV and at -60 mV in Cch compared to the same cells in SB. However, an additional introduction or facilitation of a current resulting in a  $R_{in}$  reduction cannot be excluded. Stars represent the results of Bonferroni corrected *post-hoc* tests.

(D) The sag ratio was significantly more pronounced during the bath application of Cch compared to the same cells superfused with SB when  $I_h$  was induced with a -15 or -20 mV but not a -10 mV membrane potential deflection. Stars represent the results of Bonferroni corrected *post-hoc* tests.

\*  $p < 0.05$ . \*\*  $p < 0.01$ . \*\*\*  $p < 0.001$ .

The aforementioned results from the RMP (Fig. 3.1.1A&B; suggesting an  $I_h$  enhancement, [272]) and  $R_{in}$  (Fig. 3.1.1C; suggesting an  $I_h$  blockade, [258]) implied contradictory predictions regarding the effect of Cch on  $I_h$ . This heterogeneity may reflect the controversy about the effect of muscarinic stimulation on  $I_h$  [274,209]. To obtain conclusive information about the effect of Cch on  $I_h$  in my sample, I quantified the sag ratio which represents  $I_h$  [255]. The results (Fig. 3.1.1D) indicated that  $I_h$  was significantly enhanced by the superfusion of 10  $\mu$ M Cch (3x2 two-way repeated measures ANOVA, independent variables: three  $I_h$  induction amplitudes (-10, -15, and -20 mV) two conditions (ACSF+SB only vs. ACSF+SB+10  $\mu$ M Cch), dependent variable: sag ratio,  $p < 0.001$ ), particularly when induced by a 20 ( $p < 0.01$ ) and 15 ( $p < 0.05$ ) but not by a 10 mV ( $p > 0.1$ ) hyperpolarizing voltage deflection (Bonferroni-corrected *post-hoc* tests). The facilitation of  $I_h$  by Cch was in line with the depolarization of the RMP in my sample [272].

Regarding individual action potentials (Fig. 3.1.2A), I observed a significantly more depolarized action potential (AP) threshold ( $p = 0.013$ ), a significant reduction in the AP amplitude ( $p = 0.014$ ) and a significant shortening of the action potential width at one half ( $p = 0.002$ ) and one third ( $p = 0.005$ ) of its amplitude. The latter results were in contrast to a report of a cholinergic-mediated augmentation of the action potential width at one third of its height [162].

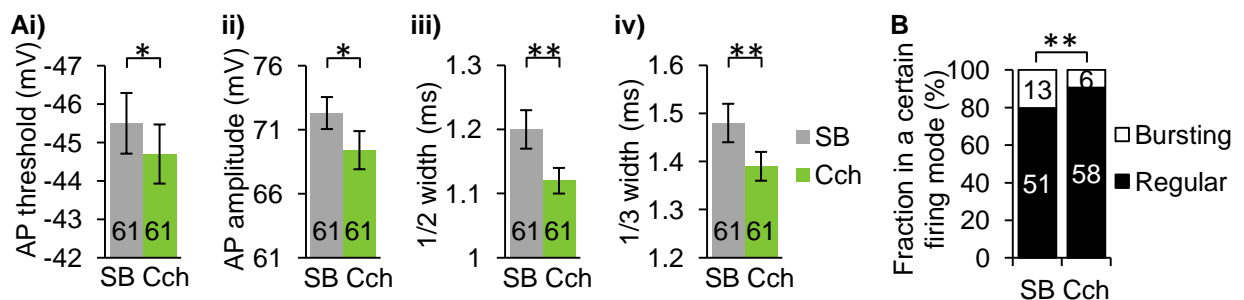


**Figure 3.1.2: Properties of individual action potentials were altered by carbachol.**

(A) The (i) action potential (AP) threshold was significantly depolarized upon the bath application of Cch. The (ii) AP amplitude, and full width at (iii) one half and (iv) one third of its amplitude were significantly reduced upon the switch from ACSF+SB (SB) to 10  $\mu$ M carbachol (Cch).

(B) The burst firing mode was significantly suppressed during the bath-application of 10  $\mu$ M carbachol.

\*  $p < 0.05$ . \*\*  $p < 0.01$ .



The propensity of CA1 pyramidal neurons to generate not only individual spikes but also bursts of action potentials was shown to be modulated by  $I_M$  [266,175]. In line with these and other [161,266,275] reports, the superfusion of Cch induced a significant (McNemar-test,  $p = 0.020$ ) reduction of the cell's likelihood to engage in burst firing (Fig. 3.1.2.B). These results indicated a blockade of  $I_M$  induced by the superfusion of Cch.

Cholinergic stimulation is well acknowledged for blocking potassium channels and attenuating post-burst AHP currents [155,175,195]. In line with these reports, I observed a significant (McNemar-test,  $p = 0.002$ ) shift from cells displaying a post-burst afterhyperpolarization (AHP) in ACSF+SB (100% AHP,  $n = 13$ ) to cells engaging in an afterdepolarization (ADP) during the bath-application of 10  $\mu\text{M}$  Cch (23% AHP, 3/13 cells). This categorical change (Fig. 3.1.3A) was also reflected in a significantly more depolarized membrane potential at the peak and at 0.2, 0.5 and 1 s after the stimulus offset (all  $p < 0.001$ , Fig. 3.1.3B). These results may indicate the suppression of hyperpolarizing outward potassium currents and/or a facilitation of a depolarizing inward current. In light of the

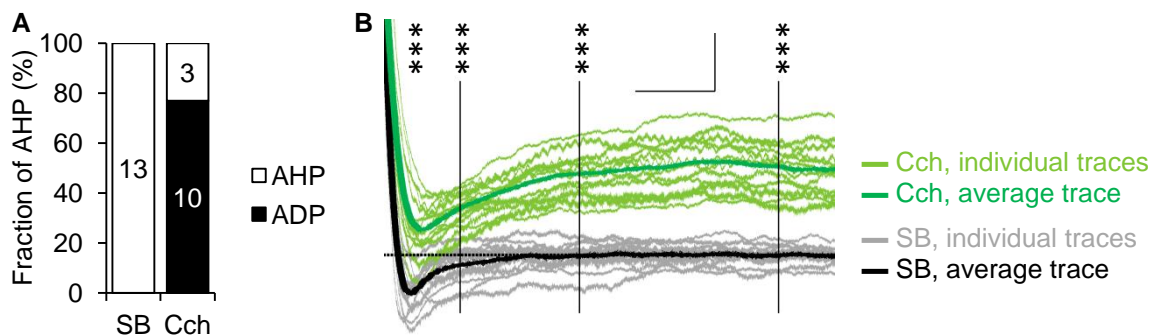


**Figure 3.1.3: The afterhyperpolarization was mostly abolished in carbachol.**

(A) While superfused with ACSF+SB (SB) all thirteen cells responded with an afterhyperpolarizing potential (AHP) to a burst of five action potentials. In contrast, during the subsequent superfusion of 10  $\mu\text{M}$  Cch (Cch) the same cells mostly responded to the same stimulation with an afterdepolarizing potential (ADP).

(B) The membrane potential after a burst of five action potentials was significantly more depolarized in the presence of Cch (green) compared to the absence of Cch (grey/black). The grey and light green traces depict the responses of all thirteen cells to a burst of five action potentials while superfused with SB and subsequently with Cch, respectively. The black and dark green trace show the averaged membrane potential across the cells in SB and Cch, respectively. The stars indicate the significant differences between the responses in SB and Cch at the peak and at 200, 500, and 1000 ms after the stimulus offset. The vertical lines specify the time points 200, 500 and 1000 ms after the stimulus offset. The horizontal dotted line indicates the baseline holding potential prior to the induction of five action potentials. Horizontal scale bar: 200 ms. Vertical scale bar: 2 mV.

\*\*\*  $p < 0.001$ .

cholinergic effect on  $R_{in}$ , (Fig. 3.1.1.C, supplementary material: Tab. 6.1.1), a depolarizing inward current which is preferentially active at more depolarized membrane potentials may be dominant in my sample. Irrespective of the underlying mechanism, the findings suggest that Cch increased the excitability of CA1 pyramidal neurons.

By modulating potassium currents, cholinergic stimulation also affects spike frequency accommodation [180,276,277]. Spike frequency accommodation is also known as adaptation and is marked by the progressive increase of the inter-spike interval during constant current injections. In ACSF+SB, cells displayed significant (2-sample  $T$ -test against one because a spike frequency accommodation equal to one corresponds to the null-hypothesis of no change throughout the stimulus interval,  $T_{47} = 4.846$ ,  $p < 0.001$ ) spike frequency accommodation ( $2.44 \pm 0.3$ ). The spike frequency accommodation was significantly reduced upon the bath application of  $10 \mu\text{M}$  Cch ( $p < 0.001$ , Fig. 3.1.4). Notably, the firing pattern in  $10 \mu\text{M}$  Cch did not display run-away excitation because the spike frequency accommodation ( $0.92 \pm 0.2$ ) was not significantly different from one (2-sample  $T$ -test,  $T_{47} = -0.351$ ,

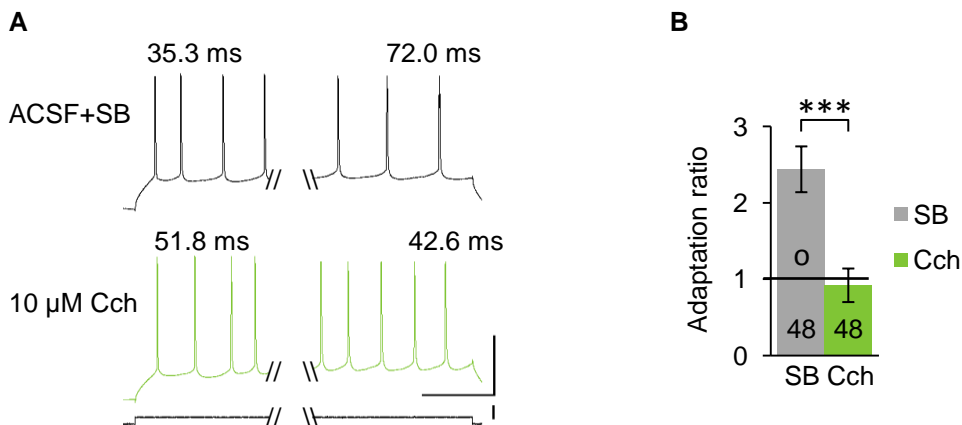


**Figure 3.1.4: Spike frequency accommodation was reduced by carbachol.**

(A) Representative traces depicting the first and last action potentials generated in response to a 100 pA current injection (bottom black trace). The duration of the first and last inter-spike interval are presented by the numbers heading the respective trace. The top black trace shows a cell superfused with ACSF+SB that exhibited an adaptation ratio of 2.04. The same cell, subsequently in the presence of  $10 \mu\text{M}$  Cch, exhibited an adaptation ratio of 0.82 and is shown by the green trace. Horizontal scale bar: 100 ms. Vertical voltage scale bar: 40 mV. Vertical current scale bar: 200 pA. ID: 140629/L3/f173 and f191.

(B) During the superfusion with ACSF+SB (SB), cells showed significant spike frequency accommodation as indicated by the adaptation ratio being significantly higher than one. However, during the presence of  $10 \mu\text{M}$  Cch (Cch), the spike frequency accommodation was significantly reduced and the adaptation ratio was no longer significantly different from one, indicating that neither a accommodation nor a ramping up was observed.

\*\*\*  $p < 0.001$ . o significantly different from one.

$p = 0.719$ ). The aforementioned Cch-induced blockade of the post-burst AHP (Fig. 3.1.3) may underlie the observed reduction in spike frequency adaptation upon the bath application of Cch. However, the significant Cch-dependent increase in  $I_h$  (Fig. 3.1.1.D), contrasted the reduction in spike frequency adaptation when assuming an involvement of  $I_h$  therein [189,277]. In summary, these results indicate that the exposure to Cch increased the excitability of CA1 pyramidal neurons.

Another common measure of cellular excitability, is the current-frequency relationship. The action potential frequency was significantly higher at current amplitudes of 100, 150 and 200 pA during the bath-application of Cch compared to the same cells afore superfused with ACSF+SB (Fig. 3.1.5A, Tab. 6.1.1). However, the current-frequency

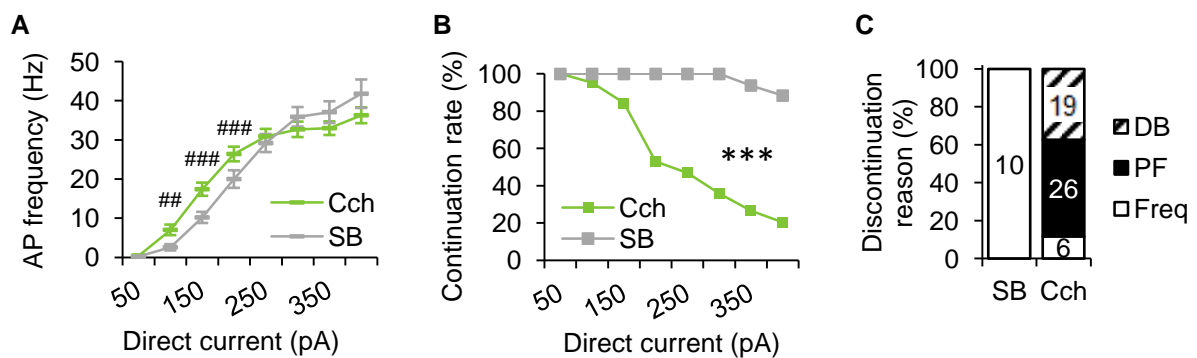


**Figure 3.1.5: Cells were more excitable in the presence of carbachol.**

(A) The graph displays the current-frequency relationship in a paired set of cells that were first superfused with ACSF+SB (SB) and subsequently with 10  $\mu$ M Cch (Cch). At lower stimulus intensities ( $\leq 200$  pA), cells generated more action potentials in the presence of Cch than they previously did in its absence. At higher stimulus intensities (300 - 400 pA) the residual paired sample generated fewer action potentials in the presence of Cch than previously in SB only. The sample size of paired recordings was 64, 61, 54, 34, 30, 24, 18, and 13 at stimulus amplitudes of 50, 100, 150, 200, 250, 300, 350, and 400 pA, respectively.

(B) The graph depicts the continuation rate of neurons during the assessment of excitability. With ascending current amplitude, a decreasing fraction of cells was examined for excitability, particularly in the presence of Cch.

(C) While superfusing SB, all ten neurons that were not transferred to a current amplitude of 400 pA were discontinued because of a high action potential firing frequency during the stimulation (Freq). During the subsequent superfusion with Cch, out of the 51 neurons that were not transferred to 400 pA again a low number of cells ( $n = 6$ ) was discontinued due to a high frequency during the stimulation. However, a high number of additional cells could not be transferred because persistent firing (PF) or depolarization block (DB) were initiated which was never observed in the absence of Cch.

##  $p < 0.00125$  (bonferroni corrected; equal to  $p < 0.01$ ). ###  $p < 0.000125$  (bonferroni corrected; equal to  $p < 0.001$ ). \*\*\*  $p < 0.001$ .

relationship of cells in ACSF+SB and Cch merged at higher stimulus intensities. This effect may be explained by a selection bias towards less excitable cells as the current amplitude increased (for details see method section 2.7.5, Fig. 2.8). This bias selectively affected neurons in Cch as evident by a significantly more pronounced drop-out rate (Kaplan-Meier survival analysis,  $\chi^2 = 66.823$ ,  $p < 0.001$ ) compared to the same cells in the absence of Cch (Fig. 3.1.5B). The reasons for discontinuation (Fig. 3.1.5C) were a high frequency during the stimulus duration in a comparably minor fraction of cells both in ACSF+SB ( $n = 10$ ) and in Cch ( $n = 6$ ). In sharp contrast, only during the presence of Cch an additional 45 out of the 64 cells (70.3%) had to be discontinued because persistent firing or depolarization block was induced. Hence, cells that were strongly affected by Cch were excluded from the paired comparison of the current frequency relationship which may explain the results obtained with high amplitude ( $\geq 250$  pA) current stimulations. These results indicate that Cch considerably enhanced the excitability of CA1 pyramidal neurons which could not be adequately captured with the current-frequency relationship. The Cch-induced reduction of the post-burst afterhyperpolarization (Fig. 3.1.3) and/or the reduction in the spike frequency adaptation (Fig. 3.1.4) may underlie this observation.

Besides expressing regular action potentials, CA1 pyramidal neurons were also reported to engage in depolarization block in the presence [236] and absence [278] of Cch. Before turning back to the paired comparisons within cells initially exposed to ACSF+SB and subsequently bathed in Cch, I first highlight descriptive statistics on all, oftentimes unpaired, recordings.

In line with previous reports [236,278], I never ( $n = 132$ ) observed depolarization block during the stimulation with a relatively weak 1 s, square pulse ranging from 50 to 400 pA (50 pA increments). In contrast, while 10  $\mu$ M Cch was superfused and the same current stimulation (max. 400 pA) was applied, 26.6% (17/64) of the cells initiated a depolarization block during the stimulation (Fig. 3.1.6B). The applied current while inducing depolarization block was  $221 \pm 20$  pA and the depolarization block lasted for  $306 \pm 47$  ms. Furthermore, 52% of these cells (9/17) maintained the depolarization block during the 100 ms following the stimulus offset (Fig. 3.1.6C). To assess whether my sample of CA1 pyramidal neurons was capable of depolarization block in the absence of Cch, 49 neurons were exposed to ascending current injections (50 pA increments) until cells showed depolarization block or up to a maximum of 1.4 nA. Therewith, depolarization block could be induced in 87.8% (43/49) of the cells in ACSF+SB (Fig. 3.1.6A). In line with a recent report [278], the current

applied during the achievement of depolarization block was  $1.037 \pm 0.03$  nA and the depolarization block lasted for  $205 \pm 21.5$  ms. However, in sharp contrast to the presence of Cch (52% stimulus-outlasting), none of the 43 cells remained in depolarization block upon the cessation of the stimulus (Fig. 3.1.6C).

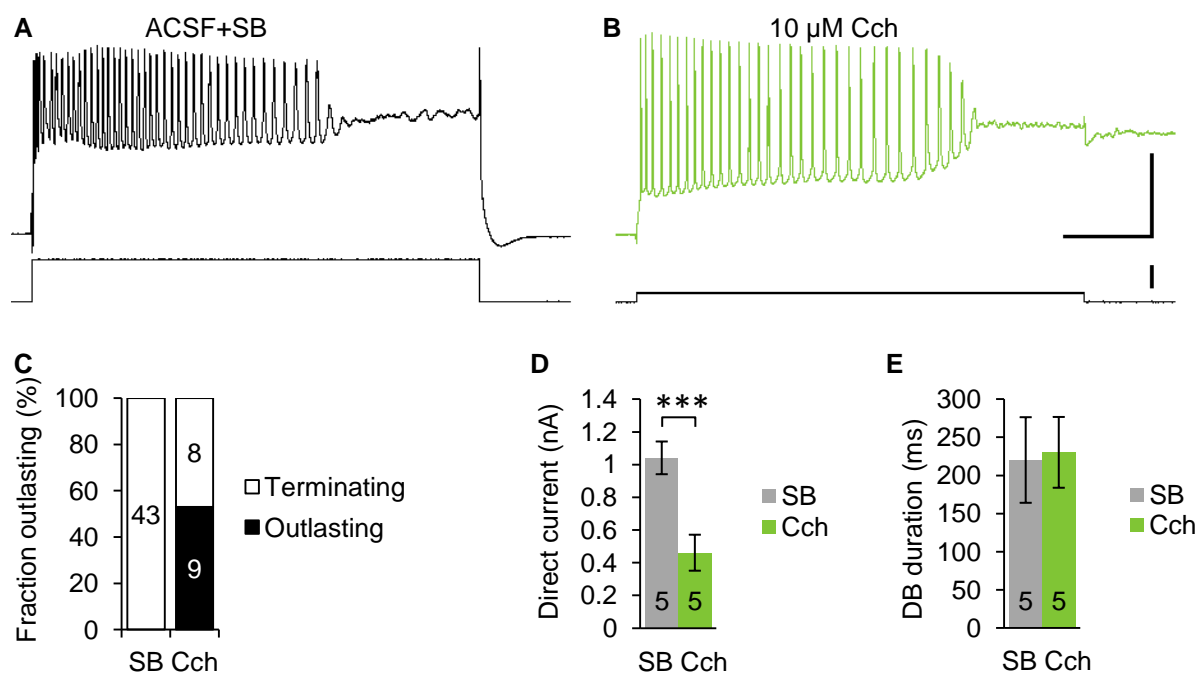


**Figure 3.1.6: Considerably lower current injections were sufficient to induce depolarization block in the presence of Cch.**

(A) The trace shows a cell during the superfusion of ACSF+SB. A 350 ms lasting depolarization block could be induced with a current injection of 950 pA. The depolarization block terminated upon the cessation of the stimulus and the cell returned back to the holding potential of -70 mV. ID: 140501/L2/f58

(B) The trace shows a different cell than in (A). During the presence of 10 μM Cch, a 150 ms lasting depolarization block could be induced with a current injection of 200 pA. In contrast to (A), the depolarization block outlasted the stimulus offset. ID: 140629/L3f191. Horizontal scale bar: 200 ms. Vertical voltage scale bar: 40 mV. Vertical current scale bar: 50 pA.

(C) The graph depicts different samples of cells in ACSF+SB (SB) and in the presence of 10 μM carbachol (Cch). The depolarization block never outlasted the stimulus duration in the absence of Cch. In contrast, in the presence of 10 μM Cch 52% of the cells remained in depolarization block despite the cessation of the stimulus.

(D) In the presence of 10 μM carbachol (Cch), a significantly lower current amplitude was sufficient to induce depolarization block, compared to the same cells before the bath application of Cch (SB).

(E) In the same cells as reported in (D), the duration of the depolarization block was indifferent between the absence (SB) and presence of 10 μM carbachol (Cch).

\*\*\*  $p < 0.001$ .

Five of these aforementioned cells were exposed to ACSF+SB and subsequently to ACSF+SB containing 10  $\mu\text{M}$  Cch which allowed for a pairwise comparison within cells (Fig. 3.1.6D&E). The results confirm that a significantly ( $p < 0.001$ ) higher current amplitude was needed to induce depolarization block in the absence of Cch compared to the presence of 10  $\mu\text{M}$  Cch (Fig. 3.1.6D). However, once the depolarization block was elicited, the duration was indistinguishable ( $p = 0.924$ ) between the absence and presence of Cch (Fig 3.1.6E).

In summary, the observation of depolarization block in the absence of Cch provided momentous replication of the findings from Bianchi et al. (2012) [278]. Furthermore, they suggest that the depolarization block is an all-or-nothing phenomenon whose induction threshold is lowered by the application of Cch. Additionally, Cch appeared to transmit the ability for stimulus-outlasting activity.

Recapitulating the aforementioned findings, Cch modulated a variety of intracellular properties in my sample of CA1 pyramidal neurons. Apart from a reduction in input resistance (Fig. 3.1.1.C, in contrast to [23]) and a narrowing of action potentials (Fig. 3.1.2A; in contrast to [162]) I replicated a multitude of previous reports [141,154,155,161] [155,154,141,161], which indicated an increase in cellular excitability induced by the stimulation with Cch.

In the previous paragraphs I highlighted the effect of Cch in contrast to its absence. To prepare the grounds for results presented in the subsequent chapters, I now very briefly summarize the differential effect of various Cch concentrations on CA1 pyramidal neurons.

Besides the aforementioned application of Cch at 10  $\mu\text{M}$  ( $n = 69$ ), I also exposed independent subsets of cells to 5 ( $n = 25$ ) and 20  $\mu\text{M}$  ( $n = 41$ ) Cch. Even though the applied Cch concentration was split into discrete groups an ANOVA could not detect subtle but gradual dose-dependent changes. On the other hand, a linear regression would be corroborated by using the technically continuous variable 'concentration' in discrete steps (5, 10 and 20  $\mu\text{M}$ ). Nevertheless, to assess whether intrinsic electrophysiological properties linearly changed with the Cch concentration I employed a linear regression (analogue analysis in Axmacher et al. (2010) [279]) and reported the averages ( $\pm$  SEM) within each group of Cch concentration. As before, results will be highlighted very briefly. The following statistical comparisons were derived from a linear regression, unless otherwise stated. The interested reader is referred to the supplementary material (Tab. 6.1.2) for details on additional dose-dependent but insignificantly subtle effects.

Increasing the Cch concentration differentially affected  $I_h$ , the post-burst membrane potential, and the excitability in a dose-dependent linear fashion (Fig. 3.1.7).

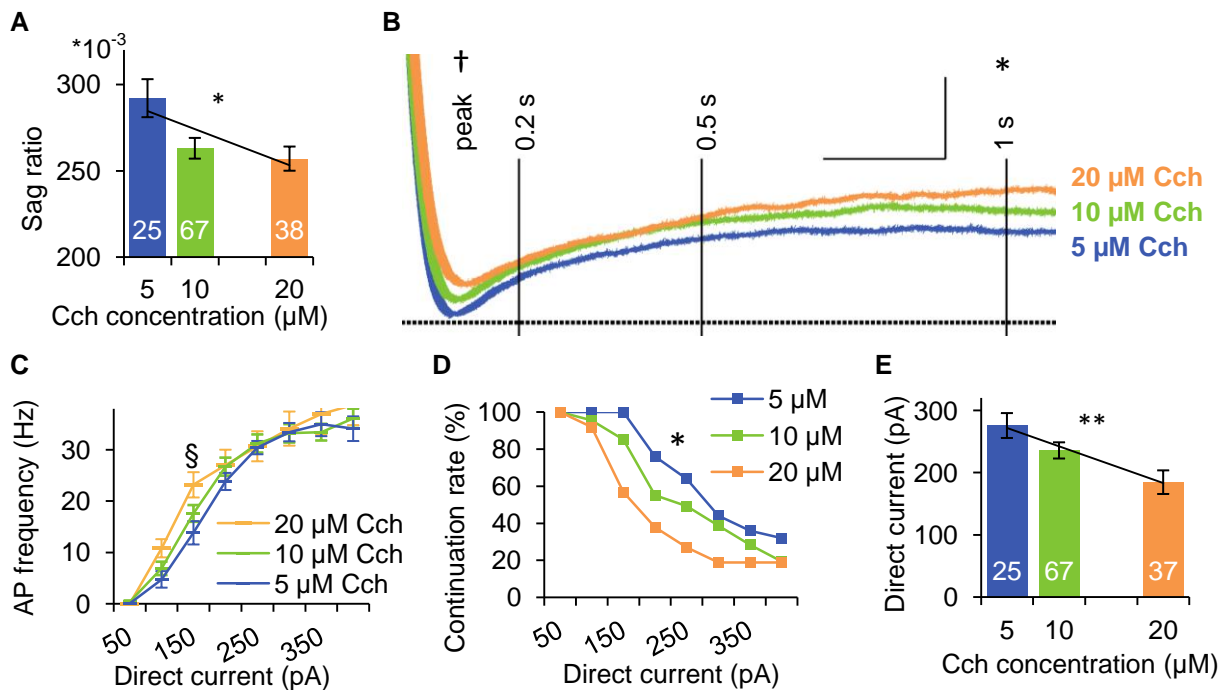


**Figure 3.1.7:  $I_h$ , post-burst potentials and firing frequency were modulated by increasing Cch concentrations.**

(A) The sag ratio induced by a -15 mV membrane potential deflection followed a significantly linear reduction with increasing carbachol (Cch) concentrations.

(B) The blue, green, and orange traces show the mean membrane potential of 13, 28, and 11 cells in the presence of 5, 10, and 20  $\mu\text{M}$  Cch, respectively. The horizontal black line represents the baseline membrane potential before the induction of five action potentials. The vertical black bars indicate the time points. The negative peak of the membrane potential following this action potential burst showed a trend towards more depolarized values at higher Cch concentrations. Following the same burst, the membrane potential at 1 s after the stimulus offset was significantly more depolarized, the higher the Cch concentration was. Horizontal scale bar: 200 ms. Vertical scale bar: 2 mV.

(C) The graph shows the current-frequency relationship of cells exposed to varying concentrations of Cch. The firing frequency showed a trend towards elevated firing frequencies at higher Cch concentrations when cells were stimulated with 150 pA. The sample size in 5/10/20  $\mu\text{M}$  Cch was 25/67/37, 25/64/34, 25/57/21, 19/37/14, 16/33/10, 11/27/7, 9/20/7, and 8/14/7 during the stimulations with 50, 100, 150, 200, 250, 300, 350, 400 pA, respectively.

(D) The graph shows the rate at which cells were transferred to subsequent increases of the current amplitude. The cumulative continuation rate was significantly different between the Cch concentrations. The lower the Cch concentration, the more cells could be transferred to subsequent increases of the current amplitude.

(E) The last current amplitude with which excitability could be assessed followed a significantly linear decrease with increasing Cch concentrations.

†  $p < 0.1$ . §  $p < 0.0125$  (bonferroni corrected trend; equal to  $p < 0.1$ ). \*  $p < 0.05$ . \*\*  $p < 0.01$ .

The sag ratio following a 15 mV hyperpolarization, decreased significantly as the Cch concentrations increased ( $p = 0.022$ ,  $R^2 = 0.035$ , Fig. 3.1.7A). The sag ratio induced by membrane deflections of -10 mV ( $p = 0.073$ ) and -20 mV ( $p = 0.098$ ) displayed comparable trends. This finding was in contrast to the increase of the sag ratio upon the introduction of 10  $\mu\text{M}$  Cch (Fig. 3.1.1.D).

The post-burst AHP could not be meaningfully assessed with a linear regression because only 7 (54%), 11 (39%), and 4 (36%) cells maintained an AHP in the presence of 5, 10, and 20  $\mu\text{M}$  Cch, respectively. Nonetheless, the membrane potential following a burst of five action potentials, irrespective if it hyperpolarized below baseline, was examined (Fig. 3.1.7B). This analysis revealed that the membrane potential at the negative peak ( $p = 0.074$ ,  $R^2 = 0.062$ ) and at 1 s after the stimulus offset ( $p = 0.048$ ,  $R^2 = 0.076$ ) was more depolarized the higher the Cch concentration was (Fig. 3.1.7B).

With regard to the excitability, the cells responded with a trend towards a linear increase of firing frequency the higher the Cch concentration was, in response to a 150 pA current injection ( $p = 0.009$ ,  $R^2 = 0.066$ , Fig. 3.1.7C, for details on bonferroni corrected  $p$  values see method section 2.8). However, the current-frequency relationship data were corroborated by a selection bias for less excitable cells at more intense current injections (for details see method section 2.7.5, Fig. 2.8). This effect was evident in the gradual reduction of the sample size available for the assessment of excitability from 25/67/37 cells stimulated with 50 pA to 8/14/7 cells stimulated with 400 pA in the presence of 5/10/20  $\mu\text{M}$  Cch, respectively. The selection bias introduced an underestimation of the Cch concentration effect. The discontinuation of cells throughout gradual increments of the current amplitude (50 pA increments) may serve as a meaningful parameter for excitability because reasons for the discontinuation were the initiation of persistent firing or depolarization block in the majority (91%) of cases. The discontinuation pattern (Fig. 3.1.7D) differed significantly between the presence of 5, 10 and 20  $\mu\text{M}$  Cch (Kaplan-Meier survival analysis,  $\chi_1^2 = 7.127$ ,  $p = 0.028$ ). In particular, the higher the Cch concentration, the earlier and the more cells were discontinued. Consequently, the average current with which cells could be stimulated before they dropped out of the sample followed a dose-dependent linear decrease ( $p = 0.002$ ,  $R^2 = 0.073$ , Fig. 3.1.7E) indicating that cells exposed to a lower concentration of Cch needed more current to engage in persistent firing or depolarization block. In summary, the results suggest that increasing Cch concentrations were accompanied by increased excitability.



### **3.1.2 Modulation of intrinsic properties by intercellular variability**

Intercellular variability may be a confounding factor when assessing neuronal responses from animals with a different sex and age obtained from different hemispheres and different locations within the hippocampus and the CA1 subfield. Furthermore, the modulation of intrinsic properties by any of these parameters could be used for assessing the impact of the naturally occurring variability within this parameter on the subsequently reported phenomena persistent firing and depolarization block. Therefore, I will firstly consider the modulation of intrinsic electrophysiological properties by the sex of the animal, the cerebral hemisphere, the maturation throughout P14-24 and aging (juvenile vs. senescent animals). Thereafter, I will compare intrinsic electrophysiological properties along the dorso-ventral and proximo-distal axis of the CA1 area. As before the data will be reported in an aggregated format and the interested reader is referred to the supplementary material for detailed information (Tab. 6.1.3 to Tab. 6.1.18). An in depth discussion is beyond the scope of this dissertation because a stronger focus will be laid on novel aspects of cholinergic effects on CA1 pyramidal neurons (Chapter 3.2) and their relation to previously reported response patterns (Chapter 3.3).

#### **3.1.2.1 No considerable modulation by the animal's sex or the cerebral hemisphere**

Despite data indicating higher excitability and differential cholinergic innervation of the hippocampus in male pups [280–283], I did not detect a substantial and consistent modulation of intrinsic electrophysiological properties by the sex of the animals from which the cells were derived, neither in ACSF+SB (Tab. 6.1.3) nor in the presence of 10  $\mu$ M Cch (Tab. 6.1.4). For details, the interested reader is referred to the supplementary material.

The evidence for hemispheric lateralization of the rodent hippocampus is scarce and heterogeneous [284–287]. I did not observe any substantial and consistent modulation of intrinsic electrophysiological properties by the brain hemisphere from which the slice was obtained, neither during the superfusion with ACSF+SB (Tab. 6.1.5) nor in the presence of 10  $\mu$ M Cch (Tab. 6.1.6). For details, the interested reader is referred to the supplementary material.

### 3.1.2.2 Maturation and aging

#### Maturation

Studies on postnatal development indicate that CA1 pyramidal neurons still mature throughout P14-24 [250,258,288]. Of particular interest, cellular properties that affect intrinsic excitability ( $I_h$ ) were reported to mature until the end of the fourth postnatal week [258]. Therefore, I assessed whether intrinsic electrophysiological properties of CA1 pyramidal neurons were modulated by the age of the animals (Tab. 6.1.7 and Tab. 6.1.8) because postnatal maturation may provide a meaningful approach to assess the differential effect of the developing property on persistent firing (chapter 3.2) and depolarization block (chapter 3.3). Unless otherwise stated, the results of linear regressions will be reported in the following because both the dependent (e.g. membrane potential or input resistance) and the independent variable (age in postnatal days) had a metric level of measurement. If a dependent variable had a lower level of measurement (i.e. nominal or ordinal; e.g. regular vs. burst firing) a binomial logistic regression was used for statistical assessment (Tab. 6.1.7 and Tab. 6.1.8).

I observed that passive properties, single spike properties, and the hyperpolarization activated current ( $I_h$ ) of neurons superfused with ACSF+SB changed significantly as animals matured (Tab. 6.1.7). In particular, the RMP hyperpolarized ( $p = 0.002$ ,  $R^2 = 0.057$ , Fig. 3.1.8D) significantly. Regarding active properties, the AP amplitude increased with progressive maturation of the animals ( $p = 0.019$ ,  $R^2 = 0.039$ ). In line with a significant augmentation of the AP peak falling slope ( $p < 0.001$ ,  $R^2 = 0.091$ , Fig. 3.1.8B), the AP full width at half ( $p = 0.017$ ,  $R^2 = 0.040$ , Fig. 3.1.8C) and at one third ( $p = 0.019$ ,  $R^2 = 0.040$ ) of its amplitude decreased significantly as animals matured. In contrast to prevalent literature [258], I detected a significant decrease in sag ratio as animals matured ( $p \leq 0.005$ ,  $R^2 \geq 0.053$ , Fig. 3.1.8A). Notably, the membrane potential following a burst of 5 action potentials (AHP in ACSF+SB, mostly ADP in Cch) was not modulated by the maturation of animals ( $p \geq 0.345$ ,  $R^2 \leq 0.012$ , Fig. 3.1.8E).

In the presence of 10  $\mu$ M Cch, the modulation of  $I_h$  and of single spike properties by maturation were preserved (Fig. 3.1.8A-C, Tab. 6.1.8). These results indicated that  $I_h$  and the action potential repolarization were not differentially affected by Cch throughout the reported age range. In contrast, the modulation of the RMP ( $p = 0.170$ ,  $R^2 = 0.077$ ) by the animal's maturation was no longer significant in the presence of Cch (Fig. 3.1.8D). However, this effect may have been due to the low number of cells ( $n = 26$ ) maintaining a RMP in the

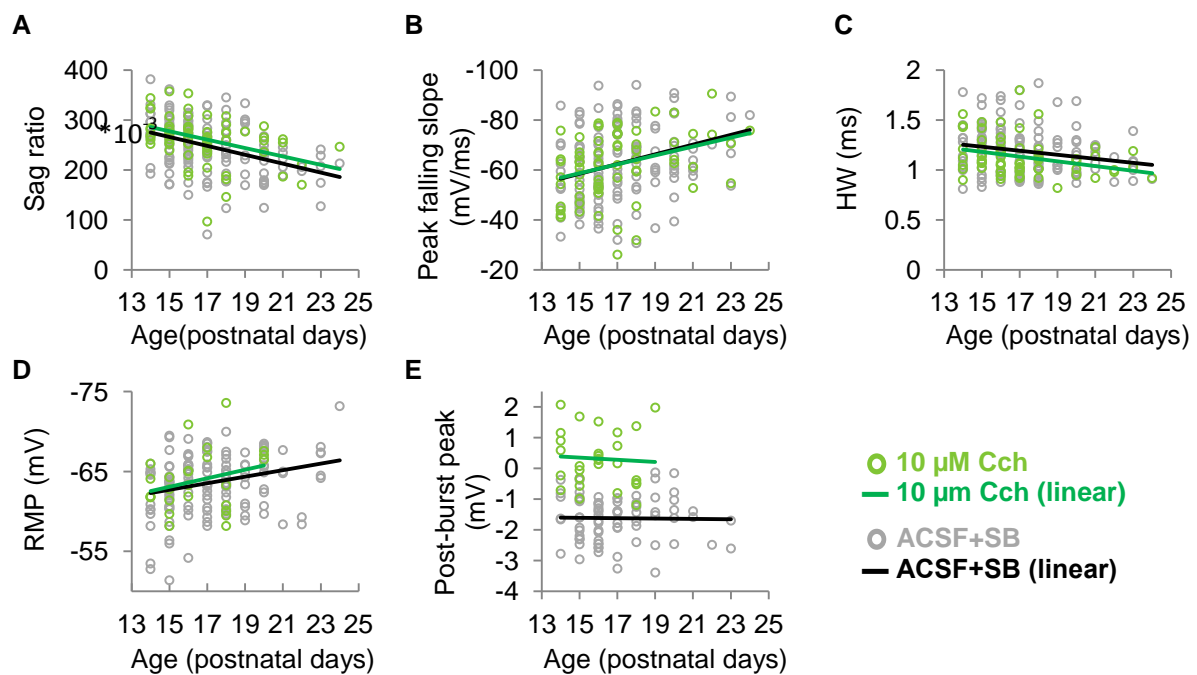


**Figure 3.1.8: The effect of maturation on intrinsic electrophysiological properties.**

(A-C) The effect of maturation on the hyperpolarization activated current ( $I_h$ ) and the spike repolarization were unaffected by the application of carbachol (Cch).

(A) The sag ratio was significantly smaller in neurons from more mature animals, both in the absence and presence of 10 μM Cch.

(B) The peak falling slope was significantly more pronounced in neurons from more mature animals, both in the absence and presence of 10 μM Cch.

(C) The full width at half amplitude (HW) was significantly shorter, in neurons from more mature the animals, both in the absence and presence of 10 μM Cch.

(D) The resting membrane potential (RMP) was significantly more hyperpolarized in neurons from more mature animals when bathed in ACSF+SB. During the superfusion of 10 μM Cch, the RMP was not modulated by maturation. However, the number of cells that maintained a RMP in the presence of 10 μM Cch was low ( $n = 26$ ) and the age range was limited to P14-20.

(E) Representative for the results on the post-burst membrane potential, the negative peak within 150 ms after stimulus offset, showed no modulation by the animal's maturation, both in the absence and presence of Cch.

presence of Cch and therewith a limited age range spanning P14 to P20. Furthermore, it is noteworthy that in the presence of Cch (Tab. 6.1.8), just as in its absence (Tab. 6.1.7), the AHP was not affected by the maturation of the animals (Fig. 3.1.8E). With regard to the mAHP, but not the sAHP, these findings are in line with previous reports [288].

In summary, these data indicated that  $I_h$  and action potential repolarization systematically co-varied with the animals maturation, even in the presence of 10 μM Cch. In the following chapters, I will assess whether this variability affected persistent firing (Chapter 3.2) and depolarization block (Chapter 3.3).

## Aging

Besides the maturation during the early lifespan [258,250], also processes during advanced age affect intrinsic electrophysiological properties like the post-burst AHP [219,289] and the effects of cholinergic stimulation on hippocampal neurons [290].

To test for the effects of aging, I analyzed the intrinsic properties of twelve CA1 pyramidal neurons from seven male Long-Evans rats at an average age of 25.3 months (SD: 0.4 months). I compared these to eleven randomly chosen neurons from seven male Long-Evans rats at an average age of 17.4 days (SD: 0.9 days) whose recordings were collected in temporal proximity to the aged animals ensuring that the same set up and the same intracellular fluid were used. Unless otherwise stated, the results of two-sample *T*-test will be reported in the following because two groups of independently sampled cells (aged vs. juvenile) were compared to one another with respect to dependent variables that had a metric level of measurement (e.g. membrane potential). I will continue to adhere to the aggregated format of data presentation. The interested reader is referred to the supplementary material for detailed information on the effects in ACSF+SB (Tab. 6.1.9) and during the bath application of 10  $\mu$ M Cch (Tab. 6.1.10)

Compared to juvenile animals, aged animals presented a significantly reduced input resistance ( $p \leq 0.012$ , Fig. 3.1.9A) and sag ratio ( $p \leq 0.015$ , Fig. 3.1.9B) at all membrane potentials tested. The action potential threshold was significantly more hyperpolarized ( $p = 0.012$ , Fig. 3.1.9C) and the AP peak falling slope was significantly more steep ( $p = 0.042$ , Fig. 3.1.9D) in cells from aged compared to juvenile animals. At various current amplitudes, the firing frequency of cells from aged animals was significantly lower when compared to cells from juvenile animals (Fig. 3.1.9E). This finding was consistent with the aforementioned effect of aging on CA1 pyramidal neurons from aged compared to those from juvenile animals (Fig. 3.1.9A-D). In contrast to prevailing literature [289,219], no differences in various measures of the post-burst afterhyperpolarization could be detected (Fig. 3.1.9F, Tab. 6.1.9)

In general, the effects of aging were insensitive to the superfusion of 10  $\mu$ M Cch. Comparable to the absence of Cch (Fig. 3.1.9), the input resistance ( $p \leq 0.092$ , Fig. 3.1.10A), the sag ratio ( $p \leq 0.036$ , Fig. 3.1.10B), the action potential width ( $p \leq 0.018$ , Fig. 3.1.10D) and the current-frequency relationship ( $p \leq 0.147$ , Fig. 3.1.10E) indicated a lower excitability in neurons from aged compared to juvenile animals.

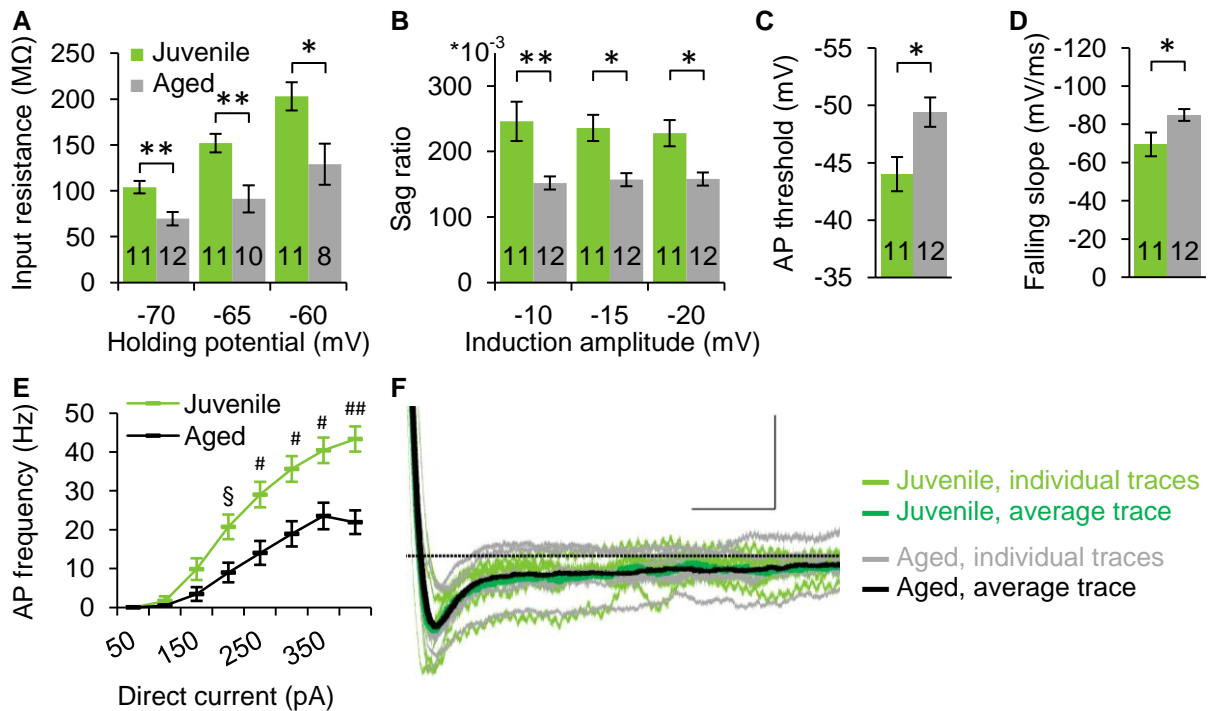


**Figure 3.1.9: In ACSF+SB various measures, but not the AHP, indicated a lower excitability in neurons from aged compared to juvenile animals.**

(A) The input resistance was significantly reduced in neurons from aged animals compared to neurons from juvenile animals at all three membrane potentials tested (-70 mV, -65 mV, -60 mV). All significant differences survived a Bonferroni correction for multiple comparisons.

(B) The sag ratio was significantly reduced in neurons from aged animals compared to neurons from juvenile animals at all three membrane potential deflections (-10 mV, -15 mV, -20 mV) used for the induction of the hyperpolarization activated current ( $I_h$ ). All significant differences survived a Bonferroni correction for multiple comparisons.

(C) The action potential threshold was significantly more hyperpolarized in neurons from aged compared to juvenile animals.

(D) The peak action potential falling slope was significantly more steep in neurons from aged compared to juvenile animals.

(E) At current amplitudes  $\geq 250$  pA, neurons from aged animals generated significantly less action potentials when stimulated with the same current injection as neurons from juvenile animals. The sample size of neurons from juvenile/aged animals was 11/12 for the current steps 50 to 350 pA and 11/10 for the 400 pA current step; respectively.

(F) The afterhyperpolarization was indistinguishable between juvenile ( $n = 6$ ) and aged ( $n = 6$ ) animals' neurons. The graph shows the individual (light colors) and average (dark colors) membrane potential following a burst of five action potentials in neurons from aged (black/grey) and juvenile (green) animals. The dotted horizontal line indicates the baseline holding potential before the induction of the action potential burst. Horizontal scale bar: 200 ms. Vertical scale bar: 2 mV

§  $p < 0.0125$  (bonferroni corrected trend; equal to  $p < 0.1$ ). \*  $p < 0.05$ . #  $p < 0.00625$  (bonferroni corrected; equal to  $p < 0.05$ ). \*\*  $p < 0.01$ . ##  $p < 0.00125$  (bonferroni corrected; equal to  $p < 0.01$ ).

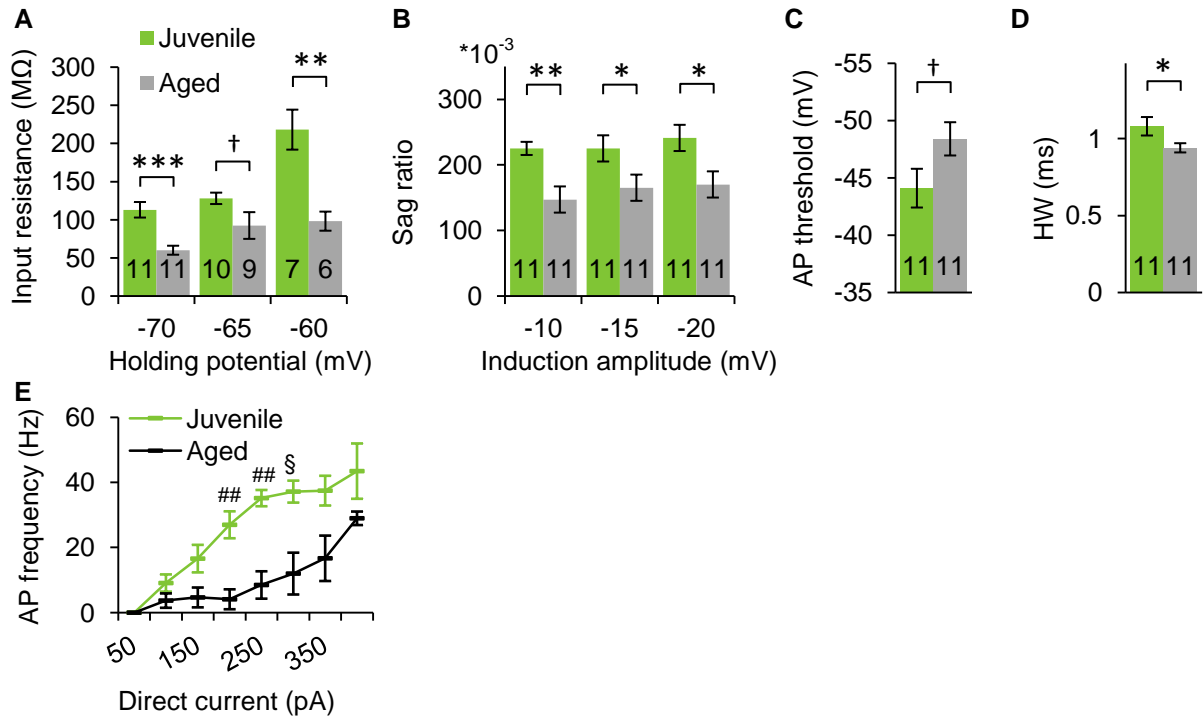


**Figure 3.1.10: The lower excitability in neurons from aged compared to juvenile animals was preserved in the presence of 10  $\mu$ M carbachol.**

(A) The input resistance was significantly lower in neurons from aged compared to juvenile animals when assessed at a holding potential of -70 mV and -60 mV. At -65 mV, the input resistance showed a trend towards lower values in neurons from aged, compared to juvenile animals

(B) The sag ratio was significantly lower in neurons from aged compared to juvenile animals, irrespective of the amplitude of the voltage deflection (-10 mV, -15 mV, -20 mV) with which the hyperpolarization activated current ( $I_h$ ) was induced.

(C) In the presence of Cch, the action potential (AP) threshold showed a trend towards more hyperpolarized values in neurons from aged compared to juvenile animals when 10  $\mu$ M Cch were superfused.

(D) The action potential full width at half height (HW) was significantly shorter in neurons from aged compared to juvenile animals.

(E) At a current injection of 200 and 250 pA, neurons from aged animals generated significantly fewer action potentials when stimulated with the same current injection as juvenile animals. The sample size of neurons from juvenile/aged animals were 11/11, 10/11, 9/9, 6/7, 6/4, 5/3, 4/3, and 2/3 for current injections of 0.05, 0.1, 0.15, 0.2, 0.25, 0.3, 0.35, 0.4 nA; respectively.

†  $p < 0.1$ . §  $p < 0.0125$  (bonferroni corrected trend; equal to  $p < 0.1$ ). \*  $p < 0.05$ . \*\*  $p < 0.01$ . ##  $p < 0.00125$  (bonferroni corrected; equal to  $p < 0.01$ ). \*\*\*  $p < 0.001$ .

### 3.1.2.3 The cell's location within CA1

The quantification of the dorso-ventral and proximo-distal location followed the previous description (method section 2.6) but is briefly recapitulated here. To quantify the dorso-ventral location, the distance of the cell from the top of the brain was calculated assuming a slice thickness of 350  $\mu\text{m}$  and a cell location at the surface on either side of the slice. A record of the slice origin (hemisphere and serial position during the slicing) and measures taken from the remainders of the brain were used for the computation. The dorso-ventral midline was approximated following anatomical considerations (method section 2.6.1). Therewith, the definitions of dorsal and ventral were supposed to represent the location within the hippocampus rather than the relative location within the sample. The proximo-distal location was the distance of the biocytin stained soma from the CA2/CA1 border in relation to the full extent of CA1 from its border with CA2 to its border with the subiculum.

Owing to the anatomically based definition of the dorso-ventral axis (method section 2.6.2), a bias towards sampling CA1 pyramidal neurons from the ventral two thirds became apparent (Fig. 3.1.11). The aspired sparing of the middle portion within the proximo-distal axis may be considered relatively successful (Fig. 3.1.11). As in previous sections, data will be presented in an aggregated format. Unless otherwise stated, the results of two-sample *T*-tests will be reported in the following section because two independent sets of cells (defined by their location) were compared with regard to dependent variables that had a metric level of measurement (e.g. membrane potential or time). If a dependent variable with a lower level of measurement (i.e. ordinal or nominal, e.g. regular vs. burst firing) was compared across the two groups, then an appropriate test out of the Chi-square test family (for details see method section 2.8.2) was chosen and explicitly indicated.

#### The dorso-ventral axis

As previously outlined (introduction section 1.1), considerable evidence suggest a dorso-ventral (aka septo-temporal) segregation of the hippocampus, including the CA1 area.

Due to the aforementioned bias towards sampling from the mid-ventral hippocampus, I compared neurons recorded in the dorsal against those recorded in the ventral half of the hippocampus (Tab. 6.1.11). The sample size in the dorsal subpopulation would be too low when using more disparate locations at the outermost thirds of the hippocampus.

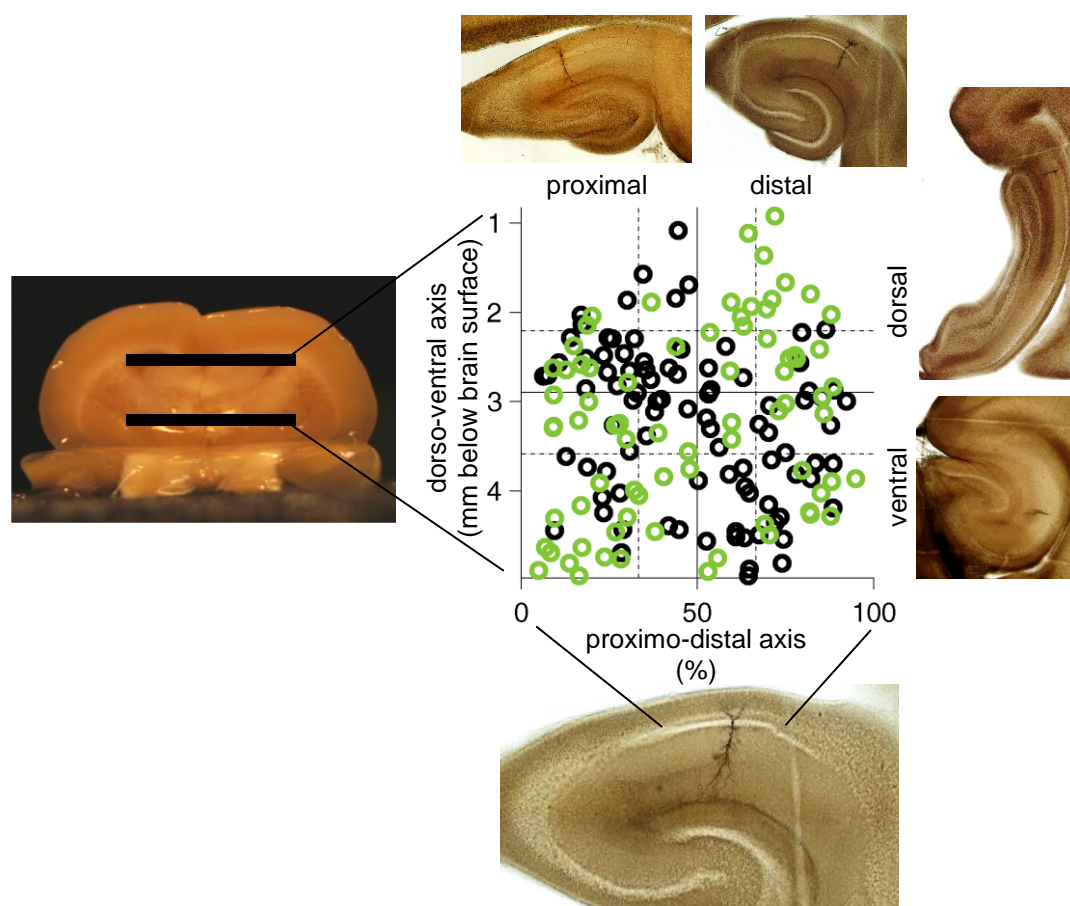


**Figure 3.1.11: The cells' location within the hippocampus.**

The scatter plot in the middle represents the location of cells for which both the proximo-distal and the dorso-ventral measures were available.

Green circles represent cells that were exposed to 10  $\mu\text{M}$  Cch. Black circles represent cells that were exposed to other concentrations of Cch, other drugs or only recorded in ACSF + SB.

The solid cross below the cell representations, indicates the 50:50 split of the dorso-ventral (at 2.895 mm below the brain surface) and proximo-distal (50%, i.e. half way between the CA2/CA1 and the CA1/subiculum) axis. The upper and lower horizontal dotted lines separate the most dorsal and ventral third of the hippocampus, respectively. The left and right vertical dotted lines separate the most proximal and distal third of the CA1 area.

The image left of the scatter plot is a view from the caudal end onto the coronal plane of an aged animal's brain (ID: 130411). The brain of an aged animal was chosen for better visibility of structures because the brains of juvenile animals appeared uniformly pale. The lines indicate the approximate correspondence of the numerical values to the anatomical location.

The image below the scatter plot shows a horizontal brain slice (ID: 140823/R4) which contains a biocytin stained CA1 pyramidal neurons. The lines indicate the approximate correspondence of the numerical values to the anatomical location within CA1.

The images right of the scatter plot represent examples of horizontal slices obtained from ventral (bottom, ID: 120812/R11, 4.58 mm below the top of the brain) and dorsal (top, ID: 121023/L1, 1.28 mm below the top of the brain) portions of the hippocampus. The dark pigmentation are biocytin stained CA1 pyramidal neurons.

The images on top of the scatter plot shows examples of biocytin stained neurons that were recorded at proximal (left, ID: 130722/R2, 6.4%) and distal (right, ID: 140421/R5, 79.0%) locations within CA1.



The fast afterhyperpolarization (fAHP) was significantly more pronounced in neurons from the dorsal, compared to the ventral half of the hippocampus ( $p = 0.043$ , Fig. 3.1.12A). In line with that, the likelihood for generating AP bursts was significantly lower in neurons from the dorsal compared to the ventral half of the hippocampus ( $\chi^2$  test,  $p = 0.005$ , Fig. 3.1.12B). In contrast to the fAHP, the post-burst AHP (mAHP and sAHP) was significantly less pronounced in neurons from the dorsal compared to the ventral half of the hippocampus ( $p \leq 0.067$ , Fig. 3.1.12C&D). Consequentially, I observed a trend towards a lower adaptation ratio in neurons from the dorsal ( $2.3 \pm 0.2$ ) compared to the ventral ( $3.0 \pm 0.4$ ) half of the hippocampus ( $p = 0.081$ ). However, these differences did not translate into significant differences in the excitability as assessed by the current-frequency relationship (Fig. 3.1.12E). In line with prevalent literature [8], a linear regression revealed that the differences in the post-burst AHP and the current-frequency relationship followed a significant linear dorso-ventral gradient (Tab. 6.1.12). In addition, the RMP was significantly more depolarized the more ventral the neurons were located (linear regression,  $p = 0.041$ ,  $R^2 = 0.026$ , Tab. 6.1.12).

In summary, I observed a significantly higher excitability in the neurons recorded from the dorsal compared to the ventral half of the hippocampus (Fig. 3.1.12) when superfused with ACSF+SB. A linear regression supported these findings and indicated a linear gradient along the dorso-ventral axis (Tab.6.1.12)

Yet, upon the bath application of 10  $\mu$ M Cch, the aforementioned differences between the dorsal and ventral half of the hippocampus vanished ( $p \geq 0.116$ , Tab. 6.1.13). Notably, the lack of significant results in the current-frequency relationship could not be explained by a selection bias for less excitable cells at higher current intensities because the selection bias affected the dorsal and ventral sample similarly (Kaplan-Meier survival analysis,  $\chi^2 = 0.930$ ,  $p = 0.335$ ). Furthermore, a significantly higher current amplitude needed for the induction of depolarization block had to be judged as type II error. The indications for equality along the dorso-ventral axis in the presence of Cch were supported by a lack of a significant linear modulation ( $p \geq 0.097$ , Tab. 6.1.14)

In summary, the data indicated that cholinergic stimulation differentially affected the dorsal and ventral portion of the hippocampus which leveled the dorso-ventral gradient observed in ACSF+SB leaving no detectable differences in the presence of Cch.

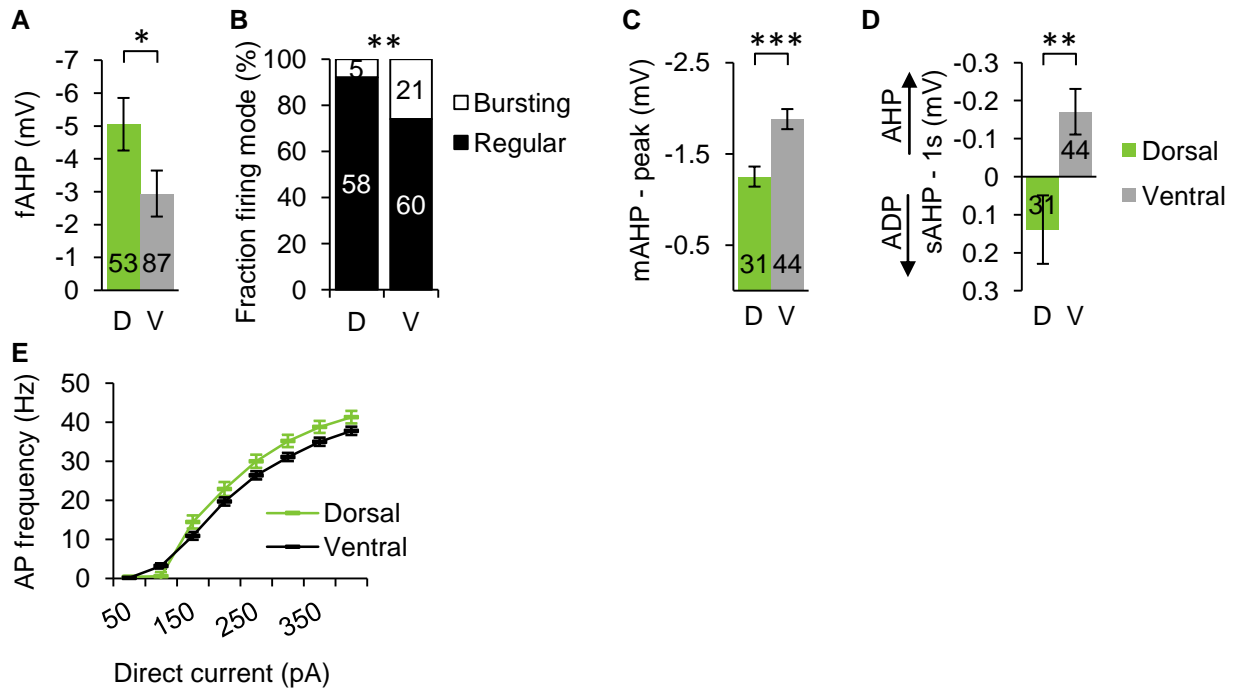


**Figure 3.1.12: Neurons in the dorsal compared to the ventral half of the hippocampus were more excitable in the absence of Cch.**

(A) The fast afterhyperpolarization (fAHP) was significantly more pronounced in neurons obtained from the dorsal (D) compared to neurons obtained from the ventral (V) half of the hippocampus.

(B) Neurons in the dorsal half of the hippocampus were significantly less likely to engage in burst firing compared to neurons in the ventral half of the hippocampus.

(C) The medium afterhyperpolarization (mAHP) was significantly less pronounced in neurons recorded in the dorsal compared to those recorded in the ventral half of the hippocampus.

(D) The slow afterhyperpolarization (sAHP) was significantly less pronounced in neurons from the dorsal compared to the ventral half of the hippocampus. Particularly, the membrane potential of neurons in the dorsal half of the hippocampus depolarized above baseline such that they exhibited an afterdepolarization (ADP) instead of an afterhyperpolarization (AHP).

(E) Neurons from the dorsal half of the hippocampus did not generate significantly more action potentials than the neurons from the ventral half of the hippocampus at any current amplitude. The sample size for the dorsal/ventral subsets were 55/89 at the stimulations 50 to 300 pA, respectively. For the stimulations with 350 and 400 pA the dorsal/ventral sample sizes were 53/87 and 49/83, respectively.

\*  $p < 0.05$ . \*\*  $p < 0.01$ . \*\*\*  $p < 0.001$ .

### The proximo-distal axis

To the best of my knowledge, in contrast to the dorso-ventral axis, only limited focus was put on a potential segregation along the proximo-distal axis of CA1 [291,38]. Nonetheless, an anatomical segregation along the proximo-distal axis has long been described [36] and is comprehensively reviewed in Cutsuridis et al. (2010) [4].

Owing to the successful avoidance of sampling in the medial portion within the proximo-distal axis, the cells' distribution (Fig. 3.1.11) allowed a comparison between the most extreme thirds along the proximo-distal axis. Unless otherwise stated, the results of two-sample *T*-test will be reported in the following.

During the superfusion of ACSF+SB, the burst firing mode was significantly more seldom in the proximal compared to the distal third of the CA1 area ( $\chi_1^2$  test,  $p = 0.025$ , Fig. 3.1.13A). In line with the burst-firing propensity (according to Graves et al. (2012) [265]), the input resistance was significantly higher in the cells obtained from the most proximal third of CA1 compared to the most distal third of CA1 ( $p \leq 0.012$ , Fig. 3.1.13B). Furthermore, in line with the higher input resistance, neurons in the most proximal third of CA1 generated significantly more action potentials than neurons in the most distal third of CA1 when stimulated with current amplitudes  $\geq 150$  pA ( $p \leq 0.00005$ , Fig. 3.1.13C). The findings obtained from comparing the disparate locations at the outermost third of the proximo-distal axis (Tab. 6.1.15) were supported by a significant linear gradient along the proximo-distal axis of neurons superfused with ACSF+SB (Tab. 6.1.16).

Similar to the leveling effect of Cch on the dorso-ventral axis effect, the superfusion of 10  $\mu$ M Cch eliminated the modulation of the input resistance by the cells' proximo-distal location ( $p \geq 0.119$ , Tab.6.1.17). However, the more intense generation of action potentials in response to current injection of 200 pA was maintained in neurons recorded in the most proximal compared to the most distal third of CA1 ( $p = 0.002$ , Fig. 3.1.13D). At higher current amplitudes ( $\geq 350$  pA) the firing frequency in proximal cells declined and the sample size was too low for a statistical comparison. Both was due to a selection bias for less excitable neurons at higher stimulus intensities. Notably, this selection bias (i.e. the rate of discontinuation) was significantly more pronounced in neurons from the most proximal compared to the most distal third of CA1 (Kaplan-Meier survival analysis,  $\chi_1^2 = 7.676$ ,  $p = 0.006$ , Fig. 3.1.13E). Furthermore, the average of the highest current to which cells could be exposed, was significantly lower in neurons from the most proximal compared to the most distal third ( $p = 0.010$ , Fig. 3.1.13F). These results indicate that the difference in excitability along the proximo-distal axis, as assessed by the current-frequency relationship, underestimated the actual excitability difference between neurons in the most proximal compared to the most distal third of CA1. The findings were supported by a significant linear gradient of the neurons' excitability along the proximo-distal axis (Fig. 6.1.18).

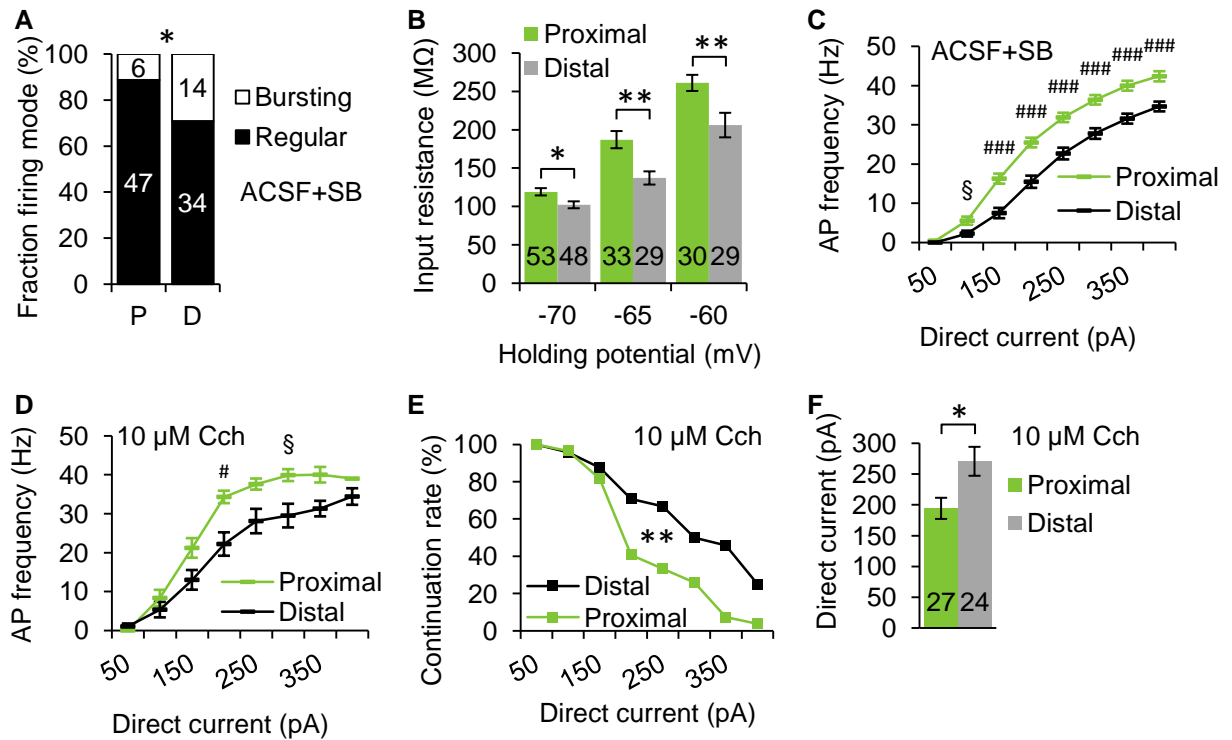


**Figure 3.1.13: The excitability was higher in neurons from the proximal compared to the distal third of CA1.**

(A) The likelihood of cells to engage in burst firing was significantly lower in cells from the most proximal (P) compared to the most distal (D) third within CA1.

(B) At all membrane potentials tested (-70 mV, -65 mV, and -60 mV) the input resistance was significantly elevated in neurons recorded in the most proximal third of CA1 compared to neurons recorded in the most distal third of CA1.

(C) The current-frequency relationship revealed that cells located within the most proximal third of CA1 generated significantly more action potentials than cells located within the most distal third of CA1 when stimulated with the same current injection while superfused with ACSF+SB. The sample size of the proximal/distal subsets were 53/48 for the 50 to 300 pA current stimulations, and 52/46 and 47/44 for the 350 pA and 400 pA current stimulations; respectively.

(D) During the bath application of 10 μM Cch, neurons in the most proximal third of CA1 generated significantly more action potentials than neurons in the most distal third of CA1 when stimulated with 200 pA. The sample size of the proximal/distal subsets were 27/24, 26/23, 22/21, 11/17, 9/16, 7/13, 2/12, 1/7 at the current amplitudes 50, 100, 150, 200, 250, 300, 350 and 400 pA.

(E) The rate of neurons being transferred from the previous to the active current amplitude (continuation rate) dropped significantly more drastic in neurons recorded in the most proximal compared to those recorded in the most distal third of CA1.

(F) The average current at which neurons could lastly be assessed for excitability was significantly lower for cells from the most proximal compared to those from the most distal third of CA1. Hence, the former exhibited persistent firing or depolarization block at lower current amplitudes which resulted in the discontinuation.

§  $p < 0.0125$  (bonferroni corrected trend; equal to  $p < 0.1$ ). \*  $p < 0.05$ . #  $p < 0.00625$  (bonferroni corrected; equal to  $p < 0.05$ ). \*\*  $p < 0.01$ . ###  $p < 0.000125$  (bonferroni corrected; equal to  $p < 0.001$ ).

In summary, in the absence of Cch, the proximal portion of CA1 was more excitable than the distal portion whereas no difference in the excitability along the dorso-ventral axis was found. The differential excitability in the proximo-distal axis appeared to be mediated by the  $R_{in}$ . Yet, the differential mAHP along the dorso-ventral axis failed to translate into an excitability difference along the dorso-ventral axis. With regard to these findings, an in depth analysis of effects within the three-dimensional configuration of the hippocampus would be worthwhile, but is beyond the scope of this dissertation. Immediately relevant to the upcoming chapters on persistent firing and depolarization block in the presence of Cch is that, upon the superfusion of Cch, differences in the mAHP and  $R_{in}$  vanished. However, the proximo-distal excitability gradient was maintained in the presence of Cch.

### **3.1.3 Summary of the cholinergic effects on CA1 pyramidal neurons**

In summary, I showed that the application of 10  $\mu$ M Cch to *in vitro* CA1 pyramidal neurons induced an increased excitability. This was evident in a wealth of effects like a depolarization of the resting membrane potential (Fig. 3.1.1A&B), the inhibition of burst firing (Fig. 3.1.2B), the conversion of afterhyperpolarizations to afterdepolarizations (Fig. 3.1.3), the reduction of and spike frequency accommodation (Fig. 3.1.4), the generation of more action potentials in response to the same current stimulation (Fig. 3.1.5) despite reduced input resistance (Fig. 3.1.1C), a reduction of the threshold for depolarization block induction (Fig. 3.1.6). A variety of these effects followed a linear concentration-dependent gradient within the range of 5 to 20  $\mu$ M carbachol (Fig. 3.1.7).

I reported that the resting membrane potential, the afterhyperpolarization activated current ( $I_h$ ) and properties of individual action potentials were significantly affected by the maturation of the animals (Fig. 3.1.8). However, cholinergic stimulation did not exert differential effects throughout the age range of 14 to 24 days (Fig. 3.1.8), indicating that the cholinergic system may have been fully mature. I presented that the excitability of CA1 pyramidal neurons from aged animals (~25 months old) was significantly reduced compared to the juvenile animals (Fig. 3.1.9). This effect persisted during the bath application of 10  $\mu$ M carbachol (Fig. 3.1.10). In contrast to prevalent literature [107,110,108], the reduction in

excitability appeared to be mediated by a reduced input resistance (Fig. 3.1.9A, Fig. 3.1.10A) and not by an enhanced post-burst afterhyperpolarization (Fig. 3.1.9F).

In contrast to the large body of evidence suggesting a higher excitability of the ventral compared to the dorsal portion of the hippocampus [15,14,13,16], I did not find such in my sample of CA1 pyramidal neurons (Fig. 3.1.12). However, in line with scarce but consistent evidence from research on epilepsy [38,40,39], I demonstrated a strikingly higher excitability of pyramidal neurons recorded in the proximal compared to the distal region of the CA1 area which was maintained during the superfusion of carbachol (Fig. 3.1.13).

## 3.2. Persistent firing

The CA1 area of the hippocampus was involved in maintaining information across temporal gaps [56,57,61] and sustained spiking activity in CA1 pyramidal neurons was recorded during the maintenance of information [211,215]. Furthermore, the cholinergic innervation of the hippocampus was crucial for the maintenance of information [93,94]. However, a possible mechanism, for how neurons in the CA1 area may accomplish the maintenance of information, was not yet proposed [61].

Cholinergic-mediated intrinsic persistent firing was observed in various temporal lobe cortices [221,225,227] and is thought to be a mechanism of short-term information maintenance [47]. Thus, cholinergic-mediated intrinsic persistent firing may be one possible mechanism underlying the sustained spiking activity *in vivo*. For the CA1 area with its sparse excitatory recurrent connections [28,29], a mechanism based on intrinsic properties of individual neurons is particularly favorable because it does not involve recurrent excitation.

In this chapter, I recapitulate some results that were previously published [63]. The inclusion criteria and the carbachol (Cch) supplier for the recapitulated data are specified in Knauer et al. (2013) [63]. Inclusion criteria and the Cch supplier for all data beyond those reported in Knauer et al. (2013) [63], follow the specifications in the methods section. Arthur Jochems contributed to the data in this chapter by sampling five out of seven cells in the experiments involving flufenamic acid. María Jesus Valero Aracama contributed to this chapter by sampling the six cells in the experiments involving atropine. Arthur Jochems supported the analysis of the post-stimulus plateau potential for the aforementioned publication [63] by providing a Matlab script which ignored membrane potential values more depolarized than -30 mV. However, owing to improvements in my programming abilities, all analysis reported in this dissertation were conducted by me, exclusively.

### 3.2.1 *In vitro* CA1 pyramidal neurons engaged in persistent firing

To elucidate whether CA1 pyramidal neurons have the propensity to show persistent firing *per se*, I studied whether *in vitro* CA1 pyramidal neurons expressed persistent firing. Therefore, I applied a transient suprathreshold current injection that elicited action potentials

and observed the cell's response following the stimulus offset, both in the absence and presence cholinergic activation.

The bath application of carbachol (Cch) served to mimic the elevated cholinergic tone during active waking [91]. However, bath application of cholinergic agonists was not only reported to block the AHP [152], but also to depolarize the RMP [153,162] which was both apparent in my sample (Fig. 3.1.3, Fig. 3.1.1; respectively). Nonetheless, neurons ought to have a comparable baseline  $V_m$ , both in the absence and presence of Cch. However, an absolute membrane potential value was rejected as standard of comparison because cells could only be kept at more hyperpolarized membrane potentials in the presence of Cch. Consequently, if the same absolute membrane potential would have been adopted in the absence of Cch, cells would have been more remote from their action potential threshold. Thus, the initial states may not have been comparable. Instead, I achieved comparability by keeping the cells at the same  $V_m$  relative to their firing threshold, i.e. just below threshold.

The cells ( $n = 15$ ) were maintained just below their firing threshold by constant direct current injection which was significantly (paired  $T$ -test;  $T_{14} = -9.120$ ,  $p < 0.001$ ) more negative in the presence of Cch (Cch;  $-39.5 \pm 8.2$  pA), compared to the absence of Cch (nACSF;  $36.1 \pm 9.4$  pA). In normal artificial cerebrospinal fluid (nACSF), the membrane potential just below firing threshold was  $-56.3 \pm 0.6$  mV. However, in Cch, the same cells could only be held at  $-60.3 \pm 0.7$  mV, which was significantly more hyperpolarized than in nACSF (paired  $T$ -test;  $T_{14} = -4.669$ ,  $p < 0.001$ ). To test for persistent firing, I injected a 2 s long and 100 pA strong square pulse. In nACSF, this stimulation elicited action potential firing at a frequency of  $22.6 \pm 2.0$  Hz. In Cch, the same stimulation elicited significantly (paired  $T$ -test;  $T_{14} = 2.937$ ,  $p = 0.011$ ) more action potentials ( $27.9 \pm 1.6$  Hz).

To examine whether persistent firing took place, I compared the cell's response after the stimulus offset. The difference between the absence and presence of Cch was readily appreciable at a phenomenological level (Fig. 3.2.1).

During the superfusion of nACSF, cells rapidly returned to their baseline membrane potential when the stimulus terminated (Fig. 3.2.1A). Two cells generated each two and eight action potentials more than  $\sim 17$  s after the stimulus offset, indicating that they were indeed maintained just below their firing threshold. A third cell also rapidly returned to baseline upon stimulus offset. However, within  $\sim 3$  s this cell depolarized and generated several action potentials while exhibiting a rather unstable membrane potential. Summarized, CA1



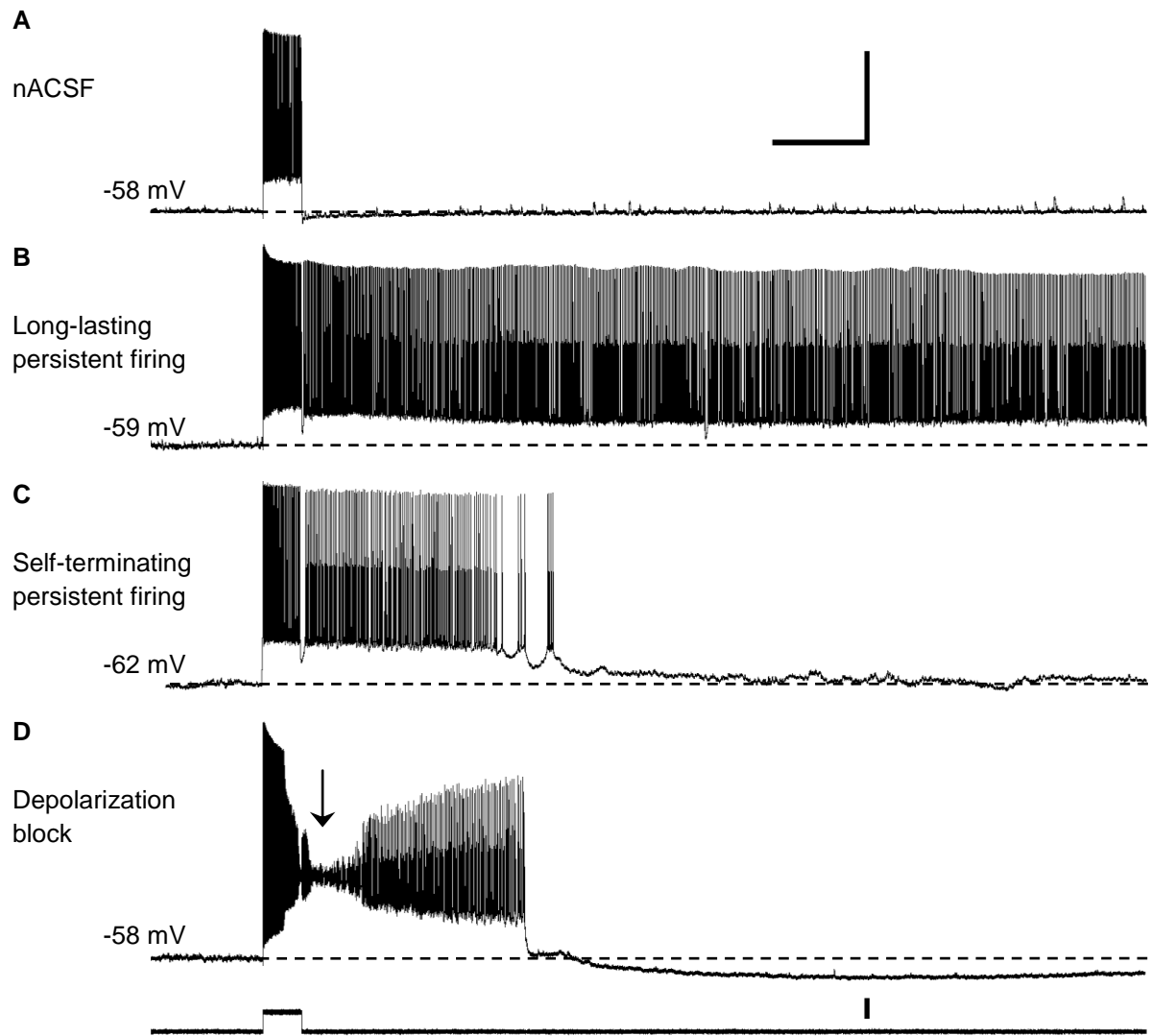


### Figure 3.2.1: CA1 pyramidal cells showed persistent firing in the presence of carbachol.

(A-D) The traces show the membrane potential from 5 s before until 30 s after a 2 s, 100 pA square current injection which is indicated at the bottom. Horizontal scale bar: 5 s. Vertical voltage scale bar: 40 mV. Vertical current scale bar: 100 pA.

(A) In the absence of carbachol (Cch), the suprathreshold current injection induced spiking which terminated upon the cessation of the stimulus and the membrane potential quickly returned to baseline. ID: 120122/R8/f70.

(B-D) During the bath application of 10  $\mu$ M Cch, cells showed different forms of persistent activity.

(B) The same cell as in (A) showed long-lasting persistent firing. I terminated the persistent firing after 56 s by injecting direct current that induced a hyperpolarization of the cell's membrane potential. ID: 120122/R8/f76.

(C) Another cell showed self-terminating persistent firing. The last action potential occurred 13 s after the stimulus offset. ID: 110901/L8/f27.

(D) Yet another cell showed run-away excitation that evolved to a transient depolarization block (arrow) and subsequently hyperpolarized while it transitionally generated action potentials before the membrane potential hyperpolarized below baseline. ID: 120123/R4/f103

Figure 1 a-d in Knauer et al. (2013) [63]; modified.

pyramidal cells did generally not show persistent firing when bathed in nACSF, which is in line with previous studies (e.g. [235,292]).

In contrast, once the superfusate contained Cch for an average of 9 min (SD: 2.7 min), the same cells resumed the generation of action potentials after the cessation of the stimulus (Fig. 3.2.1B-D). To recapitulate, these were the identical cells as before, they were again held just below their firing threshold which was more hyperpolarized, and they were exposed to the same current injection which induced more action potentials during the stimulation than in nACSF. Eleven of these fifteen cells engaged in persistent firing that lasted for more than 30 s, called long-lasting persistent firing (Fig. 3.2.1.B). Two cells demonstrated persistent firing that ceased firing 10 and 13 seconds after the stimulus offset, called self-terminating persistent firing (Fig. 3.2.1C). Another two cells exhibited run-away excitation that culminated in depolarization block (Fig. 3.2.1D). The latter will be further elaborated in the third chapter of this thesis.

The numerical data (Fig. 3.2.2A) supported the apparent phenomenon. The post-stimulus plateau potential ( $PP_{\text{fix}}$ ) was the difference between the average membrane potential across the fixed time interval at 10-20 s after the stimulus offset and the baseline membrane potential (for details method section 2.7.6). In the presence of Cch,  $PP_{\text{fix}}$  was significantly enhanced (paired  $T$ -test,  $T_{14} = 5.065$ ,  $p < 0.001$ ) compared to the absence of Cch (Fig. 3.2.2A). The post-stimulus firing frequency ( $FF_{\text{fix}}$ ) was the averaged action potential frequency at the same interval as  $PP_{\text{fix}}$  and yielded a significant increase (paired  $T$ -test,  $T_{14} = 5.542$ ,  $p < 0.001$ ) in spiking upon the switch from nACSF to Cch (Fig. 3.2.2A).

In the aforementioned experiments, the presence of Cch coincided with a longer time after gaining access to the soma. Consequently, the observed effects could have been due to the dilution of the cytosol with the intracellular fluid contained in the pipette. Wash-out experiments demonstrated that the observed effect was Cch-dependent and not mediated by diluting the cytosol (Fig. 3.2.2B). In detail, a subset of six cells was proceeded into a third condition during which nACSF with 10  $\mu\text{M}$  Cch was switched back to nACSF without Cch for an average of 16 min (SD: 3.4 min). A one-way repeated-measures analysis of variance (ANOVA; Greenhouse-Geisser correction) revealed that both  $PP_{\text{fix}}$  ( $F_{1,022,5.109} = 21.329$ ,  $p = 0.005$ ) and  $FF_{\text{fix}}$  ( $F_{1,5.002} = 32.042$ ,  $p = 0.002$ ) significantly differed across time. A Bonferroni-corrected *post-hoc* test pointed out that  $PP_{\text{fix}}$  and  $FF_{\text{fix}}$  significantly increased ( $p = 0.019$ ,  $p = 0.007$ , respectively) in response to the switch from nACSF to Cch and subsequently decreased ( $p = 0.015$ ,  $p = 0.007$ , respectively) in response to washing Cch out.

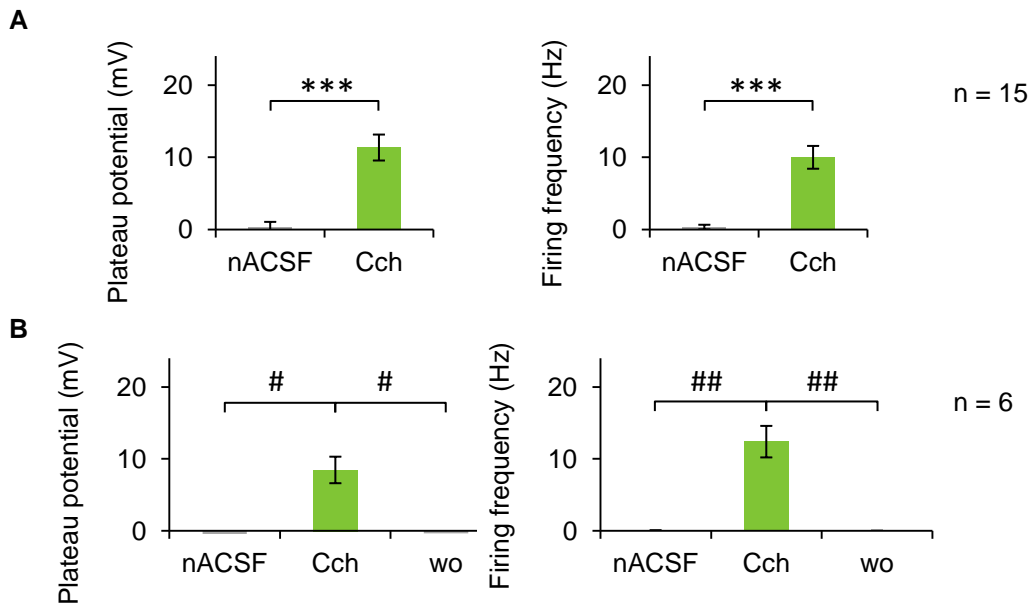


**Figure 3.2.2: Quantitative analysis of carbachol-dependent persistent firing in paired samples superfused with nACSF.**

(A) Fifteen cells were initially superfused with nACSF and subsequently with nACSF containing 10  $\mu$ M carbachol (Cch). The application of Cch induced a significant increase in the plateau potential and firing frequency ( $p < 0.001$ ) at 10-20 s after the stimulus offset, indicating that cellular activity outlasted the stimulus duration.

(B) A subset of six cells was exposed to three conditions. First nACSF, followed by Cch, and subsequently the wash out (wo) of Cch with nACSF. ANOVA signaled changes across time. A bonferroni-corrected *post-hoc* test showed that both the plateau potential ( $p \leq 0.019$ ) and the firing frequency ( $p = 0.007$ ) were significantly higher in the presence of Cch compared to its absence, indicating carbachol-dependence of the effect.

Figure 1f and g in Knauer et al. (2013) [63]; modified.

\*  $p < 0.05$ , \*\*  $p < 0.01$ . \*\*\*  $p < 0.001$ . #  $p < 0.05$ , as by bonferroni-corrected *post-hoc* tests. ##  $p < 0.01$ , as by bonferroni-corrected *post-hoc* tests.

These results indicate that persistent firing was Cch-dependent and could not be explained by the dilution of the cytosol with the intracellular fluid of the pipette.

### 3.2.2 Persistent firing was intrinsic to individual neurons

Persistent firing may be accomplished by reverberating excitation [26,27,30–32,26,27,30–32,34] or by mechanisms that are intrinsic to individual neurons [144,227]. Even though CA1 pyramidal neurons lack abundant excitatory recurrent connections [28,29] I tested the importance of fast ionotropic synaptic transmission on persistent firing. I blocked ionotropic glutamate receptors with 2 mM kynurenic acid and GABA<sub>A</sub> receptors with 0.1 mM picrotoxin in 35 cells. Despite the blocked fast ionotropic synaptic transmission (ACSF+SB), CA1

pyramidal neurons still showed persistent firing in the presence of 10  $\mu\text{M}$  Cch (Fig. 3.2.3). In particular, I observed the same response types, namely long-lasting persistent firing, self-terminating persistent firing and depolarization block, as in the absence synaptic blockers (cf. Fig. 3.2.1). A detailed comparison between nACSF and ACSF+SB in the presence of Cch is beyond the scope of this dissertation but can be found in Knauer et al. (2013) [63].

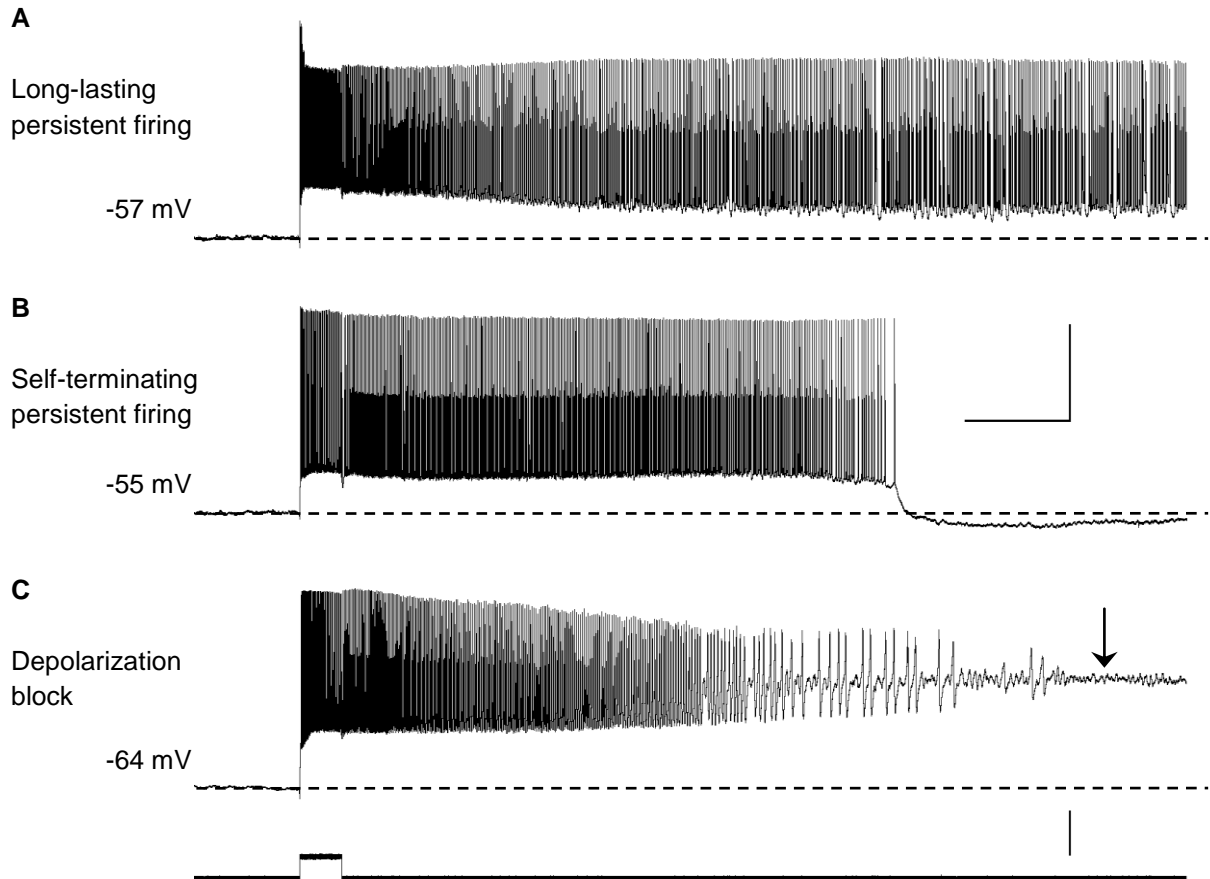


**Figure 3.2.3: Carbachol-dependent persistent firing during the blockade of fast ionotropic synaptic transmission.**

(A-C) CA1 pyramidal neurons engaged in different forms of persistent firing despite blocked ionotropic glutamate receptors (2 mM kynurenic acid) and GABA<sub>A</sub> receptors (0.1 mM picrotoxin). The trace at the bottom indicates the injected current.

(A) The majority of cells engaged in long-lasting persistent firing. Long-lasting persistent firing was marked by action potential generation for at least 30 s following the stimulus offset. ID: 111113/L7/f4.

(B) A subset of cells ceased firing within 30 s after stimulus offset. ID: 111013/R3/f6.

(C) A small subset of cells showed run-away excitation. The cell first showed persistent firing upon the cessation of the stimulus. However, the firing activity developed into depolarization block (arrow). ID: 111018/L6/f6.

Horizontal scale bar: 5 s. Vertical voltage scale bar: 40 mV. Vertical current scale bar: 100 pA.

Figure 2 a-c in Knauer et al. (2013) [63]; modified.

The fundamental insight from these experiments was that persistent firing of CA1 pyramidal neurons did apparently not require fast ionotropic synaptic transmission. In the following, the ACSF always contained synaptic blockers (ACSF+SB), unless stated otherwise.

Residual fast ionotropic synaptic transmission may have remained functional and may have supported persistent firing. If synaptic transmission would have facilitated persistent firing, the likelihood of excitatory postsynaptic potentials (EPSPs) should have been elevated during the post-stimulus interval compared to the baseline membrane potential. The EPSPs

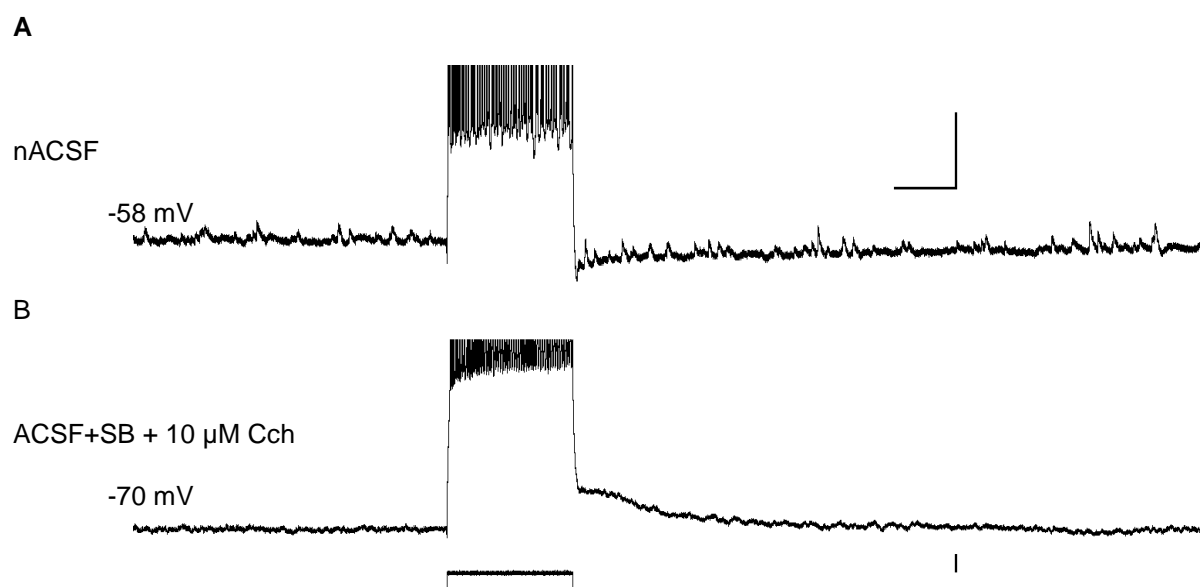


**Figure 3.2.4: In the presence of synaptic blockers, the likelihood of excitatory postsynaptic potentials was unaffected by the stimulus.**

(A, B) Traces show the cell's membrane potential 5 s preceding and 10 s following the current injection. Action potentials during the stimulation are truncated.

(A) The trace illustrates what kind of activity may be expected during the post-stimulus interval in the case of incomplete synaptic blockade. A cell in nACSF (without synaptic blockers) during the absence of carbachol (Cch) shows excitatory postsynaptic potentials (EPSPs) both before and after the 2 s current injection. ID: 120122/R8/f70.

(B) In ACSF+SB with 10  $\mu$ M Cch, a cell was held at -70 mV to allow the post-stimulus membrane potential to remain below firing threshold. The stimulus did not induce an increase in the likelihood of EPSPs during the post-stimulus interval compared to the pre-stimulus interval. These data indicate that fast ionotropic synaptic transmission was adequately blocked and did not contribute to persistent firing at more depolarized membrane potentials. ID: 110530/L2/f10.

Horizontal scale bar: 1 s. The vertical scale bar in A applies to all voltage signals: 10 mV. Vertical scale bar below (B): 0.1 nA.

could have originated from other neurons in the network whose persistent firing would have been triggered by the spiking activity of the recorded neuron during the stimulus interval. However, EPSPs during the post-stimulus interval may have been masked by action potential firing. Therefore, I maintained 13 neurons at a membrane potential of -70 mV which resulted in a subthreshold post-stimulus membrane potential. To induce a comparable number of action potentials during the stimulus interval, the amplitude of the injected current was increased to 200 pA, if necessary. The frequency of EPSPs was determined during a 5 s baseline interval and during the 10 s following the stimulus offset (Fig. 3.2.4). The stimulation did not induce a significant increase in EPSP frequency (paired *T*-test,  $T_{12} = 1.136$ ,  $p = 0.278$ ).

CA1 pyramidal neurons may not only communicate via chemical synapses. Moreover, nearby pyramidal neurons may be electrically coupled through gap junctions [293–296]. One marker for an inter-neuronal connection via gap junctions is dye coupling of neighboring cells [293]. Within the aforementioned 50 neurons, I observe dye-coupling in one cell. With regard to its electrophysiological properties, this cell was not apparently different from the remaining 49 neurons.

To assess a larger sample, I investigated all CA1 pyramidal neurons that I recorded from, irrespective of the superfusate and intracellular fluid composition, irrespective of the slice preparation method, and irrespective of the animal's age. I could evaluate potential dye-coupling in 367 of 387 (95%) pyramidal neurons whose somata were successfully stained with biocytin. Consistent documentation of any achieved whole cell configuration allowed me to confidently identify veritable dye-coupling and differentiate it from the staining of impaled but refused neurons (e.g. due to a non-silent RMP in the absence of Cch). Of the 367 neurons that could be evaluated, 22 (6%) showed some form of dye coupling. Of these 22 dye-coupled pyramidal neurons, twelve exhibited several considerably smaller spin offs that did not have a pyramidal-like morphology and were presumably interneurons. The remaining ten cells, i.e. < 3% of all stained pyramidal neurons, demonstrated dye-coupling with putative pyramidal neurons (Fig. 3.2.5). Electrotonic coupling between two pyramidal neurons could allow reciprocal excitation [293] and potentially support persistent firing. The persistent firing in these ten cells was not apparently different from the persistent firing in neurons for which no dye coupling was detected.

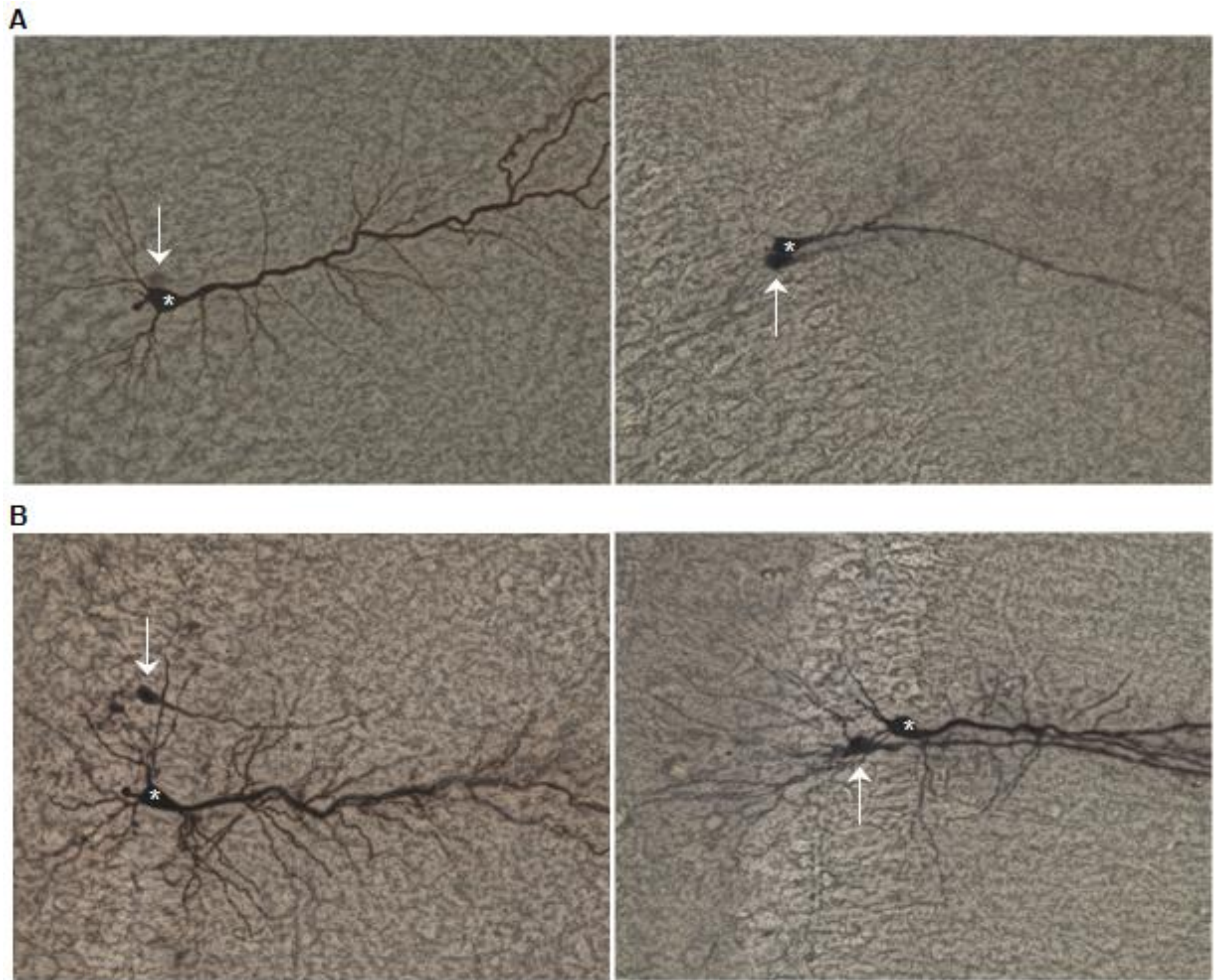


**Figure 3.2.5: Dye-coupling of CA1 pyramidal neurons occurred rarely.**

(A) In some cells, the second neuron (arrow) seemed to be in direct somatic contact to the neuron that I recorded from (star). Left ID:130709/L6. Right ID: 131223/R2.

(B) In other cells, the dendrites of the neuron that I recorded from (star) appeared to contact a second neuron (arrow). Left ID: 141024/R7. Right ID: 131222/R2.

A second indicator for electrotonic coupling are miniature action potentials\* [294]. Among the aforementioned 387 recordings from CA1 pyramidal neurons, miniature action potentials (Fig. 3.2.6, aka 'spikelets') were readily recognizable in five cell, i.e. <1.5%. Those five cells were exposed to four different combinations of intra- and extracellular fluids, which counteracted a meaningful interpretation of potential peculiarities in these recordings. Therefore, I did not pursue an in depth analysis of 'spikelets'.

\* For an alternative interpretation of 'spikelets' as field potentials from multiple nearby synchronized cells the interested reader is referred to [296].

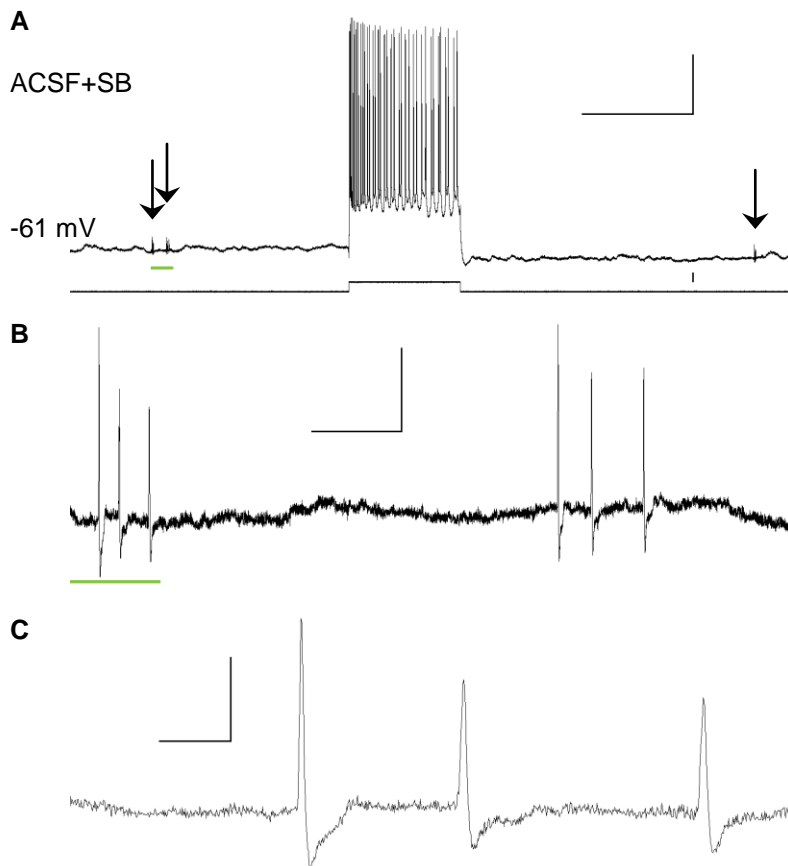


**Figure 3.2.6: Spikelets could be readily detected.**

(A) The top trace represents the membrane potential of a cell in artificial cerebrospinal fluid with synaptic blockers (ACSF+SB) from 5 s prior to a 2 s, 100 pA square pulse until 6 s after the cessation of the stimulus. Within the displayed time, three extraordinary events can be readily detected (arrows). ID:120618/R2/f93. Horizontal scale bar: 2 s. Vertical scale bar next to the voltage trace: 20 mV. Vertical scale bar between the top and bottom trace: 0.1 nA.

(B) The voltage signal shows the magnified trace of the section indicated by the green bar in (A). The graph unravels that the two pre-stimulus events are two bursts of each three events. Horizontal scale bar: 50 ms. Vertical scale bar: 2 mV.

(C) The voltage signal shows the magnified trace of the section indicated by the green bar in (B). The graph unravels an action potential like shape of the individual events within one burst. Hence, the events can be classified as miniature action potentials, aka 'spikelets'. Horizontal scale bar: 5 ms. Vertical scale bar: 2 mV.

If electrotonic coupling would be crucial for persistent firing, the robustness with which I observed persistent firing would contradict the low likelihood of indicators for electrotonic coupling. In addition to the low dye-coupling and the low 'spikelet' incidence rate, Cch was previously shown to suppress electrotonic coupling in CA1 [297]. In synopsis of the results of others and from my sample, electrotonic coupling does not appear to play a substantial role in Cch-dependent persistent firing and will not be further investigated within this dissertation.



Cch-dependent persistent firing appeared to be a phenomenon that was intrinsic to individual neurons because fast ionotropic synaptic transmission proved to be dispensable (Fig. 3.2.3), indicators for electrotonic coupling were sparse (Fig. 3.2.5, Fig. 3.2.6) and because Cch was previously shown to suppress electrotonic coupling [297].

### 3.2.3 Intrinsic persistent firing may be a physiologically plausible phenomenon

Whole cell patch clamp *in vitro* has the advantage of allowing a tight control over experimental parameters like the exposure to various chemical agents and different temperatures. However, the resemblance of the *in vivo* situation may be diminished. In the following, I address the stimulus duration and the age of the animals, and compile evidence indicating whether *in vitro* persistent firing may be physiologically plausible.

As stated earlier (cf. section 3.2.1), the firing frequency during the stimulation was significantly elevated in the presence of Cch compared to its absence. Furthermore, a 2 s long stimulation is a rather extended interval. The stimulus duration was in the order of hundreds of milliseconds in behavioral tasks which required short-term maintenance of information and during which persistent firing was recorded *in vivo* [55,213,214]. To mimic such short stimulus durations in behavioral tasks and to counteract the elevated firing frequency during the stimulus in the presence of Cch, I reduced the duration of the current injection from 2 s to 0.2 s (Fig. 3.2.7A&B). The stimulus amplitude was kept unchanged at 100 pA. Both protocols were tested in 26 cells that were bathed in ACSF+SB and 10  $\mu$ M Cch. These cells generated  $56.5 \pm 2.7$  action potentials during the 2 s long stimulus interval. In contrast, the same cells generated only  $8.1 \pm 0.4$  action potentials during the 0.2 s long stimulus interval. Generally speaking, the distribution of response types was comparable (Fig. 3.2.7C), despite the drastically reduced number of action potentials during the stimulus interval. The fraction of cells with depolarization block remained constant at 4% and that of long-lasting persistent firing was slightly reduced from 54% to 50%. Whereas the 2 s long stimulus was followed by self-terminating persistent firing in 42% of the cases, the same was true for only 27% of the responses following the 0.2 s long stimulus. This discrepancy was accompanied by the emergence of cells in which persistent firing could not be induced (0% and 19% in the 2 s and 0.2 s long stimulus protocol, respectively).  $PP_{\text{fix}}$  and  $FF_{\text{fix}}$  were not significantly affected by the reduction in the stimulus duration from 2 s to 0.2 s both in the entire sample of 26 cells (paired *T*-test,  $T_{25} \geq -1.603$ ,  $p \geq 0.112$ , Fig. 3.2.7D&E) and in the sample of nine cells that

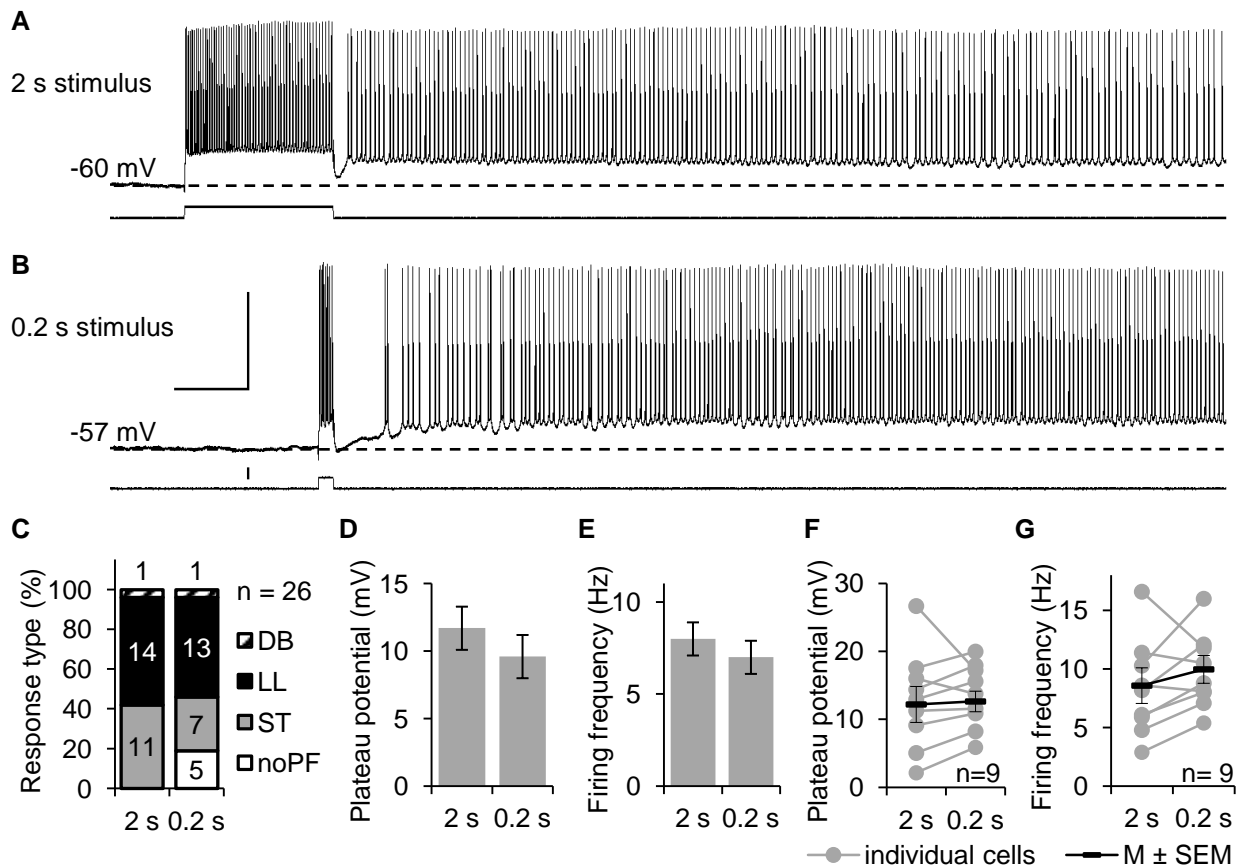


**Figure 3.2.7: Persistent firing was largely unchanged, despite a shortened stimulus duration.**

(A) The top trace shows the cell's membrane potential which exhibited persistent firing in response a 2 s, 100 pA current injection indicated at the bottom. ID: 111204/R8/f2.

(B) The top trace shows the persistent firing of the same cell which was stimulated with a 0.2 s, 100 pA current injection indicated at the bottom. Despite the shortened stimulus duration, the cell nonetheless responded with persistent firing. ID: 111204/R8/f12. Horizontal scale bar: 1s. Vertical voltage scale bar: 40 mV. Vertical current scale bar: 100 pA.

(C) The distribution of response types in the 26 tested cells was slightly altered when the stimulus duration was shortened. The likelihood of long-lasting persistent firing (LL) and depolarization block (DB) were comparable between the 2 s and the 0.2 s long stimulus durations. However, upon shortening the stimulus, the fraction of self-terminating persistent firing (ST) was reduced from 42% to 27% and gave rise to cells that did not respond with persistent firing (noPF) to the 0.2 s long stimulus.

(D&E) The plateau potential (D) and firing frequency (E) at 10-20s after the stimulus offset did not significantly change, despite the slightly altered distribution of response types (C).

(F&G) Nine cells showed long-lasting persistent firing both in response to the 2 s and the 0.2 s long stimulus. The plateau potential (F) and firing frequency (G) did not significantly change due to the shortening of the stimulus duration.

Figure 6 in Knauer et al. (2013) [63]; modified.

showed long-lasting persistent firing in both conditions (paired *T*-test,  $T_{25} \leq 1.401$ ,  $p \geq 0.199$ , Fig. 3.2.7F&G).

These results indicate that the aforementioned increase in firing frequency during the stimulus (cf. section 3.2.1) could not explain the emergence of persistent firing in the presence of Cch. Furthermore, these results show that persistent firing could also be induced with shorter stimuli that mimicked stimulus durations in behavioral tasks.

Whole cell patch clamp is the method of choice for the research project at hand because it allows tight control over intra- and extracellular media, and the study of cellular mechanisms. The throughput of this method is larger the younger the animals are. The disadvantage of investigating brains of juvenile animals is that their CA1 neurons [252,256,258,288], their hippocampal acetylcholine innervation [298] and the cell's response to cholinergic stimulation [254] might not yet be fully mature. Therefore, I tested whether persistent firing was a peculiarity of neurons from juvenile animals by comparing them to neurons from aged animals.

Aged animals showed impoverished performance in tasks that require the short-term retention of information [106]. Reduced neuronal excitability [107,110], presumably mediated by an enhanced afterhyperpolarization [109], could underlie the behavioral deficit [106,108]. Earlier in this dissertation, I replicated the reduced excitability in CA1 pyramidal neurons of aged compared to juvenile animals in the absence (Fig. 3.1.9E) and presence of Cch (Fig. 3.1.10E).

Hence, testing whether persistent firing in CA1 pyramidal neurons may be a peculiarity of immature tissue by using neurons from aged animals was a conservative approach. However this investigation could additionally provide insight into the ability of cells from aged animals to engage in persistent firing.

I obtained eleven recordings from seven male Long-Evans rats at an average age of 25.3 months (SD: 0.4 months). I compared these recordings to eleven recordings from seven randomly chosen male Long-Evans rats at an average age of 17.4 days (SD: 0.9 days). The recordings were collected in temporal proximity to the aged animals ensuring that the same set up and the same intracellular fluid were used.

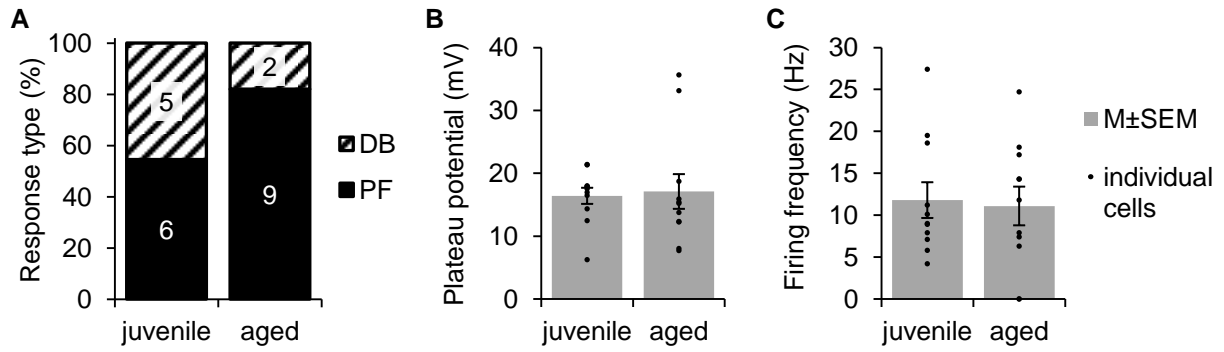


**Figure 3.2.8: Persistent firing was also observed in aged animals and was similar to that in juvenile animals.**

(A) The distribution of response types shows that persistent firing may be also elicited in CA1 pyramidal neurons from aged rats. In addition, just like in juvenile animals, run-away excitation that culminated in depolarization block was also observed in cells from aged animals.

(B&C) Neither the post-stimulus plateau potential (B) nor the post-stimulus firing frequency (C) was significantly different between neurons from juvenile and aged rats.

In the presence of 10  $\mu$ M Cch, 54.5% of the cells ( $n = 6$ ) from juvenile animals showed long-lasting persistent firing and the remaining 45.5% ( $n = 5$ ) showed depolarization block in response to a 2 s, 100 pA square current injection. During the superfusion of the same Cch concentration and the application of the same stimulus, 82% of the cells ( $n = 9$ ) from the aged animals showed long-lasting persistent firing and the remaining 18% ( $n = 2$ ) showed depolarization block. Therefore, the response-type distribution (Fig. 2.3.8A) indicated that long-lasting persistent firing was undoubtedly possible in aged animals, even though depolarization block was observed less frequently. Considering all cells, neither  $PP_{\text{fix}}$  (2-sample  $T$ -test, variance homogeneity,  $T_{20} = 0.227$ ,  $p = 0.824$ , Fig. 2.3.8B) nor  $FF_{\text{fix}}$  (2-sample  $T$ -test, variance homogeneity,  $T_{20} = -0.223$ ,  $p = 0.826$ , Fig. 2.3.8C) were significantly different between the cells from juvenile and aged animals. Furthermore, when considering only the cells that showed long-lasting persistent firing, neither the  $PP_{\text{fix}}$  (2-sample  $T$ -test, variance homogeneity,  $T_{13} = -0.821$ ,  $p = 0.427$ , juvenile:  $15.0 \pm 1.8$  mV; aged:  $13.3 \pm 1.2$  mV) nor  $FF_{\text{fix}}$  (2-sample  $T$ -test, variance homogeneity,  $T_{13} = 0.525$ ,  $p = 0.608$ , juvenile:  $11.9 \pm 2.5$  Hz; aged:  $13.6 \pm 2.0$  Hz) differed significantly between the two age groups.

These results indicate that Cch-dependent intrinsic persistent firing was not a peculiarity of neurons obtained from juvenile animals but could likewise be observed in aged animals. Thus, persistent firing in CA1 pyramidal neurons may be a physiological mechanism

in rats of any age. Furthermore, these results suggest that persistent firing was a robust phenomenon because it could be observed in CA1 pyramidal neurons of aged animals (Fig. 3.2.8) despite the curtailed excitability in these cells (Fig. 3.1.9, Fig. 3.1.10)

Because of the superior throughput while persistent firing was indistinguishable, juvenile animals were further used for studying the mechanism of persistent firing.

To recapitulate, the data indicate that intrinsic persistent firing may be a physiological mechanism supporting the short-term retention of information because it could be elicited by stimulus durations as short as those used in behavioral tasks and because it was not restricted to neurons from juvenile animals.

### 3.2.4 Mechanism underlying intrinsic persistent firing in CA1 pyramidal neurons

After having shown that CA1 pyramidal neurons have the propensity to show persistent firing (section 3.2.1), that this persistent firing is intrinsic to individual neurons (section 3.2.2) and that it may be a phenomenon with physiological relevance (section 3.2.3), I will now elaborate on the underlying mechanisms.

As outlined previously, the persistent firing in CA1 pyramidal neuron required the presence of Cch (Fig. 3.2.2B). Cch is a poorly hydrolyzable non-specific cholinergic agonist. and may act on both muscarinic and nicotinic acetylcholine receptors. Previous studies on the entorhinal cortex [119,299], the anterior cingulate cortex [229] and lateral amygdala [223] showed that muscarinic acetylcholine receptors were crucial for persistent firing. To test, whether this is also true for CA1 pyramidal neurons, the muscarinic antagonist atropine was co-applied in the presence of Cch. Out of six cells, five showed persistent firing (3x long-lasting; 2x self-terminating, Fig. 3.2.9A top) and one showed depolarization block in response to a 2s, 100 pA stimulus when bathed in ACSF+SB with 10  $\mu$ M Cch. Following an average superfusion-time of 6 min (SD: 1.7 min), the same stimulus failed to induce persistent firing in the presence of 2  $\mu$ M atropine (Fig. 3.2.9A bottom). Both  $PP_{\text{fix}}$  (paired  $T$ -test,  $T_5 = -8.599$ ,  $p < 0.001$ , Fig. 3.2.9C) and  $FF_{\text{fix}}$  (paired  $T$ -test,  $T_5 = -7.121$ ,  $p = 0.001$ , Fig. 3.2.9D) were significantly reduced when atropine was bath applied. These results indicate that Cch-dependent persistent firing was mediated by muscarinic acetylcholine receptors.

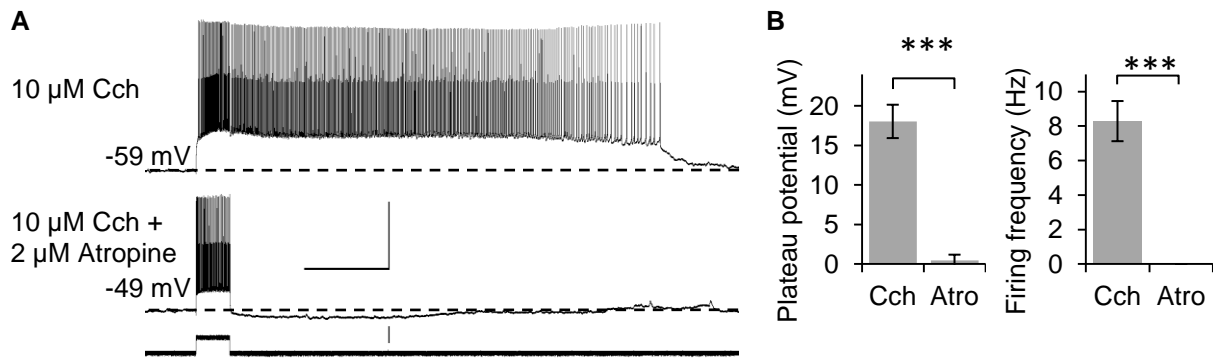


**Figure 3.2.9: Muscarinic acetylcholine receptors were required for intrinsic persistent firing of CA1 pyramidal neurons.**

(A) The top trace shows a cell that responded with self-terminating persistent firing to a 2 s, 100 pA square current injection (bottom trace) while being bathed ACSF+SB with 10 μM carbachol (Cch). ID: 111013/R3/f6. The signal in the middle shows the membrane potential of the same neuron but now additionally exposed to 2 μM atropine. In the presence of atropine, the cell no longer engaged in persistent firing. ID:111013/R3/f23. Horizontal scale bar: 5 s. Vertical voltage scale bar: 40 mV. Vertical current scale bar: 0.1 nA.

(B) Both the post-stimulus plateau potential (left) and firing frequency (right) were significantly reduced upon the co-application of atropine (Atro). \*\*\*  $p < 0.001$ .

Figure 5b, d and e in Knauer et al. (2013) [63]; modified.

The stimulation of muscarinic acetylcholine receptors (mAChRs) initiates a multitude of intracellular signaling cascades. One of these cascades induces the blockade of potassium ( $K^+$ ) channels [152,175]. Another cascade leads to the facilitation of a calcium-sensitive non-selective cationic currents ( $I_{CAN}$ ) [144]. Both signaling pathways of muscarinic stimulation have a net excitatory effect. Firstly, I will address the blockade of  $K^+$  channels. Thereafter, I will focus on the facilitation of non-selective cation currents.

The activation of mAChRs blocks voltage-gated  $K^+$  currents as well as calcium-sensitive  $K^+$  currents [300,301]. The voltage-gated potassium currents ( $I_M$ ) are mediated by  $K_{v7.2}$  and  $K_{v7.3}$  channels [181]. Despite the strong historic link between  $I_M$  and muscarinic stimulation,  $I_M$  was for example shown to be not involved in learning induced reductions of the post-burst afterhyperpolarizations [302]. The calcium-activated  $K^+$  currents are mediated by small-conductance  $K^+$  channels (SK-channels, [186,187]). Not only the synaptic subset of SK-channels are blocked by the bath application of cholinergic agonists [191–193].

To test whether the blockade of the aforementioned  $K^+$  currents may explain mAChR-dependent persistent firing, I blocked both the M and the SK currents, and injected a 2 s, 100 pA square pulse to six cells. While superfused with ACSF+SB the cells engaged in spiking activity during the stimulus and quickly returned to their just subthreshold baseline membrane

potential as soon as the stimulus terminated (Fig. 3.2.10A). During the subsequent bath-application of 20  $\mu\text{M}$  XE991 ( $I_M$  blocker, 180) together with 0.1  $\mu\text{M}$  apamin (SK2 channel blocker) for an average of 9.7 min (SD: 0.6 min), five out of six cells entered depolarization block during the stimulation. The remaining cell engaged in seemingly runaway excitation which did not culminate in depolarization block within the stimulus interval. Upon the cessation of the stimulus, all six cells quickly returned to their just subthreshold baseline membrane potential (Fig. 3.2.10B), as they did in the absence of  $\text{K}^+$  channel blockers. Neither  $\text{PP}_{\text{fix}}$  (paired  $T$ -test,  $T_5 = -1.062$ ,  $p = 0.337$ , ACSF+SB:  $-0.8 \pm 0.35$  mV,  $\text{K}^+$  channel blockers:  $-1.4 \pm 0.40$  mV) nor  $\text{FF}_{\text{fix}}$  (paired  $T$ -test,  $T_5 = -1.000$ ,  $p = 0.363$ , ACSF+SB:  $0.1 \pm 0.1$  Hz,  $\text{K}^+$  channel blockers:  $0 \pm 0$  Hz) were significantly affected by the addition of  $\text{K}^+$  channel blockers.

In line with previous reports [236], the results indicate that the muscarinic blockade of voltage-gated and calcium-activated  $\text{K}^+$  currents is insufficient to induce persistent firing.

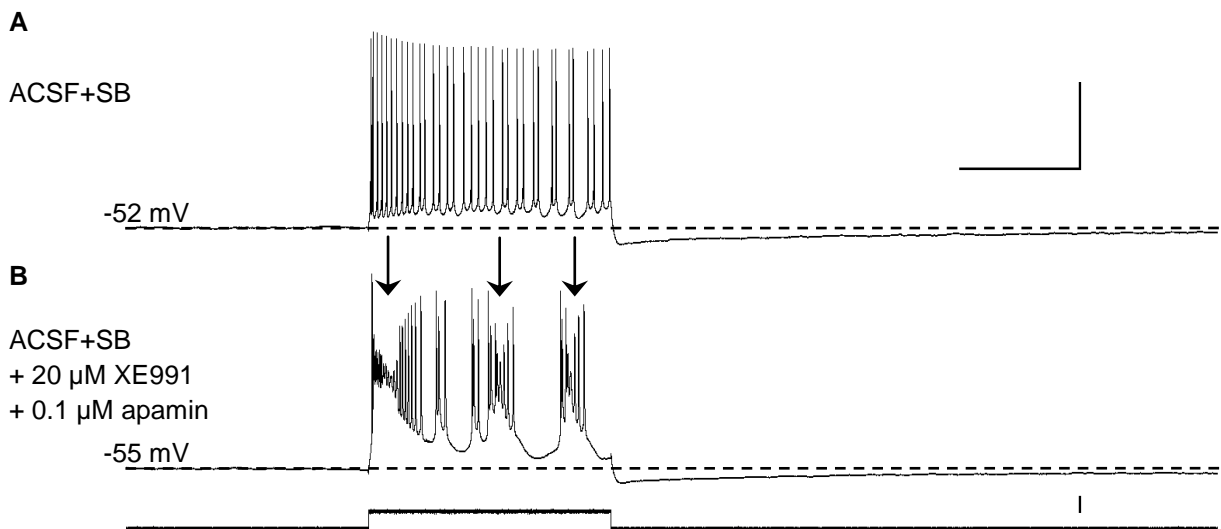


**Figure 3.2.10: Sole potassium channel blockade did not induce persistent firing.**

(A) During the superfusion of artificial cerebrospinal fluid with synaptic blockers (ACSF+SB) the CA1 pyramidal neuron responded with action potential generation during a 2 s long, 100 pA strong square pulse (bottom trace in (B)). Upon the cessation of the stimulus, the cell quickly returned to its just subthreshold baseline membrane potential. Horizontal scale bar: 1 s. Vertical scale bar: 40 mV. ID: 140428/L6/f73.

(B) While ACSF+SB with 20  $\mu\text{M}$  XE991 ( $\text{K}_{v7.2}$ ,  $\text{K}_{v7.3}$  blocker) and with 0.1  $\mu\text{M}$  apamin (SK2 blocker) was superfused, the cell responded with depolarization block (arrows) to the current stimulus. Upon the cessation of the stimulus the cell quickly returned to its just subthreshold baseline membrane potential and did not engage in persistent firing. Vertical scale bar: 100 pA. ID: 140428/L6/f90.

In addition to the blockade of  $K^+$  channels, muscarinic stimulation also facilitates the conductance of calcium-sensitive non-selective cationic currents ( $I_{CAN}$ , [303]). To test for the calcium sensitivity of this depolarizing conductance, I added the fast calcium chelator BAPTA to the intracellular fluid of nine cells. I compared their response to a 2 s, 100 pA current injection with the response of nine randomly chosen cells that were exposed to normal intracellular fluid (nICF). Of the nine randomly chosen control cells, eight showed long lasting persistent firing (Fig. 3.2.11A). The remaining cell engaged in runaway excitation that culminated in depolarization block. In contrast, of the nine cells exposed to 10 mM BAPTA in their intracellular fluid, three cells did not generate any action potentials after the stimulus offset. Two cells generated one and three action at 27 s and >22s after the stimulus offset, respectively. The remaining four cells showed faint persistent firing at frequencies below 4 Hz. In line with the apparent attenuation of persistent firing (Fig. 3.2.11B), both  $PP_{fix}$  (2-sample  $T$ -test, variance homogeneity,  $T_{16} = -6.083$ ,  $p < 0.001$ , Fig. 3.2.11C) and  $FF_{fix}$  (2-sample  $T$ -test, no variance homogeneity,  $T_{10.024} = -7.277$ ,  $p < 0.001$ , Fig. 3.2.11D) were significantly reduced in cells exposed to 10 mM BAPTA compared to control cells exposed to nICF.

These results indicate that an elevation of the intracellular calcium concentration is required for respectable persistent firing.

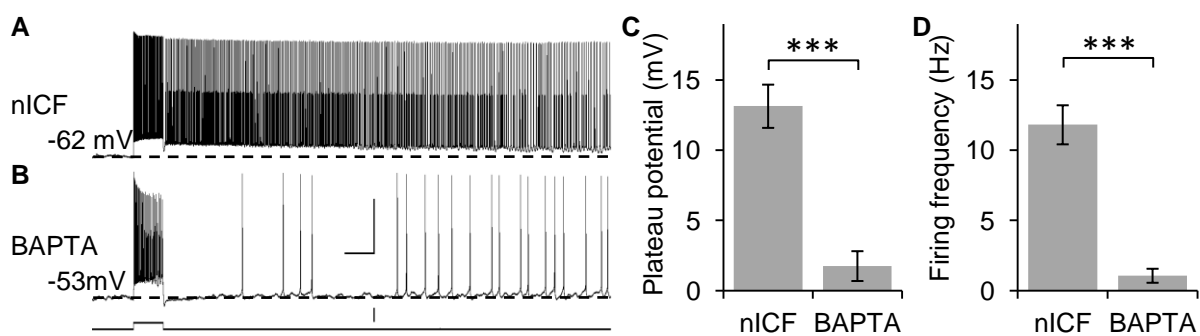


**Figure 3.2.11: Chelating intracellular calcium impeded persistent firing.**

(A) While bathed in ACSF+SB and 10  $\mu$ M Cch, a cell that was exposed to normal intracellular fluid (nICF) showed long-lasting persistent firing in response to a 2 s, 100 pA square pulse. ID: 121115/L1/f14.

(B) A different cell bathed in the same extracellular solution as the cell in (A) but exposed to intracellular fluid that contained the fast calcium chelator BAPTA (10 mM) showed faint persistent firing in response to the same current stimulation. ID: 120618/L3/f28. Horizontal scale bar: 2 s. Vertical voltage scale bar: 40 mV. Vertical current scale bar: 0.2 nA.

(C&D) Both the post-stimulus plateau potential (C) and firing frequency (D) were significantly reduced in the nine cells exposed to 10 mM BAPTA compared to nine cells exposed to nICF. \*\*\*  $p < 0.001$ .



Canonical transient receptor potential (TRPC) channels are thought to underlie  $I_{CAN}$  which is proposed to mediate persistent firing [144]. The TRPC channels 1, 4 and 5 are gated by intracellular cascades that are initiated by  $G_{q/11}$  G-proteins (see introduction chapter 3). Amongst other receptors, mAChRs couple to  $G_{q/11}$  G-proteins [175]. Hence mAChR stimulation presumably activates TRPC channels [144]. The precise gating mechanism of TRPC channels are still incompletely understood [144]. Consequently, tools that allow control over TRPC channels are scarce.

In a expression system (human embryonic kidney cells) TRPC5 channels were shown to be inhibited by intracellular adenosine triphosphate (ATP; [246]). To test for the involvement of TRPC5 channels in persistent firing, I elevated the intracellular ATP concentration from 4 mM in the nICF to 10 mM in a modified ICF. In the continuous presence of 10  $\mu$ M Cch, I compared the response to a 2 s, 100 pA square current injection from 15 cells exposed to 10 mM ATP to randomly chosen 15 cells exposed to the nICF. At the standard intracellular dilution time with an average of 23 min (SD: 6.8 min), the cells exposed to nICF and 10 mM ATP showed persistent firing in 12 and 13 out of 15 cells, respectively. The remaining 3 and 2 cells, respectively, engaged in depolarization block. In line with these phenomenological similarities (Fig. 3.2.12A), neither  $PP_{fix}$  (2-sample  $T$ -test, no variance homogeneity,  $T_{20,3097} = -0.247$ ,  $p = 0.807$ , Fig.3.2.12B) nor  $FF_{fix}$  (2-sample  $T$ -test, variance homogeneity,  $T_{28} = -0.537$ ,  $p = 0.537$ , Fig. 3.2.12C) differed significantly between the cells exposed nICF and those exposed to an elevated ATP concentration after the standard dilution time. However, diligent observation indicated a subtle but consistent attenuation of persistent firing across time in cells exposed to 10 mM ATP. Therefore, nine of the 15 cells were followed up for more prolonged dilution times. Because persistent firing may desensitize in response to prolonged dilution times, irrespective of the ICF, a simple standard time vs. late comparison within the cells exposed to 10 mM ATP would be inappropriate. Therefore, a subset of seven cells out of the aforementioned 15 cells exposed to nICF were also followed up for more prolonged dilution times (Tab. 3.2.1) .

**Table 3.2.1: Intracellular dilution times of the cells exposed to 4 and 10 mM ATP.**

Subsets of the initial 15 cells in each group were followed up for more prolonged times of intracellular dilution.

	N	standard (M $\pm$ SD)	late (M $\pm$ SD)	change (M $\pm$ SD)
4 mM ATP (nICF)	7	25 $\pm$ 1.2 min	49 $\pm$ 2.3 min	24 $\pm$ 6.5 min
10 mM ATP	9	23 $\pm$ 2.2 min	49 $\pm$ 2.4 min	26 $\pm$ 7.9 min

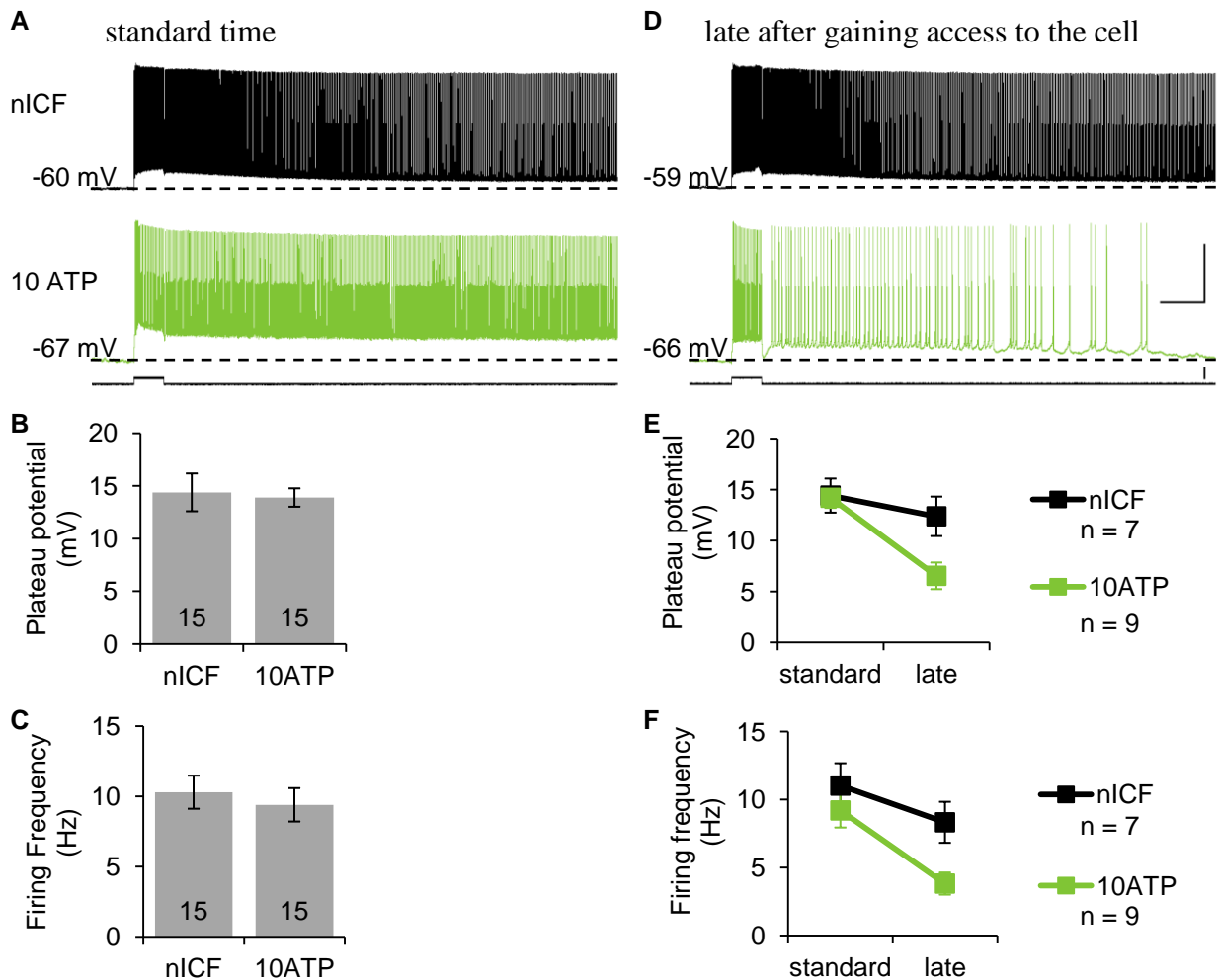


**Figure 3.2.12: Elevated ATP concentrations in the intracellular fluid attenuated persistent firing if prolonged dilution times were allowed.**

(A) During the superfusion of 10  $\mu$ M carbachol in ACSF+SB, cells were tested for persistent firing with a 2 s, 100 pA square pulse (bottom). At the standard dilution time, the persistent firing in cells exposed to the normal intracellular fluid (nICF, top, 4 mM ATP, ID: 121107/L7/f125) and those exposed to elevated ATP concentrations (middle, 10 mM ATP, ID: 121024/L8/f155) was comparable.

(B) The post-stimulus plateau potential at the standard dilution time was not significantly different between the cells exposed to 4 (nICF) or 10 mM ATP.

(C) The post-stimulus firing frequency at the standard dilution time was not significantly different between the cells exposed to 4 (nICF) or 10 mM ATP.

(D) The traces show signals from the same cells as in (A) but after a prolonged intracellular dilution. The persistent firing of the cell exposed to nICF (top, 4 mM ATP, ID: 121107/L7/f136) was unchanged. In contrast, the cell exposed to 10 mM ATP (middle, ID: 121424/L8/f181) showed attenuated persistent firing. Horizontal scale bar: 3 s. Vertical voltage scale bar: 40 mV. Vertical current scale bar: 0.2 nA.

(E) The plateau potential decreased significantly over time, irrespective of the ICF. Furthermore, this plateau potential reduction was significantly more pronounced in cells exposed to 10 mM ATP compared to 4 mM ATP.

(F) The firing frequency decreased significantly over time, irrespective of the intracellular fluid. Furthermore, there was a trend towards a lower firing frequency in cells exposed to 10 mM ATP compared to those exposed to nICF, irrespective of the time.

I conducted a mixed design 2x2 ANOVA with the subjects being CA1 pyramidal neurons, the between subject factor being the ATP concentration in the ICF (4 mM vs. 10 mM), and the within subject factor being time (standard vs. late). Irrespective of the intracellular dilution time,  $PP_{\text{fix}}$  was not significantly ( $F_{1,14} = 2.550$ ,  $p = 0.133$ ) different between the cells exposed to 4 or 10 mM ATP (i.e. no significant main effect of ATP concentration). However,  $PP_{\text{fix}}$  significantly ( $F_{1,14} = 36.016$ ,  $p < 0.001$ ) decreased over the prolonged dilution times, irrespective of the intracellular ATP concentration (i.e. significant main effect of time). Furthermore, the decrease in  $PP_{\text{fix}}$  was significantly ( $F_{1,14} = 12.102$ ,  $p = 0.004$ ) more pronounced in cells exposed to 10 mM ATP compared to those exposed to 4 mM ATP (i.e. significant time\*ATP concentration interaction). Like  $PP_{\text{fix}}$ , also  $FF_{\text{fix}}$  decreased significantly ( $F_{1,14} = 25.945$ ,  $p < 0.001$ ) over time, irrespective of the intracellular ATP concentration (i.e. significant main effect of time). However, the magnitude of the decrease over time in  $FF_{\text{fix}}$  was not significantly ( $F_{1,14} = 2.851$ ,  $p = 0.113$ ) different between the cells exposed to different concentrations of intracellular ATP (no significant time\*ATP concentration interaction). This lack of interaction could be explained by a trend ( $F_{1,14} = 3.668$ ,  $p = 0.076$ ) towards a lower  $FF_{\text{fix}}$  in cells exposed to 10 mM ATP compared to those exposed to 4 mM ATP, irrespective of the intracellular dilution time (i.e. trend towards main effect of ATP concentration).

Taken together and assuming a blockade of TRPC5 channels by intracellular ATP [246], these results indicate that TRPC5 channels support persistent firing in CA1 pyramidal neurons.

The intracellular ATP is grossly unspecific for blocking TRPC5 because it also has extensive metabolic functions (reviewed in Dunwiddie and Masino (2001) [304]) and furthermore gates ATP-sensitive potassium channels which may shape firing properties [305]. Therefore, I tested the non-selective TRPC channel blocker flufenamic acid (FFA) [306,307]. During the bath application of 10  $\mu\text{M}$  Cch in ACSF+SB, persistent firing was induced in seven cells. Four cells showed long-lasting persistent firing and three cells showed self-terminating persistent firing. Subsequently, 100  $\mu\text{M}$  FFA was bath-applied for an average of 9 min (SD: 2.6 min) together with 10  $\mu\text{M}$  Cch. Despite the presence of Cch, only one cell showed long-lasting persistent firing with a reduced firing frequency, two cells showed self-terminating persistent firing and four cells showed a complete blockade of persistent firing. In line with the apparent attenuation of persistent firing (Fig. 3.2.13A), also  $PP_{\text{fix}}$  (Fig. 3.2.13B, paired  $T$ -test,  $T_6 = -3.687$ ,  $p = 0.010$ ) and  $FF_{\text{fix}}$  (Fig. 3.2.13C, paired  $T$ -test,  $T_6 = -2.471$ ,  $p = 0.048$ ) were significantly reduced.

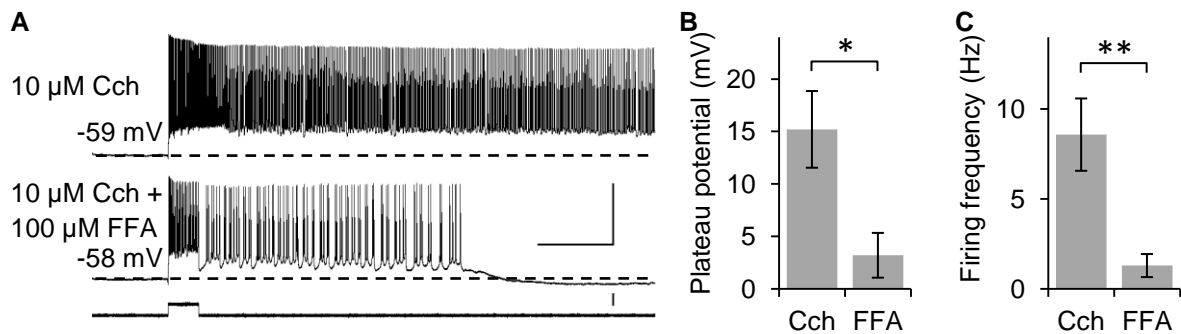


**Figure 3.2.13: Flufenamic acid attenuated carbachol-dependent persistent firing.**

(A) A cell was first superfused with artificial cerebrospinal fluid with synaptic blockers and 10  $\mu\text{M}$  Cch and showed long-lasting persistent firing. Subsequent co-application of 100  $\mu\text{M}$  flufenamic acid (FFA) attenuated persistent firing in the same cell which then showed self-terminating persistent firing. ID: 111009/L6/f5&28. Vertical voltage scale bar: 40 mV. Horizontal scale bar: 5 s. Vertical current scale bar: 0.1 nA.

(B) The post-stimulus plateau potential was significantly reduced upon the bath-application of FFA. \*  $p < 0.05$ .

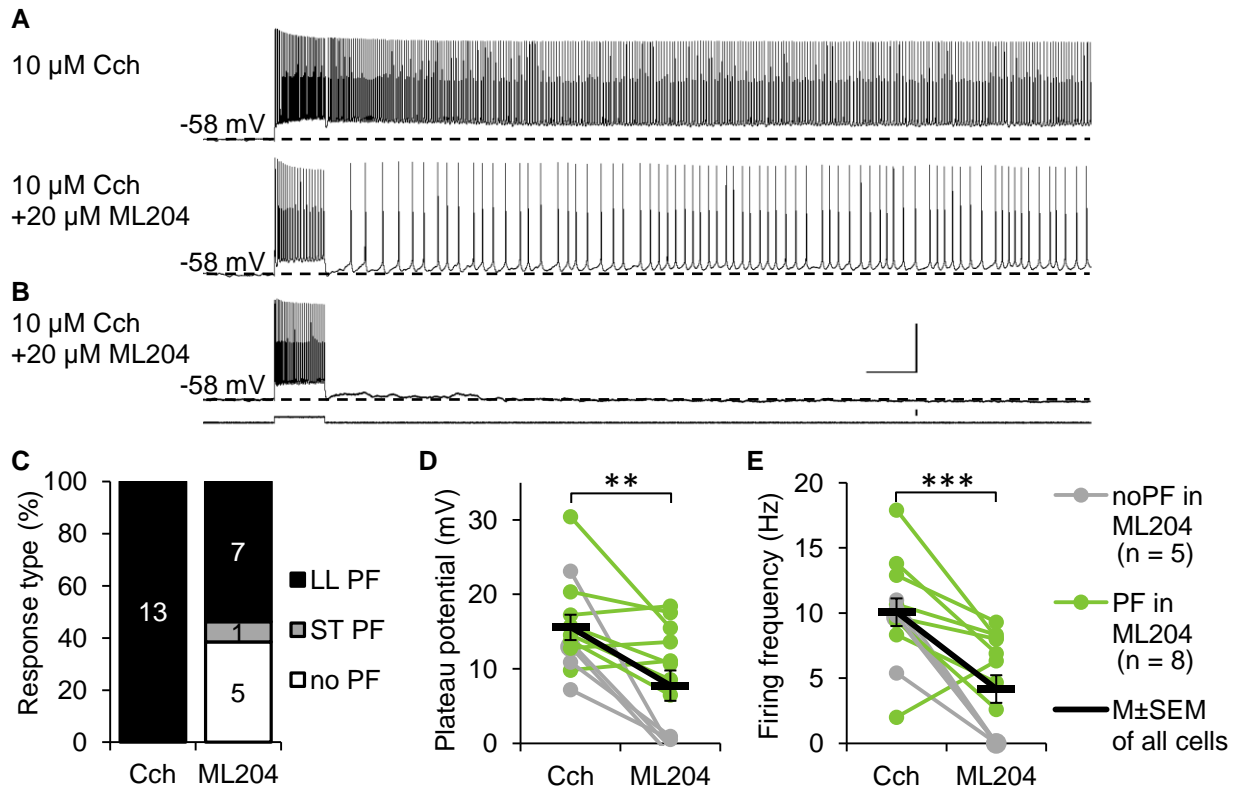
(C) The post-stimulus firing frequency was significantly reduced upon the bath-application of FFA. \*\*  $p < 0.01$ .

Figure 5c-e in Knauer et al. (2013) [63]; modified.

These results indicate that TRPC channels were involved in Cch-dependent persistent firing of CA1 pyramidal neurons.

However, FFA is not only a non-specific TRPC channel blocker but also impacts other membrane currents [308,309] which may influence the interpretation of the above mentioned results. Fortunately, a novel TRPC channel antagonist with relative selectivity for TRPC4 over TRPC3 over TRPC5 and over TRPC6 (in descending order) was introduced [244] and reported as TRPC4/5 channel antagonist [243]. Therefore; I aimed to complement the previous results suggesting an involvement of TRPC channels in persistent firing by using ML204. Due to technical challenges (for details see methods section 2.2), cells that were exposed to ML204 were maintained at a recording temperature of  $30 \pm 1^\circ\text{C}$  all along. Because I adopted a within-cell comparison of the response before and during the application of ML204, the effect of the reduced temperature (in contrast to the  $35 \pm 1^\circ\text{C}$  in all other experiments) on properties of CA1 pyramidal cells is beyond the scope of this dissertation.

Thirteen out of 23 neurons responded to a 2 s, 100 pA square pulse with long-lasting persistent firing in ACSF+SB with 10  $\mu\text{M}$  Cch maintained at  $30 \pm 1^\circ\text{C}$ . The remaining ten cells, showed depolarization block. At this point, I will focus on the thirteen cells that showed long-lasting persistent firing. When I subsequently stimulated these thirteen cells with the same current injection while they were superfused with 20  $\mu\text{M}$  ML204 in addition to the



**Figure 3.2.14: Persistent firing was attenuated by the bath-application of the TRPC4/5 channel blocker ML204.**

(A) A cell superfused with 10  $\mu\text{M}$  carbachol (Cch) showed long-lasting persistent firing in response to a 2s, 100 pA square pulse (bottom trace in (B)). The same cell showed attenuated long-lasting persistent firing during the co-application of 20  $\mu\text{M}$  ML204. ID: 140925/R6/f14&45.

(B) The trace displays a different cell bathed in 10  $\mu\text{M}$  Cch and 20  $\mu\text{M}$  ML204 exhibiting a depolarizing afterpotential (top trace) in response to the same current injection as in (A) (bottom trace). ID: 140926/R5/f44. Horizontal scale bar: 2s. Vertical voltage scale bar: 40 mV. Vertical current scale bar: 0.1 nA.

(C) The majority of the cells (61.5%,  $n = 8$ ) continued to show persistent firing in the presence of 20  $\mu\text{M}$  ML204. Among these eight cells were seven that still showed long-lasting persistent firing (LL PF). The remaining cell showing persistent firing in the presence of 20  $\mu\text{M}$  ML204 engaged in self-terminating persistent firing (ST PF). In five cells (38.5%) persistent firing could no longer be induced (no PF) while 20  $\mu\text{M}$  ML204 was co-applied.

(D&E) The connected dots represent the 13 neurons tested in the Cch-only condition (Cch) and during the subsequent co-application of ML204 (ML204). The five cells that did not show persistent firing in ML204 are colored grey. The eight cells that engaged in persistent firing despite the presence of 20  $\mu\text{M}$  ML204 are colored green. The connected black bars represent the  $M \pm \text{SEM}$  across all thirteen cells. The black indicators for significance refer to the average across all cells. \*\*  $p < 0.01$ , \*\*\*  $p < 0.001$

(D) The post-stimulus plateau potential across 10-20 s after the stimulus offset ( $PP_{\text{fix}}$ ) was significantly attenuated in the 13 cells tested. The reduction of  $PP_{\text{fix}}$  in the subset of eight cells that still exhibited persistent firing in the presence of 20  $\mu\text{M}$  ML204 (green dots) showed a trend towards significance ( $p = 0.075$ ).

(E) The post-stimulus firing frequency across 10-20 s after the stimulus offset ( $FF_{\text{fix}}$ ) was significantly diminished in the 13 cells tested. Furthermore, the reduction of  $FF_{\text{fix}}$  in the subset of eight cells that still showed persistent firing in the presence of 20  $\mu\text{M}$  ML20 (green dots), was also significant ( $p = 0.004$ ).

10  $\mu\text{M}$  Cch for an average of 16 min (SD: 2.7 min), the fraction of persistent firing cells was reduced to 61.5% (8 cells). Among those eight persistent firing cells, one ceased firing at  $\sim 27$  s after the stimulus offset and therewith showed self-terminating persistent firing. The remaining five cells (38.5%) no longer engaged in persistent firing in the presence of 20  $\mu\text{M}$  ML204 (Fig. 3.2.14C). In line with the change in response-type likelihood, the co-application of 20  $\mu\text{M}$  ML204 reduced both  $\text{PP}_{\text{fix}}$  (paired  $T$ -test,  $T_{12} = 3.786$ ,  $p = 0.003$ , Fig. 3.2.14D) and  $\text{FF}_{\text{fix}}$  (paired  $T$ -test,  $T_{12} = 4.773$ ,  $p < 0.001$ , Fig 3.2.14E) significantly, when considering all 13 cells. Even the eight cells that still showed persistent firing in the presence of ML204, mostly exhibited an attenuated response (Fig. 3.2.14B,D&E) when compared to the response of the same cells in the Cch-only condition (Fig 3.2.14A,D&E). This was also apparent in a trend towards an attenuated  $\text{PP}_{\text{fix}}$  (paired  $T$ -test,  $T_7 = -2.092$ ,  $p = 0.075$ , Cch:  $16.8 \pm 2.23$  mV, ML204:  $12.7 \pm 1.51$  mV) and a significantly diminished  $\text{FF}_{\text{fix}}$  (paired  $T$ -test,  $T_7 = -2.521$ ,  $p = 0.004$ , Cch:  $10.6 \pm 1.64$  Hz, ML204:  $6.8 \pm 0.78$  Hz) in the eight cells that still showed persistent firing in the presence of ML204.

These data indicate that TRPC4/5 channels were required for a respectable Cch-dependent persistent firing in CA1 pyramidal neurons.

### 3.2.5 Sensitivity of persistent firing to the carbachol concentration

Besides applying Cch at a concentration of 10  $\mu\text{M}$ , as throughout this chapter, I also elicited persistent firing in independent subsets of cells during the presence of 5 and 20  $\mu\text{M}$  Cch. To assess whether the Cch concentration affected persistent firing in a significantly linear fashion, I conducted a linear regression (analogue analysis in Axmacher et al. (2010) [279]). The investigation revealed that  $\text{PP}_{\text{fix}}$  ( $p = 0.047$ ,  $R^2 = 0.059$ , Fig. 3.2.15A), but not  $\text{FF}_{\text{fix}}$  ( $p = 0.231$ ,  $R^2 = 0.022$ , Fig. 3.2.15B) was significantly modulated by the carbachol concentration.

These results indicate that the Cch concentration and the accompanying changes in intrinsic cellular properties (Fig. 3.1.7) modulated the post-stimulus plateau potential which kept increasing with increasing Cch concentrations. However, the post stimulus firing frequency appeared to have reached a plateau.

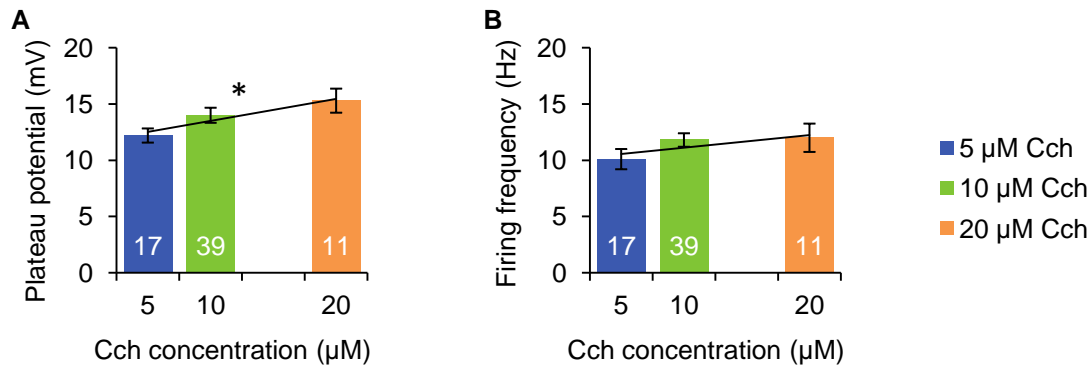


**Figure 3.2.15: Modulation of persistent firing by the carbachol concentration.**

(A) The post-stimulus plateau potential during 10 to 20 s after the cessation of a 2 s, 100 pA square pulse followed a significant linear increase with an increasing carbachol (Cch) concentration.

(B) The post-stimulus firing frequency during 10 to 20 s after the cessation of a 2 s, 100 pA square pulse was not significantly different during the presence of different concentrations of Cch.

### 3.2.6 Sensitivity of persistent firing to inter-cellular variability within CA1

To assess whether persistent firing was uniform across CA1 pyramidal cells, I investigated the linear correlation of  $PP_{fix}$  and  $FF_{fix}$  with passive membrane potential properties, the action potential properties, the animals' maturation (P14-24), the hyperpolarization activated current ( $I_h$ ), and the cell's location in the dorso-ventral and proximo-distal axis. I will report the results of linear regressions throughout this section because each of the variables that are related to one another have a metric level of measurement.

During the superfusion of 10 µM Cch,  $PP_{fix}$  correlated significantly with the action potential threshold ( $p = 0.013$ ,  $R^2 = 0.157$ ) such that  $PP_{fix}$  was more pronounced the more depolarized the action potential threshold was. Furthermore,  $PP_{fix}$  was significantly more pronounced, the more depolarized the post-burst membrane potential was ( $p \leq 0.099$ ,  $R^2 \geq 0.006$ , Tab. 6.1.19a).

During the bath application of 10 µM Cch,  $FF_{fix}$  correlated significantly with various measures of the action potential shape. In particular, the more steeply the cell repolarized ( $p = 0.008$ ,  $R^2 = 0.174$ ) and the more narrow the action potential was ( $p \leq 0.034$ ,  $R^2 \geq 0.116$ ), the higher was  $FF_{fix}$ . Like  $PP_{fix}$ ,  $FF_{fix}$  also correlated significantly with the action potential

threshold ( $p = 0.000$ ,  $R^2 = 0.425$ ) such that  $FF_{\text{fix}}$  was lower, the more depolarized the action potential threshold was. Analogous to the correlation of  $PP_{\text{fix}}$  with the post-burst membrane potential,  $FF_{\text{fix}}$  was significantly higher, the higher the firing frequency during discrete current injections was ( $p \leq 0.101$ ,  $R^2 \geq 0.022$ , Tab. 6.1.20).

Notably, I did not observe significant correlations of  $PP_{\text{fix}}$  ( $p = 0.476$ ,  $R^2 = 0.014$ , Tab. 6.1.19) or  $FF_{\text{fix}}$  ( $p = 0.060$ ,  $R^2 = 0.095$ , Tab. 6.1.20) with the location of the cells within proximo-distal axis. These results indicate that persistent firing was not significantly modulated by the cell's proximo-distal location and the accompanying differences in excitability (Fig. 3.1.13). Furthermore, neither the age of the animals, nor the sag ratio correlated significantly with either  $PP_{\text{fix}}$  ( $p \geq 0.062$ ,  $R^2 \leq 0.096$ , Tab. 6.1.19) or  $FF_{\text{fix}}$  ( $p \geq 0.197$ ,  $R^2 \leq 0.035$ , Tab. 6.1.20). These findings indicate that persistent firing was not significantly modulated by the animal's maturation or the accompanying differences in  $I_h$  (Fig. 3.1.8).

Assessing the magnitude by which each of the intrinsic properties were affected by the application of Cch did not yield new insights (data not shown).

In addition to the previously described pharmacological manipulations, these results suggest that persistent firing was mediated by currents that underlie the action potential threshold and repolarization, currents that modulate the firing frequency during a constant current injection and currents that mediate afterhyperpolarizations. These currents may include the persistent sodium current [310,311] and  $K^+$  currents [179].

However, these results also indicate that persistent firing was rather uniform in CA1 pyramidal neurons from different loci and from animals at a different age.

### **3.2.7 Summary of persistent firing in CA1 pyramidal neurons**

In summary, the results indicate that CA1 pyramidal neurons have the propensity to engage in cholinergic-dependent persistent firing (Fig. 3.2.1 and Fig. 3.2.2 in section 3.2.1). In line with the lack of abundant recurrent connections of CA1 pyramidal neurons [29,30], the persistent firing was independent of fast ionotropic synaptic transmission (Fig. 3.2.3 and Fig. 3.2.4). Furthermore, electrotonic coupling between pyramidal neurons did not appear to be crucially involved (Fig. 3.2.5 and Fig. 3.2.6). These results indicate that the cholinergic-



dependent persistent firing was based on mechanisms intrinsic to individual neurons (section 3.2.2). The data suggested that this intrinsic persistent firing was physiologically plausible (section 3.2.3). Physiological plausibility could be inferred, because intrinsic persistent firing could be elicited by shortened stimuli (Fig. 3.2.7) which mimicked the stimulus duration in behavioral tasks [55,213,214]. In addition, persistent firing was not limited to neurons from juvenile animals (Fig. 3.2.8). After having tested for the physiological relevance, I focused on the mechanism underlying intrinsic persistent firing (section 3.2.4). The data suggested that the carbachol-dependent intrinsic persistent firing was mediated by muscarinic acetylcholine receptors (Fig. 3.2.9). Subsequently, I aimed at disentangling the two main effects of muscarinic stimulation, namely the blockade of potassium currents and the gating of calcium-sensitive non-selective cationic currents ( $I_{CAN}$ ). The results indicate that the blockade of potassium channels facilitated depolarization block but did not allow stimulus outlasting persistent activity (Fig. 3.2.10). In contrast, the data suggested a calcium-sensitive mechanism because an elevation of the intracellular calcium concentration was crucial for persistent firing (Fig. 3.2.11). Moreover, the blockade of  $I_{CAN}$  via three different approaches (Fig. 3.2.12 - Fig. 3.2.14) alluded to a fundamental involvement of the  $I_{CAN}$  mediating canonical transient receptor potential (TRPC) channels in persistent firing of CA1 pyramidal neurons. Additionally, within the range of 5 to 20  $\mu$ M Cch the post-stimulus firing frequency appeared to have reached a plateau at 10 and 20  $\mu$ M, whereas the post-stimulus plateau potential kept increasing (Fig. 3.2.15). Finally, assessing the correlation of persistent firing with intrinsic electrophysiological properties alluded the involvement of  $K^+$  channels and potentially the persistent sodium current in persistent firing (section 3.2.6) .

## 3.3 Depolarization block

In the first chapter, I outlined the effects of Cch on the intrinsic properties of CA1 pyramidal neurons in my sample. While assessing cellular excitability, I highlighted that, in the absence of Cch, stimulus-confined depolarization block was feasible with intense current stimulations (~1 nA, Fig. 3.1.6A&D). These results were in line with the experimental and computational data of a thorough study on depolarization block in CA1 pyramidal neurons [278]. The application of Cch lowered the threshold for the induction of depolarization block (Fig. 3.1.6B) and endowed the cells with the ability for stimulus outlasting activity (Fig. 3.1.6B&C) whereas the duration of the depolarization block was uniform (Fig. 3.1.E).

In the second chapter, I recapitulated and deepened results on the first report of cholinergic-dependent long-lasting persistent firing in CA1 pyramidal neurons [63]. While assessing whether K<sup>+</sup> channel blockade may be sufficient for the induction of persistent firing, I observed stimulus confined depolarization block during the presence of M- and SK-channel antagonists (Fig. 3.2.10). These data were in line with a previous report concluding that potassium channel blockade was insufficient but cholinergic stimulation was required for stimulus-outlasting depolarization block [236].

Considering these previous studies [236,278] and my observations replicating their findings, I will only elaborate on the hitherto undescribed relation between the well characterized cholinergic-dependent depolarization block [141,236,241,312] and the newly reported persistent firing [63] of CA1 pyramidal neurons. An in depth investigation of the electrophysiological characteristics [236,278] and the intracellular mediation [141,241,312] of depolarization block is dispensable, due to insightful publications comprehensively covering these topics.

### 3.3.1 The mechanism underlying the switch between persistent firing and depolarization block

#### The effect of the carbachol concentration

The aforementioned publications originating from the MacVicar group usually used Cch concentrations at least twice as high (20  $\mu$ M: [236,312,241,312]; 30  $\mu$ M: [141]) as the concentration I used for inducing mostly persistent firing (10  $\mu$ M, [63]). Hence, I investigated

the effect of the Cch concentration on the probability distribution of depolarization block and persistent firing. Therefore, I applied the same current stimulation (2 s, 100 pA) in the presence of half (5  $\mu\text{M}$ ,  $n = 25$ ) and twice (20  $\mu\text{M}$ ,  $n = 41$ ) as much of the cholinergic agonist,

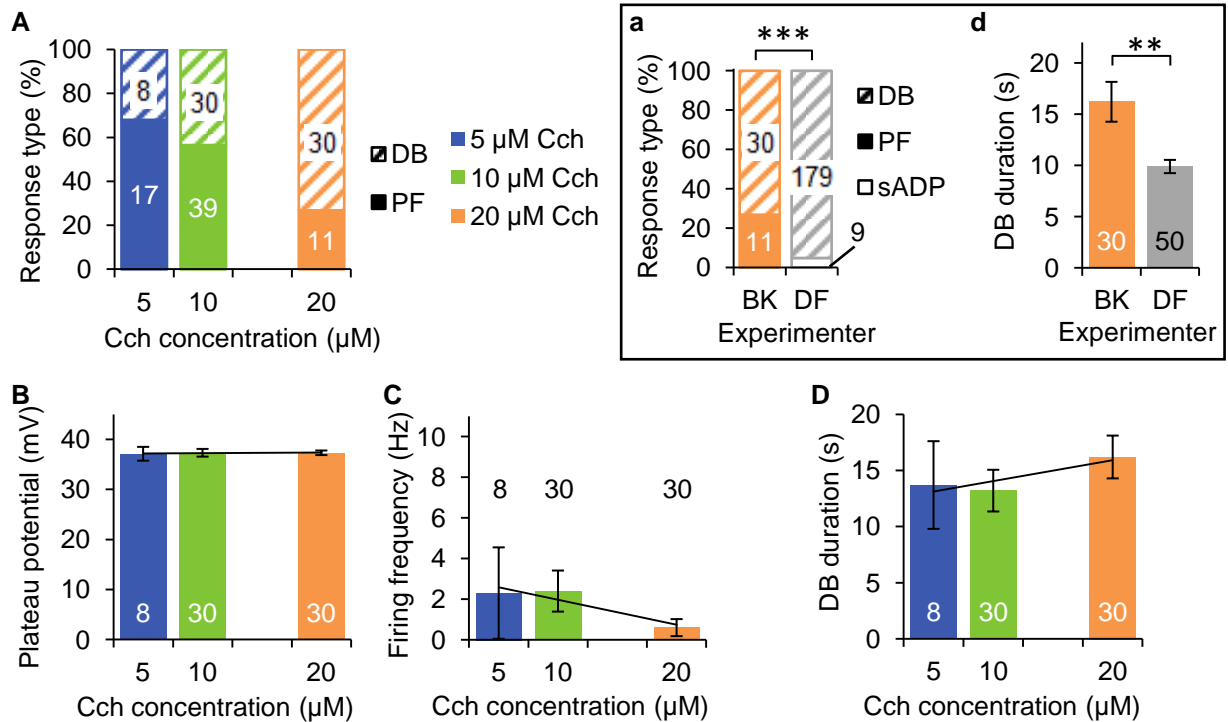


**Figure 3.3.1: The propensity for depolarization block was higher at higher carbachol concentrations but the characteristics of the depolarization block were unaffected.**

(A) The likelihood for depolarization block (DB) increased significantly as the carbachol (Cch) concentration increased. Correspondingly, the likelihood for persistent firing (PF) decreased significantly along with the increasing Cch concentration.

(B) The amplitude of the plateau potential during the most depolarized 500 ms within 30 s after the cessation of the 2s, 100 pA square pulse was unaffected by the variation of the Cch concentration.

(C) The frequency of action potential generation (Firing frequency) during the most depolarized 500 ms within 30 s after the cessation of the 2s, 100 pA square pulse was unaffected by the variation of the Cch concentration.

(D) The duration of the depolarization block within 30 s after the cessation of the 2s, 100 pA square pulse was unaffected by the variation of the Cch concentration.

Inset:

(a) Relates to (A). In 20  $\mu\text{M}$  Cch, the likelihood of observing depolarization block in my sample (Experimenter: BK) was significantly lower than the likelihood of depolarization block observed by Dr. D. Fraser [236] (Experimenter: DF). sADP: slow afterdepolarization.

(d) Relates to (D). In 20  $\mu\text{M}$  Cch, the duration of the depolarization block in my sample (Experimenter: BK) was significantly longer than the duration of the depolarization block observed by Dr. D. Fraser [236] (Experimenter: DF).

\*\*  $p < 0.01$ . \*\*\*  $p < 0.001$ .

as previously used (10  $\mu\text{M}$  Cch,  $n = 69$ ). The results showed that the likelihood for the occurrence of depolarization block significantly increased in a linear fashion the higher the Cch concentration was (binomial logistic regression,  $\chi_1^2 = 12.300$ ,  $p < 0.001$ ,  $n = 135$ , Fig. 3.3.1A). However, the characteristics of the depolarization block ( $n = 68$ ) did not significantly differ between the various Cch concentrations. The plateau potential ( $\text{PP}_{\text{max}}$ , linear regression,  $p = 0.906$ , Fig. 3.3.1B) and firing frequency ( $\text{FF}_{\text{max}}$ , linear regression,  $p = 0.130$ , Fig. 3.3.1C) during the most depolarized 500 ms within 30 s after the stimulus offset did not follow a significant linear gradient in accordance with the Cch concentration. However, due to the assessment of the most depolarized membrane potential, the insignificant result may have been mediated by a ceiling effect. Nonetheless, the duration of the depolarization block (linear regression,  $p = 0.281$ , Fig. 3.3.1D) was not significantly different across the various Cch concentrations either.

It is noteworthy, that in the presence of 20  $\mu\text{M}$  Cch, I observed depolarization block in a significantly smaller (Chi-square test,  $\chi_1^2 = 20.517$ ,  $p < 0.001$ ) fraction of cells (73.2%, 30/41 cells) than previously reported (20  $\mu\text{M}$  Cch, 95.2%, 179/188 cells) [236] (Fig. 3.3.1a). Furthermore, the duration of the depolarization which I observed in 20  $\mu\text{M}$  Cch ( $16.2 \pm 1.9$  s,  $n = 30$ ) was significantly prolonged (2-sample  $T$ -test, no variance homogeneity,  $T_{35.573} = 3.1325$ ,  $p = 0.004$ ) compared to a previously reported duration of depolarization block in 20  $\mu\text{M}$  Cch ( $9.9 \pm 0.6$  s,  $n = 50$ ) [236] (Fig. 3.3.1d).

The aforementioned data was obtained from independent samples. Hence, a sampling bias inducing a potential co-variation of cellular properties may have mediated the effects of the Cch concentration. Even though the results indicated that the introduction of Cch induced a switch to either persistent firing or to depolarization block, it remained unclear whether both phenomena could occur interchangeably within one cell. To elucidate whether individual cells were capable of exhibiting both persistent firing and depolarization block, I conducted within-cell investigations. On these grounds, I exposed seven cells that showed persistent firing in the presence of 5  $\mu\text{M}$  Cch subsequently to 20  $\mu\text{M}$  Cch (Fig. 3.3.2A). The results demonstrated that six out of seven cells were switched from persistent firing to depolarization block (Fig. 3.3.2B). In line with the categorical change,  $\text{PP}_{\text{max}}$  (paired  $T$ -test,  $T_6 = 3.493$ ,  $p = 0.013$ , Fig. 3.3.2C) and  $\text{FF}_{\text{max}}$  (paired  $T$ -test,  $T_6 = -3.711$ ,  $p = 0.010$ , Fig. 3.3.2D) changed significantly in response to the increase of the Cch concentration.

In summary, the carbachol concentration shifted the probability distribution of persistent firing and depolarization block. These results indicate that the propensity for

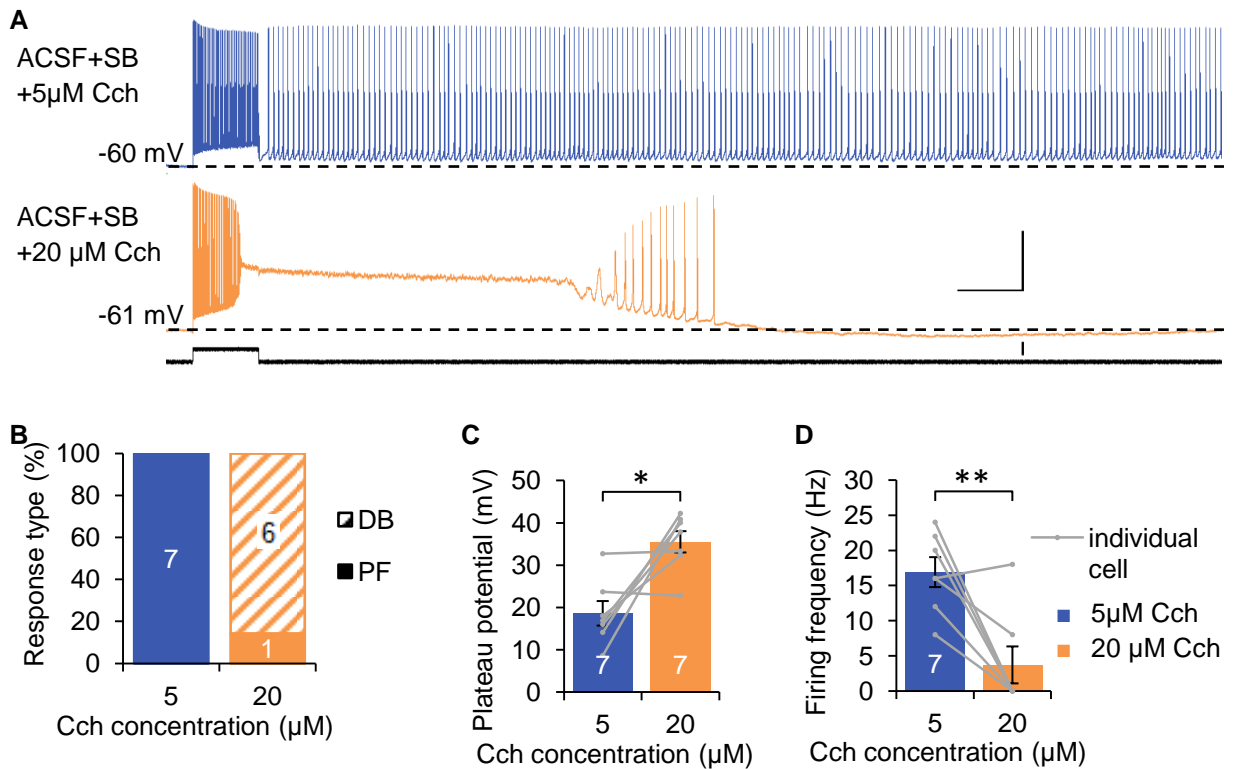


**Figure 3.3.2: Individual cells showed both persistent firing and depolarization block depending on the carbachol concentration.**

(A) The graph shows a cell's membrane potential in response to a 2 s, 100 pA square pulse (bottom black trace) during the bath application of 5  $\mu$ M carbachol (Cch, top blue trace) and subsequently during the bath application of 20  $\mu$ M Cch (middle orange trace). In the presence of 5  $\mu$ M Cch, the cell exhibited long-lasting persistent firing. In contrast, the same cell engaged in depolarization block when subsequently exposed to the four-fold concentration of Cch (20  $\mu$ M). ID: 130717/R3/f155 and f175. Horizontal scale bar: 2 s. Vertical voltage scale bar: 40 mV. Vertical current scale bar: 100 pA.

(B) The plot illustrates that six out of seven cells switched their response to a 2 s 100 pA square pulse from persistent firing to depolarization block. One cell maintained persistent firing despite the elevation of the Cch concentration.

(C) The amplitude of the membrane potential during the 500 ms of most depolarized membrane potential within 30 s following the stimulus offset increased significantly upon the increase of the Cch concentration.

(D) The frequency of action potentials during the 500 ms of most depolarized membrane potential within 30 s following the stimulus offset decreased significantly upon the increase of the Cch concentration.

\*  $p < 0.05$ . \*\*  $p < 0.01$ .

depolarization block increased linearly with an increasing Cch concentration (Fig. 3.3.1A). Furthermore, individual cells had the ability to engage in both persistent firing or depolarization block (Fig. 3.3.2). However, once elicited, the depolarization block appeared to be a rather uniform all-or-nothing phenomenon which was unaffected by the Cch concentration (Fig. 3.3.1B-D).

As previously lined out (section 3.2.4), muscarinic stimulation leads to the blockade of potassium channels [313] and the facilitation of calcium-sensitive non-selective cationic currents ( $I_{CAN}$ ) [144]. Firstly, I will assess the effect of  $K^+$  channels on the switch between persistent firing and depolarization block. Secondly, I will investigate the effect of canonical transient receptor potential (TRPC) channels on the interrelation of persistent firing and depolarization block.

### **The involvement of voltage-gated $K^+$ currents ( $I_M$ ) mediated by KCNQ channels**

The blockade of voltage-gated  $K^+$  currents was previously shown to be insufficient to induce depolarization block in the absence of Cch [236]. However, in the presence of Cch, the characteristics of the depolarization block appeared to be altered by the additional blockade of voltage-gated  $K^+$  currents [236]. Hence, I tested the involvement of the voltage-dependent and muscarinic modulated M current ( $I_M$ ) in the switching between persistent firing and depolarization block. Therefore, I blocked or enhanced  $I_M$  by the application of 20  $\mu$ M XE991 or 10  $\mu$ M retigabine [314] in cells displaying persistent firing or depolarization block, respectively.

To assess if the blockade of  $I_M$  may switch persistent firing to depolarization block, I first recorded six cells displaying persistent firing in response to a 2 s, 100 pA square pulse while superfused with 10  $\mu$ M Cch. Subsequently, I bath applied 20  $\mu$ M XE991 for an average of 10 min (SD: 5 min) in the continued presence of 10  $\mu$ M Cch and tested the same current stimulation. In the latter condition, three cells showed depolarization block and the remaining three cells continued to show persistent firing. Hence, the introduction of XE991 switched 50% of the neurons from persistent firing to depolarization block.

To assess if the enhancement of  $I_M$  may switch depolarization block to persistent firing, I first recorded 13 cells exhibiting depolarization block in response to a 2 s, 100 pA square pulse while superfused with 10 ( $n = 4$ ) or 20 ( $n = 9$ )  $\mu$ M Cch and held just below their firing threshold (Fig. 3.3.4D). Subsequently, I co-applied 10  $\mu$ M retigabine (RGB) for an average of 12 min (SD: 4.1 min) and tested the same current stimulation, again from just below threshold (Fig. 3.3.4E). Upon the cessation of the stimulus in the latter condition, one cell quickly returned to baseline, two other cells exhibited persistent firing and the majority of cells ( $n = 10$ ) continued to engage in depolarization block (Fig. 3.3.4A).

These results indicate that the presence of 10  $\mu$ M retigabine was insufficient to prevent depolarization block when the current stimulus was applied to baseline membrane potentials

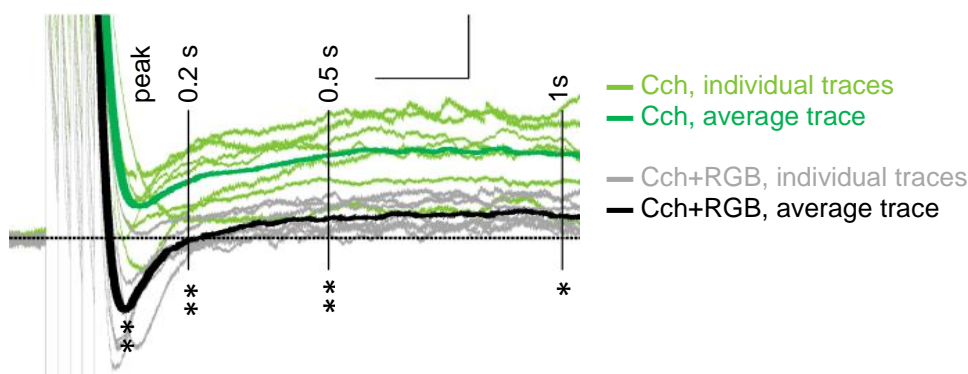


**Figure 3.3.3: Retigabine hyperpolarized the post-burst membrane potential significantly**

Retigabine (RGB, 10  $\mu\text{M}$ ) significantly hyperpolarized the post-burst membrane potential which was induced by five action potentials. In the presence of carbachol only (Cch, 10 or 20  $\mu\text{M}$ , green traces), on average (dark green trace) cells exhibited a depolarizing afterpotential. In contrast, during the co-application of 10  $\mu\text{M}$  RGB, the same cells (grey traces) on average (black trace) exhibited an afterhyperpolarization. Action potentials were truncated. Traces were normalized to their baseline membrane potential and aligned to the stimulus offset time point. The dotted horizontal line represents the baseline membrane potential. The time points at which the membrane potential was compared between Cch and RGB using paired *T*-tests are indicated by 'peak', '0.2 s', '0.5 s', and '1 s' above the traces. Stars below the peak and the vertical lines indicating the aforementioned time points represent the significance of the comparisons. Horizontal scale bar: 200 ms. Vertical scale bar: 2 mV. \*  $p < 0.05$ . \*\*  $p < 0.01$ .

just below threshold. These data could not be explained by an underestimation of the required retigabine concentration because the decision was based on a review of prevalent literature [314–316]. Testing a concentration of 25  $\mu\text{M}$  retigabine was inspired by a study showing an improved effect of 20  $\mu\text{M}$  in contrast to 10  $\mu\text{M}$  retigabine [317]. However, 25  $\mu\text{M}$  retigabine in the presence of 20  $\mu\text{M}$  Cch replicated the seemingly ineffectiveness of retigabine in preventing depolarization block ( $n = 4$ , data not shown). Furthermore, these data could not be explained by short superfusion times because the responses did not considerably change throughout  $> 30$  min retigabine exposure (10  $\mu\text{M}$ ,  $n = 7$ , M: 39 min, SD: 5.5 min, data not shown). Additionally, these data could also not be explained by a derogated health status of the cells because upon the washout of Cch and retigabine, cells recovered a firing pattern typical for the absence of Cch ( $n = 2$ , data not shown). Moreover, these data could not be explained with a hampered functionality of the product because 10  $\mu\text{M}$  retigabine significantly enhance the mAHP (paired *T*-test,  $T_6 \geq 3.371$ ,  $p \leq 0.015$ ,  $n = 7$ , Fig. 3.3.3). However, retigabine also significantly depolarized the action potential threshold compared to the bath application of Cch only (Cch:  $-45.2 \pm 1.8$  mV, Cch+RGB:  $-39.4 \pm 1.2$  mV, paired *T*-test,  $T_{12} = 5.133$ ,  $p < 0.001$ ,  $n = 13$ ). The elevated action potential threshold was also

evident in a significantly more depolarized baseline membrane potential prior to the stimulation with the 2 s, 100 pA current injection in retigabine compared to the previous subthreshold value of the same cells in Cch only (Cch:  $-59.1 \pm 1.0$  mV, Cch+RGB:  $-52.5 \pm 0.9$  mV, paired *T*-test,  $T_{12} = 6.334$ ,  $p < 0.001$   $n = 13$ , Fig. 3.3.4D&E).

To respect the action potential threshold elevation in the presence of retigabine, I injected the 2 s, 100 pA square pulse to a baseline membrane potential which was comparable to the just subthreshold baseline membrane potential before the application of retigabine. Using this approach, only two out of ten cells continued to engage in depolarization block, despite the presence of retigabine (Fig. 3.3.4B). The majority of cells did not exhibit persistent activity but quickly returned to baseline upon the cessation of the stimulus (Fig. 3.3.4F). In particular, in the eight cells that no longer exhibited depolarization block, the current stimulation induced no action potentials ( $n = 3$ ), one spike ( $n = 4$ , Fig. 3.3.4F) or a decent firing frequency ( $n = 1$ , 11 Hz) throughout the stimulus period. The two cells that continued to generate depolarization block did so already during the stimulation.

These latter two cells suggested that retigabine was incapable of terminating depolarization block once it was induced. To elaborate on this indication, I again maintained cells at a baseline membrane potential which was just subthreshold before the application of retigabine. Instead of applying the 2s, 100 pA square pulse, I increased the current amplitude (100 pA increments) until depolarization block occurred during the stimulus. These experiments were conducted in seven cells and the current amplitude had to be increased to an average of 314 pA (SD: 90 pA). In synopsis with the two cells that exhibited depolarization block in response to a 100 pA current injection, nine cells were stimulated with  $267 \pm 122$  pA and available for analysis. Five out of these nine cells continued to refrain from exhibiting depolarization block (Fig.3.3.4C). Thereof, three cells engaged in persistent firing and two cells exhibited a subthreshold depolarizing afterpotential. The remaining four cells continued to engage in stimulus-outlasting depolarization block (Fig. 3.3.4G)

These experiments elucidated that retigabine may confer its anti-epileptic effects [318,319] by shifting the action potential threshold to more depolarized values and by enhancing the post-burst hyperpolarization. According to my observations, retigabine would in the first place prevent the generation of action potentials circumventing the development of aberrant activity within one cell and/or hampering the spread of excitation within a neuronal network.



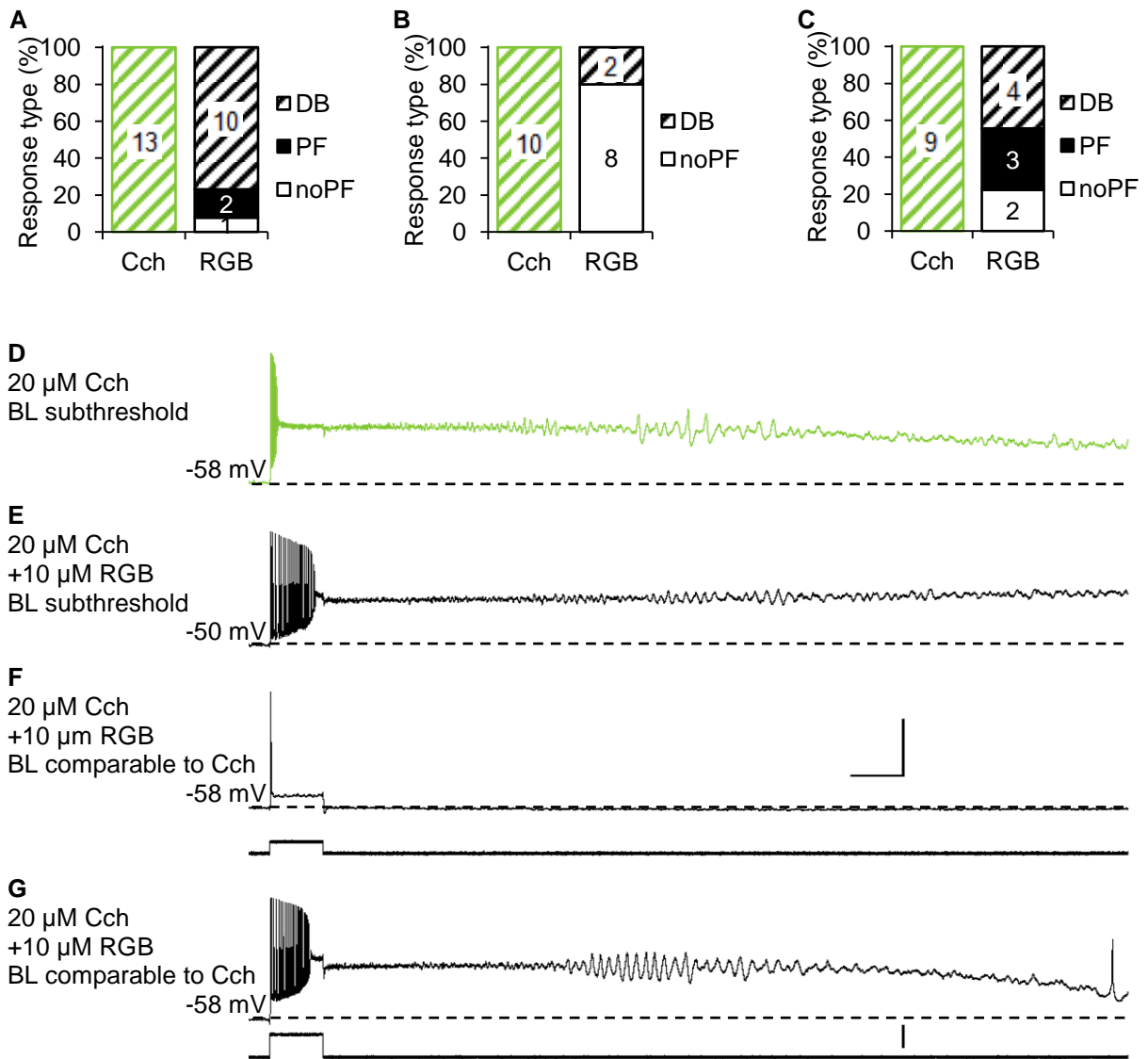


**Figure 3.3.4: Retigabine prohibited depolarization block by depressing action potentials**

(A-C) The graphs indicate the likelihood of the occurrence of depolarization block (DB), persistent firing (PF) or the lack of an apparent persistent activity (noPF). The bars represent paired samples of cells which were first tested during the superfusion with 10 or 20  $\mu$ M carbachol only (Cch) and subsequently during the co-application of 10  $\mu$ M retigabine (RGB). DB in the presence of Cch (green) was a selection criterion for the subsequent application of retigabine (RGB, black) and was therefore always 100%.

(D-E) Horizontal dotted lines indicate the baseline membrane potential (BL). Horizontal scale bar: 2 s. Vertical voltage scale bar: 40 mV. Vertical current scale bar: 200 pA. The current trace at the bottom of (F) applies to (D) and (E) as well. The current trace at the bottom of (G) applies to (G) only. ID: 141029/R3/f181, 202, 200, 207.

(A,D,E) While maintained at a BL just below the firing threshold in both conditions, the majority of the cells (12 of 15) retained their ability to engage in DB despite the presence of RGB. The current stimulation was a 2 s, 100 pA square pulse in both conditions. Related membrane potential traces are depicted in (D) and (E).

(B,D,F) In the presence of RGB, eleven of the aforementioned 15 cells were maintained at a BL which was comparable to the BL in the absence of RGB. The majority of cells (9 of 11) refrained from exhibiting DB. The current stimulation was a 2 s, 100 pA square pulse in both conditions. Related membrane potential traces are depicted in (D) and (F). Notably, cells that no longer engaged in DB, exhibited a radically ameliorated response during the stimulus period.

(C,D,G) While maintained at the aforementioned comparable BL, nine cells were stimulated with a current amplitude that induced DB during the stimulus duration. Hence; in the presence of RGB the membrane potential during the stimulation (stim- $V_m$ ) was comparable to that in the absence of RGB. DB was still observed in four cells. Related membrane potential traces are depicted in (D) and (G).

In addition, cells that still displayed depolarization block in the presence of retigabine, showed a significantly reduced  $PP_{\max}$  compared to the absence of retigabine (paired  $T$ -test,  $T_9 = -6.505$ ,  $p \leq 0.001$ , Fig. 3.3.5A). However, the duration of the depolarization block did not change significantly (Fig. 3.3.5B). Hence, retigabine may additionally convey anti-epileptic effects by curtailing the membrane potential during the depolarization block [278]. Thereby, retigabine could hamper action potential independent release of glutamate which may underlie the commencement and propagation of seizures [278].

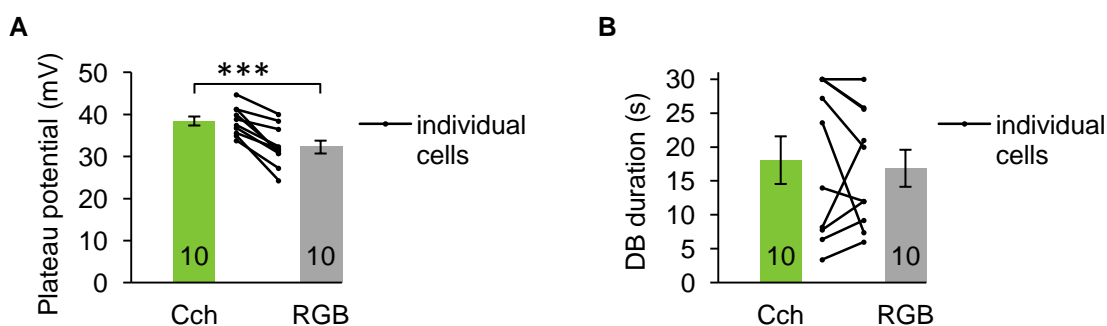


**Figure 3.3.5: The effect of voltage-gated  $K^+$  channels on the amplitude and duration of the depolarization block**

(A) Ten cells continued to exhibit depolarization block in the presence of 10 or 20  $\mu\text{M}$  Cch and 10  $\mu\text{M}$  retigabine (RGB), as they did during the application of 10 or 20  $\mu\text{M}$  Cch only (Cch). The plateau potential during the most depolarized 500 ms within 30 s following the stimulus offset was significantly reduced in the presence of retigabine, compared to its absence.

(B) The same conditions and cells as in (A). However, the graph shows that the duration of the depolarization block was unaffected by the co-application of 10  $\mu\text{M}$  retigabine.

\*\*\*  $p < 0.001$ .

These data indicate that voltage-gated  $K^+$  channels were involved in the switch between persistent firing and depolarization block and shaped the depolarization block. However, conversion of only a subset of cells in each of the experiments suggested that voltage-gated  $K^+$  channels could not fully account for the switch between persistent firing and depolarization block. These findings point to the involvement of additional currents in the switch between persistent firing and depolarization block.

### The involvement of calcium-sensitive $K^+$ currents mediated by the SK channels

As outlined in the introduction (section 1.3), calcium-sensitive  $K^+$  currents were initially found to be negligible for the induction or the shaping of depolarization block in CA1

pyramidal neurons [236]. In line with these results, I found that the blockade of SK channels (combined with the blockade of M channels) in the absence of Cch, was insufficient to induce stimulus-outlasting depolarization block (Fig. 3.2.10). However, more recent investigations suggest an involvement of SK channels in hyper-excitable states [235,239,320,321]. Considering these heterogeneous reports, I tested whether SK channel blockade or activation with apamin [186] or NS309 [277,322] had the potential to switch persistent firing to depolarization block or vice versa, respectively.

To assess the role of SK channel blockade in the switch from persistent firing to depolarization block, I first stimulated eight cells with a 2 s, 100 pA square pulse during the bath application of 10 $\mu$ M Cch only. Subsequently, I co-applied 0.1  $\mu$ M apamin for an average of 8 min (SD: 1.0 min) before testing the same stimulation again. Because it was an inclusion criterion for the acceptance in this set of experiments, all cells exhibited persistent firing in the presence of 10  $\mu$ M Cch. During the following superfusion of 0.1  $\mu$ M apamin, five of these cells were switched from persistent firing to depolarization block (Fig. 3.3.6A). The remaining three cells continued to engage in persistent firing.

To assess the role of SK channel gating in the switch from depolarization block to persistent firing, I first stimulated eight cells with a 2 s, 100 pA square pulse during the bath application of 20  $\mu$ M Cch only and subsequently while 10  $\mu$ M NS309 was co-applied for an average of 17 min (SD: 2.8 min) before I re-tested the same stimulation. Depolarization block in the presence of 20  $\mu$ M Cch only was a requirement for the inclusion of cells in this set of

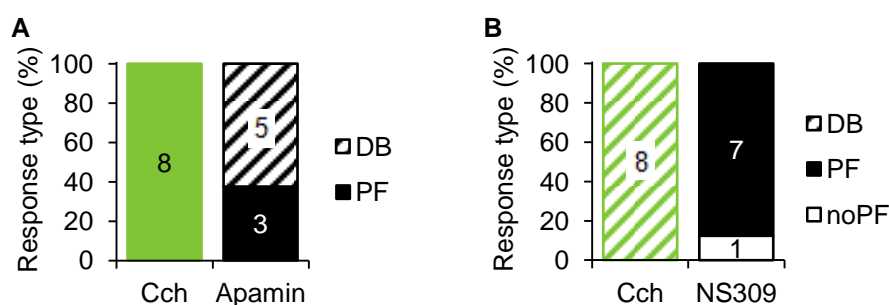


**Figure 3.3.6: SK channel activity affected the switch between persistent firing and depolarization block.**

(A) The majority of cells were switched from persistent firing (PF) in 10  $\mu$ M carbachol only (Cch) to depolarization block (DB) upon the introduction of 0.1  $\mu$ M apamin in addition to Cch (Apamin).

(B) None of the cells that engaged in depolarization block (DB) during the superfusion with 20  $\mu$ M Cch only (Cch) continued to exhibit depolarization block upon the co-application of 20  $\mu$ M NS309 (NS309). Instead, seven cells showed persistent firing (PF) and one cell presented a subthreshold depolarizing afterpotential (noPF)

experiments. Upon the presence of 10  $\mu\text{M}$  NS309, none of these cells continued to express depolarization block. Instead, seven cells engaged in persistent firing and one cell showed a subthreshold depolarizing afterpotential.

These results indicate that SK channels were involved in the switch between persistent firing and depolarization block (Fig. 3.3.6), despite having been unable to confer stimulus-outlasting activity in the absence of Cch (Fig. 3.2.10). However, as with XE991 (cf. previous section), also apamin switched only a subset of cells from persistent firing to depolarization block (Fig. 3.3.6), suggesting that SK channels were not exclusively involved in the switch from persistent firing to depolarization block.

### **Combined blockade of voltage-gated and calcium-sensitive $\text{K}^+$ currents**

As outlined before, the isolated application of XE991 or apamin (Fig. 3.3.6) only switched a subset (50% or 62.5%, respectively) of the cells from persistent firing to depolarization block. These results indicate that the blockade of either KCNQ or SK channels incompletely modulated the mechanism for the switch between persistent firing or depolarization block. This observation is in line with a study on the interplay between KCNQ and SK channels [188]. In detail, it was reported that SK channels only contributed little to the cell's intrinsic excitability, whilst KCNQ channels functioned undisturbed but adopted a crucial role in case of KCNQ failure [188]. Hence, during the solitary blockade of either KCNQ or SK channels the respective alternative channel may have prevented the induction of depolarization block.

To test for the potential rescue from the induction of depolarization block by alternative  $\text{K}^+$  channels remaining functional, I blocked both KCNQ and SK channels at once. For these experiments, I chose neurons that displayed persistent firing in the presence of 10  $\mu\text{M}$  Cch. Subsequently, I simultaneously bath applied 20  $\mu\text{M}$  XE991 and 0.1  $\mu\text{M}$  apamin in a superfusate that also contained 10  $\mu\text{M}$  Cch. All seven cells used for this investigation were switched from persistent firing to depolarization block upon the change of the extracellular medium.

These results suggest that in a subset of cells the blockade of either KCNQ or SK channels could induce depolarization block. On the other hand, in a different subset of cells, the undisturbed gating of either KCNQ or SK channels could prevent the initiation of depolarization block. In synopsis, these results indicate that KCNQ and SK channels played a cell specific role in the switch between persistent firing and depolarization block.

### **The involvement of the calcium-sensitive non-selective cationic current ( $I_{CAN}$ ) mediated by TRPC channels**

Cholinergic stimulation not only blocks the AHP which is mediated by  $K^+$  channels [151,195]. Additionally, mAChR stimulation also facilitates a calcium-sensitive non-selective cationic current ( $I_{CAN}$ ) which is thought to be mediated by canonical transient receptor potential (TRPC) channels ([199,303]; but see [200]). Hence, during the application of Cch both effects coexist and they affect vastly overlapping time periods [179,198]. This mutual masking renders the dissociate between both effects challenging. Nevertheless, to disentangle the involvement of TRPC channels from that of  $K^+$  channels, I first maximally blocked  $K^+$ . Thereby, a subsequent application of Cch would not add any further  $K^+$  channel blockade. Yet, the exposure of those cells to Cch would still introduce the non- $K^+$  channel effects, i.e. the modulation of properties presumably mediated by TRPC channels.

To investigate the specific contribution of TRPC channels to the depolarization block, I used six cells which were first exposed to 20  $\mu$ M XE991 and 0.1  $\mu$ M apamin for an average of 10 min (SD: 1.4 min). Subsequently I superfused these same cells for an average of 9 min (SD: 2.9 min) with the same solution that additionally contained 10  $\mu$ M Cch. In both media I tested for depolarization block with the 2 s, 100 pA square pulse.

During the presence of 20  $\mu$ M XE991 and 0.1  $\mu$ M apamin, five out of six cells exhibited depolarization block that was confined to the stimulus duration (Fig. 3.3.7 top; also highlighted previously: Fig. 3.2.10). The remaining cell engaged in high frequency (37 Hz) action potential discharge which was also confined to the stimulus interval. In contrast, during the subsequent co-application of 10  $\mu$ M Cch, depolarization block was initiated during the stimulus period in all six cells. Momentously, the depolarization block then outlasted the cessation of the stimulus by  $11.0 \pm 4.2$  s (Fig. 3.3.7 bottom).

These results indicate that a conductance other than the blocked  $K^+$  currents may be involved in stimulus outlasting depolarization block. This conductance could potentially be the TRPC channel mediated  $I_{CAN}$  due to its sensitivity to muscarinic stimulation [199] and its role in persistent activity [144] and depolarization block [141]. However, it remained unclear whether  $I_{CAN}$  was also involved in the switch between persistent firing and depolarization block.

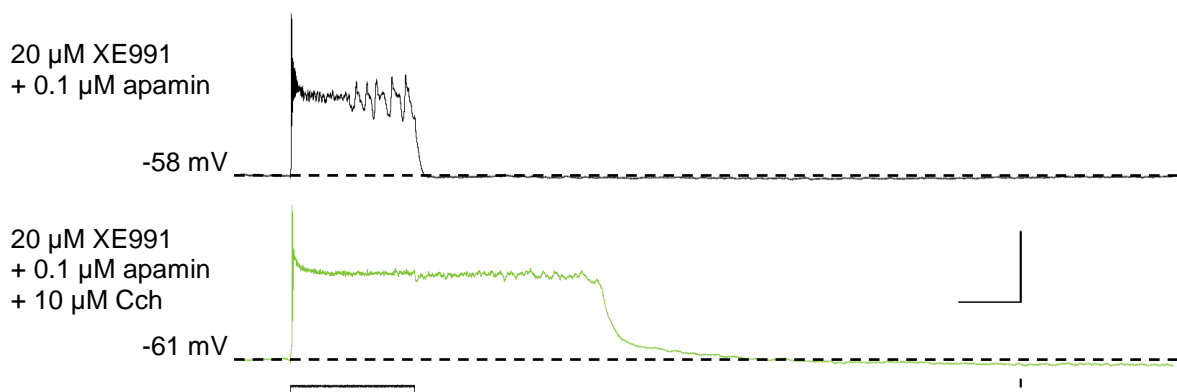


**Figure 3.3.7: Non- $K^+$  channel effects of cholinergic stimulation endowed cells with the ability to engage in persistent activity.**

During the bath application of 20  $\mu$ M XE991 and 0.1  $\mu$ M apamin (top black trace) the cell's membrane potential quickly culminated to depolarization block upon the onset of the 2 s, 100 pA square pulse (bottom black trace). However, the depolarization block quickly ceased with the termination of the stimulus injection.

In contrast, during the addition of 10  $\mu$ M Cch to the previously used superfusate, the same cell responded to the same current injection with stimulus-outlasting depolarization block. Furthermore, depolarization block was achieved even more quickly and the just subthreshold baseline membrane potential was already achieved at a more hyperpolarized membrane potential.

The horizontal dotted lines represent the baseline membrane potential. Horizontal scale bar: 1 s. Vertical voltage scale bar: 40 mV. Vertical current scale bar: 100 pA. ID: 140427/L5/f96&104.

To elucidate whether  $I_{CAN}$  may be involved in the switch between persistent firing and depolarization block, I used the TRPC channel antagonist ML204 [243,244]. First, I superfused 23 cells with 10  $\mu$ M Cch maintained at  $30 \pm 1$   $^{\circ}$ C (for details see method section 2.2). Thereof, I chose the ten cells that responded with depolarization block to a 2 s, 100 pA current injection at a membrane potential just below threshold (Fig. 3.3.8B). Subsequently, I co-applied 20  $\mu$ M ML204 for an average of 14 min (SD: 2.4 min). Re-testing the same cells with the same current injection yielded that none of them maintained the ability to engage in depolarization block (Fig. 3.3.8A). In contrast, three cells exhibited a subthreshold depolarizing afterpotential (Fig. 3.3.8B) and the majority of the cells ( $n = 7$ ) showed persistent firing (3.3.8C).

These results suggest that the TRPC channel mediated  $I_{CAN}$  was involved in the switch between persistent firing and depolarization block.

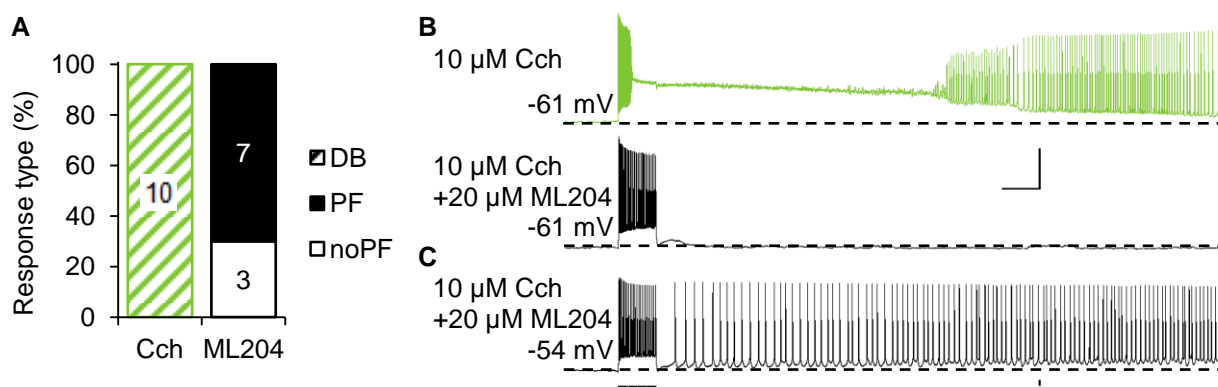


**Figure 3.3.8: Depolarization block was suppressed by the bath-application of the TRPC4/5 channel blocker ML204.**

(A) Although all cells displayed depolarization block in response to a 2 s, 100 pA square pulse during the bath application of 10  $\mu$ M carbachol (Cch), the same stimulus could not induce depolarization block in any of these cells during the subsequent co-application of 20  $\mu$ M ML204. Instead, seven cells engaged in persistent firing (PF) and three cells showed a subthreshold depolarizing afterpotential (noPF).

(B) The graph depicts the membrane potential of a cell that was first superfused with 10  $\mu$ M Cch and responded with depolarization block (green trace) to a 2 s, 100 pA current stimulation (bottom black trace in (C)). The same cell was subsequently exposed to 20  $\mu$ M ML204 in addition to 10  $\mu$ M Cch and then responded with a subthreshold depolarizing after potential (black trace) to the same stimulation. ID: 141002/R5/f49&67

(C) A different cell engaged in persistent firing during the presence of 20  $\mu$ M ML204 along with 10  $\mu$ M Cch. ID: 140924/R5/f80.

The horizontal dotted lines represent the baseline membrane potential. Horizontal scale bar: 2s. Vertical voltage scale bar: 40 mV. Vertical current scale bar: 100 pA.

The evidence presented here and reported by others [137,138,140,141] suggest that the enhancement of  $I_{CAN}$  would facilitate the occurrence of depolarization block. Unfortunately, the gating mechanisms of TRPC channels are yet incompletely understood [144]. Pharmacological agents allowing the modulation of TRPC channels are therefore scarce [243,244]. Consequently I could not test whether the enhancement of TRPC channel conductance would facilitate the occurrence of depolarization block.

### 3.3.2 Sensitivity of depolarization block to inter-cellular variability

To assess the sensitivity of the depolarization block to inter-cellular variability, I analyzed the linear relationship between the duration of the depolarization block to the age of the animals, the anatomical location of the pyramidal neurons within CA1 and intrinsic electrophysiological properties of CA1 pyramidal neurons.

The analysis of  $PP_{\max}$  and  $FF_{\max}$  revealed a striking lack of linear relationships with any of the aforementioned parameters (data not shown). This observation may have been due to ceiling and floor effects in  $PP_{\max}$  and  $FF_{\max}$ , respectively. The comprised variability of  $PP_{\max}$  and  $FF_{\max}$  within cells exhibiting depolarization block, was based on the analysis of the most depolarized 500 ms interval within the 30 s following the stimulus offset. Therefore, I focused on examining the relation between the more variable duration of the depolarization block and the aforementioned characteristics of the neurons.

A linear regression analysis revealed that the duration of the depolarization block in 10  $\mu\text{M}$  Cch ( $n = 30$ ) was neither affected by the animal's age ( $p = 0.158$ , Tab. 6.1.21) nor the cell's location within the dorso-ventral ( $p = 0.553$ ) or proximo-distal ( $p = 0.411$ ) axis of CA1 (Tab. 6.1.21). Furthermore, except for  $I_h$ , none of the intrinsic properties in the presence of 10  $\mu\text{M}$  Cch co-varied with the duration of the depolarization block (Tab. 6.1.21). Regarding  $I_h$ , I found that the depolarization block in 10  $\mu\text{M}$  Cch lasted significantly longer, the higher the sag ratio was, when induced by a 15 mV ( $n = 30$ ,  $p = 0.008$ ,  $R^2 = 0.223$ ) or a 20 mV ( $n = 30$ ,  $p = 0.003$ ,  $R^2 = 0.282$ , Fig. 3.3.9) hyperpolarizing step during the bath application of 10  $\mu\text{M}$  Cch.

The lack of modulation, particularly by the post-burst membrane potential ( $n = 17$ ) and post-burst afterhyperpolarization ( $n = 6$ ), may have been due to a limited sample size. Therefore, I scaled the sample size up by including cells that exhibited depolarization block in the presence of 5 and 20  $\mu\text{M}$  Cch. Pooling the data was justified because the depolarization block did not significantly differ across the variation of the Cch concentration (Fig. 3.3.1). A linear regression analysis of the pooled data set confirmed the results obtained from cells bathed in 10  $\mu\text{M}$  Cch and did not yield any novel insights (data not shown).



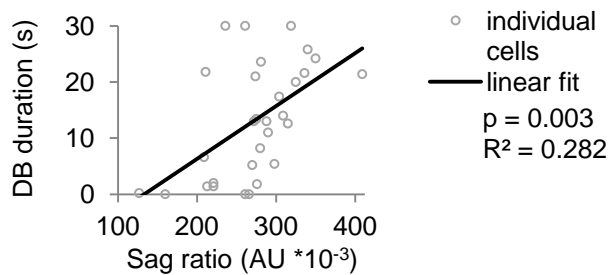


**Figure 3.3.9: The sag ratio correlated significantly with the depolarization block duration.**

The sag ratio in response to a 20 mV hyperpolarizing membrane deflection from a baseline membrane potential of -70 mV in the presence of 10  $\mu$ M Cch significantly correlated with the duration cells spent in depolarization block (DB) following a 2 s, 100 pA square pulse while superfused with 10  $\mu$ M Cch as well.

Note: Cells were classified as engaging in depolarization block if they did so at any point in time following the stimulus onset. Thus, a depolarization block duration of zero seconds represents cells that engaged in depolarization block during the stimulation and proceeded with persistent firing upon the cessation of the stimulus.

The lacking modulation of the depolarization block duration by intrinsic properties in the presence of Cch may have been due to neglecting the cell's intrinsic electrophysiological properties prior to the application of Cch. Therefore, I assessed the linear relation between the duration of the depolarization block and the magnitude by which 5, 10 or 20  $\mu$ M Cch affected the intrinsic properties. Several intrinsic properties were differentially affected by a varying Cch concentration (Fig. 3.1.7). However, this increase in variability was desirable for assessing the correlation between the change of intrinsic cellular properties that was induced by Cch and the duration of the depolarization block in the presence of Cch. The results revealed no significant correlations, except for a significant elongation of the depolarization block duration the more the action potential broadened by the application of Cch ( $n = 64$ ,  $p = 0.36$ ,  $R^2 = 0.069$ ). Particularly, despite  $I_h$  having been significantly elevated by the introduction of Cch (Fig. 3.1.1), the magnitude of this change in individual cells did not significantly correlate with the depolarization block duration in the same cells ( $p \geq 0.059$ ,  $R^2 \leq 0.055$ ).

The positive correlation between the duration of the depolarization block and  $I_h$  in the presence of Cch is in line with reports demonstrating effects of HCN channels on excitability [189] and their role in depolarization block [241] of CA1 pyramidal neurons.

In summary, the depolarization block appeared to be unaffected by the animal's age, the cell's location and most of the intrinsic electrophysiological properties of the CA1 pyramidal neurons. These findings may suggest that the depolarization block was a rather uniform all-or-nothing phenomenon once it was elicited and that merely the threshold for depolarization block induction may have been modulated.

### **3.3.3 Aspects of inter-cellular variability modulating the occurrence of persistent firing and depolarization block**

In the presence of 10  $\mu\text{M}$  Cch for example, 56.5% of the cells displayed persistent firing and the remaining 43.5% displayed depolarization block (Fig. 3.3.1). Up until now; I showed that both the pharmacological manipulation of  $\text{K}^+$  channels (Fig. 3.3.4, Fig. 3.3.5) and TRPC channels (Fig. 3.3.7) contributed to the switch between persistent firing and depolarization block. However, it remained unclear whether  $\text{K}^+$  and TRPC channels were also involved in the naturally occurring variability of the response spectrum. In addition, the observed disparity may have also been mediated by other factors, such as the cell's location (section 3.1.2.3) or  $I_h$  (Fig. 3.3.1, Fig. 3.1.7).

To recapitulate, within cells that exhibited persistent firing (section 3.2.6) and within cells exhibited depolarization block (section 3.3.2), I observed only sparse correlations of the persistent activity with different aspects of intercellular variability. In conjunction, these data suggest a categorical difference between cells displaying persistent firing (PF cells) or depolarization block (DB cells). In the following I will line out the findings of investigating which, if any, cellular properties were significantly different between PF or DB cells. Therefore, I pooled cells exposed to 5, 10 and 20  $\mu\text{M}$  Cch to increase the variability of the cholinergic effect because cells showed an increased likelihood of engaging in depolarization block at increased Cch concentrations (Fig. 3.3.1). Unless stated otherwise, I will report the results of two-sample *T*-tests in the following sections because I compared dependent variables that had a metric level of measurement (e.g. membrane potential) between two discrete groups of the independent variable (i.e. response type: PF or DB). If the dependent variable had a lower level of measurement (i.e. nominal or ordinal; e.g. existence of an AHP [yes or no]), I used the appropriate test out of the family of Chi-square tests for assessing the significance of the findings and explicitly indicated its use.

### The animal's age and co-varying intrinsic electrophysiological properties

Despite reports suggesting ongoing maturation throughout the age range of the experimental animals I used [250,254,258,288,298] and the modulation of intrinsic electrophysiological properties by the animal's maturation in my sample (Fig. 3.1.8), I did not observe a significant relationship between the cells' response type (PF or DB) and the animals' age ( $p = 0.302$ ). Earlier in this dissertation, I showed that  $I_h$ , the AP peak falling slope, the AP width and the RMP were significantly modulated by the maturation of the animals (Fig. 3.1.8). In accordance with the absent modulation of the response type (PF or DB) by maturation, I did not detect a significant difference of  $I_h$  ( $p \geq 0.799$ ), the AP peak falling slope ( $p = 0.379$ ), the AP width ( $p \geq 0.180$ ) or the RMP ( $p \geq 0.659$ ) between PF and DB cells.

These results suggest that the variability of  $I_h$  along an age range of ten days does not considerably affect the cells propensity to engage in either PF or DB, despite reports suggesting an involvement of  $I_h$  [189,209,241].

### The cell's location within CA1

The segregation of the hippocampus along its dorso-ventral axis is well recognized [5,15–17,19,36,323–325]. In line with the absence of a significant modulation of the cell's excitability along the dorso-ventral axis as outlined in chapter one (Fig. 3.1.12), I did not find a significant relation between the cell's dorso-ventral location and the occurrence of PF or DB ( $p = 0.626$ ).

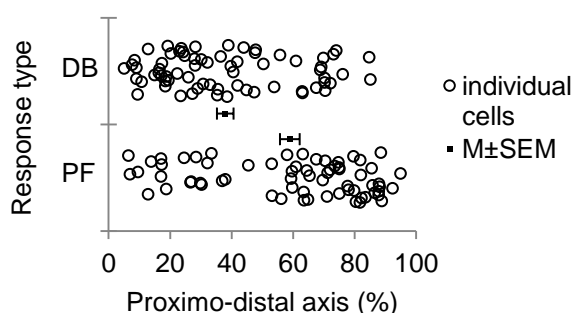


**Figure 3.3.10: Cells exhibiting persistent firing or depolarization block were recorded at disparate locations in the proximo-distal axis.**

The plot displays the proximo-distal location of cells displaying persistent firing (PF) or depolarization block (DB). The border between CA2 and CA1 (proximal) corresponded to 0% and the border between CA1 and subiculum (distal) corresponded to 100%. Neurons that exhibited persistent firing were recorded at significantly more distal locations when compared to the cells that exhibited depolarization block.

In contrast to the dorso-ventral axis, the reports concentrating on the proximo-distal axis are, to the best of my knowledge, scarce but consistently suggest a higher vulnerability of the proximal CA1 [39,40]. Accordingly, prior to and still during the cholinergic stimulation, the excitability of proximal cells in my sample was significantly higher than that of distal cells (Fig. 3.1.13). In line with that, I detected a significant disparity in the average proximo-distal location (0% = CA2/CA1 border, 100% = CA1/subiculum border) of PF and DB cells (PF:  $58.9 \pm 3.2\%$ , DB:  $37.9 \pm 2.7\%$ ,  $p < 0.001$ , Fig. 3.3.10).

These results suggest that CA1 pyramidal neurons differed along the proximo-distal but not the dorso-ventral axis in properties that mediated the differential propensity for exhibiting persistent firing and depolarization block.

### **Passive membrane properties and action potential characteristics**

To investigate which, intrinsic electrophysiological property may mediate the discriminative location of PF and DB cells in the proximo-distal axis (Fig. 3.3.10), I assessed  $R_{in}$  and properties of individual action potentials.

In line with the extinction of  $R_{in}$  differences along the proximo-distal axis (Fig. 3.1.13) upon the bath application of Cch,  $R_{in}$  was not differentially expressed in PF and DB cells ( $p \geq 0.586$ ). With regard to the AP waveform, I observed a significantly steeper AP rising slope (PF:  $243 \pm 9$  mV/ms, DB:  $283 \pm 11$  mV/ms,  $p = 0.005$ ) and a significantly higher AP amplitude (PF:  $69.2 \pm 1.3$  mV, DB:  $73.2 \pm 1.4$  mV,  $p = 0.036$ ) in DB cells compared to PF cells. None of the other AP properties differed between PF and DB cells (Tab. 6.1.22).

The results of an enhanced AP upstroke indicate that a sodium current [326] may be differentially expressed in PF or DB cells.

### **Excitability during sustained current injections**

Assessing persistent firing and depolarization block in response to a 2 s, 100 pA at a baseline just below threshold and the excitability in response to a 1 s square pulse with incrementing (50 pA) current amplitude at a baseline of -70 mV involved circular reasoning. Therefore, the results may not be interpreted as significant mediators of the cells' propensity to engage in persistent firing or depolarization block. However, the data may be inspected as it served for the validation of the Kaplan-Meier survival analysis to assess the excitability in the presence of Cch (Fig. 2.8, Table 6.1.22).

### Post-burst properties

Earlier in this dissertation, I demonstrated that  $K^+$  channels were involved in the switch between persistent firing and depolarization block (Fig. 3.3.5, Fig. 3.3.6). Therefore, differential expression of the post-burst AHP could mediate the mAChR-dependent variability in the cell's propensity to engage in either persistent firing or depolarization block (Fig. 3.3.2). In contrast to these prospects, neither of the post-burst membrane potential characteristics differed significantly between PF and DB cells that still showed an AHP ( $n = 15$  and  $n = 7$ , respectively;  $p \geq 0.081$ ). Even if all cells were considered, irrespective if they expressed an AHP, the amplitude of the post-burst membrane potential was not significantly different between PF and DB cells ( $n = 26$  each,  $p \geq 0.056$ , Fig. 3.3.11, Tab. 6.1.22). Nonetheless, the actual expression of an AHP significantly differed between PF and DB cells ( $\chi^2$ -test,  $\chi_1^2 = 5.042$ ,  $p = 0.025$ ). Only 26.5% (7 of 26) of the DB cells maintained an AHP in the presence of Cch. In contrast, 57.7% (15 of 26) of the PF cells sustained an AHP in the presence of Cch.

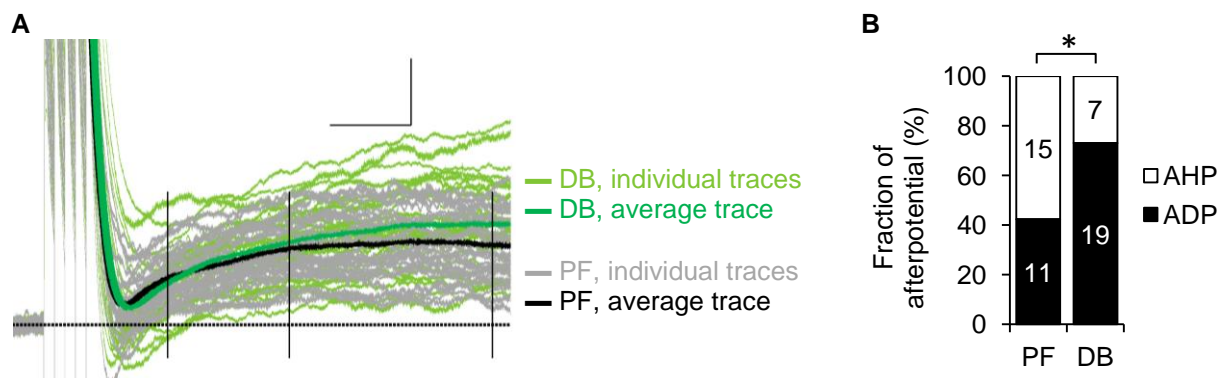


**Figure 3.3.11: The post-burst membrane potential in cells exhibiting persistent firing or depolarization block.**

(A) The graph displays the membrane potential following a burst of five action potentials (truncated) of 26 persistent firing (PF) cells (light green) and 26 depolarization block (DB) cells (grey). The average traces of the PF cells (dark green) and DB cells (black) were not significantly different at the assessed time points (peak, 0.2, 0.5, and 1 s). Traces were normalized to their baseline membrane potential and aligned to the stimulus offset time point. The dotted horizontal line represents the baseline membrane potential. The time points 0.2, 0.5 and 1 s after the stimulus offset are indicated by vertical black lines. Horizontal scale bar: 200 ms. Vertical scale bar: 2 mV.

(B) The plot shows the significantly higher likelihood of an afterhyperpolarization (AHP) in cells that exhibited persistent firing (PF) in contrast to cells that exhibited depolarization block (DB). The latter were more prone to exhibiting an afterdepolarization (ADP).

These results suggest that differences in the AHP that may mediate the switch between persistent firing and depolarization block were so subtle that I could not detect them. Alternatively, the expression of persistent firing or depolarization block could be mainly mediated by the categorical switch whether cells retained an AHP or expressed an ADP and could be rather insensitive to the precise magnitude of the post-burst membrane potential.

### **Considering the magnitude of the cholinergic effect on intrinsic properties**

The scarce finding of differences in cellular properties between PF and DB cells could have been due to the neglect of the cell's property prior to the application of Cch. However, an investigation of the magnitude by which cells were affected by the bath application of Cch did not yield fundamentally different results (data not shown).

### **Summary**

In summary, I showed that cells which exhibited persistent firing and those that exhibited depolarization block did not greatly differ along a multitude of intrinsic properties. The most striking finding was a higher likelihood of depolarization block to occur in the proximal compared to the distal portion of CA1 which is in line with prevalent literature [38–40]. Furthermore, the  $K^+$  channels mediating the post-burst AHP and sodium channels mediating the action potential upstroke were distinct between cells engaging in persistent firing or depolarization block.

## **3.3.4 Summary of the interrelation between persistent firing and depolarization block**

To recapitulate, I showed that the propensity of depolarization block increased significantly with increasing carbachol concentrations (Fig. 3.3.1) and that individual cells could be switched from persistent firing to depolarization block by increasing the carbachol concentration (Fig. 3.3.2). I demonstrated that the pharmacological modulation of both  $K^+$  and TRPC channels induced a switch between persistent firing and depolarization block (Fig. 3.3.3 & Fig. 3.3.4). Additionally, I highlighted that the depolarization block, once elicited, appeared to be an all-or-nothing response (section 3.3.2). Finally, I showed that the occurrence of a depolarization block was associated with a proximal location of the cell (Fig. 3.3.10) and the absence of an AHP (Fig. 3.3.11):

# 4 Discussion

## 4.1 Overall summary of the data

4.1.1 Effects of cholinergic stimulation on CA1 pyramidal neurons

4.1.2 Cholinergic excitation enabled intrinsic persistent firing in CA1 pyramidal neurons

4.1.3 Interrelation between persistent firing and depolarization block

## 4.2 Interpretation and discussion with regard to *in vitro* data of others

4.2.1 Persistent firing as potential mechanism for the short-term retention of novel information

4.2.2 Heterogeneous responses during potassium channel blockade

4.2.3 A potential explanation for the late report of persistent firing in CA1 pyramidal neurons

## 4.3 Interpretation and discussion with regard to the potential situation *in vivo*

4.3.1 The role of aging

4.3.2 Relation between *in vitro* and *in vivo* data of epileptiform activity and seizures

4.3.3 Relation between *in vitro* and *in vivo* data of persistent firing

4.3.4 Input specificity

4.3.5 Interaction with concurrent neurotransmission

4.3.6 Embedding persistent firing in neuronal networks

4.3.7 Questioning the interpretation of persistent-firing and depolarization block as either memory- or seizure-related activity

## 4.4 Conclusion

In the following, I will first highlight the results obtained from the study of intrinsic electrophysiological properties of CA1 pyramidal cells regarding cholinergic-dependent persistent firing and depolarization block which are associated with mnemonic function and seizures, respectively. Subsequently, I will focus on specifics of the presented data by addressing the heterogeneous results of potassium channel blockade and discussing the disparity between previous studies on depolarization block in CA1 pyramidal cells and my report on persistent firing in the same cell type. Finally, I will turn to a broader perspective. Firstly, I will relate the reports of persistent firing *in vitro* and *in vivo* with one another. Thereafter, I will discuss whether and how input specificity may be accomplished. Subsequently, I will embed cholinergic mediated persistent firing in concurrent neurotransmission and neuronal networks. Finally, I will question the interpretation of persistent firing and depolarization as either memory- or seizure related activity.

## 4.1 Overall summary of the data

Firstly, I will recapitulate the effects of cholinergic stimulation on CA1 pyramidal neurons from P14-24 Long-Evans rats. Secondly, I will summarize the findings of the newly discovered cholinergic-dependent persistent firing in the aforementioned cells. Lastly, I will integrate this intrinsic persistent firing with the well established cholinergic-dependent depolarization block.

### 4.1.1 Effects of cholinergic stimulation on CA1 pyramidal neurons

In the first chapter, I showed that the application of carbachol (Cch) induced an increase of the excitability in CA1 pyramidal neurons. This elevated excitability was apparent in (i) a significant depolarization of the resting membrane potential (Fig. 3.1.1A&B), (ii) an elevation of  $I_h$  (Fig. 3.1.1D), (iii) a largely abolished afterhyperpolarization which converted to an afterdepolarization (Fig. 3.1.3), (iv) a suppression of the burst firing mode (Fig. 3.1.2), (v) a reduction in the spike frequency accommodation in regular spiking cells (Fig. 3.1.4), (vi) a modulation of the current-frequency relationship (Fig. 3.1.5), and (vii) a facilitation of depolarization block (Fig. 3.1.6). The effects on  $I_h$ , the post-burst afterhyperpolarization, and the excitability were linearly concentration-dependent (Fig. 3.1.7). Notably, in contrast to



prevailing literature [313], I observed a reduction in the input resistance, particularly at more depolarized membrane potentials (Fig. 3.1.1C).

## **4.1.2 Cholinergic excitation enabled intrinsic persistent firing in CA1 pyramidal neurons**

In the second chapter, I demonstrated that CA1 pyramidal neurons *in vitro* exhibited persistent firing (Fig. 3.2.1, Fig. 3.2.2) which was presumably mediated by a mechanism that was intrinsic to individual neurons (Fig. 3.2.3 - Fig. 3.2.6). After having concluded that intrinsic persistent firing may be a physiological mechanism for short-term retention of information (Fig. 3.2.7, Fig. 3.2.8), I showed that this intrinsic mechanism was mediated by muscarinic acetylcholine receptors (Fig. 3.2.9). Furthermore, I highlighted that the blockade of voltage-gated and calcium-dependent potassium channels did not allow persistent activity (Fig. 3.2.10). I reported that intrinsic persistent firing was nonetheless supported by a calcium-dependent mechanism (Fig. 3.2.11). Moreover, I accumulated evidence that intrinsic persistent firing in CA1 pyramidal neurons may be supported by the calcium-sensitive non-selective cationic current ( $I_{CAN}$ ) which was mediated by canonical transient receptor potential (TRPC) channels (Fig. 3.2.12 - Fig. 3.2.14). Finally, I concluded by pointing out that the post-stimulus firing frequency, but not the post-stimulus plateau potential reached a plateau at higher carbachol concentrations.

## **4.1.3 Interrelation between persistent firing and depolarization block**

In the third chapter, I focused on the interrelation between persistent firing and depolarization block because cholinergic-dependent depolarization block in CA1 pyramidal neurons has been thoroughly characterized in the past [236,296,312,241,141]. I demonstrated that the propensity of cells to display depolarization block increased with an increasing carbachol-concentration (Fig. 3.3.1A, Fig. 3.3.2AandB). I reported that the modulation of both voltage-gated and calcium-sensitive potassium channels switched cells between persistent firing and depolarization block (Fig. 3.3.4 - Fig. 3.3.6). Moreover, I showed that the calcium-sensitive non-selective cationic current ( $I_{CAN}$ ) was involved in the switch between persistent firing and depolarization block (Fig. 3.3.7, Fig. 3.3.8). However, the characteristics of the depolarization block were virtually unaffected by electrophysiological and other

characteristics of the neurons (section 3.3.2). Nevertheless, the occurrence of depolarization block was significantly more likely in cells located in the proximal compared to distal region of the CA1 field (Fig. 3.3.10). Finally, the occurrence of depolarization block was associated with an abolishment of the post-burst afterhyperpolarization and its conversion into an afterdepolarization upon the superfusion of carbachol (Fig. 3.3.11)

## **4.2 Interpretation and discussion with regard to *in vitro* data of others**

### **4.2.1 Persistent firing as potential mechanism for the short-term retention of novel information**

The discovery of persistent firing in CA1 pyramidal neurons [63] expanded the wealth of cerebral regions in which cholinergic- [119,221,224,225,299] or metabotropic- [228,229] mediated intrinsic persistent firing was confirmed. My data offered a potentially underlying mechanism for the recordings of *in vivo* persistent activity in the CA1 area of the hippocampus [211,212,214–217] despite its lack of recurrent excitatory connections [28,29] by emphasizing the role of intrinsic properties of individual neurons [63]. Persistent firing in the CA1 area may support the short-term retention of novel information [47,51,63]. Thereby, my results propose a mechanism for the involvement of area CA1 in tasks that require the short-term retention of novel information [57,61,62]. Persistent firing based on intrinsic properties of individual neurons appears to be a particularly suitable candidate mechanism for the retention of novel information because it does not require the prior establishment of networks for maintaining the information [47].

### **4.2.2 Heterogeneous responses during potassium channel blockade**

The blockade of either voltage-gated (KCNQ2 and KCNQ3, 50% switched to depolarization block) or calcium-sensitive (SK2 and SK3, 62.5% switched to depolarization block) K<sup>+</sup> channels displayed a considerable inter-cellular variability. This finding may support the coadjutant role of KCNQ and SK channels in CA1 pyramidal neurons [188]. In

detail, this means that the functionality of SK channels may preserve neurons from exhibiting depolarization block in case KCNQ channels fail [188]. In the reverse, SK channel malfunction may not be crucial because they were shown to have only a secondary role in case of proper KCNQ functionality [188]. Hence, the whole-cell response during the blockade of either channel would not only depend on the effect on the target channel but also crucially on the functionality of the respective alternative. This would lead to an increase in variability of the whole cell response during blockade of either KCNQ or SK channels. Furthermore, the specific subunit composition and presence or absence of auxiliary proteins [327–329] would additionally increase this variability. The importance of the remaining  $K^+$  current is demonstrated by the reliable switch of all cells from persistent firing to depolarization block when KCNQ and SK channels were blocked simultaneously (section 3.3.1).

### **4.2.3 A potential explanation for the late report of persistent firing in CA1 pyramidal neurons**

The effects of muscarinic acetylcholine receptor stimulation on  $K^+$  currents [153,154,162,190] and a calcium-sensitive non-selective cationic current ( $I_{CAN}$ ) [141,200] on CA1 pyramidal neurons were intensely investigated. Mainly focusing on the latter, seizure-related depolarization block in CA1 pyramidal neurons was researched [141,236,241,312]. Therewith, the underlying intracellular signaling cascades [312], the involvement of  $I_{CAN}$  [141] and  $I_h$  [241] as well as the effect of a synaptic induction [312] were thoroughly delineated.

In a second line of research, the involvement of  $I_{CAN}$  in cholinergic-dependent persistent firing of entorhinal cortex neurons has been investigated elegantly and extensively, both by adopting computational [227] and pharmacological [119,230,330] approaches. However, the link to seizures and epilepsy is rarely described [331,332].

Despite the intense work on cholinergic-mediated electrophysiological effects in CA1 pyramidal neurons and the studies of cholinergic-dependent persistent firing in the entorhinal cortex, accounts of cholinergic-mediated persistent firing in CA1 pyramidal neurons were, to the best of my knowledge, not available until my report [63].

In the following I aim at integrating both lines of research, i.e. persistent firing, e.g. in the entorhinal cortex, and depolarization block in CA1 pyramidal neurons. My goal is to explain the disparity between the absence of persistent firing in the observations by the MacVicar group [141,236,241,312] and the discovery of persistent firing in my sample [63].

#### 4.2.3.1 Interpretation of the input resistance in my sample in the light of other reports

As previously mentioned, I found a Cch-induced reduction of the input resistance, particularly at more depolarized membrane potentials (Fig. 3.1.1C). This observation is not necessarily in contrast to previous reports. That is because the Cch-dependent blockade of  $K^+$  currents [153] and the Cch-induced facilitation of  $I_{CAN}$  [141] were both previously described for CA1 pyramidal neurons. The former leads to an increase [313] and the latter leads to a reduction of the input resistance [236]. Hence, the reduced input resistance in my sample may demonstrate the dominance of the facilitatory effect over the blocking effect. Emphatically, this does not argue against a concomitant but, with regard to the input resistance, a masked blockade of  $K^+$  currents in my sample.

In line with a multitude of previous studies since the early 1980s [313,155], Fraser and MacVicar (1996) found a Cch-dependent increase in input resistance [236]. This suggests that the blockade of  $K^+$  currents was dominant in their sample. In contrast to my report [63], Dr. Fraser never observed persistent firing (personal communication [333]). The only two responses he found were the reported slow afterdepolarization below the threshold for depolarization block initiation and the depolarization block [236].

#### 4.2.3.2 Postulates and supporting evidence

##### Potassium channel blockade

Firstly, I postulate that the discovery of persistent firing in my sample was based on a hampered blockade of  $K^+$  currents. The blockade of  $K^+$  currents is generally accepted to increase neuronal excitability [175,195]. Notably, I argue that the blockade of  $K^+$  currents did not endow the cells with the ability to exhibit activity that considerably outlasted the stimulus duration.

The effects of a sole blockade of  $K^+$  currents may support this postulate. Inhibiting  $K^+$  currents in the absence of other pharmacological manipulations was previously reported to result in a short lived but pronounced afterdepolarization (5 mM 4-AP, Fig. 10B1 in [236]) and even depolarization block (10 mM TEA, Fig. 10A1 in [236]). Importantly, this exclusive  $K^+$  current inhibition was insufficient to induce stimulus-outlasting depolarization block. Both forms of activity were confined to the stimulus interval [236]. These results are in line with my finding that exclusive blockade of  $K^+$  currents (20  $\mu$ M XE991 and 0.1  $\mu$ M apamin) induced depolarization block in five out of six cells. Crucially, this depolarization block was also confined to the stimulus duration (Fig. 3.2.10, Fig. 3.3.7).

The enhancement of calcium-sensitive  $K^+$  currents may furthermore support this postulate. The application of the  $K^+$  current facilitator NS309 resulted in a replacement of depolarization block by persistent firing in seven out of eight cells (Fig. 3.3.6B, no persistent activity in the remaining cell). Hence, the propensity for inducing depolarization block was abolished. Momentously, however, the likelihood for perpetuating the initiated activity was largely unaltered.

The results obtained from the enhancement of voltage-gated  $K^+$  channels were more complex due to a variety of side effects, like the elevation of the action potential threshold. Therefore, the integration of these data should be viewed with caution. That said, cells which still displayed depolarization block during the enhancement of voltage-gated  $K^+$  channels displayed a significantly reduced amplitude of the depolarization block (Fig. 3.3.5A), whereas the duration of the depolarization block was not systematically affected (Fig. 3.3.5B). Furthermore, while voltage-gated  $K^+$  currents were enhanced, still seven out of nine cells showed stimulus-outlasting activity (Fig. 3.3.4C).

### **TRPC channel facilitation**

Secondly, I postulate that the discovery of long-lasting persistent firing in my sample was based on a stronger facilitation of  $I_{CAN}$ .  $I_{CAN}$  is broadly acknowledged for enabling the cell to display an activity that outlasts the stimulus duration [230,141]. Notably, I argue that the modulation of  $I_{CAN}$  was secondary for the induction of depolarization block.

This postulate may be supported by a between-cells observation concluding that stimulus-outlasting depolarization block required the presence of carbachol whereas exclusive  $K^+$  current blockade was insufficient [236]. This is in line with my results obtained from within-cell comparisons showing that stimulus-outlasting activity was only enabled by the presence of Cch but not by the previous blockade of  $K^+$  currents only (Fig. 3.3.7).

The involvement of an enhanced conductance during the post-stimulus interval is supported by a reduction of the input resistance during the depolarization block after the cessation of the stimulus (Fig. 11B in Fraser and MacVicar (1996) [236]). If the stimulus-outlasting component had been dominated by the blockade of  $K^+$  currents, the input resistance would have increased.

In another report [141], TRPC channels were blocked (either with 2-APB or with SKF96365) and a significant reduction of the current after the stimulus offset was demonstrated. Even though not explicitly analyzed in this publication, the presented current clamp (Fig. 2F in 141) calcium imaging (Fig. 2I in 141) data suggest that the induction of depolarization block during the stimulation was unaffected by the TRPC blockade (Fig.

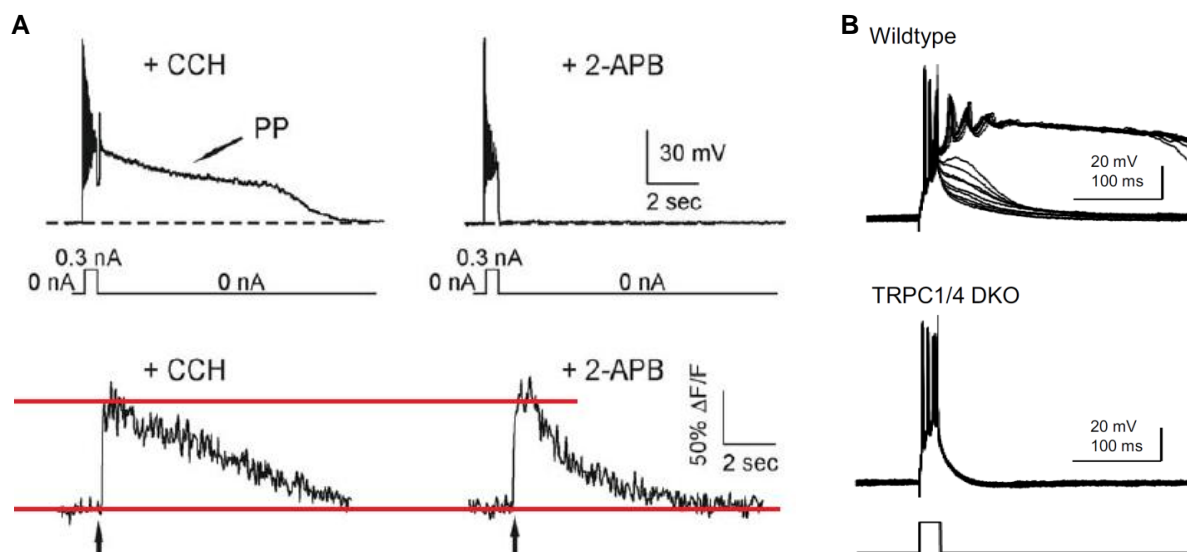


**Figure 4.1: Previously reported TRPC channel blockade or knock out may have left the induction of depolarization block unaffected.**

(A) Top: The graphs depict the membrane potential and the current command. Left: While 30  $\mu$ M carbachol (+CCH) were superfused, the cell showed a steep depolarization and a reduction of action potential amplitude during the 0.8 s, 300 pA square pulse. Upon the cessation of the stimulus, the depolarization block (PP - plateau potential) is sustained for about 8 s. Right: In contrast, during the co-application of the non-specific TRPC channel blocker 2-APB, the cell quickly returned to baseline upon the cessation of the stimulus. However, the steep depolarization and the reduction of action potential amplitude during the stimulus appears unaffected.

Bottom: The graphs depicts fluorescence imaging of transient changes in the intracellular calcium concentration. Left: While 30  $\mu$ M carbachol (+CCH) were superfused, the intracellular calcium concentration increased rapidly upon the onset of the stimulation (arrow) and was sustained for a substantial duration. Right: In contrast, during the co-application of the non-specific TRPC channel blocker 2-APB, the decay of the intracellular calcium concentration was considerably faster. However, the magnitude of the calcium-signal following immediately after the stimulus onset (arrow) appeared unchanged.

Figure 2 E,F,H and I in Tai et al. (2011) [141]; modified.

(B) Top: the graph shows the overlay of repeated (every 10 s) membrane potential traces obtained from a wildtype mouse during the ongoing superfusion of metabotropic glutamate receptor (mGluR) agonists. The membrane potential response was elicited by a 0.02 s, 800 pA square pulse indicated at the bottom. In the presence of sufficient mGluR agonists, the cell displays stimulus-outlasting depolarization block.

Bottom: The same as in Top, but in a mouse with the TRPC1 and TRPC4 channels knocked out. The cell did not engage in stimulus-outlasting activity. However, the steep depolarization and the action potential amplitude reduction appears to be comparable to the wildtype. Yet, the stimulation was too short to judge whether stimulus-confined depolarization block would have been induced and the overlay makes it hard to judge whether the steepness intensified with an increasing mGluR concentration. DKO: double knock-out.

Figure 3B in Phelan et al. (2012) [140]; modified

4.1A). In TRPC1/4 double knock-out mice, very short (0.02 s, 0.8 nA) current injections to neurons in the dorsal septum were applied during the stimulation with metabotropic glutamate receptors [140]. The post-stimulus activity in these neurons was significantly blocked (Fig. 3B in [140]). Even though not explicitly analyzed in that publication, the steep depolarization and the reduction of the action potential amplitude during the stimulus (Fig. 4.1B) strongly suggest that depolarization block would have been induced with longer stimulations as the MacVicar group [236,312,241,141] (0.8 s) or I [63] (2 s) used. While this interpretation is speculative, spontaneous (i.e. not current injection induced) generation of metabotropic glutamate-receptor mediated paroxysmal depolarization shifts in TRPC7 [137] and TRPC5 [138] channel knock-out mice may support the interpretation. These data indicate that TRPC channels may not be crucial for the induction of depolarization block but essential for sustaining whatever activity was induced during the stimulus.

Furthermore, I showed that the blockade of  $I_{CAN}$  switched depolarization block to persistent firing (Fig. 3.3.8). Hence, in addition to perpetuating whatever activity was in process,  $I_{CAN}$  may potentially play a role in the induction of depolarization block. However, further investigations on the role of TRPC channels in the induction of depolarization block (in contrast to its maintenance which was thoroughly studied by the MacVicar group) may have to await the introduction of more selective positive TRPC channel modulators [334].

Due to the technical challenge of applying the TRPC channel blocker ML204 (for details see method section 2.2) I propose that  $I_{CAN}$  may have been blocked inconsistently, despite using a rather high (20  $\mu$ M) concentration [243,244]. Hence, in the presence of ML204, residual  $I_{CAN}$  may have allowed the perpetuation of the stimulus-induced action potential generation in a total of 15 out of 23 cells (65%) (Fig. 3.2.14C, Fig. 3.3.8A). Due to the delicate stability of ML204, the degree of  $I_{CAN}$  blockade in my sample cannot be determined reliably and without circular reasoning. Therefore, my observations do not allow for an estimation about how much  $I_{CAN}$  is needed for perpetuating activity and at what extent it facilitates depolarization block.

To summarize, the cardinal role of  $I_{CAN}$  may be the perpetuation of whatever activity was induced. However, if strongly activated,  $I_{CAN}$  may additionally facilitate the induction of depolarization block.

Noteworthy, the potential involvement of the persistent sodium current [311] or the hyperpolarization activated current [241,209,231] cannot be excluded at this point.

#### 4.2.3.3 Integration and potential explanation

To recapitulate, it may be assumed that the facilitation of  $I_{CAN}$  was dominant over the blockade of  $K^+$  currents in my sample, as indicated by the reduction of the input resistance (Fig. 3.1.1C). This relative dominance may be established by a hampered  $K^+$  current blockade, an enhanced facilitation of  $I_{CAN}$ , or both.

Firstly, I argue that the magnitude of  $K^+$  current blockade may be crucial for the initiation of depolarization block. Hence, an assumed hampered blockade of  $K^+$  currents in my sample may explain why depolarization block was induced in a significantly lower fraction of cells than previously reported [236] (Fig. 3.3.1a). In other words, this moderate but concentration-dependent blockade of  $K^+$  currents (Fig. 3.1.7B) may have enabled a concentration-dependent fraction of cells to remain below the threshold of depolarization block induction (Fig. 3.3.1A)

Secondly, in line with previous reports [141,230], I argue that  $I_{CAN}$  endowed the cells with the ability to perpetuate whatever activity was initiated during the stimulus, e.g. action potential generation. Furthermore, the magnitude of  $I_{CAN}$  facilitation may be positively related with the duration of the persistent activity. Hence, an enhanced facilitation of  $I_{CAN}$  could explain why the persistent activity lasted significantly longer in my sample than previously reported [236] (Fig. 3.3.1d).

Accordingly, I suggest that both a hampered blockade of  $K^+$  currents (enabling the cells to remain below depolarization block) and a strengthened facilitation of  $I_{CAN}$  (endowing long lasting perpetuation), may underlie the reduction of input resistance. This shifted balance between the blockade of  $K^+$  currents and the facilitation  $I_{CAN}$  may explain the occurrence of long-lasting persistent firing in my sample [63].

Maybe due to the initial report of a minor role of  $K^+$  currents in depolarization block [236] subsequent investigations did not address  $K^+$  currents [141,241,312]. Hence, the presumably strong blockade of  $K^+$  currents in the CA1 pyramidal neurons of the MacVicar group was not experimentally modified in later publications [141,241,312]. Therefore, depolarization block was constantly induced during the stimulus. Consequently, the mechanism of activity maintenance — and not depolarization block induction — was studied. This research, together with the reports of persistent firing in the entorhinal cortex [227,119,230] and other brain areas [223,221] established TRPC channel conductance ( $I_{CAN}$ ) as a generic mechanism for sustaining activity. However, other mechanisms, e.g.  $K^+$  currents, may determine what form of activity is available for perpetuation.



#### 4.2.3.4 Conclusion

With the aforementioned considerations, I potentially isolated two effects of muscarinic stimulation in CA1 pyramidal neurons which may determine whether action potential generation or depolarization block occurs ( $K^+$  channel blockade) and whether this activity outlasts the stimulus (TRPC channel facilitation). To the best of my knowledge, this explicit delineation of the muscarinic effects with respect to the dissociation of persistent firing and depolarization block in CA1 pyramidal neurons was not yet reported.

#### 4.2.3.5 Outlook

It still remains open what may underlie this presumed shift in the balance of  $K^+$  current blockade and  $I_{CAN}$  facilitation by cholinergic stimulation in my sample compared to other reports [236].

The observed differences may not be attributed to slightly different stimulation protocols because adopting the stimulation protocols of the MacVicar group (shortened in duration and increased in amplitude compared to my 2 s, 100 pA square pulse) did not yield a noteworthy change in response types (data not shown). The presumed shifted balance between  $K^+$  currents and  $I_{CAN}$  may not be attributed to differences in the intracellular and extracellular fluids, because I adopted the fluid formula reported by Fraser and MacVicar [236] and still observed a considerable fraction of cells (50%, 9/18) engaging in persistent firing (data not shown).

The mode of slice preparation may not be excluded as mediating the differences. By adopting the preparation methods of Fraser and MacVicar (1996) [236], I could not generate healthy slices (15 pyramidal neurons from 15 animals). Notably, I replicated their method except for extracting the hippocampus from the brain because the goal was to also locate cells in the dorso-ventral axis. This may have been the crucial difference because the preparation protocol of Fraser and MacVicar (1996) did not involve a trans-cardiac perfusion of the brain [236]. A trans-cardiac perfusion replaces the blood with a low-calcium ACSF, such that hyperexcitability is prevented which may promote the generation of healthy slices. Because the ACSF used for perfusion is ice-cold, it is able to quickly cool the brain even at the innermost nuclei. This cooling process may promote the generation of healthy slices. In contrast, when the animal is not perfused and the hippocampus is maintained within the brain, it takes longer until the hippocampus is exposed to the ice-cold ACSF. That delayed exposure to the ice-cold ACSF may hamper the generation of healthy slices. When a trans-cardiac perfusion is not performed and the tissue is sliced, blood-containing blood vessels are severed. This leakage of blood into the tissue by the disruption of the blood-brain barrier may

hamper the generation of healthy brain slices. Furthermore, when the entire posterior portion of the brain is sliced, the cutting procedure takes longer compared to the slicing of only the hippocampus. Thus, a prolonged cutting procedure may hamper the generation of healthy slices. Hence, with not using trans-cardiac perfusion and slicing the posterior brain at whole, I combined two approaches that interfere with the generation of healthy slices.

The site of recording could have had an effect because I found that proximal cells showed a significantly higher propensity to engage in persistent firing (Figure 3.3.1). However, data on the precise recording site is not available in the reports of the MacVicar group [236,312,241,141].

The strain of rats may also have an effect. Research on persistent firing in the entorhinal cortex usually involved Long-Evans rats [223,230,251,299,330,221]. In contrast, the MacVicar lab used Sprague-Dawley rats [236,312,241,141]. However, persistent firing has also been observed in the prefrontal cortex [222] and the perirhinal cortex [225] of Sprague-Dawley rats; and in the primary cortices of mice [224].

In light of these data, I would consider two approaches most reasonable if one aims at resolving the open question of what might mediate the shifted balance between  $K^+$  currents and  $I_{CAN}$ . Firstly, it may be insightful to characterize the differences between cells in the proximal compared to cell in the distal region of CA1 with regard to  $K^+$  and TRPC channels. Secondly, it may be worthwhile to assess inter-strain differences in the electrophysiological properties and/or protein expression of CA1 pyramidal neurons from Long-Evans and Sprague-Dawley rats.

## **4.3 Interpretation and discussion with regard to the potential situation *in vivo***

### **4.3.1 The role of aging**

In a subset of experiments, aged animals were used to test whether persistent firing may be a peculiarity of CA1 pyramidal neurons from juvenile animals (Fig. 3.2.8). Furthermore, intrinsic properties were compared between CA1 pyramidal neurons from the aged animals against those from the juvenile animals.

In contrast to prior reports [219,289], I did not detect a significant reduction in the post-burst afterhyperpolarization (Fig. 3.1.8F). Nevertheless, I observed a reduced excitability of neurons from aged animals compared to those from juvenile animals both in the absence (Fig. 3.1.8E) and in the presence (Fig. 3.1.9E) of 10  $\mu$ M Cch. The discrepancy in excitability may have been mediated by a lower input resistance (Fig. 3.1.8A & Fig. 3.1.9A), and a more depolarized action potential threshold (Fig. 3.1.8C & Fig. 3.1.9C) in the neurons from the aged animals compared to those from the juvenile animals.

Despite the hampered excitability, CA1 pyramidal neurons of aged animals showed persistent firing that was indistinguishable of that from juvenile animals (Fig. 3.2.8B&C). Yet, only two out of eleven (2/11) neurons from the aged animals engaged in depolarization block whereas five out of eleven (5/11) neurons from the juvenile animals engaged in depolarization block (Fig. 3.2.8A). The assessment whether this difference was significant was not feasible because of the small sample size (sample size in at least one group < 5 and grand sum of the sample < 50; for details see method section 2.8.2).

The data leaves a mixed impression. Neurons from the aged animals showed a reduced excitability (Fig. 3.1.9E and 3.1.10E) compared to those from juvenile animals. However, I could not replicate (Fig. 3.1.8F) previous reports of a more pronounced post-burst afterhyperpolarization [219,289] in aged, compared to juvenile animals. Furthermore, neurons from the aged animals showed a potentially reduced likelihood to engage in depolarization block compared to those from juvenile animals (Fig. 3.2.8A). On the other hand, persistent firing was indistinguishable between the neurons from both age groups (Fig. 3.2.8B&C).

The data indicates that acetylcholine receptors and the intracellular signaling cascades allowing persistent firing were intact in the aged animals. This interpretation is in line with *in vivo* studies showing that impaired performance of aged animals could be rescued by systemic application of acetylcholine esterase blockers [106,108]. The *in vitro* study was not designed for detecting age-related cholinergic effects but rather to assessing whether neurons from aged animals have, under the same circumstances as those from juvenile animals, the propensity to engage in persistent firing. Accordingly, flooding the cells with cholinergic stimulation by using the bath application of a rather high dose of carbachol (10  $\mu$ M Cch; [312]) did not allow for inferences about potentially fine grained differences in the number of expressed acetylcholine receptors, the efficacy of the cholinergic receptors, or the efficacy of intracellular cascades between both age groups. Furthermore, because carbachol is a poorly

hydrolyzable cholinergic agonist potential age-dependent changes in acetylcholine esterase activity may not be assessed either.

Besides the aforementioned peculiarities of the *in vitro* study, the animals were derived from a variable background. Five out of the seven animals were exposed to a two-week training in the hippocampus-dependent morris water maze task. These five animals, provided eight of the eleven cells tested in 10  $\mu$ M Cch. Previous reports showed that learning may enhance the excitability of CA1 pyramidal neurons [219,289,302]. However, the two cells that exhibited depolarization block (Fig. 3.2.8A) were derived from the two animals that did not undergo water maze training. The remaining cell was derived from an animal that was not trained on the water maze task and exhibited persistent firing. The training on the water maze task did not yield behavioral data that may have allowed a differentiation into aged-impaired and aged-unimpaired animals. Because of the absent behavioral data, the uncontrolled duration between the last day of training and brain slicing (range: 26 - 34 days), as well as the small sample size of the un-trained group, the training must be interpreted as confounder.

In summary, the data obtained from neurons of aged animals demonstrated the capability of these cells to exhibit persistent firing and thereby highlighted that persistent firing was not a peculiarity of juvenile animals. Furthermore, the data suggested that the G-protein coupled intracellular cascades leading to persistent firing were sufficiently functional when cells were flooded with cholinergic stimulation. In light of the aforementioned limitations, I regard an interpretation beyond this summary as highly speculative and refrain from speculating.

### **4.3.2 Relation between *in vitro* and *in vivo* data of epileptiform activity and seizures**

My data support the role of the cholinergic system [128] and intrinsic cellular properties [335,336] in seizures. Despite epilepsy being a network phenomenon [68,137], the network is comprised by individual cells and these may either hamper or facilitate the maintenance and/or spread of aberrant activity [335,336].

The involvement of TRPC channels in the cholinergic-dependent switch between persistent firing and depolarization block (Fig. 3.3.8) supports the role of TRPC1/4 heteromeric channels in pilocarpine induced status epilepticus and in metabotropic glutamate

receptor induced depolarization block [140]. Thus, in addition to the network-mediated anti-epileptic role of TRPC channel blockade [137,138] my results strengthen the view that also the effects of TRPC channel blockade on intrinsic cellular properties may affect the likelihood of cells to engage in epileptiform activity (Fig. 3.3.8; and [140]) and its detrimental effects on a systems level [140].

My data on the involvement of potassium channels in the cholinergic-dependent switch between persistent firing and depolarization block (Fig. 3.3.4 to Fig. 3.3.6) support the role of KCNQ [149,316,331] and SK channels [239,321,337] in epileptiform activity. Especially the need for combined blockade of KCNQ and SK channels for reliable switch from persistent firing to depolarization block (p. 118) supports the relation between KCNQ and SK channels as mutually supportive systems against over-excitation [188]. Particularly for the role of SK channels, older reports [320,321] and my data draw the attention to effects of SK channel modulation on intrinsic properties whereas more recent literature focused on the resultant network effects [239]. Furthermore, my data elucidated that retigabine may pass its anti-epileptic effects [149] in CA1 pyramidal neurons rather by elevating the action potential threshold and thereby preventing aberrant activity to occur in the first place and rather not by terminating excessive excitation (Fig. 3.3.4 and Fig. 3.3.5).

### **4.3.3 Relation between *in vitro* and *in vivo* data of persistent firing**

While exposed to cholinergic activation, all *in vitro* CA1 pyramidal neurons engaged in stimulus-outlasting activity (Fig. 3.3.1). In contrast, a subset of about 10% to 20% of the recorded cells are reported to engage in stimulus-outlasting activity throughout the retention period of various tasks involving the short-term retention of information [213,214,216,338,339]. However, these estimates consider all recorded cells. Yet, when only behaviorally relevant cells are considered, this fraction was shown to increase to about 40% [216]. The activity of cells showing persistent firing throughout the delay phase is rarely set into relation with the behavioral performance [216]. Nevertheless, one report concluded that the activity of cells showing persistent firing throughout the delay phase was not predictive of the behavioral performance [216]. Yet, I propose that this finding may be explained by the employed limited delay duration of six seconds. It was later reported [340] that delay-dependent errors only increase upon the prolongation of the delay interval beyond five seconds (Fig. 4.2). In detail, the majority of errors in a short-term retention of information

task was due to miscoding (~10% of all trials and 54% of the errors) while the temporal gap was shorter than 15 s. At such short delay of <15 s, the fraction of delay-dependent errors was comparably low (<5% of all trials and <27% of the errors). At longer delays of 15 - 30 s, the fraction of miscoding errors remained constant. However, the likelihood of delay-dependent errors increased drastically (~20% of all trials and ~75% of the errors) when the delay period was 15 - 30 s long [340].

These data may indicate that the animals examined by Otto and Eichenbaum (1992) [216] committed a negligible number of delay-dependent errors while the majority of errors may have been due to miscoding. Consequently, the conclusion that persistent action potential generation throughout the delay interval was not predictive of the behavior may be confined to short delay periods. I predict that the frequency of persistent activity during the delay phase will correlate with behavioral performance when retention delays are longer and delay-dependent errors are committed more frequently.

I conclude that revisiting the behavioral relevance of cells showing persistent generation of action potentials throughout the delay phase of a short-term memory task with a delay longer than 15 s may be worthwhile.

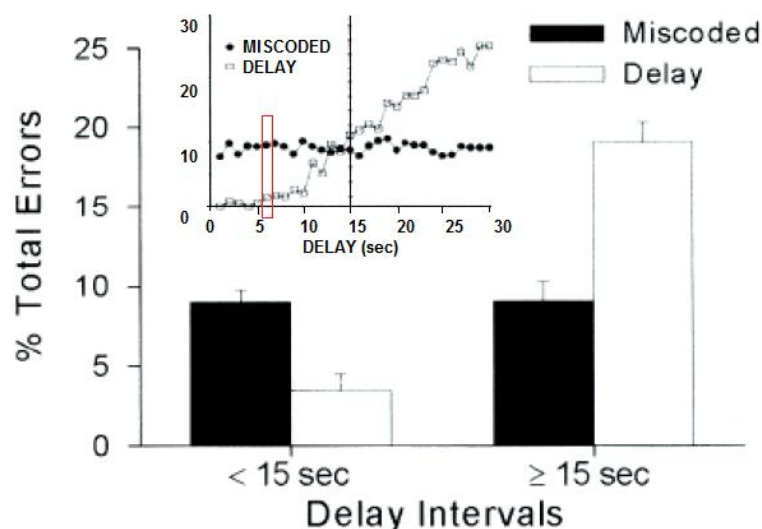


**Figure 4.2: Low fraction of delay-related errors at delay intervals of six seconds**

The bar graph shows that the fraction of delay-related errors at delay intervals shorter than 15 s is lower than at delay intervals longer than 15 s. The scatter plot depicts the linear increase of delay-related errors as the delay interval was prolonged. The red rectangle indicates the delay interval used by Otto and Eichenbaum (1992) [216].

Figure 10E in Deadwyler et al. (1996) [340]; modified.

Furthermore, these data indicate that my *in vitro* investigations merely assess the ability of neurons to engage in persistent firing. Whether a cell will be behaviorally relevant is presumably determined by other factors. Moreover, in case of behavioral relevance of the cell's activity, again other factors may determine whether the cell will engage in persistent firing throughout the delay interval. This matter will be addressed in the subsequent section.

### **4.3.4 Input specificity**

Cholinergic stimulation of the hippocampus is thought to provide rather a tone of activation via volume transmission in contrast to a wired signal transmission [84,86,88]. This mode of activation appears most prominent for acetylcholine but is was also observed for noradrenergic and serotonergic but not for GABAergic neurotransmission [84]. The high prevalence of volume transmission may suggest that muscarinic stimulation may not convey highly specific activation. However, the activity of acetylcholine esterase, which degrades acetylcholine, is known to be highly potent and may rapidly [89] limit the amount of freely available acetylcholine. Thus, despite volume transmission appearing to be the most prevalent mode of cholinergic signal transduction, short lived transients in the sub-second range may nonetheless occur in the hippocampus [111]. However, evidence for such transients is currently limited to the prefrontal cortex [89]. Furthermore, the muscarinic acetylcholine receptor M<sub>2</sub> is known to be an autoreceptor which may limit the excretion of acetylcholine via a positive feedback loop [341]. Due to the volume transmission this positive feedback may potentially affect not only the releasing varicosity but also neighboring nerve endings whose acetylcholine excretion would then be inhibited [84].

These data on the cholinergic transmission mode indicate that muscarinic signaling may not be highly selective. Hence, cholinergic stimulation may endow enhanced responsiveness to a large population of neurons. However, this disposition may not provide input specificity. For the modulatory effects to have an impact, suprathreshold stimulation is required to initiate activity. Hence, the activity of up-stream neurons and the efficacy of synaptic contacts may determine whether an individual neuron exhibits persistent firing or not.

### 4.3.5 Interaction with concurrent neurotransmission

As outlined in the preceding section, wired synaptic transmission may provide input specificity to the rather unspecific facilitating effect of muscarinic excitation. One limitation of the data presented in this dissertation is that only one neuromodulator (acetylcholine) was addressed. However, the conditions *in vivo* are far more complex because they involve a multitude of simultaneously occurring modulation of neuronal activity. One of these is glutamatergic neurotransmission.

As elegantly laid out for attentional processes in the prefrontal cortex [111], the interplay between cholinergic and glutamatergic signaling on the network level may similarly affect the hippocampus. As highlighted in the introduction (Fig. 1.4), the actions of acetylcholine on nicotinic receptors may enhance glutamatergic entorhinal input to CA1 ([112], but see [342]). Simultaneously, the actions of acetylcholine on muscarinic receptors at pre-synapses were shown to block recurrent glutamatergic excitation [115] and the transmission of glutamatergic signals at Schaffer collateral synapses [117,118,343]. On top of that, the actions of acetylcholine on post-synaptic receptors were found to enhance intrinsic excitability of principal neurons [119,154]. Taken together, these effects may mediate a switch from retrieval [112] or consolidation [114] towards focusing attention to environmental cues [114], maintaining the detected information for short periods of time [63,119] up to the point of encoding information [112,114]. The enhancement of intrinsic excitability may be particularly crucial for novel information for which no previously established networks exist [47,97]. The recent proposal of a mechanism that mediates the cholinergic-dependent switch between the aforementioned modes of activity incorporated the excitatory role of the calcium-dependent non-specific cationic current at its core [344].

My research provided evidence that cholinergic activation in conjunction with current injection to CA1 pyramidal neurons may allow for stimulus-induced physiological and potentially behaviorally relevant persistent firing [63]. The discrete current injection may have mimicked glutamatergic excitatory input which may induce persistent firing in a pyramidal neuron that was activated by exposure to acetylcholine. This was of interest because up until then previous reports showed an elevation of the resting membrane potential which may have resulted in repetitive action potential generation but did not show prolonged maintenance of activity induced by a discrete current stimulation [154]. Furthermore, my report demonstrated that CA1 pyramidal neurons may be able to engage in forms of persistent activity that are associated with the short-term retention of information [119] and not



associated with seizure-related hyperexcitation [236]. Hence, my research was located at a basic level showing the feasibility of intrinsic persistent firing in CA1 pyramidal neurons. Further research may elucidate the role of the persistent firing in CA1 pyramidal neurons for the short-term maintenance of information in tasks involving tens of seconds lasting delay periods, as highlighted previously (section 4.3.3)

### 4.3.6 Embedding persistent firing in neuronal networks

The persistent firing I observed lasted for several tens of seconds up to minutes. Such a prolonged undisturbed activity may not be plausible *in vivo*. In the intact behaving animal, activity of interneurons would presumably confine the duration of persistent firing by providing hyperpolarizing impulses. Yet, during the constant wide-spread presence of cholinergic agonists, persistent firing was shown to be robust against perturbation [227]. However, despite the volume transmission of acetylcholine in the hippocampus [84,86,88] the potent degradation of acetylcholine by acetylcholine esterase may confine the cholinergic signal to transients [89,111]. Additionally, in light of the three-dimensional extent of a pyramidal cell and the density of the extracellular matrix which may not be approximated with an aqueous solution, I do not consider a homogeneous cholinergic activation of the entire neuron physiological. Hence, excitatory glutamatergic input may reach the cell at a cholinergically facilitated or unaffected site. Furthermore, the synergistic cholinergic and glutamatergic excitation of the cell [345] may compete with its synaptic inhibition by interneurons.

With regard to the aforementioned considerations, the method adopted in this dissertation is valid for discerning an ability within the response spectrum of a neuron. Advantageously, it allows the decoding of underlying processes and mechanisms. However, it clearly is an oversimplification of the processes in an intact organism, both by wresting the cell from its integration in networks and by providing it with unambiguous signals.

In an intact organism, I envision a neuron to constantly face "uncertainty" with regard to its incoming signals. In that light, I think that information processing, even in individual neurons, may be governed by probabilistic mechanisms in terms of signal detection theory or Bayesian stochastic [346]. The signal detection theory is well acknowledged in the field of decision making [347–350]. However, it may be applied to a broader scope of topics [349]. These probabilistic considerations may potentially describe which output will be generated on the single cell level, on the network level and on the systems level. In short, signal detection

theory covers the principles underlying the choice of a response in the light of a multitude and potentially contradictory information. In neurons, the response may be the generation of action potentials. Importantly, the choice may not be viewed as a conscious, deliberate and explicit process but rather as the result of mechanistically integrating available information. Such information may be provided by the immediate environment and/or the internal state of the neuron. The neuron's immediate environment would be the aforementioned complexity of cholinergic, GABAergic, glutamatergic and, to remain within the scope of this dissertation, further unspecified components (e.g. dopaminergic signaling [351]). The internal state may be established by short- or long-lasting effects. The short-term history of either responding or not responding to a previous signal may be encoded by the metabolic state of the neuron (presumably with a special role of ATP-sensitive potassium channels [352] and store-operated channels [145]). The long-term history of either responding or not responding to a signal is thought to be encoded by synaptic modifications via long-term potentiation, long-term depression or metaplasticity [353–357].

In the light of these considerations, I conclude that the next step would be an investigation on the role of persistent firing in short-term retention of information with delay intervals spanning several tens of seconds ( section 4.3.3) by adopting *in vivo* techniques,

Recently, the discovery of time cells [358] stimulated investigations on the delay interval of behavioral tasks involving the short-term retention of information [359,360]. Time cells are neurons that, across multiple repetitions, reliably generate action potentials at about the same time interval within a delay period, if information has to be retained throughout the delay (Fig. 4.3A). The alignment of cells in a systematic succession with regard to their time field within the delay period, illustrate that a multiplicity of neurons covers the entire delay period (Fig. 4.3B). Intriguingly, the activity of the cell assembly was shown to be associated with behavior [358].

These studies may provide an insight into the potential role of persistent firing. However, the data suggest that long-lasting sustained delay activity may be an exception in these tasks because the neuronal activity of individual cells was confined to shorter intervals than observed *in vitro* [63]. This is in line with the previously mentioned concept that *in vitro* studies merely detect the potentials within the response spectrum of a cell whereas *in vivo* studies may delineate the physiological implementation. Hence, CA1 pyramidal neurons may

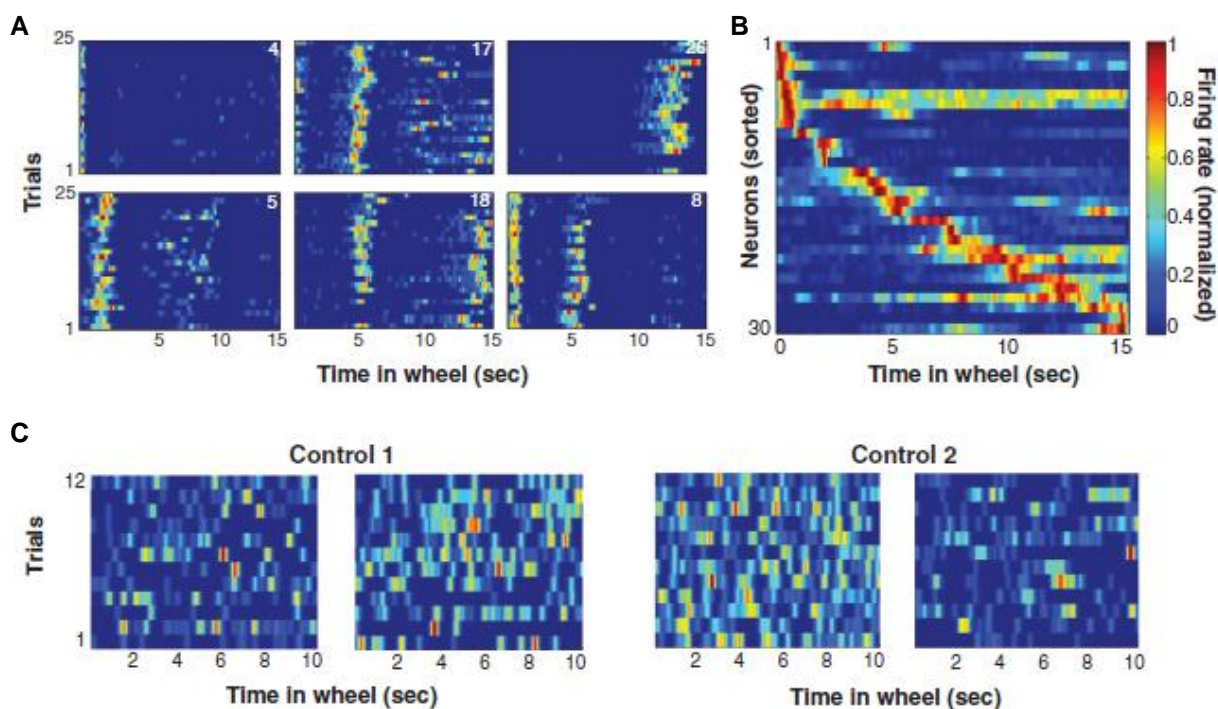


**Figure 4.3: Time cells cover a well defined interval during a delay period.**

(A) The heat maps represent the firing rate of six individual neurons during a 15 seconds long delay interval (x axis). The cells display reproducible spike timings across 25 trials (y axis).

(B) For each neuron, the firing rate was averaged over the trials, normalized to the maximum firing frequency and is presented by one line each (30 neurons, y axis). The graph shows that neurons may be sorted such that their firing occurs in a sequence which spans the entire delay period (x axis).

(C) Related to (A). Neurons recorded during control tasks where no retention of information or behavioral planning was required did not show temporally confined and reproducible activity during the delay period.

Figure 1D and E and figure 3A in Pastalkova et al. (2008) [358]; modified.

potentially have had the ability to generate long-lasting persistent firing [63] but did not usually display it [358–360]. Instead, well timed rather short lasting activity was exhibited (Fig. 4.3A,B).

The theoretical model [47], suggests that sustained intrinsic activity of CA1 pyramidal neuron may be crucial for the short-term retention of novel information. In the following I will discuss three recent studies that investigated time cells and point out why they may not investigate the short-term maintenance of novel information by CA1 pyramidal neurons.

First, in the time-cell experiments of MacDonald et al. (2011) [359], animals were trained to criterion (>70% correct on three consecutive sessions) prior to the implantation surgery. Hence, the animals were highly familiar with the task and potentially with the presented objects and odors.

Second, in the experiments of Pastalkova et al. (2008) [358] (Fig. 4.3) animals were not exposed to a distinct novel stimulus. The information that animals had to retain was their behavioral response during the previous trial. This may not be considered a novel stimulus for which no previously established networks exist. Furthermore, the behavior of the animals may have been shaped prior to the recordings because the demands were rather specific and the error rates were astonishingly low (3, 9 and 13 erroneous choices in the rats 1, 2 and 3; respectively). In detail, animals had to learn that they were required to alternate their responses. Furthermore, they had to learn to operate the running wheel in one direction only. Hence, animals were presumably highly familiar to any detail of the test apparatus. Importantly for the role of CA1 in the short-term retention of information, animals were not exposed to novel stimuli while recording.

Third, in the experiments of Modi et al. (2014) [360] animals were naïve to the task requirements prior to recording because the aim was to delineate the time course as well as the mechanism underlying the generation of the aforementioned time cell activity. Modi et al. (2014) [360] *"concluded that sustained cell activation is not the mechanism used by the hippocampus to maintain a stimulus representation."* However, in my eyes, the investigation undertaken by Modi et al. (2014) [360] may not be conclusive for the involvement of CA1 pyramidal cells in the short-term retention of novel information. I base this statement on the following four specifics of the task. **(I)** First, the trace-conditioning task was comprised by repeated exposure to the same tone serving as a conditioned stimulus. Thus, after a few exposures, this tone may no longer be considered a novel stimulus. **(II)** Second, animals were not naïve to the tone stimulus even at the first application during the trace conditioning paradigm. Prior to the trace conditioning and the calcium imaging, animals were habituated to the tone only. Therefore the animals had been exposed to the tone 30 times within a pre-training session. **(III)** Third, the presence of sustained activity throughout the delay period was assessed once animals reached the conditioned response criterion after an average of 26 (SD: 5) trials. Hence, by that time animals were exposed to the tone up to 60 times. Furthermore, once animals reached the response criterion they had learned that the tone predicted the upcoming unconditioned stimulus. Hence, it is not necessarily the representation of the tone that has to be maintained for successfully avoiding the unconditioned stimulus. Alternatively, it may be sufficient to initiate signaling that merely predicts the time point at which the expected aversive stimulus occurs. The characteristics of the tone (pitch, loudness, duration) may be irrelevant and may therefore not necessarily be retained. **(IV)** Fourth, animals were naïve to the task requirements because they did not know that the retention of

the tone may support them in detecting the contingency with the air puff to the eye. In particular, due to the prior exposure to the tone only, animals had 30 repetitions for potentially learning that no consequence followed the tone and that it may not be a salient stimulus. Upon the onset of the trace conditioning task prediction errors and the potentially associated dopaminergic signaling [361] may thus have mediated the (re)learning that the tone stimulus was indeed a salient stimulus which helped the animals to avoid unpleasant air puffs. In summary, the data presented by Modi et al. (2014) [360] may serve for comprehensively describing the emergence of time cell activity during a delay interval, during which eventually highly familiar stimuli or merely a plan for consecutive actions has to be retained.

In conclusion, I suggest to adopt a task involving the short-term retention of information in which animals are allowed to learn the rules of the task, including the potential exposure to novel stimuli, prior to electrode implantation. Given that the animals know the rules of the task and what they are required to do (i.e. transiently retaining whatever information they will be presented) this would then permit the recording of neurons during the short-term retention of novel information for which no prior networks were established. This task could elucidate whether CA1 pyramidal neurons adopt long-lasting sustained activity throughout the retention period.

### **4.3.7 Questioning the interpretation of persistent-firing and depolarization block as either memory- or seizure-related activity**

A computational study hypothesized that any modulation of neuronal conductances that favor excitation may lower the threshold for depolarization block induction [278]. Cholinergic stimulation appears to be one of these modulators. This is supported by my explicit demonstration that the threshold for the induction of depolarization block was significantly reduced by the application of 10  $\mu$ M Cch (Fig. 3.1.6). However, whether this activity may be considered functionally relevant or if it represents a disease state is untouched by this mechanistic description.

For reasons of clarity, I have consistently associated the depolarization block with seizures; up until now. However, the simplified distinction between memory-related persistent firing and seizure-related depolarization block may be inadequate.

In 2012, Bianchi et al. [278] alluded to a potential functional role of the depolarization block in limiting action potential generation during strong synaptic stimulation. Notably, the

amplitude of the current stimulation was still considered physiological with regard to the multiple excitatory input an individual neuron may receive [278]. Therewith, the depolarization block was ascribed with a potentially compensatory role against hyperexcitation. However, this should be put into perspective of the membrane potential value during the steady state of the depolarization block. Bianchi et al. (2012) [278] highlighted that this protective interpretation may only be applicable if the membrane potential during the steady state of the depolarization block adopts values more hyperpolarized than -35 mV. At more depolarized membrane potentials, action potential independent neurotransmitter release may be enabled [278]. Consequently, a depolarization block that involves a steady state membrane potential more depolarized than -35 mV could contribute to the spread of excitation [278]. Hence, the balance between a physiological preclusion of hyperexcitation and the potentially detrimental spread of hyperexcitation appears to be very delicate. In that light, the association between seizures and the depolarization block observed by the MacVicar group may still be reasonable because the membrane potential at 200 ms after the stimulus offset was reported to be  $-19 \pm 1$  mV (range: -25 to -11 mV, n = 50) and thus consistently more depolarized than -35 mV.

Evidence for a limited coherence between the ability of individual cell to sustain (metabotropic glutamate receptor induced) depolarization block and the induction of seizures by pilocarpine injections is presented by Phelan et al. [140,138,137]. Depolarization block that outlasted a very brief stimulation was blocked in TRPC1/4 double knock-out mice [140]. However, the seizure severity in response to the same dose of pilocarpine was comparable with that of wildtype animals [140]. Yet, the mortality and the damage to individual neurons was lower in TRPC1/4 double knock-out mice compared to wildtype mice [140]. In contrast, TRPC5 knock-out mice still exhibited spontaneous metabotropic glutamate receptor induced bursts that were indistinguishable from those of wild type animals [138]. However, the severity of seizures (at the highest dose of pilocarpine), the mortality and the damage to individual neurons was significantly lower in TRPC5 knock-out mice compared to wildtype mice [138]

The most parsimonious explanation for the incoherence between single cell activity *in vitro* and the effects on behavioral as well as cellular survival may be the use of two different TRPC stimulants. *In vivo*, the cholinergic agonist pilocarpine was used to induce seizures. However, *in vitro*, metabotropic glutamate receptor agonists were used to mimic the *in vivo* state. Current evidence indicates a common intracellular signal transduction cascade that leads to the activation of TRPC channels both by the stimulation of muscarinic acetylcholine

receptors and group I metabotropic glutamate receptors [144]. However, due to the currently incomplete clarification of the mode of TRPC channel activation [144], potential differences between muscarinic cholinergic and metabotropic glutamatergic intracellular signaling with respect to TRPC channels may not be excluded. Furthermore, differential effects on other channels, that may affect seizure susceptibility, should be considered [362].

The latest report on the association of TRPC channels with seizures took network mechanisms into consideration [137]. This new model may potentially resolve the apparent discrepancies in previous publications [138,140]. The data showed that *in vitro* epileptiform burst firing (often comprising depolarization block) remained intact in CA1 but was significantly reduced in CA3 of TRPC7 knock-out mice compared to wildtype mice [137]. In the light of these results, Phelan et al. (2014) [137] proposed a seizure mechanism that was supported by network activity. In detail, they argue that TRPC7 channels are involved in

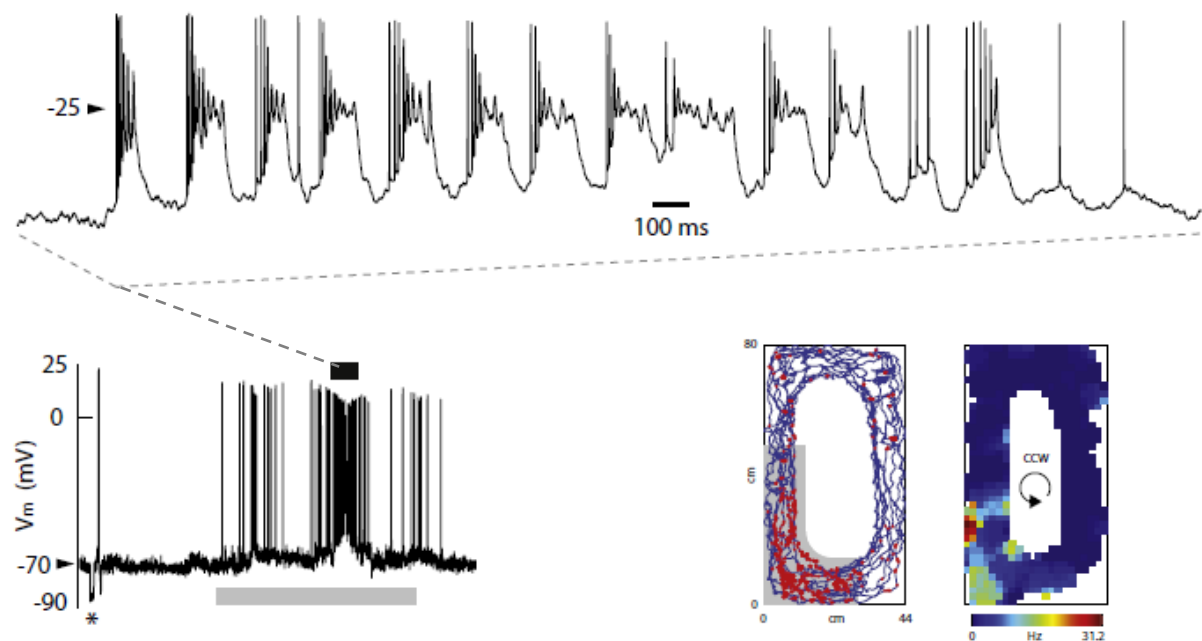


**Figure 4.4: Depolarization block during place field traversal.**

(A) The trace represents the neuronal activity of a neuron in the dorsal portion of the hippocampal CA1 area of a rat while it traversed this neuron's place field on a circular track.

(B) The trace displays the activity of the same neuron at a larger time scale. The time the animal spent in the neuron's place field is indicated by the grey bar.

(C) The right graph illustrates the trajectory (blue) and spike timings (red) of an animal going along the circular track. The heat map on the right shows the firing frequency of the same cell.

Figure 2 A, B and E in Epsztein et al. (2011) [363]; modified.

enhancement of long-term potentiation that depends on NMDA receptors. They suggest that the enhanced efficacy of synapses at recurrent collaterals in CA3 may initiate epileptiform bursts in CA3 pyramidal neurons. Notably, the strengthened network would overrule the neuron's reduced intrinsic propensity to engage in depolarization block. Via the likewise strengthened Schaffer collateral synapses from CA3 to CA1 the epileptiform activity would then be transmitted to CA1. The synaptically transmitted hyperexcitability from CA3 would encounter CA1 neurons whose intrinsic propensity to engage in depolarization block is unaltered. Therewith, a behaviorally overt seizure may potentially be initiated.

Evidence for a functional role of the depolarization block was presented by Epsztein et al. (2011) [363]. While rats were running on a circular maze single cell activity was recorded. Interestingly, when animals passed through the place field of the recorded neuron the membrane potential frequently culminated in depolarization block (Fig. 4.4). Epsztein et al. (2011) interpreted the depolarization block as calcium-mediated and associated it with the induction of metabolic processes that may mediate long-term plasticity which may underlie the stabilization of place fields [363].

## 4.4 Conclusion

With the data presented in this dissertation, I showed that CA1 pyramidal neurons may have the ability to engage in persistent firing. Persistent firing is the sustained generation of action potentials despite the absence of sensory stimulation. With these characteristics, persistent firing may serve as mechanism for short-term retention of information. Importantly, I showed that CA1 pyramidal neurons hold intrinsic mechanisms that enable them to exhibit persistent firing that may be maintained even in the absence of synaptic input. According to that, CA1 pyramidal neurons may potentially be relevant for sustaining information for which no efficient networks have yet been established. Electrophysiological recordings in behaving animals have shown the presence of sustained single cell activity. However, I claim that behavioral data does not yet conclusively show whether this activity is crucial for the animal's performance. Therefore, I have suggested a potential experimental design that may allow to put the hypothesis at test.

The clear-cut distinction between memory-related persistent firing and seizure-related depolarization block may be questioned because the depolarization block may also serve to



prevent hyperexcitation or support long-term plasticity processes via the considerable calcium transients. However, to date one might just start a debate on that matter.

## 5 References

1. Wiesmann, W. (2012). Hansi und Lilo oder wie man ein guter König wird. Parabel ; [Roman] (Pfalzfeld: Kontrast-Verl).
2. Burwell, R.D. and Agster, K.L. (2008). Anatomy of the hippocampus and the declarative memory system. In *Learning and memory. A comprehensive reference*, J.H. Byrne, ed. (Oxford, UK, San Diego, CA: Elsevier), pp. 47–66.
3. Eichenbaum, H., Dudchenko, P., Wood, E., Shapiro, M. and Tanila, H. (1999). The hippocampus, memory, and place cells: is it spatial memory or a memory space? *Neuron* 23, 209–226.
4. Cutsuridis, V., Graham, B., Cobb, S. and Vida, I. (2010). *Hippocampal microcircuits. A computational modeler's resource book* (New York: Springer).
5. Laurberg, S. (1979). Commissural and intrinsic connections of the rat hippocampus. *The Journal of comparative neurology* 184, 685–708.
6. Chang, L.W. and Dyer, R.S. (1985). Septotemporal gradients of trimethyltin-induced hippocampal lesions. *Neurobehavioral toxicology and teratology* 7, 43–49.
7. van Groen, T. and Lopes da Silva, F.H. (1985). Septotemporal distribution of entorhinal projections to the hippocampus in the cat: electrophysiological evidence. *The Journal of comparative neurology* 238, 1–9.
8. Strange, B.A., Witter, M.P., Lein, E.S. and Moser, E.I. (2014). Functional organization of the hippocampal longitudinal axis. *Nature reviews. Neuroscience* 15, 655–669.
9. Moser, E., Moser, M.B. and Andersen, P. (1993). Spatial learning impairment parallels the magnitude of dorsal hippocampal lesions, but is hardly present following ventral lesions. *The Journal of neuroscience : the official journal of the Society for Neuroscience* 13, 3916–3925.
10. Hoz, L. de, Knox, J. and Morris, Richard G M (2003). Longitudinal axis of the hippocampus: both septal and temporal poles of the hippocampus support water maze spatial learning depending on the training protocol. *Hippocampus* 13, 587–603.
11. Stevens, R. and Cowey, A. (1973). Effects of dorsal and ventral hippocampal lesions on spontaneous alternation, learned alternation and probability learning in rats. *Brain research* 52, 203–224.
12. Beer, Z., Chwiesko, C. and Sauvage, M.M. (2014). Processing of spatial and non-spatial information reveals functional homogeneity along the dorso-ventral axis of CA3, but not CA1. *Neurobiology of learning and memory* 111, 56–64.
13. Bragdon, A.C., Taylor, D.M. and Wilson, W.A. (1986). Potassium-induced epileptiform activity in area CA3 varies markedly along the septotemporal axis of the rat hippocampus. *Brain research* 378, 169–173.
14. Gilbert, M., Racine, R.J. and Smith, G.K. (1985). Epileptiform burst responses in ventral vs dorsal hippocampal slices. *Brain research* 361, 389–391.
15. Racine, R., Rose, P.A. and Burnham, W.M. (1977). Afterdischarge thresholds and kindling rates in dorsal and ventral hippocampus and dentate gyrus. *The Canadian journal of neurological sciences. Le journal canadien des sciences neurologiques* 4, 273–278.

16. Ekstrand, J.J., Pouliot, W., Scheerlinck, P. and Dudek, F.E. (2011). Lithium pilocarpine-induced status epilepticus in postnatal day 20 rats results in greater neuronal injury in ventral versus dorsal hippocampus. *Neuroscience* 192, 699–707.
17. Marcelin, B., Lugo, J.N., Brewster, A.L., Liu, Z., Lewis, A.S., McClelland, S., Chetkovich, D.M., Baram, T.Z., Anderson, A.E., Becker, A., et al. (2012). Differential dorso-ventral distributions of Kv4.2 and HCN proteins confer distinct integrative properties to hippocampal CA1 pyramidal cell distal dendrites. *The Journal of biological chemistry* 287, 17656–17661.
18. Dougherty, K.A., Nicholson, D.A., Diaz, L., Buss, E.W., Neuman, K.M., Chetkovich, D.M. and Johnston, D. (2013). Differential expression of HCN subunits alters voltage-dependent gating of h-channels in CA1 pyramidal neurons from dorsal and ventral hippocampus. *Journal of neurophysiology* 109, 1940–1953.
19. Pandis, C., Sotiriou, E., Kouvaras, E., Asproдини, E., Papatheodoropoulos, C. and Angelatou, F. (2006). Differential expression of NMDA and AMPA receptor subunits in rat dorsal and ventral hippocampus. *Neuroscience* 140, 163–175.
20. Sotiriou, E., Papatheodoropoulos, C. and Angelatou, F. (2005). Differential expression of gamma-aminobutyric acid--a receptor subunits in rat dorsal and ventral hippocampus. *Journal of neuroscience research* 82, 690–700.
21. Sarantis, K., Sotiriou, E., Papatheodoropoulos, C., Matsokis, N. and Angelatou, F. (2008). Differential pharmacological properties of GABAA/benzodiazepine receptor complex in dorsal compared to ventral rat hippocampus. *Neurochemistry international* 52, 1019–1029.
22. Papatheodoropoulos, C., Moschovos, C. and Kostopoulos, G. (2005). Greater contribution of N-methyl-D-aspartic acid receptors in ventral compared to dorsal hippocampal slices in the expression and long-term maintenance of epileptiform activity. *Neuroscience* 135, 765–779.
23. Hönigsperger, C., Marosi, M., Murphy, R. and Storm, J.F. (2014). Dorsoventral differences in Kv7/M-current and its impact on resonance, temporal summation and excitability in rat hippocampal pyramidal cells. *The Journal of physiology*.
24. Marcelin, B., Liu, Z., Chen, Y., Lewis, A.S., Becker, A., McClelland, S., Chetkovich, D.M., Migliore, M., Baram, T.Z., Esclapez, M., et al. (2012). Dorsoventral differences in intrinsic properties in developing CA1 pyramidal cells. *The Journal of neuroscience : the official journal of the Society for Neuroscience* 32, 3736–3747.
25. Petrides, T., Georgopoulos, P., Kostopoulos, G. and Papatheodoropoulos, C. (2007). The GABAA receptor-mediated recurrent inhibition in ventral compared with dorsal CA1 hippocampal region is weaker, decays faster and lasts less. *Experimental brain research* 177, 370–383.
26. Ishizuka, N., Weber, J. and Amaral, D.G. (1990). Organization of intrahippocampal projections originating from CA3 pyramidal cells in the rat. *The Journal of comparative neurology* 295, 580–623.
27. Li, X.G., Somogyi, P., Ylinen, A. and Buzsáki, G. (1994). The hippocampal CA3 network: an in vivo intracellular labeling study. *The Journal of comparative neurology* 339, 181–208.
28. Amaral, D.G. (1993). Emerging principles of intrinsic hippocampal organization. *Current opinion in neurobiology* 3, 225–229.
29. Cenquizca, L.A. and Swanson, L.W. (2006). Analysis of direct hippocampal cortical field CA1 axonal projections to diencephalon in the rat. *The Journal of comparative neurology* 497, 101–114.
30. Hebb, D.O. (1949). *The Organization of Behavior: A Neuropsychological Theory* (New York, USA: Wiley).
31. Marr, D. (1971). Simple Memory: A Theory for Archicortex. *Philosophical Transactions of the Royal Society B: Biological Sciences* 262, 23–81.

32. McNaughton, B.L. and Morris, R. (1987). Hippocampal synaptic enhancement and information storage within a distributed memory system. *Trends in Neurosciences* *10*, 408–415.
33. Willshaw, D.J. and Buckingham, J.T. (1990). An assessment of Marr's theory of the hippocampus as a temporary memory store. *Philosophical transactions of the Royal Society of London. Series B, Biological sciences* *329*, 205–215.
34. Wiebe, S.P., Stäubli, U.V. and Ambros-Ingerson, J. (1997). Short-term reverberant memory model of hippocampal field CA3. *Hippocampus* *7*, 656–665.
35. Witter, M.P. and Amaral, D.G. (2004). Hippocampal formation. In *The rat nervous system*, G. Paxinos, ed. (Amsterdam [etc.]: Elsevier Academic Press), pp. 637–703.
36. Tamamaki, N. and Nojyo, Y. (1995). Preservation of topography in the connections between the subiculum, field CA1, and the entorhinal cortex in rats. *The Journal of comparative neurology* *353*, 379–390.
37. Henriksen, E.J., Colgin, L.L., Barnes, C.A., Witter, M.P., Moser, M.-B. and Moser, E.I. (2010). Spatial representation along the proximodistal axis of CA1. *Neuron* *68*, 127–137.
38. Hatanpaa, K.J., Raisanen, J.M., Herndon, E., Burns, D.K., Foong, C., Habib, A.A. and White, C.L. (2014). Hippocampal sclerosis in dementia, epilepsy, and ischemic injury: differential vulnerability of hippocampal subfields. *Journal of neuropathology and experimental neurology* *73*, 136–142.
39. Chang, P.Y., Taylor, P.E. and Jackson, M.B. (2007). Voltage imaging reveals the CA1 region at the CA2 border as a focus for epileptiform discharges and long-term potentiation in hippocampal slices. *Journal of neurophysiology* *98*, 1309–1322.
40. Meldrum, B. (1991). Excitotoxicity and epileptic brain damage. *Epilepsy research* *10*, 55–61.
41. Fanselow, M.S. and Dong, H.-W. (2010). Are the dorsal and ventral hippocampus functionally distinct structures? *Neuron* *65*, 7–19.
42. Scoville, W.B. and Milner, B. (1957). Loss of recent memory after bilateral hippocampal lesions. *Journal of neurology, neurosurgery, and psychiatry* *20*, 11–21.
43. Annese, J., Schenker-Ahmed, N.M., Bartsch, H., Maechler, P., Sheh, C., Thomas, N., Kayano, J., Ghatan, A., Bresler, N., Frosch, M.P., et al. (2014). Postmortem examination of patient H.M.'s brain based on histological sectioning and digital 3D reconstruction. *Nature communications* *5*, 3122.
44. Corkin, S. (2002). What's new with the amnesic patient H.M.? *Nature reviews. Neuroscience* *3*, 153–160.
45. Rempel-Clower, N.L., Zola, S.M., Squire, L.R. and Amaral, D.G. (1996). Three cases of enduring memory impairment after bilateral damage limited to the hippocampal formation. *The Journal of neuroscience : the official journal of the Society for Neuroscience* *16*, 5233–5255.
46. Zola-Morgan, S., Squire, L.R. and Amaral, D.G. (1986). Human amnesia and the medial temporal region: enduring memory impairment following a bilateral lesion limited to field CA1 of the hippocampus. *The Journal of neuroscience : the official journal of the Society for Neuroscience* *6*, 2950–2967.
47. Hasselmo, M.E. and Stern, C.E. (2006). Mechanisms underlying working memory for novel information. *Trends in Cognitive Sciences* *10*, 487–493.
48. Hartley, T., Bird, C.M., Chan, D., Cipolotti, L., Husain, M., Vargha-Khadem, F. and Burgess, N. (2007). The hippocampus is required for short-term topographical memory in humans. *Hippocampus* *17*, 34–48.
49. Hannula, D.E., Tranel, D. and Cohen, N.J. (2006). The long and the short of it: relational memory impairments in amnesia, even at short lags. *The Journal of neuroscience : the official journal of the Society for Neuroscience* *26*, 8352–8359.

50. Cashdollar, N., Malecki, U., Rugg-Gunn, F.J., Duncan, J.S., Lavie, N. and Duzel, E. (2009). Hippocampus-dependent and -independent theta-networks of active maintenance. *Proceedings of the National Academy of Sciences of the United States of America* *106*, 20493–20498.
51. Ranganath, C. and D'Esposito, M. (2001). Medial temporal lobe activity associated with active maintenance of novel information. *Neuron* *31*, 865–873.
52. Ranganath, C., Cohen, M.X. and Brozinsky, C.J. (2005). Working memory maintenance contributes to long-term memory formation: neural and behavioral evidence. *Journal of cognitive neuroscience* *17*, 994–1010.
53. Weiss, C., Bouwmeester, H., Power, J.M. and Disterhoft, J.F. (1999). Hippocampal lesions prevent trace eyeblink conditioning in the freely moving rat. *Behavioural brain research* *99*, 123–132.
54. McEchron, M.D., Tseng, W. and Disterhoft, J.F. (2000). Neurotoxic lesions of the dorsal hippocampus disrupt auditory-cued trace heart rate (fear) conditioning in rabbits. *Hippocampus* *10*, 739–751.
55. McEchron, M.D. and Disterhoft, J.F. (1999). Hippocampal encoding of non-spatial trace conditioning. *Hippocampus* *9*, 385–396.
56. Tseng, W., Guan, R., Disterhoft, J.F. and Weiss, C. (2004). Trace eyeblink conditioning is hippocampally dependent in mice. *Hippocampus* *14*, 58–65.
57. Kesner, R.P., Hunsaker, M.R. and Gilbert, P.E. (2005). The role of CA1 in the acquisition of an object-trace-odor paired associate task. *Behavioral neuroscience* *119*, 781–786.
58. Ainge, J.A., van der Meer, Matthijs A A, Langston, R.F. and Wood, E.R. (2007). Exploring the role of context-dependent hippocampal activity in spatial alternation behavior. *Hippocampus* *17*, 988–1002.
59. Bangasser, D.A., Waxler, D.E., Santollo, J. and Shors, T.J. (2006). Trace conditioning and the hippocampus: the importance of contiguity. *The Journal of neuroscience : the official journal of the Society for Neuroscience* *26*, 8702–8706.
60. Kim, J.J., Clark, R.E. and Thompson, R.F. (1995). Hippampectomy impairs the memory of recently, but not remotely, acquired trace eyeblink conditioned responses. *Behavioral neuroscience* *109*, 195–203.
61. Farovik, A., Dupont, L.M. and Eichenbaum, H. (2010). Distinct roles for dorsal CA3 and CA1 in memory for sequential nonspatial events. *Learning & memory (Cold Spring Harbor, N.Y.)* *17*, 12–17.
62. Suh, J., Rivest, A.J., Nakashiba, T., Tominaga, T. and Tonegawa, S. (2011). Entorhinal cortex layer III input to the hippocampus is crucial for temporal association memory. *Science (New York, N.Y.)* *334*, 1415–1420.
63. Knauer, B., Jochems, A., Valero-Aracama, M.J. and Yoshida, M. (2013). Long-lasting intrinsic persistent firing in rat CA1 pyramidal cells: a possible mechanism for active maintenance of memory. *Hippocampus* *23*, 820–831.
64. Chatzikonstantinou, A. (2014). Epilepsy and the hippocampus. *Frontiers of neurology and neuroscience* *34*, 121–142.
65. Engel, J. (1996). Introduction to temporal lobe epilepsy. *Epilepsy research* *26*, 141–150.
66. Leonardi, M. and Ustun, T.B. (2002). The global burden of epilepsy. *Epilepsia* *43 Suppl 6*, 21–25.
67. WHO (2012). Epilepsy. Fact sheet No 999.
68. Caciagli, L., Bernhardt, B.C., Hong, S.-J., Bernasconi, A. and Bernasconi, N. (2014). Functional network alterations and their structural substrate in drug-resistant epilepsy. *Frontiers in neuroscience* *8*, 411.

69. Han, C.-L., Hu, W., Stead, M., Zhang, T., Zhang, J.-G., Worrell, G.A. and Meng, F.-G. (2014). Electrical stimulation of hippocampus for the treatment of refractory temporal lobe epilepsy. *Brain research bulletin* *109*, 13–21.
70. Babb, T.L., Lieb, J.P., Brown, W.J., Pretorius, J. and Crandall, P.H. (1984). Distribution of pyramidal cell density and hyperexcitability in the epileptic human hippocampal formation. *Epilepsia* *25*, 721–728.
71. Kása, P. (1986). The cholinergic systems in brain and spinal cord. *Progress in neurobiology* *26*, 211–272.
72. Frotscher, M., Schlander, M. and Léránth, C. (1986). Cholinergic neurons in the hippocampus. A combined light- and electron-microscopic immunocytochemical study in the rat. *Cell and tissue research* *246*, 293–301.
73. Freund, T.F. and Buzsáki, G. (1996). Interneurons of the hippocampus. *Hippocampus* *6*, 347–470.
74. Houser, C.R., Crawford, G.D., Barber, R.P., Salvaterra, P.M. and Vaughn, J.E. (1983). Organization and morphological characteristics of cholinergic neurons: an immunocytochemical study with a monoclonal antibody to choline acetyltransferase. *Brain research* *266*, 97–119.
75. Frotscher, M., Vida, I. and Bender, R. (2000). Evidence for the existence of non-GABAergic, cholinergic interneurons in the rodent hippocampus. *Neuroscience* *96*, 27–31.
76. Yi, F., Catudio-Garrett, E., Gábel, R., Wilhelm, M., Erdelyi, F., Szabo, G., Deisseroth, K. and Lawrence, J. (2015). Hippocampal "cholinergic interneurons" visualized with the choline acetyltransferase promoter: anatomical distribution, intrinsic membrane properties, neurochemical characteristics, and capacity for cholinergic modulation. *Frontiers in synaptic neuroscience* *7*, 4.
77. Woolf, N.J. (1991). Cholinergic systems in mammalian brain and spinal cord. *Progress in neurobiology* *37*, 475–524.
78. Dutar, P., Bassant, M.H., Senut, M.C. and Lamour, Y. (1995). The septohippocampal pathway: structure and function of a central cholinergic system. *Physiological reviews* *75*, 393–427.
79. Matthews, D.A., Salvaterra, P.M., Crawford, G.D., Houser, C.R. and Vaughn, J.E. (1987). An immunocytochemical study of choline acetyltransferase-containing neurons and axon terminals in normal and partially deafferented hippocampal formation. *Brain research* *402*, 30–43.
80. Lewis, P.R., Shute, C.C. and Silver, A. (1967). Confirmation from choline acetylase analyses of a massive cholinergic innervation to the rat hippocampus. *The Journal of physiology* *191*, 215–224.
81. Krnjević, K. and Ropert, N. (1981). Septo-hippocampal pathway modulates hippocampal activity by a cholinergic mechanism. *Canadian journal of physiology and pharmacology* *59*, 911–914.
82. Amaral, D.G. and Kurz, J. (1985). An analysis of the origins of the cholinergic and noncholinergic septal projections to the hippocampal formation of the rat. *The Journal of comparative neurology* *240*, 37–59.
83. Woolf, N.J. (1997). A possible role for cholinergic neurons of the basal forebrain and pontomesencephalon in consciousness. *Consciousness and cognition* *6*, 574–596.
84. Umbriaco, D., Garcia, S., Beaulieu, C. and Descarries, L. (1995). Relational features of acetylcholine, noradrenaline, serotonin and GABA axon terminals in the stratum radiatum of adult rat hippocampus (CA1). *Hippocampus* *5*, 605–620.
85. Sarter, M., Parikh, V. and Howe, W.M. (2009). Phasic acetylcholine release and the volume transmission hypothesis: time to move on. *Nature reviews. Neuroscience* *10*, 383–390.

86. Yamasaki, M., Matsui, M. and Watanabe, M. (2010). Preferential localization of muscarinic M1 receptor on dendritic shaft and spine of cortical pyramidal cells and its anatomical evidence for volume transmission. *The Journal of neuroscience : the official journal of the Society for Neuroscience* 30, 4408–4418.
87. Teles-Grilo Ruivo, L.M. and Mellor, J.R. (2013). Cholinergic modulation of hippocampal network function. *Frontiers in synaptic neuroscience* 5, 2.
88. Descarries, L., Gisiger, V. and Steriade, M. (1997). Diffuse transmission by acetylcholine in the CNS. *Progress in neurobiology* 53, 603–625.
89. Parikh, V., Kozak, R., Martinez, V. and Sarter, M. (2007). Prefrontal acetylcholine release controls cue detection on multiple timescales. *Neuron* 56, 141–154.
90. Paolone, G., Angelakos, C.C., Meyer, P.J., Robinson, T.E. and Sarter, M. (2013). Cholinergic control over attention in rats prone to attribute incentive salience to reward cues. *The Journal of neuroscience : the official journal of the Society for Neuroscience* 33, 8321–8335.
91. Kametani, H. and Kawamura, H. (1990). Alterations in acetylcholine release in the rat hippocampus during sleep-wakefulness detected by intracerebral dialysis. *Life Sciences* 47, 421–426.
92. Burmeister, J.J., Pomerleau, F., Huettl, P., Gash, C.R., Werner, C.E., Bruno, J.P. and Gerhardt, G.A. (2008). Ceramic-based multisite microelectrode arrays for simultaneous measures of choline and acetylcholine in CNS. *Biosensors & bioelectronics* 23, 1382–1389.
93. Rawlins, J.N., Feldon, J. and Butt, S. (1985). The effects of delaying reward on choice preference in rats with hippocampal or selective septal lesions. *Behavioural brain research* 15, 191–203.
94. Fontán-Lozano, A., Troncoso, J., Múnera, A., Carrión, A.M. and Delgado-García, J.M. (2005). Cholinergic septo-hippocampal innervation is required for trace eyeblink classical conditioning. *Learning & memory (Cold Spring Harbor, N.Y.)* 12, 557–563.
95. Asaka, Y., Seager, M.A., Griffin, A.L. and Berry, S.D. (2000). Medial septal microinfusion of scopolamine disrupts hippocampal activity and trace jaw movement conditioning. *Behavioral neuroscience* 114, 1068–1077.
96. Schon, K., Atri, A., Hasselmo, M.E., Tricarico, M.D., LoPresti, M.L. and Stern, C.E. (2005). Scopolamine reduces persistent activity related to long-term encoding in the parahippocampal gyrus during delayed matching in humans. *The Journal of neuroscience : the official journal of the Society for Neuroscience* 25, 9112–9123.
97. McGaughy, J., Koene, R.A., Eichenbaum, H. and Hasselmo, M.E. (2005). Cholinergic deafferentation of the entorhinal cortex in rats impairs encoding of novel but not familiar stimuli in a delayed nonmatch-to-sample task. *The Journal of neuroscience : the official journal of the Society for Neuroscience* 25, 10273–10281.
98. Giacobini, E. (2003). Cholinergic function and Alzheimer's disease. *International journal of geriatric psychiatry* 18, S1-5.
99. Muir, J.L. (1997). Acetylcholine, aging, and Alzheimer's disease. *Pharmacology, biochemistry, and behavior* 56, 687–696.
100. Whitehouse, P.J., Price, D.L., Struble, R.G., Clark, A.W., Coyle, J.T. and Delon, M.R. (1982). Alzheimer's disease and senile dementia: loss of neurons in the basal forebrain. *Science (New York, N.Y.)* 215, 1237–1239.
101. Levey, A.I. (1996). Muscarinic acetylcholine receptor expression in memory circuits: implications for treatment of Alzheimer disease. *Proceedings of the National Academy of Sciences of the United States of America* 93, 13541–13546.
102. NIH (2014). Alzheimer's disease medication facts sheet.
103. Bartus, R.T., Dean, R.L., Beer, B. and Lippa, A.S. (1982). The cholinergic hypothesis of geriatric memory dysfunction. *Science (New York, N.Y.)* 217, 408–414.

104. Dumas, J.A. and Newhouse, P.A. (2011). The cholinergic hypothesis of cognitive aging revisited again: cholinergic functional compensation. *Pharmacology, biochemistry, and behavior* 99, 254–261.
105. Ta, A.T., Huang, S.-E., Chiu, M.-J., Hua, M.-S., Tseng, W.-Y.I., Chen, S.-H.A. and Qiu, A. (2012). Age-related vulnerabilities along the hippocampal longitudinal axis. *Human brain mapping* 33, 2415–2427.
106. Disterhoft, J.F., Kronforst-Collins, M., Oh, M.M., Power, J.M., Preston, A.R. and Weiss, C. (1999). Cholinergic facilitation of trace eyeblink conditioning in aging rabbits. *Life Sciences* 64, 541–548.
107. Disterhoft, J.F. and Oh, M.M. (2007). Alterations in intrinsic neuronal excitability during normal aging. *Aging cell* 6, 327–336.
108. Oh, M.M., Power, J.M., Thompson, L.T., Moriearty, P.L. and Disterhoft, J.F. (1999). Metrifonate increases neuronal excitability in CA1 pyramidal neurons from both young and aging rabbit hippocampus. *The Journal of neuroscience : the official journal of the Society for Neuroscience* 19, 1814–1823.
109. Power, J.M., Wu, W.W., Sametsky, E., Oh, M.M. and Disterhoft, J.F. (2002). Age-related enhancement of the slow outward calcium-activated potassium current in hippocampal CA1 pyramidal neurons in vitro. *The Journal of neuroscience : the official journal of the Society for Neuroscience* 22, 7234–7243.
110. Oh, M.M., Oliveira, F.A. and Disterhoft, J.F. (2010). Learning and aging related changes in intrinsic neuronal excitability. *Frontiers in aging neuroscience* 2, 2.
111. Hasselmo, M.E. and Sarter, M. (2011). Modes and models of forebrain cholinergic neuromodulation of cognition. *Neuropsychopharmacology : official publication of the American College of Neuropsychopharmacology* 36, 52–73.
112. Hasselmo, M.E. (2006). The role of acetylcholine in learning and memory. *Current opinion in neurobiology* 16, 710–715.
113. Blokland, A. (1995). Acetylcholine: a neurotransmitter for learning and memory? *Brain research. Brain research reviews* 21, 285–300.
114. Hasselmo, M.E. and McGaughy, J. (2004). High acetylcholine levels set circuit dynamics for attention and encoding and low acetylcholine levels set dynamics for consolidation. *Progress in brain research* 145, 207–231.
115. Hasselmo, M.E. and McClelland, J.L. (1999). Neural models of memory. *Current opinion in neurobiology* 9, 184–188.
116. Fernández de Sevilla, D., Cabezas, C., de Prada, A.N., Sánchez-Jiménez, A. and Buño, W. (2002). Selective muscarinic regulation of functional glutamatergic Schaffer collateral synapses in rat CA1 pyramidal neurons. *The Journal of physiology* 545, 51–63.
117. Hasselmo, M.E. and Schnell, E. (1994). Laminar selectivity of the cholinergic suppression of synaptic transmission in rat hippocampal region CA1: computational modeling and brain slice physiology. *The Journal of neuroscience : the official journal of the Society for Neuroscience* 14, 3898–3914.
118. Hounsgaard, J. (1978). Presynaptic inhibitory action of acetylcholine in area CA1 of the hippocampus. *Experimental neurology* 62, 787–797.
119. Egorov, A.V., Hamam, B.N., Fransén, E., Hasselmo, M.E. and Alonso, A.A. (2002). Graded persistent activity in entorhinal cortex neurons. *Nature* 420, 173–178.
120. McLaughlin, F.L. (1933). ACETYLCHOLINE IN THE TREATMENT OF EPILEPSY. *British medical journal* 1, 997–998.
121. Lloyd, J.E. (1933). Acetylcholine therapy in epilepsy. *British medical journal* 1, 999.
122. Carter, S. and Merritt, H.H. (1955). Convulsive disorders. *Disease-a-month : DM*, 1–40.



123. Ferguson, J.H. and Cornblath, D.R. (1975). Acetylcholine epilepsy: relationship of surface concentration, chronicity of denervation, and focus size. *Experimental neurology* *46*, 302–314.
124. Turski, L., Ikonomidou, C., Turski, W.A., Bortolotto, Z.A. and Cavalheiro, E.A. (1989). Review: cholinergic mechanisms and epileptogenesis. The seizures induced by pilocarpine: a novel experimental model of intractable epilepsy. *Synapse (New York, N.Y.)* *3*, 154–171.
125. Turski, L., Cavalheiro, E.A., Czuczwar, S.J., Turski, W.A. and Kleinrok, Z. (1987). The seizures induced by pilocarpine: behavioral, electroencephalographic and neuropathological studies in rodents. *Polish journal of pharmacology and pharmacy* *39*, 545–555.
126. Kandravicius, L., Balista, P.A., Lopes-Aguiar, C., Ruggiero, R.N., Umeoka, E.H., Garcia-Cairasco, N., Bueno-Junior, L.S. and Leite, J.P. (2014). Animal models of epilepsy: use and limitations. *Neuropsychiatric disease and treatment* *10*, 1693–1705.
127. Scorza, F.A., Arida, R.M., Naffah-Mazzacoratti, Maria da Graça, Scerni, D.A., Calderazzo, L. and Cavalheiro, E.A. (2009). The pilocarpine model of epilepsy: what have we learned? *Anais da Academia Brasileira de Ciências* *81*, 345–365.
128. Friedman, A., Behrens, C.J. and Heinemann, U. (2007). Cholinergic dysfunction in temporal lobe epilepsy. *Epilepsia* *48 Suppl 5*, 126–130.
129. Dupont, S., Semah, F., Loc'h, C., Strijckmans, V., Baulac, M., Samson, Y. and Mazière, B. (1999). In vivo imaging of muscarinic cholinergic receptors in temporal lobe epilepsy with a new PET tracer: [76Br]4-bromodexetimide. *Journal of nuclear medicine : official publication, Society of Nuclear Medicine* *40*, 935–941.
130. Boundy, K.L., Rowe, C.C., Black, A.B., Kitchener, M.I., Barnden, L.R., Sebben, R., Kneebone, A., Kassiou, M., Katsifis, A. and Lambrecht, R. (1996). Localization of temporal lobe epileptic foci with iodine-123 iododexetimide cholinergic neuroreceptor single-photon emission computed tomography. *Neurology* *47*, 1015–1020.
131. Rogawski, M.A. and Löscher, W. (2004). The neurobiology of antiepileptic drugs. *Nature reviews. Neuroscience* *5*, 553–564.
132. Vajda, Frank J E and Eadie, M.J. (2014). The clinical pharmacology of traditional antiepileptic drugs. *Epileptic disorders : international epilepsy journal with videotape* *16*, 395–408.
133. D'Antuono, M., Kawasaki, H., Palmieri, C., Curia, G., Biagini, G. and Avoli, M. (2007). Antiepileptic drugs and muscarinic receptor-dependent excitation in the rat subiculum. *Neuropharmacology* *52*, 1291–1302.
134. Löscher, W., Klitgaard, H., Twyman, R.E. and Schmidt, D. (2013). New avenues for anti-epileptic drug discovery and development. *Nature reviews. Drug discovery* *12*, 757–776.
135. Cohen-Gadol, A.A., Wilhelmi, B.G., Collignon, F., White, J.B., Britton, J.W., Cambier, D.M., Christianson, Teresa J H, Marsh, W.R., Meyer, F.B. and Cascino, G.D. (2006). Long-term outcome of epilepsy surgery among 399 patients with nonlesional seizure foci including mesial temporal lobe sclerosis. *Journal of neurosurgery* *104*, 513–524.
136. Ramey, W.L., Martirosyan, N.L., Lieu, C.M., Hasham, H.A., Lemole, G.M. and Weinand, M.E. (2013). Current management and surgical outcomes of medically intractable epilepsy. *Clinical neurology and neurosurgery* *115*, 2411–2418.
137. Phelan, K.D., Shwe, U.T., Abramowitz, J., Birnbaumer, L. and Zheng, F. (2014). Critical role of canonical transient receptor potential channel 7 in initiation of seizures. *Proceedings of the National Academy of Sciences of the United States of America* *111*, 11533–11538.
138. Phelan, K.D., Shwe, U.T., Abramowitz, J., Wu, H., Rhee, S.W., Howell, M.D., Gottschall, P.E., Freichel, M., Flockerzi, V., Birnbaumer, L., et al. (2013). Canonical transient receptor channel 5 (TRPC5) and TRPC1/4 contribute to seizure and excitotoxicity by distinct cellular mechanisms. *Molecular pharmacology* *83*, 429–438.
139. Zeng, C., Zhou, P., Jiang, T., Yuan, C., Ma, Y., Feng, L., Liu, R., Tang, W., Long, X., Xiao, B., et al. (2014). Upregulation and Diverse Roles of TRPC3 and TRPC6 in Synaptic

- Reorganization of the Mossy Fiber Pathway in Temporal Lobe Epilepsy. *Molecular neurobiology*.
140. Phelan, K.D., Mock, M.M., Kretz, O., Shwe, U.T., Kozhemyakin, M., Greenfield, L.J., Dietrich, A., Birnbaumer, L., Freichel, M., Flockerzi, V., et al. (2012). Heteromeric canonical transient receptor potential 1 and 4 channels play a critical role in epileptiform burst firing and seizure-induced neurodegeneration. *Molecular pharmacology* 81, 384–392.
  141. Tai, C., Hines, D.J., Choi, H.B. and MacVicar, B.A. (2011). Plasma membrane insertion of TRPC5 channels contributes to the cholinergic plateau potential in hippocampal CA1 pyramidal neurons. *Hippocampus* 21, 958–967.
  142. Kim, D.-S., Ryu, H.J., Kim, J.-E. and Kang, T.-C. (2013). The reverse roles of transient receptor potential canonical channel-3 and -6 in neuronal death following pilocarpine-induced status epilepticus. *Cellular and molecular neurobiology* 33, 99–109.
  143. Zhou, F.-W. and Roper, S.N. (2014). TRPC3 mediates hyperexcitability and epileptiform activity in immature cortex and experimental cortical dysplasia. *Journal of neurophysiology* 111, 1227–1237.
  144. Reboreda, A., Jiménez-Díaz, L. and Navarro-López, J.D. (2011). TRP channels and neural persistent activity. *Advances in experimental medicine and biology* 704, 595–613.
  145. Sun, Y., Sukumaran, P., Bandyopadhyay, B.C. and Singh, B.B. (2014). Physiological Function and Characterization of TRPCs in Neurons. *Cells* 3, 455–475.
  146. D'Adamo, M.C., Catacuzzeno, L., Di Giovanni, G., Franciolini, F. and Pessia, M. (2013). K(+) channelepsy: progress in the neurobiology of potassium channels and epilepsy. *Frontiers in cellular neuroscience* 7, 134.
  147. Zhou, P., Zhang, Y., Xu, H., Chen, F., Chen, X., Li, X., Pi, X., Wang, L., Zhan, L., Nan, F., et al. (2015). P-retigabine: an N-propargyld retigabine with improved brain distribution and enhanced antiepileptic activity. *Molecular pharmacology* 87, 31–38.
  148. Wehner, T., Chinnasami, S., Novy, J., Bell, G.S., Duncan, J.S. and Sander, J.W. (2014). Long term retention of retigabine in a cohort of people with drug resistant epilepsy. *Seizure* 23, 878–881.
  149. Gunthorpe, M.J., Large, C.H. and Sankar, R. (2012). The mechanism of action of retigabine (ezogabine), a first-in-class K<sup>+</sup> channel opener for the treatment of epilepsy. *Epilepsia* 53, 412–424.
  150. Fisher, R.S. (2015). Stimulation of the medial septum should benefit patients with temporal lobe epilepsy. *Medical hypotheses*.
  151. Krnjević, K., Pumain, R. and Renaud, L. (1971). The mechanism of excitation by acetylcholine in the cerebral cortex. *The Journal of physiology* 215, 247–268.
  152. Halliwell, J.V. and Adams, P.R. (1982). Voltage-clamp analysis of muscarinic excitation in hippocampal neurons. *Brain research* 250, 71–92.
  153. Cole, A.E. and Nicoll, R.A. (1983). Acetylcholine mediates a slow synaptic potential in hippocampal pyramidal cells. *Science (New York, N.Y.)* 221, 1299–1301.
  154. Benardo, L.S. and Prince, D.A. (1981). Acetylcholine induced modulation of hippocampal pyramidal neurons. *Brain research* 211, 227–234.
  155. Cole, A.E. and Nicoll, R.A. (1984). Characterization of a slow cholinergic post-synaptic potential recorded in vitro from rat hippocampal pyramidal cells. *The Journal of physiology* 352, 173–188.
  156. Cole, A.E. and Nicoll, R.A. (1984). The pharmacology of cholinergic excitatory responses in hippocampal pyramidal cells. *Brain research* 305, 283–290.
  157. Benardo, L.S. and Prince, D.A. (1982). Cholinergic pharmacology of mammalian hippocampal pyramidal cells. *Neuroscience* 7, 1703–1712.

158. Ropert, N. and Krnjević, K. (1982). Pharmacological characteristics of facilitation of hippocampal population spikes by cholinomimetics. *Neuroscience* 7, 1963–1977.
159. Sakmann, B. and Neher, E. (1984). Patch clamp techniques for studying ionic channels in excitable membranes. *Annual review of physiology* 46, 455–472.
160. Wilson, W.A. and Goldner, M.M. (1975). Voltage clamping with a single microelectrode. *Journal of neurobiology* 6, 411–422.
161. Azouz, R., Jensen, M.S. and Yaari, Y. (1994). Muscarinic modulation of intrinsic burst firing in rat hippocampal neurons. *The European journal of neuroscience* 6, 961–966.
162. Figenschou, A., Hu, G.Y. and Storm, J.F. (1996). Cholinergic modulation of the action potential in rat hippocampal neurons. *The European journal of neuroscience* 8, 211–219.
163. Power, J.M. and Sah, P. (2002). Nuclear calcium signaling evoked by cholinergic stimulation in hippocampal CA1 pyramidal neurons. *The Journal of neuroscience : the official journal of the Society for Neuroscience* 22, 3454–3462.
164. Dasari, S. and Gullidge, A.T. (2011). M1 and M4 receptors modulate hippocampal pyramidal neurons. *Journal of neurophysiology* 105, 779–792.
165. Martinson, E.A., Goldstein, D. and Brown, J.H. (1989). Muscarinic receptor activation of phosphatidylcholine hydrolysis. Relationship to phosphoinositide hydrolysis and diacylglycerol metabolism. *The Journal of biological chemistry* 264, 14748–14754.
166. Sudweeks, S.N. and Yakel, J.L. (2000). Functional and molecular characterization of neuronal nicotinic ACh receptors in rat CA1 hippocampal neurons. *The Journal of physiology* 527 Pt 3, 515–528.
167. McQuiston, A.R. and Madison, D.V. (1999). Nicotinic receptor activation excites distinct subtypes of interneurons in the rat hippocampus. *The Journal of neuroscience : the official journal of the Society for Neuroscience* 19, 2887–2896.
168. Frazier, C.J., Rollins, Y.D., Breese, C.R., Leonard, S., Freedman, R. and Dunwiddie, T.V. (1998). Acetylcholine activates an alpha-bungarotoxin-sensitive nicotinic current in rat hippocampal interneurons, but not pyramidal cells. *The Journal of neuroscience : the official journal of the Society for Neuroscience* 18, 1187–1195.
169. McQuiston, A.R. (2014). Acetylcholine release and inhibitory interneuron activity in hippocampal CA1. *Frontiers in synaptic neuroscience* 6, 20.
170. Caulfield, M.P., Robbins, J., Higashida, H. and Brown, D.A. (1993). Postsynaptic actions of acetylcholine: the coupling of muscarinic receptor subtypes to neuronal ion channels. *Progress in brain research* 98, 293–301.
171. Caulfield, M.P. (1993). Muscarinic receptors--characterization, coupling and function. *Pharmacology & therapeutics* 58, 319–379.
172. Hulme, E.C., Birdsall, N.J. and Buckley, N.J. (1990). Muscarinic receptor subtypes. *Annual review of pharmacology and toxicology* 30, 633–673.
173. Levey, A.I., Edmunds, S.M., Koliatsos, V., Wiley, R.G. and Heilman, C.J. (1995). Expression of m1-m4 muscarinic acetylcholine receptor proteins in rat hippocampus and regulation by cholinergic innervation. *The Journal of neuroscience : the official journal of the Society for Neuroscience* 15, 4077–4092.
174. Hulme, E.C. (1990). Muscarinic acetylcholine receptors: typical G-coupled receptors. *Symposia of the Society for Experimental Biology* 44, 39–54.
175. Brown, D.A. and Passmore, G.M. (2009). Neural KCNQ (Kv7) channels. *British journal of pharmacology* 156, 1185–1195.
176. Peralta, E.G., Ashkenazi, A., Winslow, J.W., Ramachandran, J. and Capon, D.J. (1988). Differential regulation of PI hydrolysis and adenylyl cyclase by muscarinic receptor subtypes. *Nature* 334, 434–437.

177. Bonner, T.I. (1992). Domains of muscarinic acetylcholine receptors that confer specificity of G protein coupling. *Trends in pharmacological sciences* *13*, 48–50.
178. Alger, B.E. and Nicoll, R.A. (1980). Epileptiform burst afterhyperpolarization: calcium-dependent potassium potential in hippocampal CA1 pyramidal cells. *Science (New York, N.Y.)* *210*, 1122–1124.
179. Storm, J.F. (1990). Potassium currents in hippocampal pyramidal cells. *Progress in brain research* *83*, 161–187.
180. Hu, H., Vervaeke, K. and Storm, J.F. (2007). M-channels (Kv7/KCNQ channels) that regulate synaptic integration, excitability, and spike pattern of CA1 pyramidal cells are located in the perisomatic region. *The Journal of neuroscience : the official journal of the Society for Neuroscience* *27*, 1853–1867.
181. Wang, H. (1998). KCNQ2 and KCNQ3 Potassium Channel Subunits: Molecular Correlates of the M-Channel. *Science* *282*, 1890–1893.
182. Storm, J.F. (1989). An after-hyperpolarization of medium duration in rat hippocampal pyramidal cells. *The Journal of physiology* *409*, 171–190.
183. Dutar, P. and Nicoll, R.A. (1988). Stimulation of phosphatidylinositol (PI) turnover may mediate the muscarinic suppression of the M-current in hippocampal pyramidal cells. *Neuroscience letters* *85*, 89–94.
184. Andrade, R., Foehring, R.C. and Tzingounis, A.V. (2012). The calcium-activated slow AHP: cutting through the Gordian knot. *Frontiers in cellular neuroscience* *6*, 47.
185. Hotson, J.R. and Prince, D.A. (1980). A calcium-activated hyperpolarization follows repetitive firing in hippocampal neurons. *Journal of neurophysiology* *43*, 409–419.
186. Stocker, M., Krause, M. and Pedarzani, P. (1999). An apamin-sensitive Ca<sup>2+</sup>-activated K<sup>+</sup> current in hippocampal pyramidal neurons. *Proceedings of the National Academy of Sciences of the United States of America* *96*, 4662–4667.
187. Stocker, M. (2004). Ca(2+)-activated K<sup>+</sup> channels: molecular determinants and function of the SK family. *Nature reviews. Neuroscience* *5*, 758–770.
188. Chen, S., Benninger, F. and Yaari, Y. (2014). Role of small conductance Ca<sup>2+</sup>-activated K<sup>+</sup> channels in controlling CA1 pyramidal cell excitability. *The Journal of neuroscience : the official journal of the Society for Neuroscience* *34*, 8219–8230.
189. Gu, N., Vervaeke, K., Hu, H. and Storm, J.F. (2005). Kv7/KCNQ/M and HCN/h, but not KCa2/SK channels, contribute to the somatic medium after-hyperpolarization and excitability control in CA1 hippocampal pyramidal cells. *The Journal of physiology* *566*, 689–715.
190. Gullledge, A.T. and Kawaguchi, Y. (2007). Phasic cholinergic signaling in the hippocampus: functional homology with the neocortex? *Hippocampus* *17*, 327–332.
191. Buchanan, K.A., Petrovic, M.M., Chamberlain, Sophie E L, Marrion, N.V. and Mellor, J.R. (2010). Facilitation of long-term potentiation by muscarinic M(1) receptors is mediated by inhibition of SK channels. *Neuron* *68*, 948–963.
192. Giessel, A.J. and Sabatini, B.L. (2010). M1 muscarinic receptors boost synaptic potentials and calcium influx in dendritic spines by inhibiting postsynaptic SK channels. *Neuron* *68*, 936–947.
193. Maylie, J. and Adelman, J.P. (2010). Cholinergic signaling through synaptic SK channels: it's a protein kinase but which one? *Neuron* *68*, 809–811.
194. Sah, P. and Isaacson, J.S. (1995). Channels underlying the slow afterhyperpolarization in hippocampal pyramidal neurons: neurotransmitters modulate the open probability. *Neuron* *15*, 435–441.
195. Benardo, L.S. and Prince, D.A. (1982). Ionic mechanisms of cholinergic excitation in mammalian hippocampal pyramidal cells. *Brain research* *249*, 333–344.

196. Tzingounis, A.V. and Nicoll, R.A. (2008). Contribution of KCNQ2 and KCNQ3 to the medium and slow afterhyperpolarization currents. *Proceedings of the National Academy of Sciences of the United States of America* *105*, 19974–19979.
197. Kim, K.S., Kobayashi, M., Takamatsu, K. and Tzingounis, A.V. (2012). Hippocalcin and KCNQ channels contribute to the kinetics of the slow afterhyperpolarization. *Biophysical journal* *103*, 2446–2454.
198. Partridge, L.D. and Swandulla, D. (1988). Calcium-activated non-specific cation channels. *Trends in Neurosciences* *11*, 69–72.
199. Yan, H.-D., Villalobos, C. and Andrade, R. (2009). TRPC Channels Mediate a Muscarinic Receptor-Induced Afterdepolarization in Cerebral Cortex. *The Journal of neuroscience : the official journal of the Society for Neuroscience* *29*, 10038–10046.
200. Dasari, S., Abramowitz, J., Birnbaumer, L. and Gullledge, A.T. (2013). Do canonical transient receptor potential channels mediate cholinergic excitation of cortical pyramidal neurons? *Neuroreport* *24*, 550–554.
201. Pedersen, S.F., Owsianik, G. and Nilius, B. (2005). TRP channels: an overview. *Cell calcium* *38*, 233–252.
202. Talavera, K., Nilius, B. and Voets, T. (2008). Neuronal TRP channels: thermometers, pathfinders and life-savers. *Trends in Neurosciences* *31*, 287–295.
203. Ambudkar, I.S. and Ong, H.L. (2007). Organization and function of TRPC channelosomes. *Pflügers Archiv : European journal of physiology* *455*, 187–200.
204. Strübing, C., Krapivinsky, G., Krapivinsky, L. and Clapham, D.E. (2001). TRPC1 and TRPC5 form a novel cation channel in mammalian brain. *Neuron* *29*, 645–655.
205. Fowler, M.A., Sidiropoulou, K., Ozkan, E.D., Phillips, C.W. and Cooper, D.C. (2007). Corticolimbic expression of TRPC4 and TRPC5 channels in the rodent brain. *PloS one* *2*, e573.
206. Chung, Y.H., Sun Ahn, H., Kim, D., Hoon Shin, D., Su Kim, S., Yong Kim, K., Bok Lee, W. and Ik Cha, C. (2006). Immunohistochemical study on the distribution of TRPC channels in the rat hippocampus. *Brain research* *1085*, 132–137.
207. Cheng, K.T., Ong, H.L., Liu, X. and Ambudkar, I.S. (2013). Contribution and regulation of TRPC channels in store-operated Ca<sup>2+</sup> entry. *Current topics in membranes* *71*, 149–179.
208. Santoro, B. and Tibbs, G.R. (1999). The HCN gene family: molecular basis of the hyperpolarization-activated pacemaker channels. *Annals of the New York Academy of Sciences* *868*, 741–764.
209. Pian, P., Bucchi, A., Decostanzo, A., Robinson, R.B. and Siegelbaum, S.A. (2007). Modulation of cyclic nucleotide-regulated HCN channels by PIP(2) and receptors coupled to phospholipase C. *Pflügers Archiv : European journal of physiology* *455*, 125–145.
210. Major, G. and Tank, D. (2004). Persistent neural activity: prevalence and mechanisms. *Current opinion in neurobiology* *14*, 675–684.
211. Solomon, P.R., Vander Schaaf, E R, Thompson, R.F. and Weisz, D.J. (1986). Hippocampus and trace conditioning of the rabbit's classically conditioned nictitating membrane response. *Behavioral neuroscience* *100*, 729–744.
212. Colombo, M. and Gross, C.G. (1994). Responses of inferior temporal cortex and hippocampal neurons during delayed matching to sample in monkeys (*Macaca fascicularis*). *Behavioral neuroscience* *108*, 443–455.
213. Hampson, R.E., Pons, T.P., Stanford, T.R. and Deadwyler, S.A. (2004). Categorization in the monkey hippocampus: a possible mechanism for encoding information into memory. *Proceedings of the National Academy of Sciences of the United States of America* *101*, 3184–3189.

214. McEchron, M.D., Weible, A.P. and Disterhoft, J.F. (2001). Aging and learning-specific changes in single-neuron activity in CA1 hippocampus during rabbit trace eyeblink conditioning. *Journal of neurophysiology* 86, 1839–1857.
215. Griffin, A.L., Asaka, Y., Darling, R.D. and Berry, S.D. (2004). Theta-contingent trial presentation accelerates learning rate and enhances hippocampal plasticity during trace eyeblink conditioning. *Behavioral neuroscience* 118, 403–411.
216. Otto, T. and Eichenbaum, H. (1992). Neuronal activity in the hippocampus during delayed non-match to sample performance in rats: evidence for hippocampal processing in recognition memory. *Hippocampus* 2, 323–334.
217. Hampson, R.E. and Deadwyler, S.A. (2000). Cannabinoids reveal the necessity of hippocampal neural encoding for short-term memory in rats. *The Journal of neuroscience : the official journal of the Society for Neuroscience* 20, 8932–8942.
218. Weible, A.P., O'Reilly, J.-A., Weiss, C. and Disterhoft, J.F. (2006). Comparisons of dorsal and ventral hippocampus cornu ammonis region 1 pyramidal neuron activity during trace eyeblink conditioning in the rabbit. *Neuroscience* 141, 1123–1137.
219. Matthews, E.A., Linardakis, J.M. and Disterhoft, J.F. (2009). The fast and slow afterhyperpolarizations are differentially modulated in hippocampal neurons by aging and learning. *The Journal of neuroscience : the official journal of the Society for Neuroscience* 29, 4750–4755.
220. McKay, B.M., Oh, M.M., Galvez, R., Burgdorf, J., Kroes, R.A., Weiss, C., Adelman, J.P., Moskal, J.R. and Disterhoft, J.F. (2012). Increasing SK2 channel activity impairs associative learning. *Journal of neurophysiology* 108, 863–870.
221. Yoshida, M. and Hasselmo, M.E. (2009). Persistent firing supported by an intrinsic cellular mechanism in a component of the head direction system. *The Journal of neuroscience : the official journal of the Society for Neuroscience* 29, 4945–4952.
222. Dembrow, N.C., Chitwood, R.A. and Johnston, D. (2010). Projection-specific neuromodulation of medial prefrontal cortex neurons. *The Journal of neuroscience : the official journal of the Society for Neuroscience* 30, 16922–16937.
223. Egorov, A.V., Unsicker, K. and von Bohlen und Halbach, Oliver (2006). Muscarinic control of graded persistent activity in lateral amygdala neurons. *The European journal of neuroscience* 24, 3183–3194.
224. Rahman, J. and Berger, T. (2011). Persistent activity in layer 5 pyramidal neurons following cholinergic activation of mouse primary cortices. *The European journal of neuroscience* 34, 22–30.
225. Navaroli, V.L., Zhao, Y., Boguszewski, P. and Brown, T.H. (2012). Muscarinic receptor activation enables persistent firing in pyramidal neurons from superficial layers of dorsal perirhinal cortex. *Hippocampus* 22, 1392–1404.
226. Esclassan, F., Coutureau, E., Di Scala, G. and Marchand, A.R. (2009). A cholinergic-dependent role for the entorhinal cortex in trace fear conditioning. *The Journal of neuroscience : the official journal of the Society for Neuroscience* 29, 8087–8093.
227. Fransén, E., Tahvildari, B., Egorov, A.V., Hasselmo, M.E. and Alonso, A.A. (2006). Mechanism of graded persistent cellular activity of entorhinal cortex layer v neurons. *Neuron* 49, 735–746.
228. Yoshida, M., Fransén, E. and Hasselmo, M.E. (2008). mGluR-dependent persistent firing in entorhinal cortex layer III neurons. *The European journal of neuroscience* 28, 1116–1126.
229. Zhang, Z. and Séguéla, P. (2010). Metabotropic induction of persistent activity in layers II/III of anterior cingulate cortex. *Cerebral cortex (New York, N.Y. : 1991)* 20, 2948–2957.

230. Zhang, Z., Reboresda, A., Alonso, A., Barker, P.A. and Séguéla, P. (2011). TRPC channels underlie cholinergic plateau potentials and persistent activity in entorhinal cortex. *Hippocampus* 21, 386–397.
231. Thuault, S.J., Malleret, G., Constantinople, C.M., Nicholls, R., Chen, I., Zhu, J., Panteleyev, A., Vronskaya, S., Nolan, M.F., Bruno, R., et al. (2013). Prefrontal cortex HCN1 channels enable intrinsic persistent neural firing and executive memory function. *The Journal of neuroscience : the official journal of the Society for Neuroscience* 33, 13583–13599.
232. Zhang, Z., Cordeiro Matos, S., Jegu, S., Adamantidis, A. and Séguéla, P. (2013). Norepinephrine drives persistent activity in prefrontal cortex via synergistic  $\alpha 1$  and  $\alpha 2$  adrenoceptors. *PloS one* 8, e66122.
233. Maljevic, S. and Lerche, H. (2013). Potassium channels: a review of broadening therapeutic possibilities for neurological diseases. *Journal of neurology* 260, 2201–2211.
234. Miceli, F., Soldovieri, M.V., Ambrosino, P., Maria, M. de, Migliore, M., Migliore, R. and Tagliatalata, M. (2015). Early-Onset Epileptic Encephalopathy Caused by Gain-of-Function Mutations in the Voltage Sensor of Kv7.2 and Kv7.3 Potassium Channel Subunits. *The Journal of neuroscience : the official journal of the Society for Neuroscience* 35, 3782–3793.
235. Anderson, N.J., Slough, S. and Watson, W.P. (2006). In vivo characterisation of the small-conductance KCa (SK) channel activator 1-ethyl-2-benzimidazolinone (1-EBIO) as a potential anticonvulsant. *European journal of pharmacology* 546, 48–53.
236. Fraser, D.D. and MacVicar, B.A. (1996). Cholinergic-dependent plateau potential in hippocampal CA1 pyramidal neurons. *The Journal of neuroscience : the official journal of the Society for Neuroscience* 16, 4113–4128.
237. Qiu, C., Johnson, B.N. and Tallent, M.K. (2007). K<sup>+</sup> M-current regulates the transition to seizures in immature and adult hippocampus. *Epilepsia* 48, 2047–2058.
238. Oliveira, M.S., Skinner, F., Arshadmansab, M.F., Garcia, I., Mello, C.F., Knaus, H.-G., Ermolinsky, B.S., Otalora, Luis F Pacheco and Garrido-Sanabria, E.R. (2010). Altered expression and function of small-conductance (SK) Ca(2+)-activated K<sup>+</sup> channels in pilocarpine-treated epileptic rats. *Brain research* 1348, 187–199.
239. Schulz, R., Kirschstein, T., Brehme, H., Porath, K., Mikkat, U. and Köhling, R. (2012). Network excitability in a model of chronic temporal lobe epilepsy critically depends on SK channel-mediated AHP currents. *Neurobiology of disease* 45, 337–347.
240. Reid, C.A., Phillips, A.M. and Petrou, S. (2012). HCN channelopathies: pathophysiology in genetic epilepsy and therapeutic implications. *British journal of pharmacology* 165, 49–56.
241. Kuzmiski, J.B. and MacVicar, B.A. (2001). Cyclic nucleotide-gated channels contribute to the cholinergic plateau potential in hippocampal CA1 pyramidal neurons. *The Journal of neuroscience : the official journal of the Society for Neuroscience* 21, 8707–8714.
242. Ting, J.T. (2015). Brain slice methods. <http://www.brainslicemethods.com/#!recipes/czv4>.
243. Miller, M., Shi, J., Zhu, Y., Kustov, M., Tian, J.-B., Stevens, A., Wu, M., Xu, J., Long, S., Yang, P., et al. (2011). Identification of ML204, a novel potent antagonist that selectively modulates native TRPC4/C5 ion channels. *The Journal of biological chemistry* 286, 33436–33446.
244. Miller, M.R., Shi, J., Wu, M., Engers, J., Hopkins, C.R., Lindsley, C.W., Salovic, J.M., Zhu, Y., Tian, J.-B., Zhu, M.X., et al. (2011). Novel Chemical Inhibitor of TRPC 4 Channels. *Probe Reports from the NIH Molecular Libraries Program*, 1–35.
245. Tsien, R.Y. (1980). New calcium indicators and buffers with high selectivity against magnesium and protons: design, synthesis, and properties of prototype structures. *Biochemistry* 19, 2396–2404.
246. Dattilo, M., Penington, N.J. and Williams, K. (2008). Inhibition of TRPC5 channels by intracellular ATP. *Molecular pharmacology* 73, 42–49.

247. Guedel, A.E. (1951). *Inhalation Anesthesia: A Fundamental Guide*, 2nd Edition (New York, USA: The Macmillan Company).
248. Brehme, H., Kirschstein, T., Schulz, R. and Köhling, R. (2014). In vivo treatment with the casein kinase 2 inhibitor 4,5,6,7-tetrabromotriazole augments the slow afterhyperpolarizing potential and prevents acute epileptiform activity. *Epilepsia* *55*, 175–183.
249. Malenka, R.C. and Nicoll, R.A. (1986). Dopamine decreases the calcium-activated afterhyperpolarization in hippocampal CA1 pyramidal cells. *Brain research* *379*, 210–215.
250. Chen, S., Yue, C. and Yaari, Y. (2005). A transitional period of Ca<sup>2+</sup>-dependent spike afterdepolarization and bursting in developing rat CA1 pyramidal cells. *The Journal of physiology* *567*, 79–93.
251. Reboreda, A., Raouf, R., Alonso, A. and Séguéla, P. (2007). Development of cholinergic modulation and graded persistent activity in layer v of medial entorhinal cortex. *Journal of neurophysiology* *97*, 3937–3947.
252. Giglio, A.M. and Storm, J.F. (2014). Postnatal development of temporal integration, spike timing and spike threshold regulation by a dendrotoxin-sensitive K<sup>+</sup> current in rat CA1 hippocampal cells. *The European journal of neuroscience* *39*, 12–23.
253. Sánchez-Alonso, J.L., Sánchez-Aguilera, A., Vicente-Torres, M.A. and Colino, A. (2012). Intrinsic excitability is altered by hypothyroidism in the developing hippocampal CA1 pyramidal cells. *Neuroscience* *207*, 37–51.
254. Reece, L.J. and Schwartzkroin, P.A. (1991). Effects of cholinergic agonists on immature rat hippocampal neurons. *Brain research. Developmental brain research* *60*, 29–42.
255. Pape, H.C. (1996). Queer current and pacemaker: the hyperpolarization-activated cation current in neurons. *Annual review of physiology* *58*, 299–327.
256. Bender, R.A., Brewster, A., Santoro, B., Ludwig, A., Hofmann, F., Biel, M. and Baram, T.Z. (2001). Differential and age-dependent expression of hyperpolarization-activated, cyclic nucleotide-gated cation channel isoforms 1-4 suggests evolving roles in the developing rat hippocampus. *Neuroscience* *106*, 689–698.
257. Vasilyev, D.V. and Barish, M.E. (2002). Postnatal development of the hyperpolarization-activated excitatory current I<sub>h</sub> in mouse hippocampal pyramidal neurons. *The Journal of neuroscience : the official journal of the Society for Neuroscience* *22*, 8992–9004.
258. Surges, R., Brewster, A.L., Bender, R.A., Beck, H., Feuerstein, T.J. and Baram, T.Z. (2006). Regulated expression of HCN channels and cAMP levels shape the properties of the h current in developing rat hippocampus. *The European journal of neuroscience* *24*, 94–104.
259. Paxinos, G. and Watson, C. (2007). *The rat brain in stereotaxic coordinates*, 6th ed Edition (Amsterdam, Boston: Elsevier).
260. Blasiak, T., Czubak, W., Ignaciak, A. and Lewandowski, M.H. (2010). A new approach to detection of the bregma point on the rat skull. *Journal of neuroscience methods* *185*, 199–203.
261. Bandeira, F., Lent, R. and Herculano-Houzel, S. (2009). Changing numbers of neuronal and non-neuronal cells underlie postnatal brain growth in the rat. *Proceedings of the National Academy of Sciences of the United States of America* *106*, 14108–14113.
262. Sekerli, M., Del Negro, Christopher A, Lee, R.H. and Butera, R.J. (2004). Estimating action potential thresholds from neuronal time-series: new metrics and evaluation of methodologies. *IEEE transactions on bio-medical engineering* *51*, 1665–1672.
263. Naundorf, B., Wolf, F. and Volgushev, M. (2006). Unique features of action potential initiation in cortical neurons. *Nature* *440*, 1060–1063.
264. Henze, D.A. and Buzsáki, G. (2001). Action potential threshold of hippocampal pyramidal cells in vivo is increased by recent spiking activity. *Neuroscience* *105*, 121–130.



265. Graves, A.R., Moore, S.J., Bloss, E.B., Mensh, B.D., Kath, W.L. and Spruston, N. (2012). Hippocampal pyramidal neurons comprise two distinct cell types that are countermodulated by metabotropic receptors. *Neuron* 76, 776–789.
266. Yue, C. and Yaari, Y. (2004). KCNQ/M channels control spike afterdepolarization and burst generation in hippocampal neurons. *The Journal of neuroscience : the official journal of the Society for Neuroscience* 24, 4614–4624.
267. Feldman, H.H., Pirttila, T., Dartigues, J.F., Everitt, B., van Baelen, B., Schwalen, S. and Kavanagh, S. (2009). Treatment with galantamine and time to nursing home placement in Alzheimer's disease patients with and without cerebrovascular disease. *International journal of geriatric psychiatry* 24, 479–488.
268. Ruxton, G.D. (2006). The unequal variance t-test is an underused alternative to Student's t-test and the Mann-Whitney U test. *Behavioral Ecology* 17, 688–690.
269. Lumley, T., Diehr, P., Emerson, S. and Chen, L. (2002). The importance of the normality assumption in large public health data sets. *Annual review of public health* 23, 151–169.
270. Hoffman, J.I.D. (1975). The incorrect use of Chi-square analysis for aird data. *Clin Exp Immunol* 24, 227–229.
271. Leonhart, R. (2004). *Lehrbuch Statistik. Einstieg und Vertiefung*, 1. Aufl Edition (Bern, Göttingen, Toronto, Seattle: Huber).
272. Maccaferri, G., Mangoni, M., Lazzari, A. and DiFrancesco, D. (1993). Properties of the hyperpolarization-activated current in rat hippocampal CA1 pyramidal cells. *Journal of neurophysiology* 69, 2129–2136.
273. Surges, R., Freiman, T.M. and Feuerstein, T.J. (2004). Input resistance is voltage dependent due to activation of I<sub>h</sub> channels in rat CA1 pyramidal cells. *Journal of neuroscience research* 76, 475–480.
274. Agopyan, N., Krnjević, K. and Leblond, J. (1989). Mediation of acetylcholine's excitatory actions in central neurons. *EXS* 57, 77–87.
275. Alroy, G., Su, H. and Yaari, Y. (1999). Protein kinase C mediates muscarinic block of intrinsic bursting in rat hippocampal neurons. *The Journal of physiology* 518 ( Pt 1), 71–79.
276. Otto, J.F., Yang, Y., Frankel, W.N., White, H.S. and Wilcox, K.S. (2006). A spontaneous mutation involving *Kcnq2* (Kv7.2) reduces M-current density and spike frequency adaptation in mouse CA1 neurons. *The Journal of neuroscience : the official journal of the Society for Neuroscience* 26, 2053–2059.
277. Pedarzani, P., McCutcheon, J.E., Rogge, G., Jensen, B.S., Christophersen, P., Hougaard, C., Strøbaek, D. and Stocker, M. (2005). Specific enhancement of SK channel activity selectively potentiates the afterhyperpolarizing current I(AHP) and modulates the firing properties of hippocampal pyramidal neurons. *The Journal of biological chemistry* 280, 41404–41411.
278. Bianchi, D., Marasco, A., Limongiello, A., Marchetti, C., Marie, H., Tirozzi, B. and Migliore, M. (2012). On the mechanisms underlying the depolarization block in the spiking dynamics of CA1 pyramidal neurons. *Journal of computational neuroscience* 33, 207–225.
279. Axmacher, N., Henseler, M.M., Jensen, O., Weinreich, I., Elger, C.E. and Fell, J. (2010). Cross-frequency coupling supports multi-item working memory in the human hippocampus. *Proceedings of the National Academy of Sciences of the United States of America* 107, 3228–3233.
280. Moore, C.L. and Morelli, G.A. (1979). Mother rats interact differently with male and female offspring. *Journal of comparative and physiological psychology* 93, 677–684.
281. Moriyama, C., Galic, M.A., Mychasiuk, R., Pittman, Q.J., Perrot, T.S., Currie, R.W. and Esser, M.J. (2013). Prenatal transport stress, postnatal maternal behavior, and offspring sex differentially affect seizure susceptibility in young rats. *Epilepsy & behavior : E&B* 29, 19–27.

282. Liu, D., Diorio, J., Day, J.C., Francis, D.D. and Meaney, M.J. (2000). Maternal care, hippocampal synaptogenesis and cognitive development in rats. *Nature neuroscience* 3, 799–806.
283. Champagne, F.A., Francis, D.D., Mar, A. and Meaney, M.J. (2003). Variations in maternal care in the rat as a mediating influence for the effects of environment on development. *Physiology & Behavior* 79, 359–371.
284. Arias, N., Morán, J., Conejo, N. and Arias, J.L. (2013). Sexual metabolic differences in the rat limbic brain. *Psicothema* 25, 461–467.
285. Hami, J., Kheradmand, H. and Haghiri, H. (2014). Gender differences and lateralization in the distribution pattern of insulin-like growth factor-1 receptor in developing rat hippocampus: an immunohistochemical study. *Cellular and molecular neurobiology* 34, 215–226.
286. Klur, S., Muller, C., Pereira de Vasconcelos, Anne, Ballard, T., Lopez, J., Galani, R., Certa, U. and Cassel, J.-C. (2009). Hippocampal-dependent spatial memory functions might be lateralized in rats: An approach combining gene expression profiling and reversible inactivation. *Hippocampus* 19, 800–816.
287. Zaichenko, M.I. (2009). Comparative analysis of spike activity of neurons in hippocampal field CA1 and CA3 in rats of different typological groups on exposure to emotional stimuli. *Neuroscience and behavioral physiology* 39, 901–908.
288. Costa, P.F., Santos, A.I. and Ribeiro, M.A. (1992). Slow and medium afterhyperpolarizations in maturing rat hippocampal CA1 neurones. *Neuroreport* 3, 555–558.
289. Disterhoft, J.F., Thompson, L.T., Moyer, J.R. and Mogul, D.J. (1996). Calcium-dependent afterhyperpolarization and learning in young and aging hippocampus. *Life Sciences* 59, 413–420.
290. Decker, M.W. (1987). The effects of aging on hippocampal and cortical projections of the forebrain cholinergic system. *Brain research* 434, 423–438.
291. Jarsky, T., Mady, R., Kennedy, B. and Spruston, N. (2008). Distribution of bursting neurons in the CA1 region and the subiculum of the rat hippocampus. *The Journal of comparative neurology* 506, 535–547.
292. Spruston, N. and Johnston, D. (1992). Perforated patch-clamp analysis of the passive membrane properties of three classes of hippocampal neurons. *Journal of neurophysiology* 67, 508–529.
293. Mercer, A. (2012). Electrically coupled excitatory neurones in cortical regions. *Brain research* 1487, 192–197.
294. Mercer, A., Bannister, A.P. and Thomson, A.M. (2006). Electrical coupling between pyramidal cells in adult cortical regions. *Brain cell biology* 35, 13–27.
295. MacVicar, B.A. and Dudek, F.E. (1981). Electrotonic coupling between pyramidal cells: a direct demonstration in rat hippocampal slices. *Science (New York, N.Y.)* 213, 782–785.
296. MacVicar, B.A. and Dudek, F.E. (1980). Dye-coupling between CA3 pyramidal cells in slices of rat hippocampus. *Brain research* 196, 494–497.
297. Velazquez, J.L., Han, D. and Carlen, P.L. (1997). Neurotransmitter modulation of gap junctional communication in the rat hippocampus. *The European journal of neuroscience* 9, 2522–2531.
298. Aznavour, N., Watkins, K.C. and Descarries, L. (2005). Postnatal development of the cholinergic innervation in the dorsal hippocampus of rat: Quantitative light and electron microscopic immunocytochemical study. *The Journal of comparative neurology* 486, 61–75.
299. Tahvildari, B., Fransén, E., Alonso, A.A. and Hasselmo, M.E. (2007). Switching between "On" and "Off" states of persistent activity in lateral entorhinal layer III neurons. *Hippocampus* 17, 257–263.

300. Brown, D.A. (2010). Muscarinic acetylcholine receptors (mAChRs) in the nervous system: some functions and mechanisms. *Journal of molecular neuroscience : MN* *41*, 340–346.
301. Nicoll, R.A. (1985). The septo-hippocampal projection: a model cholinergic pathway. *Trends in Neurosciences*, 533–536.
302. Kuo, A.G., Lee, G., McKay, B.M. and Disterhoft, J.F. (2008). Enhanced neuronal excitability in rat CA1 pyramidal neurons following trace eyeblink conditioning acquisition is not due to alterations in I M. *Neurobiology of learning and memory* *89*, 125–133.
303. Haj-Dahmane, S. and Andrade, R. (1996). Muscarinic activation of a voltage-dependent cation nonselective current in rat association cortex. *The Journal of neuroscience : the official journal of the Society for Neuroscience* *16*, 3848–3861.
304. Dunwiddie, T.V. and Masino, S.A. (2001). The role and regulation of adenosine in the central nervous system. *Annual review of neuroscience* *24*, 31–55.
305. Lemak, M.S., Voloshanenko, O., Draguhn, A. and Egorov, A.V. (2014). KATP channels modulate intrinsic firing activity of immature entorhinal cortex layer III neurons. *Front. Cell. Neurosci.* *8*.
306. Partridge, L.D. and Valenzuela, C.F. (2000). Block of hippocampal CAN channels by flufenamate. *Brain research* *867*, 143–148.
307. Shaw, T., Lee, R.J. and Partridge, L.D. (1995). Action of diphenylamine carboxylate derivatives, a family of non-steroidal anti-inflammatory drugs, on [Ca<sup>2+</sup>]<sub>i</sub> and Ca(2<sup>+</sup>)-activated channels in neurons. *Neuroscience letters* *190*, 121–124.
308. Di Wang, Grillner, S. and Wallén, P. (2006). Effects of flufenamic acid on fictive locomotion, plateau potentials, calcium channels and NMDA receptors in the lamprey spinal cord. *Neuropharmacology* *51*, 1038–1046.
309. Yau, H.-J., Baranauskas, G. and Martina, M. (2010). Flufenamic acid decreases neuronal excitability through modulation of voltage-gated sodium channel gating. *The Journal of physiology* *588*, 3869–3882.
310. Azouz, R., Jensen, M.S. and Yaari, Y. (1996). Ionic basis of spike after-depolarization and burst generation in adult rat hippocampal CA1 pyramidal cells. *The Journal of physiology* *492 ( Pt 1)*, 211–223.
311. Yamada-Hanff, J. and Bean, B.P. (2013). Persistent sodium current drives conditional pacemaking in CA1 pyramidal neurons under muscarinic stimulation. *The Journal of neuroscience : the official journal of the Society for Neuroscience* *33*, 15011–15021.
312. Fraser, D.D., Doll, D. and MacVicar, B.A. (2001). Serine/threonine protein phosphatases and synaptic inhibition regulate the expression of cholinergic-dependent plateau potentials. *Journal of neurophysiology* *85*, 1197–1205.
313. Benardo, L.S. and Prince, D.A. (1982). Cholinergic excitation of mammalian hippocampal pyramidal cells. *Brain research* *249*, 315–331.
314. Rundfeldt, C. (1997). The new anticonvulsant retigabine (D-23129) acts as an opener of K<sup>+</sup> channels in neuronal cells. *European journal of pharmacology* *336*, 243–249.
315. Armand, V., Rundfeldt, C. and Heinemann, U. (1999). Effects of retigabine (D-23129) on different patterns of epileptiform activity induced by 4-aminopyridine in rat entorhinal cortex hippocampal slices. *Naunyn-Schmiedeberg's archives of pharmacology* *359*, 33–39.
316. Boehlen, A., Schwake, M., Dost, R., Kunert, A., Fidzinski, P., Heinemann, U. and Gebhardt, C. (2013). The new KCNQ2 activator 4-Chlor-N-(6-chlor-pyridin-3-yl)-benzamid displays anticonvulsant potential. *British journal of pharmacology* *168*, 1182–1200.
317. Armand, V., Rundfeldt, C. and Heinemann, U. (2000). Effects of retigabine (D-23129) on different patterns of epileptiform activity induced by low magnesium in rat entorhinal cortex hippocampal slices. *Epilepsia* *41*, 28–33.

318. Slomko, A.M., Naseer, Z., Ali, S.S., Wongvavit, J.P. and Friedman, L.K. (2014). Retigabine calms seizure-induced behavior following status epilepticus. *Epilepsy & behavior : E&B* 37, 123–132.
319. Sachdeo, R., Partiot, A., Biton, V., Rosenfeld, W.E., Nohria, V., Tompson, D., DeRossett, S. and Porter, R.J. (2014). A novel design for a dose finding, safety, and drug interaction study of an antiepileptic drug (retigabine) in early clinical development. *International journal of clinical pharmacology and therapeutics* 52, 509–518.
320. Empson, R.M. and Jefferys, J.G. (2001). Ca(2+) entry through L-type Ca(2+) channels helps terminate epileptiform activity by activation of a Ca(2+) dependent afterhyperpolarisation in hippocampal CA3. *Neuroscience* 102, 297–306.
321. Lappin, S.C., Dale, T.J., Brown, J.T., Trezise, D.J. and Davies, C.H. (2005). Activation of SK channels inhibits epileptiform bursting in hippocampal CA3 neurons. *Brain research* 1065, 37–46.
322. Strøbaek, D., Teuber, L., Jørgensen, T.D., Ahring, P.K., Kjaer, K., Hansen, R.S., Olesen, S.P., Christophersen, P. and Skaaning-Jensen, B. (2004). Activation of human IK and SK Ca<sup>2+</sup> - activated K<sup>+</sup> channels by NS309 (6,7-dichloro-1H-indole-2,3-dione 3-oxime). *Biochimica et biophysica acta* 1665, 1–5.
323. Dougherty, K.A., Islam, T. and Johnston, D. (2012). Intrinsic excitability of CA1 pyramidal neurones from the rat dorsal and ventral hippocampus. *The Journal of physiology* 590, 5707–5722.
324. Jung, M.W., Wiener, S.I. and McNaughton, B.L. (1994). Comparison of spatial firing characteristics of units in dorsal and ventral hippocampus of the rat. *The Journal of neuroscience : the official journal of the Society for Neuroscience* 14, 7347–7356.
325. Moser, M.B., Moser, E.I., Forrest, E., Andersen, P. and Morris, R.G. (1995). Spatial learning with a minislab in the dorsal hippocampus. *Proceedings of the National Academy of Sciences of the United States of America* 92, 9697–9701.
326. Sah, P., Gibb, A.J. and Gage, P.W. (1988). The sodium current underlying action potentials in guinea pig hippocampal CA1 neurons. *The Journal of general physiology* 91, 373–398.
327. Gamper, N., Stockand, J.D. and Shapiro, M.S. (2003). Subunit-specific modulation of KCNQ potassium channels by Src tyrosine kinase. *The Journal of neuroscience : the official journal of the Society for Neuroscience* 23, 84–95.
328. Tinel, N., Diochot, S., Lauritzen, I., Barhanin, J., Lazdunski, M. and Borsotto, M. (2000). M-type KCNQ2–KCNQ3 potassium channels are modulated by the KCNE2 subunit. *FEBS Letters* 480, 137–141.
329. Wen, H. and Levitan, I.B. (2002). Calmodulin is an auxiliary subunit of KCNQ2/3 potassium channels. *The Journal of neuroscience : the official journal of the Society for Neuroscience* 22, 7991–8001.
330. Tahvildari, B., Alonso, A.A. and Bourque, C.W. (2008). Ionic basis of ON and OFF persistent activity in layer III lateral entorhinal cortical principal neurons. *Journal of neurophysiology* 99, 2006–2011.
331. Maslarova, A., Salar, S., Lapilover, E., Friedman, A., Veh, R.W. and Heinemann, U. (2013). Increased susceptibility to acetylcholine in the entorhinal cortex of pilocarpine-treated rats involves alterations in KCNQ channels. *Neurobiology of disease* 56, 14–24.
332. Dickson, C.T. and Alonso, A. (1997). Muscarinic induction of synchronous population activity in the entorhinal cortex. *The Journal of neuroscience : the official journal of the Society for Neuroscience* 17, 6729–6744.
333. Douglas Fraser (2012). Personal communication about specifics that were not reported in the publications from 1996 (*J. Neurosci*) and 2001 (*J Neurophysiol*). E-mail.

334. Richter, J.M., Schaefer, M. and Hill, K. (2014). Riluzole activates TRPC5 channels independently of PLC activity. *British journal of pharmacology* *171*, 158–170.
335. Bogaard, A., Parent, J., Zochowski, M. and Booth, V. (2009). Interaction of cellular and network mechanisms in spatiotemporal pattern formation in neuronal networks. *The Journal of neuroscience : the official journal of the Society for Neuroscience* *29*, 1677–1687.
336. Bazhenov, M., Timofeev, I., Fröhlich, F. and Sejnowski, T.J. (2008). Cellular and network mechanisms of electrographic seizures. *Drug discovery today. Disease models* *5*, 45–57.
337. Blank, T., Nijholt, I., Kye, M.-J. and Spiess, J. (2004). Small conductance Ca<sup>2+</sup>-activated K<sup>+</sup> channels as targets of CNS drug development. *Current drug targets. CNS and neurological disorders* *3*, 161–167.
338. McEchron, M.D. and Disterhoft, J.F. (1997). Sequence of single neuron changes in CA1 hippocampus of rabbits during acquisition of trace eyeblink conditioned responses. *Journal of neurophysiology* *78*, 1030–1044.
339. McEchron, M.D., Tseng, W. and Disterhoft, J.F. (2003). Single neurons in CA1 hippocampus encode trace interval duration during trace heart rate (fear) conditioning in rabbit. *The Journal of neuroscience : the official journal of the Society for Neuroscience* *23*, 1535–1547.
340. Deadwyler, S.A., Bunn, T. and Hampson, R.E. (1996). Hippocampal ensemble activity during spatial delayed-nonmatch-to-sample performance in rats. *The Journal of neuroscience : the official journal of the Society for Neuroscience* *16*, 354–372.
341. Hoss, W., Messer, W.S., Monsma, F.J., Miller, M.D., Ellerbrock, B.R., Scranton, T., Ghodsi-Hovsepian, S., Price, M.A., Balan, S. and Mazloum, Z. (1990). Biochemical and behavioral evidence for muscarinic autoreceptors in the CNS. *Brain research* *517*, 195–201.
342. Leão, R.N., Mikulovic, S., Leão, K.E., Munguba, H., Gezelius, H., Enjin, A., Patra, K., Eriksson, A., Loew, L.M., Tort, Adriano B L, et al. (2012). OLM interneurons differentially modulate CA3 and entorhinal inputs to hippocampal CA1 neurons. *Nature neuroscience* *15*, 1524–1530.
343. Fernández de Sevilla, D. and Buño, W. (2003). Presynaptic inhibition of Schaffer collateral synapses by stimulation of hippocampal cholinergic afferent fibres. *The European journal of neuroscience* *17*, 555–558.
344. Saravanan, V., Arabali, D., Jochems, A., Cui, A.-X., Gootjes-Dreesbach, L., Cutsuridis, V. and Yoshida, M. (2015). Example between encoding and consolidation/replay dynamics via cholinergic modulation of CAN current: A modeling study. *Hippocampus*.
345. Park, J.-Y. and Spruston, N. (2012). Synergistic actions of metabotropic acetylcholine and glutamate receptors on the excitability of hippocampal CA1 pyramidal neurons. *The Journal of neuroscience : the official journal of the Society for Neuroscience* *32*, 6081–6091.
346. Trimmer, P.C. and Houston, A.I. (2014). An evolutionary perspective on information processing. *Topics in cognitive science* *6*, 312–330.
347. Atkinson, R.C. (1963). A variable sensitivity theory of signal detection. *Psychological review* *70*, 91–106.
348. Broadbent, D.E. and Gregory, M. (1963). Division of attention and the decision theory of signal detection. *Proceedings of the Royal Society of London. Series B, Biological sciences* *158*, 222–231.
349. Shadlen, M.N. and Kiani, R. (2013). Decision making as a window on cognition. *Neuron* *80*, 791–806.
350. Stüttgen, M.C. and Schwarz, C. (2008). Psychophysical and neurometric detection performance under stimulus uncertainty. *Nature neuroscience* *11*, 1091–1099.
351. Hansen, N. and Manahan-Vaughan, D. (2014). Dopamine D1/D5 receptors mediate informational saliency that promotes persistent hippocampal long-term plasticity. *Cerebral cortex (New York, N.Y. : 1991)* *24*, 845–858.

352. Chen, B.-S. and Wu, S.-N. (2011). Functional role of the activity of ATP-sensitive potassium channels in electrical behavior of hippocampal neurons: experimental and theoretical studies. *Journal of theoretical biology* 272, 16–25.
353. Braunewell, K.H. and Manahan-Vaughan, D. (2001). Long-term depression: a cellular basis for learning? *Reviews in the neurosciences* 12, 121–140.
354. Artola, A. and Singer, W. (1993). Long-term depression of excitatory synaptic transmission and its relationship to long-term potentiation. *Trends in Neurosciences* 16, 480–487.
355. Frey, U. and Morris, R.G. (1997). Synaptic tagging and long-term potentiation. *Nature* 385, 533–536.
356. Lisman, J. (1989). A mechanism for the Hebb and the anti-Hebb processes underlying learning and memory. *Proceedings of the National Academy of Sciences of the United States of America* 86, 9574–9578.
357. Zhang, L., Kirschstein, T., Sommersberg, B., Merkens, M., Manahan-Vaughan, D., Elgersma, Y. and Beck, H. (2005). Hippocampal synaptic metaplasticity requires inhibitory autophosphorylation of Ca<sup>2+</sup>/calmodulin-dependent kinase II. *The Journal of neuroscience : the official journal of the Society for Neuroscience* 25, 7697–7707.
358. Pastalkova, E., Itskov, V., Amarasingham, A. and Buzsáki, G. (2008). Internally generated cell assembly sequences in the rat hippocampus. *Science (New York, N.Y.)* 321, 1322–1327.
359. MacDonald, C.J., Lepage, K.Q., Eden, U.T. and Eichenbaum, H. (2011). Hippocampal "time cells" bridge the gap in memory for discontinuous events. *Neuron* 71, 737–749.
360. Modi, M.N., Dhawale, A.K. and Bhalla, U.S. (2014). CA1 cell activity sequences emerge after reorganization of network correlation structure during associative learning. *eLife* 3, e01982.
361. Bromberg-Martin, E.S., Matsumoto, M. and Hikosaka, O. (2010). Dopamine in motivational control: rewarding, aversive, and alerting. *Neuron* 68, 815–834.
362. Pedarzani, P. and Storm, J.F. (1996). Evidence that Ca/calmodulin-dependent protein kinase mediates the modulation of the Ca<sup>2+</sup>-dependent K<sup>+</sup> current, IAHP, by acetylcholine, but not by glutamate, in hippocampal neurons. *Pflügers Archiv : European journal of physiology* 431, 723–728.
363. Epsztein, J., Brecht, M. and Lee, A.K. (2011). Intracellular determinants of hippocampal CA1 place and silent cell activity in a novel environment. *Neuron* 70, 109–120.

# 6 Appendix

6.1 Supplemental data

6.2 Curriculum Vitae

6.3 List of publications

6.4 Acknowledgements

## 6.1 Supplemental data

### **Specifics about the tumor in one aged animal**

The tumor started at an approximate Bregma position of -8 mm, extended to more ventral areas, was located medial, presumably affected the mammillothalamic and mammilothegmental tract, the nigrostriatal bundle, the posterior hypothalamic nucleus, the ansa lenticularis and the fasciculus retroflexus, but spared the cerebral peduncle and the internal capsule. The animal showed an obese phenotype (888 g).



## Whole slice staining protocol

(Traditional version based on but modified from Nathalie - August 2002)

Changes in red made by Beate

### Labeling and Fixing the cell:

Label cells with 1% Biocytin in the intra-cellular solution.

Place slices in 4% Paraformaldehyde in 0.1 M NaPB (sodium phosphate buffer) at 4°C for 1 to 20 days.

### Staining Protocol for DAB:

#### Day 1

start out with less!!

1. Check if there is enough ABC and DAB kit.
2. Prepare 0.1 M NaPB solution. 35 ml for 1 slice.  
- 0.013 M/L  $\text{NaH}_2\text{PO}_4$  (FW=137.99) = 1.7939g/l = 0.1794g/100ml  
- 0.087 M/L  $\text{Na}_2\text{HPO}_4$  (FW=177.99) = 15.4851g/l = 1.5485g/100ml
3. Rinse slices for 5 min, 3 times in 0.1 M NaPB on a rotating table
4. While waiting, prepare NaPB + Gelatin (0.2%) + Triton (0.25%).  
17 ml for 1 slice. (Triton is like soap → don't shake)  
- Warm up 100 ml NaPB, dissolve 0.2g Gelatin, filter, cool down to room temp, add 250µl of Triton X-100 and mix well.
5. Suppress endogenous peroxidase with 2%  $\text{H}_2\text{O}_2$  in NaPB for 30 min.  
1.5 ml for 1 slice.  
- For 10 ml, 0.67 ml of 30%  $\text{H}_2\text{O}_2$  + 9.33 ml of NaPB. Fill the wells up.
6. Rinse slices for 5 min, 3 times in 0.1 M NaPB on a rotating table (keep rest of NaPB because needed on day 3)
7. This step makes holes in the cell membrane and blocks antibody with NaPB + Triton (0.25%) + Gelatin (0.2%) for 30 min.
8. While waiting, prepare AB Complex on rotating table and wait for 30 min before use.  
1.5 ml for 1 slice.  
- For 10 ml NaPB, mix 2 drops of A and 2 drops of B  
- 30 µl Triton X-100
9. Transfer to AB Complex over night.

Use 1 to 1,5 ml per slice. Calculate with exact amount of slices because safety amount is within the amount for 1 slice already.

\_\_\_ ml for \_\_\_ slices  
\_\_\_  $\text{NaH}_2\text{PO}_4$ : \_\_\_ g  
\_\_\_  $\text{Na}_2\text{HPO}_4$ : \_\_\_ g

\_\_\_ ml for \_\_\_ slices  
< \_\_\_ ml NaPB  
\_\_\_ g Gelatin  
\_\_\_ ml Triton  
\_\_\_ X-100

\_\_\_ ml for \_\_\_ slices  
\_\_\_ ml 30%  $\text{H}_2\text{O}_2$   
\_\_\_ ml NaPB

\_\_\_ ml for \_\_\_ slices  
\_\_\_ ml NaPB  
\_\_\_ drops of A  
and B  
\_\_\_ µl Triton  
X-100

#### Day 2

Long wash with NaPB / gelatine / Triton.

1. Rinse slices for 5 min, 4 times.
2. 6 more washes. 1 hour, 6 times.
3. Final wash overnight.

#### Day 3

1. Rinse in 0.1 M Tris Buffered Saline (TBS) for 10 min, 3 times.  
4,5 ml for 1 slice.  
For in 100 ml of water add  
Trizma Base (FW= 121.1) 1.2g + NaCl (FW = 58.44) 1g.  
Then adjust pH to 7.6 using HCl.
2. While waiting, prepare a new well, syringe, filter, needle, etc. for DAB.
3. Wear gloves and mask, and prepare DAB solution (light sensitive)  
For 10 slices, in 10ml distilled water, add:  
4 drops of Buffer Stock Solution and mix well (stirring platform)  
8 drops of DAB Stock Solution  
4 drops of Hydrogen Peroxide solution  
4 drops of Nickel Solution
4. Filter (0.2 µm) and place DAB solution in a new well dish.  
Transfer slices using a brush.  
Keep the well on a dark surface and cover it (light sensitive)  
wait until slices get purplish.  
(~3min. /up to 15 min. Check for staining under microscope)
5. Stop the reaction by rinsing in NaPB (10 min, 3 times) 1.5 ml for 1 slice.
6. Prepare slides (write slice names), coverslips, unfreeze mowiol.
7. Put slice on a glass slide and check for a cell under the microscope.  
Turn the slice with the cell facing up (ease things by noting the orientation immediately after recording)  
Let the slice dry for ~2 min. Put 3 drops of Mowiol (in a bath @ 37-40°C)  
Put cover slips on from straight above. When just above the slice, let the cover slip become damp before letting go.  
Avoid bubbles and avoid distorting the shape
8. Soak all containers that touch DAB solution in bleach.
9. Place slides in darkness for overnight.
10. Reserve microscope for next day photographing.

\_\_\_ ml for \_\_\_ slices  
< \_\_\_ ml dH<sub>2</sub>O  
\_\_\_ g Trizma Base  
\_\_\_ g NaCl

\_\_\_ ml for \_\_\_ slices  
\_\_\_ drops Buffer  
\_\_\_ drops DAB  
\_\_\_ drops H<sub>2</sub>O<sub>2</sub>  
\_\_\_ drops Nickel

KEEP TRACK OF WHAT TOUCHED DAB AND STORE IT FOR BLEACHING

\_\_\_ ml NaPB  
CHECK IF  
ENOUGH LEFT!  
3 \* 1.5ml \* slices

## 4% PFA in 0,1M NaPB

### NaPB

Compound	Concentration (M/L)	MW( g/M)			
dH <sub>2</sub> O			0,25l	0,5l	1l
NaH <sub>2</sub> PO <sub>4</sub>	0,019	137,99	0,655 g	1,31 g	2,62 g
Na <sub>2</sub> HPO <sub>4</sub>	0,081	177,99	3,60 g	7,21 g	14,4 g

Fill about half of NaPB in a bottle (or beaker) and put on heating/stirring platform (amount is very important if beaker is being used, because shaking not possible then)

Heat up NaPB

### Caution:

**PFA is very toxic! Wear labcoat, mask, gloves and eyeglasses! Only handle PFA under the hood!**

Add 1,0g PFA per 25ml NaPB

Shake to get PFA that's stuck on the inside of the bottle

Add the rest of NaPB

Put lid on the bottle (minimize evaporation of PFA) but don't screw the lid close (danger of exploding)

Heat (~80°C) but not boil until clear (~135-145°C on our stirrer platform)

Cool down when clear (*speeding it up by using ice does not deteriorate the solution; but make sure not to break the glass with too sudden coldness*)

Adjust pH to 7,4 to 7,6 using NaOH (10~40 µl of 6 M/L)

Paper filter and store

Stability if stored at -20°C: up to 6 month

Stability if stored at +4°C: up to 1 month

## Mowiol by Babak (Tahvildari, kept by Lisa Giokomo, gotten from Moto)

- 1) Prepare 100ml, 0.2M Tris-HCl (Sigam T-3253), pH=8.5 using NaOH  
 < 100 ml dH<sub>2</sub>O  
 3.152 g Tris-HCl  
 adjust pH with 6M NaOH (2.4 g NaOH in 10 ml d H<sub>2</sub>O.  
*Be careful with NaOH!  
 add NaOH pellets stepwise  
 because dH<sub>2</sub>O will warm up  
 needed slightly more than 2 ml NaOH in 80 ml,  
 change is not linear!*  
 fill up to 100 ml  
 readjust pH
- 2) Dissolve 20gr. Mowiol (Calbiochem 475904) in the above solution by heating up to 50-60°C with stirring (what I myself do is to warm it up in a bath, instead of heating it directly, by heating directly lots of solution evaporates and this will cause to have a thick Mowiol, you should avoid that)  
 dissolving takes a long time  
 Look closely. The particles seen might as well be bubbles because the solution is very thick.
- 3) After cooling add 20 ml Glycerol and stir
- 4) Centrifuge at 500rpm for 15 min and store in aliquots at -20C  
 For getting bubbles out  
 2 ml aliquots can be centrifuged as well (minimum at Magdalena's centrifuge = 800 rpm)  
 Do not aliquot exactly 2 ml because there needs to be some space for letting the pipette stand in when using it.

red are the specifications Beate added

**Table 6.1.1: Effects of 10  $\mu$ M carbachol on intrinsic electrophysiological properties.**

The table summarizes comparisons within the same cells which were first superfused with ACSF+SB only and subsequently in the presence of 10  $\mu$ M Cch.

	ACSF+SB	10 $\mu$ M Cch	N (SB/Cch)	T or $\chi^2$	p	
<b>Passive properties</b>						
RMP (%silent)	100% (n = 69)	37.7 (n = 26)	69	43	.000	***
RMP (mV)	-65.2 $\pm$ 0.49	-63.8 $\pm$ 0.74	26	2.439	.022	*
-70 mV R <sub>in</sub> (M $\Omega$ ) <sup>+</sup>	111 $\pm$ 4.56	108 $\pm$ 5.03	63	-0.601	.550	
-65 mV R <sub>in</sub> (M $\Omega$ ) <sup>+</sup>	155 $\pm$ 7.47	123 $\pm$ 6.19	44	-3.854	.000	***
-60 mV R <sub>in</sub> (M $\Omega$ ) <sup>+</sup>	229 $\pm$ 10.1	191 $\pm$ 11.3	35	-3.880	.000	***
<b>Hyperpolarization activated current</b>						
Sag (-10 mV step) <sup>++</sup>	0.244 $\pm$ 0.01	0.247 $\pm$ 0.01	64	0.349	.729	
Sag (-15 mV step) <sup>++</sup>	0.247 $\pm$ 0.01	0.262 $\pm$ 0.01	64	2.763	.007	**
Sag (-20 mV step) <sup>++</sup>	0.248 $\pm$ 0.01	0.269 $\pm$ 0.01	64	3.760	.000	***
<b>Action potential properties</b>						
Threshold (mV)	-45.5 $\pm$ 0.79	-44.7 $\pm$ 0.77	61	2.559	.013	*
Amplitude (mV)	72.3 $\pm$ 1.25	69.4 $\pm$ 1.49	61	-2.527	.014	*
Rising slope (mV/ms)	253 $\pm$ 9.66	248 $\pm$ 9.73	61	-0.550	.584	
falling slope (mV/ms)	-62.8 $\pm$ 2.04	-62.9 $\pm$ 1.68	61	-0.045	.965	
1/2 width (ms)	1.20 $\pm$ 0.03	1.12 $\pm$ 0.02	61	-3.179	.002	**
1/3 width (ms)	1.48 $\pm$ 0.04	1.39 $\pm$ 0.03	61	-2.907	.005	**
fAHP (mV)	-3.74 $\pm$ 0.68	-3.20 $\pm$ 0.58	61	1.916	.060	†
firing type (%regular)	79.7 (n = 51)	90.6 (n = 58)	64	5.444	.020	*
<b>Post-burst properties</b>						
AHP (%exist)	100 (n = 13)	23.1 (n = 3)	13	10.000	.002	**
AHP duration (s)	0.323 $\pm$ 0.12	0.052 $\pm$ 0.02	3			
AHP area (mV*s)	-0.243 $\pm$ 0.07	0.023 $\pm$ 0.02	3			
mAHP latency (ms)	30.8 $\pm$ 4.19	22.6 $\pm$ 10.9	3			
mAHP peak (mV)	-2.12 $\pm$ 0.13	-0.471 $\pm$ 0.27	3			
AHP decay $\tau$ (ms)	66.9 $\pm$ 11.8	16.8 $\pm$ 9.00	3			
sAHP at 0.5 s (mV)	0.159 $\pm$ 0.15	2.06 $\pm$ 0.24	3			
sAHP at 1 s (mV)	0.281 $\pm$ 0.09	2.13 $\pm$ 0.13	3			
V <sub>m</sub> at peak (mV)	-1.55 $\pm$ 0.20	0.690 $\pm$ 0.25	13	12.023	.000	***
V <sub>m</sub> at 0.2 s (mV)	-0.358 $\pm$ 0.16	1.62 $\pm$ 0.17	13	9.200	.000	***
V <sub>m</sub> at 0.5 s (mV)	-0.035 $\pm$ 0.14	2.81 $\pm$ 0.21	13	11.539	.000	***
V <sub>m</sub> at 1 s (mV)	-0.041 $\pm$ 0.09	3.04 $\pm$ 0.24	13	12.461	.000	***

Data represented as M  $\pm$  SEM. Paired T-test, unless otherwise stated. †  $p < 0.1$ , \*  $p < 0.05$ , \*\*  $p < 0.01$ , \*\*\*  $p < 0.001$ .

RMP: resting membrane potential. R<sub>in</sub>: input resistance at the specified holding membrane potential. Sag: Sag ratio induced by a hyperpolarizing voltage step as specified. rising slope: the peak of the rising slope. falling slope: the peak of the falling slope 1/2 width: Full width of the action potential at one half of its amplitude. 1/3 width: Full width of the action potential at one third of its amplitude. AHP: afterhyperpolarization. fAHP: Fast AHP. mAHP: Medium AHP. sAHP: Slow AHP. V<sub>m</sub> at: Membrane potential at the specified time after a burst of five action potentials, irrespective of the occurrence of an AHP.

**Continuation of Table 6.1.1:**

	ACSF+SB	10 $\mu$ M Cch	N (SB/Cch)	T or $\chi^2$	p	
<b>Excitability</b>						
Adaptation ratio	2.44 $\pm$ 0.30	0.920 $\pm$ 0.22	48	-4.845	.000	***
Discontinuation rate	see N (SB)	see N (Cch)	1	66.823	.000	***
Last current (pA)	389 $\pm$ 3.4	231 $\pm$ 14	64	-10.676	.000	***
50 pA step (Hz)	0.219 $\pm$ 0.219	0.391 $\pm$ 0.285	64 (64/64)	0.474	.637	
100 pA step (Hz)	2.56 $\pm$ 0.80	7.02 $\pm$ 1.35	61 (64/61)	3.963	.000	***
150 pA step (Hz)	10.2 $\pm$ 1.42	17.4 $\pm$ 1.69	54 (64/54)	5.771	.000	***
200 pA step (Hz)	20.0 $\pm$ 2.25	26.4 $\pm$ 1.87	34 (64/34)	4.875	.000	***
250 pA step (Hz)	29.2 $\pm$ 2.31	30.9 $\pm$ 1.91	30 (64/30)	1.128	.269	
300 pA step (Hz)	35.9 $\pm$ 2.50	32.7 $\pm$ 1.97	24 (64/24)	-1.783	.088	†
350 pA step (Hz)	37.1 $\pm$ 2.78	33.0 $\pm$ 1.74	18 (60/18)	-2.063	.055	†
400 pA step (Hz)	41.8 $\pm$ 3.64	36.3 $\pm$ 2.03	13 (54/13)	-2.023	.066	†
DB (%exist)	83.3 (n = 5)	100 (n = 6)	6	1.000	.317	
DB current (nA)	1.04 $\pm$ 0.10	0.46 $\pm$ 0.11	5	-10.770	.000	***
DB duration (ms)	220 $\pm$ 56.1	230 $\pm$ 46.4	5	0.102	.924	

Data represented as M  $\pm$  SEM. Paired T-test, unless otherwise stated. †  $p < 0.1$ , \*  $p < 0.05$ , \*\*  $p < 0.01$ , \*\*\*  $p < 0.001$ .

Discontinuation rate: Degree of the cell's drop out from the assessment for excitability a 1 s current stimulations with incrementing (50 pA) amplitude. Last current: The amplitude of the last current amplitude with which the excitability could be assessed. DB: Depolarization block. DB current: Amplitude of the direct current necessary for the first induction of DB.

#### \*Elaboration on the complex but potentially meaningful effects of Cch on $R_{in}$ :

To assess the effect of Cch on  $R_{in}$ , I analyzed 33 cells from which  $R_{in}$  measures were obtained at the three holding potentials -70, -65, and -60 mV and both in the absence and presence of Cch.

	ACSF+SB	10 $\mu$ M Cch	N
<b>Passive properties</b>			
-70 mV $R_{in}$ (M $\Omega$ )	103 $\pm$ 6.38	108 $\pm$ 4.98	33
-65 mV $R_{in}$ (M $\Omega$ )	155 $\pm$ 9.35	112 $\pm$ 5.96	33
-60 mV $R_{in}$ (M $\Omega$ )	228 $\pm$ 10.7	193 $\pm$ 11.9	33

Data represented as M  $\pm$  SEM. †  $p < 0.1$ , \*  $p < 0.05$ , \*\*  $p < 0.01$ , \*\*\*  $p < 0.001$ .  
 $R_{in}$ : input resistance at the specified holding membrane potential.

To assess the effects of Cch and the holding potential on  $R_{in}$ , I conducted a 3x2 two-way repeated measures ANOVA on a sample of 33 neurons which were recorded at the three membrane potentials -70, -65, and -60 mV both in the absence and presence of Cch. Firstly, this analysis yielded a significant voltage-dependence of  $R_{in}$  ( $F_{(2,64)} = 89.518$ ,  $p < 0.001$ ), whereby  $R_{in}$  increased as the membrane potential depolarized (Fig. 3.1.1C). Secondly, the bath-application of Cch significantly decreased  $R_{in}$  ( $F_{(1,32)} = 18.996$ ,  $p < 0.001$ ). Lastly, the voltage-dependence of  $R_{in}$  was significantly affected by the superfusion of Cch (Greenhouse-Geisser correction,  $F_{(1,657,53,030)} = 7.704$ ,  $p = 0.002$ ). In particular, during the superfusion of Cch, the voltage-dependence was reduced at the more hyperpolarized membrane potentials. Bonferroni-corrected post-hoc tests are specified in figure 3.1.1C. Notably,  $R_{in}$  values could only be obtained if the neuron did not generate action potentials at the respective membrane potential (methods). This may have introduced a bias towards assessing the  $R_{in}$  from neurons that were only moderately affected by Cch. Thus, the aforementioned results may underestimate the effects exerted by Cch.

The main effect of a Cch-dependent  $R_{in}$  reduction was in contrast to prevalent literature (Benardo and Prince, 1982; Hönigsperger et al., 2014). Nonetheless, the reduced  $R_{in}$  indicated the relative dominance of an increased membrane conductance over the blockade of trans-membrane currents upon the application of Cch in my sample. In light of the observed RMP depolarization (Fig. 3.1.1A&B), this facilitated conductance may have been the hyperpolarization activated cyclic nucleotide-gated cationic current ( $I_h$ ) because enhancement of  $I_h$  was reported to depolarize the RMP (Maccaferri et al., 1993). Yet,  $I_h$  was also reported to mediate the voltage-dependence of  $R_{in}$ , particularly at membrane potentials more hyperpolarized than -65 mV (Surges et al., 2004). Based on that, the pattern of  $R_{in}$  modulation by Cch indicated a blockade of  $I_h$  because I observed a hampered voltage-dependence specifically at -65 to -70 mV (Fig. 3.1.1C). This effect on the voltage-dependence of  $R_{in}$  may have introduced the  $R_{in}$  discrepancy between ACSF+SB and Cch at -65 and -60 mV. However, a functional reduction of  $I_h$ , restricted to membrane potentials more hyperpolarized than -65 mV may not necessarily account for the remaining  $R_{in}$  difference at -60 mV. Therefore, an enhancement of a current that exerts its effects at more depolarized membrane

potentials and thereby establishes a  $R_{in}$  reduction at depolarized membrane potentials may be possible as well.

In summary, the facilitation of a current particularly at more depolarized membrane potentials may have dominated an oftentimes reported (Benardo and Prince, 1982; Cole and Nicoll, 1983) Cch-dependent blockade of potassium currents which I also observed in my sample as evident by the Cch-mediated suppression of the AHP (Fig. 3.1.3).

#### \*\* Elaboration on the sag ratio:

All previously reported cells were recorded with all three membrane potential deflections (-10, -15, and -20 mV) and both in the absence and presence of Cch. Therefore, the sample used for the 3x2 repeated-measures ANOVA was identical to the above mentioned sample. However, a Bonferroni-corrected post hoc test on the differences between Cch and ACSF+SB at -15 and -20 mV yielded a significance values of  $p < 0.05$  and  $p < 0.01$ , respectively.

The analysis revealed a significant augmentation of  $I_h$  with more intense membrane deflections (Greenhouse-Geisser correction,  $F_{(1,474,126)} = 10.167$ ,  $p < 0.001$ ) and a significant increase of  $I_h$  by the bath application of Cch ( $F_{(1,63)} = 5.167$ ,  $p = 0.026$ ). Furthermore, the sag ratio dependence on the hyperpolarization amplitude was significantly more pronounced in the presence of Cch, than in ACSF+SB only (Greenhouse-Geisser correction,  $F_{(1,457,126)} = 3.887$ ,  $p = 0.036$ ). Bonferroni-corrected post-hoc tests (Fig. 3.1.X) revealed that the more pronounced induction of  $I_h$  by more intense hyperpolarizations was entirely mediated by this effect in the presence of Cch because it was absent in the absence of Cch.

**Table 6.1.2: Effects of 5, 10, and 20  $\mu\text{M}$  carbachol on intrinsic electrophysiological properties.**

The table summarizes comparisons across three independent samples of cells which were exposed to 5, 10, or 20  $\mu\text{M}$  carbachol (Cch).

	5 $\mu\text{M}$ Cch(5)	10 $\mu\text{M}$ Cch (10)	20 $\mu\text{M}$ Cch (20)	N (5/10/20)	N (all)	R <sup>2</sup>	p	Slope of the linear fit	
<b>Passive properties</b>									
RMP (%silent)	12.0 (n = 3)	37.7 (n = 26)	17.1 (n = 7)	25/69/41	130				
RMP (mV) <sup>†</sup>	-61.9 $\pm$ 1.68	-63.8 $\pm$ 0.74	-59.2 $\pm$ 1.23	3/26/7	36	.149	.020	+0.35 mV/ $\mu\text{M}$	*
-70 mV R <sub>in</sub> (M $\Omega$ )	101 $\pm$ 8.08	108 $\pm$ 4.94	102 $\pm$ 4.04	25/66/38	129	.000	.810		
-65 mV R <sub>in</sub> (M $\Omega$ )	127 $\pm$ 8.91	123 $\pm$ 6.21	131 $\pm$ 10.50	21/45/15	81	.002	.721		
-60 mV R <sub>in</sub> (M $\Omega$ )	181 $\pm$ 18.90	191 $\pm$ 10.98	228 $\pm$ 22.62	16/36/9	61	.047	.095	+3.23 m $\Omega$ / $\mu\text{M}$	†
<b>Hyperpolarization activated current</b>									
Sag (-10 mV step)	0.280 $\pm$ 0.012	0.247 $\pm$ 0.006	0.246 $\pm$ 0.009	25/67/38	130	.025	.073	-0.002 AU/ $\mu\text{M}$	†
Sag (-15 mV step)	0.292 $\pm$ 0.011	0.263 $\pm$ 0.006	0.257 $\pm$ 0.007	25/67/38	130	.035	.033	-0.002 AU/ $\mu\text{M}$	*
Sag (-20 mV step)	0.301 $\pm$ 0.010	0.268 $\pm$ 0.006	0.270 $\pm$ 0.008	25/67/38	130	.021	.098	-0.001 AU/ $\mu\text{M}$	†
<b>Action potential properties</b>									
Threshold (mV)	-42.9 $\pm$ 1.42	-44.6 $\pm$ 0.72	-45.8 $\pm$ 0.83	25/68/41	134	.023	.079	-0.166 mV/ $\mu\text{M}$	†
Amplitude (mV)	72.2 $\pm$ 1.85	69.0 $\pm$ 1.40	74.4 $\pm$ 1.70	25/68/41	134	.021	.096	+0.29 mV/ $\mu\text{M}$	†
Rising slope (mV/ms)	268 $\pm$ 15.7	246 $\pm$ 9.64	288 $\pm$ 14.9	25/68/41	134	.025	.067	+2.40 mVs <sup>-1</sup> / $\mu\text{M}$	†
falling slope (mV/ms)	-64.5 $\pm$ 2.44	-62.2 $\pm$ 1.62	-65.9 $\pm$ 2.13	25/68/41	134	.006	.365		
1/2 width (ms)	1.07 $\pm$ 0.03	1.14 $\pm$ 0.02	1.07 $\pm$ 0.02	25/68/41	134	.004	.459		
1/3 width (ms)	1.34 $\pm$ 0.04	1.41 $\pm$ 0.03	1.34 $\pm$ 0.03	25/68/41	134	.003	.539		
fAHP (mV)	-4.84 $\pm$ 1.23	-3.28 $\pm$ 0.58	-3.12 $\pm$ 0.80	25/68/41	134	.008	.318		
firing type (%regular)	92.0 (n = 23)	92.4 (n = 61)	94.6 (n = 35)	25/66/37					

Linear regression, unless otherwise stated. †  $p < 0.1$ , \*  $p < 0.05$ , \*\*  $p < 0.01$ , \*\*\*  $p < 0.001$ .

RMP: resting membrane potential. R<sub>in</sub>: input resistance at the specified holding membrane potential. Sag: Sag ratio induced by a hyperpolarizing voltage step as specified. rising slope: the peak of the rising slope. falling slope: the peak of the falling slope. 1/2 width: Full width of the action potential at one half of its amplitude. 1/3 width: Full width of the action potential at one third of its amplitude. AHP: afterhyperpolarization. fAHP: fast AHP.

Continuation of Table 6.1.2:

	5 $\mu\text{M}$ Cch(5)	10 $\mu\text{M}$ Cch (10)	20 $\mu\text{M}$ Cch (20)	N (5/10/20)	N (all)	R <sup>2</sup>	p	Slope of the linear fit	
<b>Post-burst properties</b>									
AHP (%exist)	53.8 (n = 7)	39.3 (n = 11)	36.4 (n = 4)	13/28/11					
AHP duration (s)	0.082 $\pm$ 0.02	0.054 $\pm$ 0.01	0.102 $\pm$ 0.02	7/11/4	22	.043	.354		
AHP area (mV*s)	-0.048 $\pm$ 0.02	-0.022 $\pm$ 0.01	-0.044 $\pm$ 0.01	7/11/4	22	.001	.912		
mAHP latency (ms)	32.4 $\pm$ 5.84	25.7 $\pm$ 3.07	37.4 $\pm$ 5.85	7/11/4	22	.023	.502		
mAHP peak (mV)	-0.817 $\pm$ 0.23	-0.564 $\pm$ 0.10	-0.699 $\pm$ 0.14	7/11/4	22	.007	.706		
AHP decay $\tau$ (ms)	33.0 $\pm$ 11.05	19.4 $\pm$ 3.12	42.2 $\pm$ 13.46	7/11/4	22	.027	.467		
sAHP at 0.5 s (mV)	1.92 $\pm$ 0.52	2.17 $\pm$ 0.22	1.94 $\pm$ 0.50	7/11/4	22	.000	.989		
sAHP at 1 s (mV)	2.19 $\pm$ 0.56	2.53 $\pm$ 0.26	2.45 $\pm$ 0.54	7/11/4	22	.006	.731		
V <sub>m</sub> at peak (mV)	-0.171 $\pm$ 0.25	0.319 $\pm$ 0.17	0.644 $\pm$ 0.43	13/28/11	52	.062	.074	+0.05 mV/ $\mu\text{M}$	†
V <sub>m</sub> at 200 ms (mV)	1.07 $\pm$ 0.22	1.37 $\pm$ 0.11	1.46 $\pm$ 0.40	13/28/11	52	.020	.319		
V <sub>m</sub> at 500 ms (mV)	2.07 $\pm$ 0.27	2.47 $\pm$ 0.15	2.60 $\pm$ 0.39	13/28/11	52	.029	.231		
V <sub>m</sub> at 1 s (mV)	2.24 $\pm$ 0.29	2.72 $\pm$ 0.19	3.24 $\pm$ 0.51	13/28/11	52	.076	.048	+0.06 mV/ $\mu\text{M}$	*
<b>Excitability</b>									
Adaptation ratio	0.609 $\pm$ 0.15	1.086 $\pm$ 0.28	0.751 $\pm$ 0.19	5/42/4	51	.000	.986		
Discontinuation rate	see N(5 $\mu\text{M}$ )	see N (10 $\mu\text{M}$ )	see N (20 $\mu\text{M}$ )		129		.028	$\chi^2 = 7.127$ , Kaplan-Meier analysis*	
Last current (pA)	276 $\pm$ 20.2	236 $\pm$ 13.8	185 $\pm$ 19.3	25/67/37	129	.073	.002	-5.72 pA/ $\mu\text{M}$	**
50 pA step (Hz)	0.040 $\pm$ 0.04	0.373 $\pm$ .027	0.00 $\pm$ 0.00	25/67/37	129	.002	.586		
100 pA step (Hz)	4.67 $\pm$ 1.61	6.91 $\pm$ 1.304	10.8 $\pm$ 1.78	25/64/34	123	.047	.016	+0.40 Hz/ $\mu\text{M}$	*
150 pA step (Hz)	13.8 $\pm$ 2.27	17.6 $\pm$ 1.63	23.2 $\pm$ 2.46	25/57/21	103	.066	.009	+0.61 Hz/ $\mu\text{M}$	**
200 pA step (Hz)	23.8 $\pm$ 1.67	26.7 $\pm$ 1.75	27.0 $\pm$ 3.03	19/37/14	70	.009	.424		
250 pA step (Hz)	30.4 $\pm$ 1.30	31.2 $\pm$ 1.76	30.7 $\pm$ 2.93	16/33/10	59	.007	.957		
300 pA step (Hz)	33.5 $\pm$ 1.79	33.2 $\pm$ 1.79	34.1 $\pm$ 3.33	11/27/7	45	.001	.853		
350 pA step (Hz)	35.0 $\pm$ 2.33	33.5 $\pm$ 1.63	37.0 $\pm$ 4.03	9/20/7	36	.012	.526		
400 pA step (Hz)	34.1 $\pm$ 2.40	36.1 $\pm$ 1.89	38.7 $\pm$ 3.89	8/14/7	29	.046	.265		

Linear regression, unless otherwise stated. †  $p < 0.1$ , \*  $p < 0.05$ , \*\*  $p < 0.01$ , \*\*\*  $p < 0.001$ .

AHP: afterhyperpolarization. mAHP: medium AHP. sAHP: slow AHP. Discontinuation rate: Degree of the cell's drop out from the assessment for excitability by incrementing (50 pA) 1 s current stimulations. Last current: The amplitude of the last current amplitude with which the excitability could be assessed.

**Continuation of Table 6.1.2:**

	<b>5 <math>\mu</math>M Cch(5)</b>	<b>10 <math>\mu</math>M Cch (10)</b>	<b>20 <math>\mu</math>M Cch (20)</b>	<b>N (5/10/20)</b>	<b>N (all)</b>	<b>R<sup>2</sup></b>	<b>p</b>	<b>Slope of the linear fit</b>
DB (%exist)	32.0 (n = 8)	25.4 (n = 17)	54.1 (n = 20)	25/67/37	129			
DB current (nA)	0.275 $\pm$ 0.03	0.221 $\pm$ 0.02	0.218 $\pm$ 0.02	8/17/20	45	.026	.655	
DB duration (ms)	281 $\pm$ 47.19	306 $\pm$ 47.14	278 $\pm$ 41.73	8/17/20	45	.002	.847	
postDB (%exist)	62.5 (n = 5)	52.9 (n = 9)	55.0 (n = 11)	8/17/20	45			
Hi-DB (%exist)	100 (n = 14)	85.7 (n = 6)	100 (n = 27)	14/7/27	48			
Hi-DB current (nA)	0.621 $\pm$ 0.09	0.583 $\pm$ 0.15	0.496 $\pm$ 0.07	14/6/27	47	.029	.253	
Hi-DB duration (ms)	196 $\pm$ 31.21	225 $\pm$ 38.19	253 $\pm$ 26.94	14/6/27	47	.040	.179	
Hi-postDB (% exist)	14.3 (n = 2)	33.3 (n = 2)	36.0 (n = 9)	14/6/27	47			

Linear regression, unless otherwise stated. †  $p < 0.1$ , \*  $p < 0.05$ , \*\*  $p < 0.01$ , \*\*\*  $p < 0.001$ .

DB: Depolarization block. Tested up to a current amplitude of 400 pA. DB current: Amplitude of the direct current necessary for the first induction of DB. Hi-DB: Occurrence of DB tested by current stimulations up to 1.4 nA Hi-DB current: Amplitude of the direct current necessary for the first induction of DB.

Even though the experimental animals I used were sacrificed at a pre-pubertal age (Clark, 2002; Stanko et al., 2010) evidence indicates that the sex may nonetheless affect cellular properties. The maternal care of rats was reported to be more intense towards male than female offspring (Moore and Morelli, 1979). Variability in maternal care were related to differential development of the central nervous system, including the cholinergic innervation of the hippocampus (Liu et al., 2000; Champagne et al., 2003). In particular interest for the memory-related aspects of this dissertation, intensive maternal care improved hippocampus-dependent learning and memory (Liu et al., 2000; Champagne et al., 2003). With special relevance to the seizure-related aspects of this dissertation, the offspring from mothers investing in intensive maternal care and male pups had an increased seizure susceptibility (Moriyama et al., 2013). In summary, indicators for a differential modulation by cholinergic stimulation and/or increased intrinsic excitability of cells from male pups could be expected.

**Table 6.1.3: Effects of the animals' sex on intrinsic electrophysiological properties of CA1 pyramidal neurons while superfused with ACSF+SB.**

The table summarizes comparisons between the independent samples of cells derived from male or female animals at a postnatal age of 14-24 days.

	Male (M)	Female (F)	N (M/F)	df	T or $\chi^2$	p*
<b>Passive properties</b>						
RMP (mV)	-63.2 ± 0.4	-63.7 ± 0.4	62/97	157	-0.759	.443
-70 mV R <sub>in</sub> (MΩ)	110 ± 4.5	112 ± 3.4	48/95	141	0.269	.789
-65 mV R <sub>in</sub> (MΩ)	165 ± 8.2	156 ± 9.2	38/52	88	-0.712	.478
-60 mV R <sub>in</sub> (MΩ)	234 ± 12	226 ± 12	36/48	82	-0.444	.658
<b>Hyperpolarization activated current</b>						
Sag (-10 mV step)	0.248 ± 0.01	0.231 ± 0.01	49/95	142	-1.612	.109
Sag (-15 mV step)	0.247 ± 0.01	0.246 ± 0.01	49/95	142	-0.160	.873
Sag (-20 mV step)	0.253 ± 0.01	0.247 ± 0.01	49/95	142	-0.639	.524
<b>Action potential properties</b>						
Threshold (mV)	-45.1 ± 0.86	-46.0 ± 0.72	48/92	138	-0.754	.452
Amplitude (mV)	74.3 ± 1.6	73.0 ± 1.0	48/92	138	-0.759	.449
rising slope (mV/ms)	274 ± 14	254 ± 7.6	48/92	75.748	-1.268	.209
falling slope (mV/ms)	-63.4 ± 2.5	-62.7 ± 1.4	48/92	138	0.235	.815
1/2 width (ms)	1.19 ± 0.03	1.18 ± 0.02	48/92	138	-0.288	.774
1/3 width (ms)	1.48 ± 0.04	1.46 ± 0.03	48/92	138	-0.446	.656
fAHP (mV)	-3.80 ± 0.74	-3.70 ± 0.67	48/92	138	0.091	.927
firing type (%regular)	79.6 (n = 39)	83.2 (n = 79)	49/95	1	0.278	.598

Data represented as M ± SEM. Two-sample T-test, unless otherwise stated. † p < 0.1, \* p < 0.05, \*\* p < 0.01, \*\*\* p < 0.001.

RMP: resting membrane potential. R<sub>in</sub>: input resistance at the specified holding membrane potential. Sag: Sag ratio induced by a hyperpolarizing voltage step as specified. rising slope: the peak of the rising slope. falling slope: the peak of the falling slope 1/2 width: Full width of the action potential at one half of its amplitude. 1/3 width: Full width of the action potential at one third of its amplitude. AHP: afterhyperpolarization. fAHP: fast AHP.

**Continuation of Table 6.1.3:**

	Male (M)	Female (F)	N (M/F)	df	T or $\chi^2$	p*
<b>Post-burst properties</b>						
AHP (%exist)	100 (n = 24)	98.1 (n = 51)	24/52			.684
AHP duration (s)	0.541 ± 0.15	0.495 ± 0.10	24/51	73	-0.261	.795
AHP area (mV*s)	-0.349 ± 0.1	-0.315 ± 0.06	24/51	73	0.768	.296
mAHP latency (ms)	34.6 ± 2.6	30.6 ± 1.79	24/51	73	-1.260	.212
mAHP peak (mV)	-1.63 ± 0.12	-1.62 ± 0.12	24/51	73	0.053	.958
AHP decay τ (ms)	98.4 ± 19	91.7 ± 17.3	24/51	73	-0.235	.815
sAHP at 0.5 s (mV)	-0.098 ± 0.1	-0.034 ± 0.06	24/51	73	0.558	.579
sAHP at 1 s (mV)	-0.146 ± 0.09	0.006 ± 0.06	24/51	73	1.375	.173
<b>Excitability</b>						
Adaptation ratio	2.54 ± 0.33	2.79 ± 0.30	39/79	116	0.497	.620
50 pA step (Hz)	0.367 ± 0.30	0.168 ± 0.11	49/95	61.013	-0.633	.529
100 pA step (Hz)	3.35 ± 0.94	4.61 ± 0.74	49/95	142	1.030	.305
150 pA step (Hz)	10.9 ± 1.47	13.0 ± 1.13	49/95	142	1.089	.278
200 pA step (Hz)	19.6 ± 1.66	21.6 ± 1.15	49/95	142	0.978	.330
250 pA step (Hz)	26.7 ± 1.69	28.3 ± 1.09	49/95	142	0.840	.402
300 pA step (Hz)	32.0 ± 1.61	33.0 ± 1.07	49/95	142	0.531	.596
350 pA step (Hz)	36.0 ± 1.61	36.7 ± 1.06	49/91	138	0.381	.704
400 pA step (Hz)	38.5 ± 1.70	39.4 ± 1.06	44/88	130	0.510	.611

Data represented as M ± SEM. Two-sample T-test, unless otherwise stated. † p < 0.1, \* p < 0.05, \*\* p < 0.01, \*\*\* p < 0.001.

AHP: afterhyperpolarization. mAHP: medium AHP. sAHP: slow AHP.

**Table 6.1.4: Effects of the animals' sex on intrinsic electrophysiological properties of CA1 pyramidal neurons during the bath application of 10 μM Cch.**

The table summarizes comparisons between the independent samples of cells derived from male or female animals at a postnatal age of 14-24 days.

	Male (M)	Female (F)	N (M/F)	df	T or $\chi^2$	p
<b>Passive properties</b>						
RMP (%silent)	41.9 (n = 13)	34.2 (n = 13)	31/38	1	0.434	.510
RMP (mV)	-63.8 ± 1.09	-63.9 ± 1.05	13/13	24	-0.092	.927
-70 mV R <sub>in</sub> (MΩ)	101 ± 6.94	114 ± 6.90	31/35	64	1.387	.170
-65 mV R <sub>in</sub> (MΩ)	112 ± 7.0	131 ± 9.06	18/27	43	1.466	.150
-60 mV R <sub>in</sub> (MΩ)	206 ± 18.4	180 ± 13.3	15/21	34	-1.202	.238
<b>Hyperpolarization activated current</b>						
Sag (-10 mV step)	0.247 ± 0.01	0.247 ± 0.01	31/36	65	-0.040	.968
Sag (-15 mV step)	0.254 ± 0.01	0.270 ± 0.01	31/36	44.947	1.245	.219
Sag (-20 mV step)	0.261 ± 0.01	0.274 ± 0.01	31/36	47.407	0.942	.351

Data represented as M ± SEM. Two-sample T-test, unless otherwise stated. † p < 0.1, \* p < 0.05, \*\* p < 0.01, \*\*\* p < 0.001.

RMP: resting membrane potential. R<sub>in</sub>: input resistance at the specified holding membrane potential. Sag: Sag ratio induced by a hyperpolarizing voltage step as specified.



Continuation of Table 6.1.4:

	Male (M)	Female (F)	N (M/F)	df	T or $\chi^2$	p
<b>Action potential properties</b>						
Threshold (mV)	-44.3 ± 1.15	-45.0 ± 0.93	31/37	66	-0.468	.641
Amplitude (mV)	69.7 ± 1.94	68.4 ± 2.01	31/37	66	-0.470	.640
rising slope (mV/ms)	250 ± 13.9	242 ± 13.5	31/37	66	-0.484	.630
falling slope (mV/ms)	-62.0 ± 2.45	-62.4 ± 2.18	31/37	66	-0.109	.913
1/2 width (ms)	1.14 ± 0.04	1.13 ± 0.03	31/37	66	-0.186	.853
1/3 width (ms)	1.42 ± 0.05	1.40 ± 0.04	31/37	66	-0.395	.694
fAHP (mV)	-2.83 ± 0.77	-3.66 ± 0.85	31/37	66	-0.705	.483
firing type (%regular)	96.8 (n = 30)	88.6 (n = 31)	31/35	1	1.580	.209
<b>Post-burst properties</b>						
AHP (%exist)	30.0 (n = 3)	44.4 (n = 8)	10/18			
AHP duration (s)	0.047 ± 0.00	0.056 ± 0.01	3/8	7.810	1.109	.300
AHP area (mV*s)	-0.015 ± 0.00	-0.025 ± 0.01	3/8	7.057	-1.336	.223
mAHP latency (ms)	24.3 ± 2.75	26.2 ± 4.19	3/8	9	0.266	.796
mAHP peak (mV)	-0.515 ± 0.03	-0.582 ± 0.14	3/8	7.519	-0.466	.655
AHP decay $\tau$ (ms)	16.3 ± 1.28	20.51 ± 4.28	3/8	9	0.576	.579
sAHP at 0.5 s (mV)	2.15 ± 0.52	2.17 ± 0.25	3/8	9	0.041	.969
sAHP at 1 s (mV)	2.46 ± 0.59	2.55 ± 0.30	3/8	9	0.164	.873
V <sub>m</sub> at peak (mV)	0.497 ± 0.290	0.220 ± 0.21	10/18	26	-0.767	.450
V <sub>m</sub> at 200 ms (mV)	1.36 ± 0.19	1.37 ± 0.15	10/18	26	0.057	.955
V <sub>m</sub> at 500 ms (mV)	2.37 ± 0.32	2.43 ± 0.16	10/18	26	0.477	.637
V <sub>m</sub> at 1 s (mV)	2.61 ± 0.33	2.78 ± 0.23	10/18	26	0.436	.666
<b>Excitability</b>						
Adaptation ratio	1.07 ± 0.24	1.00 ± 0.34	29/30	57	-0.155	.877
Discontinuation rate	see N(M)	see N(F)	65	1	0.085	.770
Last current (pA)	247 ± 20	226 ± 19	31/36	65	-0.733	.466
50 pA step (Hz)	0.516 ± 0.52	0.250 ± 0.25	31/36	43.668	-0.464	.645
100 pA step (Hz)	5.79 ± 1.78	7.83 ± 1.88	29/35	62	0.775	.441
150 pA step (Hz)	16.0 ± 2.25	19.1 ± 2.35	27/30	55	0.959	.342
200 pA step (Hz)	25.1 ± 2.69	28.4 ± 2.23	19/18	35	0.950	.348
250 pA step (Hz)	30.4 ± 3.12	32.1 ± 1.6	17/16	23.814	0.489	.630
300 pA step (Hz)	31.9 ± 3.26	34.7 ± 1.31	14/13	17.080	0.808	.430
350 pA step (Hz)	32.2 ± 2.72	35.0 ± 1.43	11/9	14.883	0.916	.374
400 pA step (Hz)	35.2 ± 5.02	36.7 ± 1.37	5/9	4.608	0.282	.790
DB (%exist)	19.4 (n = 6)	30.6 (n = 11)	31/36	1	1.104	.294
DB current (nA)	0.283 ± 0.05	0.186 ± 0.02	6/11	15	-2.297	.036 *
DB duration (ms)	325 ± 104	295 ± 50.2	6/11	15	-0.291	.775

Data represented as M ± SEM. Two-sample T-test, unless otherwise stated. † p < 0.1, \* p < 0.05, \*\* p < 0.01, \*\*\* p < 0.001.

Rising slope: the peak of the rising slope. Falling slope: the peak of the falling slope 1/2 width: Full width of the action potential at one half of its amplitude. 1/3 width: Full width of the action potential at one third of its amplitude. AHP: afterhyperpolarization. fAHP: Fast AHP. mAHP: Medium AHP. sAHP: Slow AHP. V<sub>m</sub> at: Membrane potential at the specified time after a burst of five action potentials, irrespective of the occurrence of an AHP. Discontinuation rate: Degree of the cell's drop out from the assessment for excitability by incrementing (50 pA) 1 s current stimulations. Last current: The amplitude of the last current amplitude with which the excitability could be assessed. DB: Depolarization block. DB current: Amplitude of the direct current necessary for the first induction of DB.

Table 6.1.5: Effects of the cerebral hemisphere on intrinsic electrophysiological properties of CA1 pyramidal neurons while superfused with ACSF+SB.

The table summarizes comparisons between the independent samples of cells derived from the left or the right cerebral hemisphere.

	left (L)	right (R)	N (L/R)	df	T or $\chi^2$	p*
<b>Passive properties</b>						
RMP (mV)	-63.8 ± 0.38	-63.1 ± 0.41	92/66	156	1.292	.153
-70 mV R <sub>in</sub> (MΩ)	113 ± 3.77	109 ± 3.89	84/59	141	-0.812	.418
-65 mV R <sub>in</sub> (MΩ)	169 ± 9.37	148 ± 7.56	51/39	87.503	-1.756	.083 †
-60 mV R <sub>in</sub> (MΩ)	246 ± 12.9	209 ± 10.1	47/37	80.968	-2.225	.029 *
<b>Hyperpolarization activated current</b>						
Sag (-10 mV step)	0.228 ± 0.01	0.249 ± 0.01	85/59	142	2.078	.039 *
Sag (-15 mV step)	0.241 ± 0.01	0.254 ± 0.01	85/59	142	1.524	.130
Sag (-20 mV step)	0.241 ± 0.01	0.260 ± 0.01	85/59	142	2.057	.042 *
<b>Action potential properties</b>						
Threshold (mV)	-46.1 ± 0.72	-45.0 ± 0.88	83/57	138	1.031	.304
Amplitude (mV)	73.1 ± 1.0	73.9 ± 1.42	83/57	138	0.452	.652
rising slope (mV/ms)	260 ± 8.22	263 ± 12.1	83/57	138	0.209	.835
falling slope (mV/ms)	-64.3 ± 1.50	-61.0 ± 2.23	83/57	138	1.283	.202
1/2 width (ms)	1.164 ± 0.02	1.22 ± 0.03	83/57	138	1.376	.171
1/3 width (ms)	1.43 ± 0.03	1.51 ± 0.04	83/57	100.400	1.533	.128
fAHP (mV)	-3.725 ± 0.69	-3.75 ± 0.73	83/57	138	-0.023	.982
firing type (%regular)	78.8 (n = 67)	86.4 (n = 51)	85/59	1	1.366	.243 †
<b>Post-burst properties</b>						
AHP (%exist)	97.7 (n = 43)	100 (n = 32)	44/32		Fisher-Yates test	.684
AHP duration (s)	0.482 ± 0.10	0.547 ± 0.14	43/32	73	0.399	.691
AHP area (mV*s)	-0.305 ± 0.06	-0.354 ± 0.09	43/32	73	-0.466	.643
mAHP latency (ms)	32.4 ± 2.25	31.3 ± 1.73	43/32	72.156	-0.363	.717
mAHP peak (mV)	-1.63 ± 0.12	-1.61 ± 0.13	43/32	73	0.128	.851
AHP decay $\tau$ (ms)	98.36 ± 20.0	87.7 ± 15.7	43/32	72.443	-0.419	.677
sAHP at 0.5 s (mV)	-0.037 ± 0.07	-0.077 ± 0.08	43/32	73	-0.372	.711
sAHP at 1 s (mV)	-0.019 ± 0.07	-0.045 ± 0.08	43/32	73	-0.530	.598
<b>Excitability</b>						
Adaptation ratio	2.38 ± 0.26	3.14 ± 0.40	67/51	88.476	1.603	.112
50 pA step (Hz)	0.318 ± 0.20	0.119 ± 0.08	85/59	111.358	-0.919	.360
100 pA step (Hz)	4.71 ± 0.82	3.42 ± 0.78	85/59	142	-1.085	.280
150 pA step (Hz)	13.0 ± 1.21	11.2 ± 1.32	85/59	142	-0.947	.345
200 pA step (Hz)	21.8 ± 1.24	19.6 ± 1.45	85/59	142	-1.171	.243
250 pA step (Hz)	28.7 ± 1.19	26.5 ± 1.45	85/59	142	-1.160	.248
300 pA step (Hz)	33.5 ± 1.17	31.4 ± 1.37	85/59	142	-1.183	.239
350 pA step (Hz)	37.1 ± 1.17	35.5 ± 1.36	81/59	138	-0.894	.373
400 pA step (Hz)	40.0 ± 1.18	37.8 ± 1.39	79/53	130	-1.214	.227

Data represented as M ± SEM. Two-sample T-test, unless otherwise stated. † p < 0.1, \* p < 0.05, \*\* p < 0.01, \*\*\* p < 0.001.

RMP: resting membrane potential. R<sub>in</sub>: input resistance at the specified holding membrane potential. Sag: Sag ratio induced by a hyperpolarizing voltage step as specified. rising slope: the peak of the rising slope. falling slope: the peak of the falling slope 1/2 width: Full width of the action potential at one half of its amplitude. 1/3 width: Full width of the action potential at one third of its amplitude. AHP: afterhyperpolarization. fAHP: fast AHP. mAHP: medium AHP. sAHP: slow AHP.

The data from cells superfused with ACSF+SB indicated a lower input resistance ( $R_{in}$ ) in CA1 pyramidal neurons from the right compared to the left hemisphere at more depolarized membrane potentials ( $p \geq 0.029$ ). Somewhat inconsistently, this data set also suggested a more pronounced hyperpolarization activated current ( $I_h$ ) in cells from the right compared to the left hemisphere ( $p \geq 0.039$ ). In synopsis, these hemispheric effects on  $R_{in}$  and  $I_h$  were contradictory to one another (Surges et al., 2004) and did not translate to differences in excitability between the left and right hemisphere ( $p \geq 0.227$ ). Therefore, these findings may potentially be attributed to a type I error and will not be further elaborated.

**Table 6.1.6: Effects of the cerebral hemisphere on intrinsic electrophysiological properties of CA1 pyramidal neurons during the bath application of 10  $\mu$ M Cch.**

The table summarizes comparisons between the independent samples of cells derived from the left or the right cerebral hemisphere.

	left (L)	right (R)	N (L/R)	df	T or $\chi^2$	p
<b>Passive properties</b>						
RMP (%silent)	37.2 (n = 16)	38.5 (n = 10)	43/26	1	0.011	.917
RMP (mV)	-64.4 $\pm$ 1.08	-63.0 $\pm$ 0.85	16/10	24	0.920	.367
-70 mV $R_{in}$ (M $\Omega$ )	113 $\pm$ 6.51	98.8 $\pm$ 7.26	41/25	64	-1.445	.153
-65 mV $R_{in}$ (M $\Omega$ )	130 $\pm$ 8.14	115 $\pm$ 9.46	26/19	43	-1.217	.230
-60 mV $R_{in}$ (M $\Omega$ )	205 $\pm$ 11.7	170 $\pm$ 20.7	22/14	34	-1.579	.124
<b>Hyperpolarization activated current</b>						
Sag (-10 mV step)	0.245 $\pm$ 0.01	0.251 $\pm$ 0.01	42/25	65	0.519	.606
Sag (-15 mV step)	0.261 $\pm$ 0.01	0.265 $\pm$ 0.01	42/25	65	0.250	.803
Sag (-20 mV step)	0.271 $\pm$ 0.01	0.263 $\pm$ 0.01	42/25	65	-0.643	.522
<b>Action potential properties</b>						
Threshold (mV)	-45.9 $\pm$ 0.76	-42.5 $\pm$ 1.36	42/26	40.481	2.177	.035 *
Amplitude (mV)	69.3 $\pm$ 1.54	68.5 $\pm$ 2.71	42/26	66	-0.268	.790
rising slope (mV/ms)	248 $\pm$ 10.6	243 $\pm$ 18.7	42/26	66	-0.227	.821
falling slope (mV/ms)	-63.2 $\pm$ 1.68	-60.7 $\pm$ 3.26	42/26	38.407	0.694	.492
1/2 width (ms)	1.1 $\pm$ 0.02	1.2 $\pm$ 0.05	42/26	35.823	0.967	.340
1/3 width (ms)	1.38 $\pm$ 0.03	1.45 $\pm$ 0.06	42/26	36.406	1.122	.269
fAHP (mV)	-2.77 $\pm$ 0.65	-4.11 $\pm$ 1.09	42/26	66	-1.129	.263
firing type (%regular)	90.5 (n = 38)	95.8 (n = 23)	42/24	1	0.626	.429

Data represented as M  $\pm$  SEM. Two-sample T-test, unless otherwise stated. †  $p < 0.1$ , \*  $p < 0.05$ , \*\*  $p < 0.01$ , \*\*\*  $p < 0.001$ .

RMP: resting membrane potential.  $R_{in}$ : input resistance at the specified holding membrane potential. Sag: Sag ratio induced by a hyperpolarizing voltage step as specified. rising slope: the peak of the rising slope. falling slope: the peak of the falling slope. 1/2 width: Full width of the action potential at one half of its amplitude. 1/3 width: Full width of the action potential at one third of its amplitude. AHP: afterhyperpolarization. fAHP: fast AHP.

**Continuation of Table 6.1.6:**

	left (L)	right (R)	N (L/R)	df	T or $\chi^2$	p
<b>Post-burst properties</b>						
AHP (%exist)	44.4 (n = 8)	30.0 (n = 3)	18/10			
AHP duration (s)	0.05 $\pm$ 0.01	0.06 $\pm$ 0.01	8/3	9	0.361	.726
AHP area (mV*s)	-0.025 $\pm$ 0.01	-0.017 $\pm$ 0.01	8/3	9	0.643	.536
mAHP latency (ms)	24.9 $\pm$ 3.89	27.8 $\pm$ 5.27	8/3	9	0.408	.693
mAHP peak (mV)	-0.60 $\pm$ 0.13	-0.47 $\pm$ 0.12	8/3	9	0.546	.598
AHP decay $\tau$ (ms)	20.1 $\pm$ 3.75	17.5 $\pm$ 6.72	8/3	9	-0.351	.734
sAHP at 0.5 s (mV)	2.35 $\pm$ 0.24	1.67 $\pm$ 0.42	8/3	9	-1.474	.175
sAHP at 1 s (mV)	2.66 $\pm$ 0.33	2.18 $\pm$ 0.33	8/3	9	-0.813	.437
$V_m$ at peak (mV)	0.197 $\pm$ 0.22	0.539 $\pm$ 0.28	18/10	26	0.955	.348
$V_m$ at 200 ms (mV)	1.32 $\pm$ 0.14	1.46 $\pm$ 0.19	18/10	26	0.615	.544
$V_m$ at 500 ms (mV)	2.42 $\pm$ 0.21	2.55 $\pm$ 0.21	18/10	26	0.403	.690
$V_m$ at 1 s (mV)	2.71 $\pm$ 0.25	2.73 $\pm$ 0.29	18/10	26	0.048	.962
<b>Excitability</b>						
Adaptation ratio	1.18 $\pm$ 0.32	0.76 $\pm$ 0.14	38/21	49.092	-1.218	.229
Discontinuation rate	see N(L)	see N(R)	65	1	2.775	.096 †
Last current (pA)	224 $\pm$ 16	256 $\pm$ 25	42/25	65	1.129	.263
50 pA step (Hz)	0.595 $\pm$ 0.43	0.00 $\pm$ 0.00	42/25	41.000	-1.376	.176
100 pA step (Hz)	8.87 $\pm$ 1.86	3.84 $\pm$ 1.48	39/25	62	-2.113	.039 *
150 pA step (Hz)	17.6 $\pm$ 2.07	17.6 $\pm$ 2.72	35/22	55	0.011	.991
200 pA step (Hz)	27.7 $\pm$ 1.95	24.9 $\pm$ 3.52	24/13	35	-0.754	.456
250 pA step (Hz)	33.1 $\pm$ 1.49	28.0 $\pm$ 4.05	21/12	14.030	-1.182	.257
300 pA step (Hz)	35.1 $\pm$ 1.63	30.9 $\pm$ 3.46	15/12	15.824	-1.085	.294
350 pA step (Hz)	33.1 $\pm$ 1.55	33.7 $\pm$ 2.74	9/11	18	0.184	.856
400 pA step (Hz)	34.0 $\pm$ 2.13	37.8 $\pm$ 2.88	6/8	12	0.982	.345
DB (%exist)	21.4 (n = 9)	32.0 (n = 8)	42/25	1	0.925	.336
DB current (nA)	0.239 $\pm$ 0.03	0.200 $\pm$ 0.03	9/8	15	-0.847	.410
DB duration (ms)	294 $\pm$ 72.9	319 $\pm$ 62.6	9/8	15	0.250	.806

Data represented as M  $\pm$  SEM. Two-sample T-test, unless otherwise stated. †  $p < 0.1$ , \*  $p < 0.05$ , \*\*  $p < 0.01$ , \*\*\*  $p < 0.001$ .

AHP: afterhyperpolarization. mAHP: Medium AHP. sAHP: Slow AHP.  $V_m$  at: Membrane potential at the specified time after a burst of five action potentials, irrespective of the occurrence of an AHP. Discontinuation rate: Degree of the cells' drop out from the assessment for excitability by incrementing (50 pA) 1 s current stimulations. Last current: The amplitude of the last current amplitude with which the excitability could be assessed. DB: Depolarization block. DB current: Amplitude of the direct current necessary for the first induction of DB.

**Table 6.1.7: Effects of maturation on intrinsic electrophysiological properties of CA1 pyramidal neurons while superfused with ACSF+SB.**

The table summarizes linear regressions of intrinsic electrophysiological properties by the maturation of the experimental animals through postnatal day 14 to 24.

	N	R <sup>2</sup>	$\rho$	Slope of the linear fit
<b>Passive properties</b>				
RMP (mV)	159	.057	.002 **	-0.36 mV/day
-70 mV R <sub>in</sub> (M $\Omega$ )	143	.016	.130	
-65 mV R <sub>in</sub> (M $\Omega$ )	90	.012	.297	
-60 mV R <sub>in</sub> (M $\Omega$ )	84	.000	.901	
<b>Hyperpolarization activated current</b>				
Sag (-10 mV step)	144	.053	.005 **	-0.006 AU/day
Sag (-15 mV step)	144	.157	.000 ***	-0.009 AU/day
Sag (-20 mV step)	144	.147	.000 ***	-0.009 AU/day
<b>Action potential properties</b>				
Threshold (mV)	140	.020	.097 †	-0.400 mV/day
Amplitude (mV)	140	.039	.019 *	+0.834 mV/day
Rising slope (mV/ms)	140	.023	.077 †	+5.25 mVms <sup>-1</sup> /day
falling slope (mV/ms)	140	.091	.000 ***	-1.95 mVms <sup>-1</sup> /day
1/2 width (ms)	140	.040	.017 *	-0.020 ms/day
1/3 width (ms)	140	.040	.019 *	-0.025 ms/day
fAHP (mV)	140	.003	.490	
firing type (%regular)	81.9 (118/144)	.001	.828	binomial logistic regression
<b>Post-burst properties</b>				
AHP (%exist)	98.7 (75/76)			
AHP duration (s)	75	.000	.940	
AHP area (mV*s)	75	.000	.878	
mAHP latency (ms)	75	.012	.345	
mAHP peak (mV)	75	.000	.896	
AHP decay $\tau$ (ms)	75	.005	.550	
sAHP at 0.5 s (mV)	75	.001	.845	
sAHP at 1 s (mV)	75	.011	.377	

Linear regression, unless otherwise stated. †  $p < 0.1$ , \*  $p < 0.05$ , \*\*  $p < 0.01$ , \*\*\*  $p < 0.001$ .

RMP: resting membrane potential. R<sub>in</sub>: input resistance at the specified holding membrane potential. Sag: Sag ratio induced by a hyperpolarizing voltage step as specified. rising slope: the peak of the rising slope. falling slope: the peak of the falling slope 1/2 width: Full width of the action potential at one half of its amplitude. 1/3 width: Full width of the action potential at one third of its amplitude. AHP: afterhyperpolarization. fAHP: Fast AHP. mAHP: Medium AHP. sAHP: Slow AHP. Vm at Membrane potential at the specified time after a burst of five action potentials, irrespective of the occurrence of an AHP.

**Continuation of Table 6.1.7:**

	N	R <sup>2</sup>	$\rho$	Slope of the linear fit
<b>Excitability</b>				
Adaptation ratio	118	.018	.145	
DB (%exist)	0.0 (0/132)			
50 pA step (Hz)	144	.000	.908	
100 pA step (Hz)	144	.013	.183	
150 pA step (Hz)	144	.020	.092 †	+0.654 Hz/day
200 pA step (Hz)	144	.015	.148	
250 pA step (Hz)	144	.015	.137	
300 pA step (Hz)	144	.016	.132	
350 pA step (Hz)	140	.017	.122	
400 pA step (Hz)	132	.017	.130	

Linear regression, unless otherwise stated. †  $p < 0.1$ , \*  $p < 0.05$ , \*\*  $p < 0.01$ , \*\*\*  $p < 0.001$ . DB: Depolarization block.

**Table 6.1.8: Effects of maturation on intrinsic electrophysiological properties of CA1 pyramidal neurons during the bath application of 10  $\mu$ M Cch.**

The table summarizes linear regressions of intrinsic electrophysiological properties by the maturation of the experimental animals through postnatal day 14 to 24.

	N	age range (days)	R <sup>2</sup>	$\rho$	slope of the linear fit
<b>Passive properties</b>					
RMP (%silent)**	37.7 (26/69)	14-24	.041	.166	binomial logistic regression
RMP (mV)	26	14-20	.077	.170	
-70 mV R <sub>in</sub> (M $\Omega$ )	66	14-24	.001	.769	
-65 mV R <sub>in</sub> (M $\Omega$ )	45	14-23	.005	.644	
-60 mV R <sub>in</sub> (M $\Omega$ )	36	14-23	.068	.125	
<b>Hyperpolarization activated current</b>					
Sag (-10 mV step)	67	14-24	.099	.009 **	-0.007 AU**/day
Sag (-15 mV step)	67	14-24	.147	.001 **	-0.008 AU**/day
Sag (-20 mV step)	67	14-24	.152	.001 **	-0.009 AU**/day
<b>Action potential properties</b>					
Threshold (mV)	68	14-24	.002	.702	
Amplitude (mV)	68	14-24	.000	.893	
rising slope (mV/ms)	68	14-24	.002	.726	
falling slope (mV/ms)	68	14-24	.110	.006 **	-1.792 mVms <sup>-1</sup> /day
1/2 width (ms)	68	14-24	.092	.012 *	-0.024 ms/day
1/3 width (ms)	68	14-24	.099	.009 **	-0.031 ms/day
fAHP (mV)	68	14-24	.020	.253	
firing type (%regular)**	91.0 (61/67)	14-24			the six animals exhibiting bursting cells were 15, 16, 3x18 and 20 days old

Linear regression, unless otherwise stated. †  $p < 0.1$ , \*  $p < 0.05$ , \*\*  $p < 0.01$ , \*\*\*  $p < 0.001$ .

RMP: resting membrane potential. R<sub>in</sub>: input resistance at the specified holding membrane potential. Sag: Sag ratio induced by a hyperpolarizing voltage step as specified. rising slope: the peak of the rising slope. falling slope: the peak of the falling slope 1/2 width: Full width of the action potential at one half of its amplitude. 1/3 width: Full width of the action potential at one third of its amplitude. AHP: afterhyperpolarization. fAHP: fast AHP.

Continuation of Table 6.1.8:

	N	age range (days)	R <sup>2</sup>	p	slope of the linear fit
<b>Post-burst properties</b>					
AHP (%exist)	39.3 (11/28)	14-19	.006	.720	binomial logistic regression
AHP duration (s)	11	14-18	.008	.799	
AHP area (mV*s)	11	14-18	.012	.747	
mAHP latency (ms)	11	14-18	.007	.805	
mAHP peak (mV)	11	14-18	.073	.420	
AHP decay $\tau$ (ms)	11	14-18	.003	.869	
sAHP at 0.5 s (mV)	11	14-18	.345	.058	† +0.249 mV/day
sAHP at 1 s (mV)	11	14-18	.372	.046	* +0.304 mV/day
V <sub>m</sub> at peak	28	14-19	.004	.762	
V <sub>m</sub> at 200 ms	28	14-19	.001	.851	
V <sub>m</sub> at 500 ms	28	14-19	.013	.557	
V <sub>m</sub> at 1 s	28	14-19	.044	.284	
<b>Excitability</b>					
Adaptation ratio	59	14-24	.013	.388	
Last current (pA)	67	14-24	.020	.257	
50 pA step (Hz)	67	14-24	.002	.724	
100 pA step (Hz)	64	14-24	.000	.906	
150 pA step (Hz)	57	14-24	.004	.641	
200 pA step (Hz)	37	14-22	.013	.586	
250 pA step (Hz)	33	14-22	.001	.847	
300 pA step (Hz)	27	14-22	.001	.871	
350 pA step (Hz)	20	14-22	.015	.608	
400 pA step (Hz)	14	14-22	.080	.753	
DB exist	25.4 (17/67)	14-24	.000	.919	binomial logistic regression
DB current (nA)	17	14-24	.026	.540	
DB duration (ms)	17	14-24	.177	.092	† +33.4 ms/day

Linear regression, unless otherwise stated. †  $p < 0.1$ , \*  $p < 0.05$ , \*\*  $p < 0.01$ , \*\*\*  $p < 0.001$ .

AHP: afterhyperpolarization. mAHP: medium AHP. sAHP: slow AHP. V<sub>m</sub> at: Membrane potential at the specified time after a burst of five action potentials, irrespective of the occurrence of an AHP. Last current: The amplitude of the last current amplitude with which the excitability could be assessed. DB: Depolarization block. DB current: Amplitude of the direct current necessary for the first induction of DB.

Table 6.1.9: Effects of aging on intrinsic electrophysiological properties of CA1 pyramidal neurons while superfused with ACSF+SB.

The table summarizes the comparison of intrinsic electrophysiological properties between neurons obtained from juvenile and aged animals.

	Juvenile (J)	Aged (A)	N (J/A)	df	T	p
<b>Passive properties</b>						
RMP (mV)	-62.7 ± 1.37	-65.0 ± 1.36	11/12	21	-1.195	.245
-70 mV R <sub>in</sub> (M $\Omega$ )	104 ± 6.80	69.6 ± 7.32	11/12	21	-3.464	.002 **
-65 mV R <sub>in</sub> (M $\Omega$ )	152 ± 10.1	91.2 ± 14.8	11/10	19	-3.462	.003 **
-60 mV R <sub>in</sub> (M $\Omega$ )	203 ± 15.4	129 ± 22.4	11/8	17	-2.827	.012 *
<b>Hyperpolarization activated current</b>						
Sag (-10 mV step)	0.246 ± 0.03	0.152 ± 0.01	11/12	12,596	-3.094	.009 **
Sag (-15 mV step)	0.236 ± 0.02	0.157 ± 0.01	11/12	14,630	-2.874	.012 *
Sag (-20 mV step)	0.228 ± 0.02	0.158 ± 0.01	11/12	14,491	-2.759	.015 *
<b>Action potential properties</b>						
Threshold (mV)	-44.0 ± 1.49	-49.4 ± 1.28	11/12	21	-2.744	.012 *
Amplitude (mV)	72.8 ± 3.22	77.3 ± 2.23	11/12	21	1.162	.258
Rising slope (mV/ms)	269 ± 26.1	278 ± 15.8	11/12	21	0.305	.763
falling slope (mV/ms)	-69.5 ± 6.22	-84.9 ± 3.09	11/12	14,729	-2.223	.042 *
1/2 width (ms)	1.13 ± 0.08	0.94 ± 0.03	11/12	12,314	-2.150	.052 †
1/3 width (ms)	1.40 ± 0.11	1.16 ±	11/12	12,205	-2.076	.060 †
fAHP (mV)	-5.07 ± 1.32	-2.22 ± 1.30	11/12	21	1.54	.138
firing type (%regular)	72.7 (n = 8)	75.0 (n = 9)	11/12			
<b>Post-burst properties</b>						
AHP (%exist)	100 (n = 6)	85.7 (n = 6)	7/6			
AHP duration (s)	0.846 ± 0.33	1.20 ± 0.40	6/6	10	0.680	.512
AHP area (mV*s)	-0.543 ± 0.26	-0.648 ± 0.28	6/6	10	-0.278	.787
mAHP latency (ms)	36.3 ± 3.40	37.1 ± 3.74	6/6	10	0.150	.884
mAHP peak (mV)	-1.80 ± 0.31	-1.58 ± 0.30	6/6	10	0.512	.620
AHP decay $\tau$ (ms)	175 ± 66.8	158 ± 83.6	6/6	10	-0.157	.878
sAHP at 0.5 s (mV)	-0.233 ± 0.12	-0.405 ± 0.23	6/6	10	-0.665	.521
sAHP at 1 s (mV)	-0.289 ± 0.16	-0.347 ± 0.15	6/6	10	-0.264	.797
<b>Excitability</b>						
Adaptation ratio	1.13 ± 0.26	2.31 ± 0.54	8/9	11,387	1.964	.074 †
50 pA step (Hz)	0.0 ± 0.0	0.0 ± 0.0	11/12			
100 pA step (Hz)	1.64 ± 1.19	0.42 ± 0.42	11/12	12,421	-0.965	.353
150 pA step (Hz)	9.82 ± 2.79	3.42 ± 1.77	11/12	21	-1.973	.062 †
200 pA step (Hz)	20.7 ± 3.17	8.59 ± 2.52	11/12	21	-3.021	.006 **
250 pA step (Hz)	29.0 ± 3.28	14.0 ± 3.08	11/12	21	-3.335	.003 **
300 pA step (Hz)	35.6 ± 3.31	18.9 ± 3.25	11/12	21	-3.582	.002 **
350 pA step (Hz)	40.4 ± 3.28	23.5 ± 3.41	11/12	21	-3.547	.002 **
400 pA step (Hz)	43.3 ± 3.24	21.9 ± 3.04	11/10	19	-4.778	.000 ***

Data represented as M ± SEM. Two-sample T-test, unless otherwise stated. †  $p < 0.1$ , \*  $p < 0.05$ , \*\*  $p < 0.01$ , \*\*\*  $p < 0.001$ .

RMP: resting membrane potential. R<sub>in</sub>: input resistance at the specified holding membrane potential. Sag: Sag ratio induced by a hyperpolarizing voltage step as specified. rising slope: the peak of the rising slope. falling slope: the peak of the falling slope. 1/2 width: Full width of the action potential at one half of its amplitude. 1/3 width: Full width of the action potential at one third of its amplitude. AHP: afterhyperpolarization. fAHP: fast AHP. mAHP: medium AHP. sAHP: slow AHP.

**Table 6.1.10: Effects of aging on intrinsic electrophysiological properties of CA1 pyramidal neurons during the bath application of 10  $\mu$ M Cch.**

The table summarizes the comparison of intrinsic electrophysiological properties between neurons obtained from juvenile and aged animals.

	Juvenile (J)	Aged (A)	N (J/A)	df	T or $\chi^2$	p
<b>Passive properties</b>						
RMP (%silent)	27.3 (n = 3)	0.0 (n = 0)	11/11			
RMP (mV)	-64.8 $\pm$ 4.40		3/0			
-70 mV R <sub>in</sub> (M $\Omega$ )	113 $\pm$ 10.2	60.0 $\pm$ 5.89	11/11	20	-4.478	.000 ***
-65 mV R <sub>in</sub> (M $\Omega$ )	128 $\pm$ 7.45	92.4 $\pm$ 17.5	10/9	10.830	-1.851	.092 †
-60 mV R <sub>in</sub> (M $\Omega$ )	218 $\pm$ 26.2	98.1 $\pm$ 12.5	7/6	11	-3.900	.002 **
<b>Hyperpolarization activated current</b>						
Sag (-10 mV step)	0.225 $\pm$ 0.01	0.147 $\pm$ 0.02	11/11	20	-3.308	.004 **
Sag (-15 mV step)	0.225 $\pm$ 0.02	0.165 $\pm$ 0.02	11/11	20	-2.247	.036 *
Sag (-20 mV step)	0.241 $\pm$ 0.02	0.170 $\pm$ 0.02	11/11	20	-2.532	.020 *
<b>Action potential properties</b>						
Threshold (mV)	-44.1 $\pm$ 1.69	-48.4 $\pm$ 1.45	11/11	20	-1.927	.068 †
Amplitude (mV)	70.4 $\pm$ 2.43	72.6 $\pm$ 2.64	11/11	20	0.607	.551
Rising slope (mV/ms)	257 $\pm$ 20.4	256 $\pm$ 17.2	11/11	20	-0.044	.965
falling slope (mV/ms)	-67.2 $\pm$ 3.78	-81.2 $\pm$ 4.10	11/11	20	-2.509	.021
1/2 width (ms)	1.08 $\pm$ 0.04	0.940 $\pm$ 0.03	11/11	20	-2.770	.012 *
1/3 width (ms)	1.34 $\pm$ 0.06	1.16 $\pm$ 0.03	11/11	20	-2.582	.018 *
fAHP (mV)	-4.25 $\pm$ 1.14	-1.75 $\pm$ 1.3	11/11	20	1.446	.164
firing type (%regular)	100 (n = 11)	90.9 (n = 1)	11/11			
<b>Post-burst properties</b>						
AHP (%exist)	50.0 (n = 2)	0.0 (n = 0)	4/3			
AHP duration (s)	0.046 & 0.051		2/0			
AHP area (mV*s)	-0.014 & -0.016		2/0			
mAHP latency (ms)	23.9 & 29.3		2/0			
mAHP peak (mV)	-0.514 & -0.467		2/0			
AHP decay $\tau$ (ms)	13.9 & 16.9		2/0			
sAHP at 0.5 s (mV)	2.95 & 2.33		2/0			
sAHP at 1 s (mV)	3.50 & 2.40		2/0			
V <sub>m</sub> at peak (mV)	0.142 $\pm$ 0.44	1.74 $\pm$ 0.46	4/3			
V <sub>m</sub> at 200 ms (mV)	1.25 $\pm$ 0.26	2.10 $\pm$ 0.40	4/3			
V <sub>m</sub> at 500 ms (mV)	2.30 $\pm$ 0.55	3.22 $\pm$ 0.13	4/3			
V <sub>m</sub> at 1 s (mV)	2.58 $\pm$ 0.49	3.56 $\pm$ 0.15	4/3			

Data represented as M  $\pm$  SEM. Two-sample T-test, unless otherwise stated. †  $p < 0.1$ , \*  $p < 0.05$ , \*\*  $p < 0.01$ , \*\*\*  $p < 0.001$ .

RMP: resting membrane potential. R<sub>in</sub>: input resistance at the specified holding membrane potential. Sag: Sag ratio induced by a hyperpolarizing voltage step as specified. rising slope: the peak of the rising slope. falling slope: the peak of the falling slope 1/2 width: Full width of the action potential at one half of its amplitude. 1/3 width: Full width of the action potential at one third of its amplitude. AHP: afterhyperpolarization. fAHP: Fast AHP. mAHP: Medium AHP. sAHP: Slow AHP. V<sub>m</sub> at: Membrane potential at the specified time after a burst of five action potentials, irrespective of the occurrence of an AHP.

**Continuation of Table 6.1.10:**

	Juvenile (J)	Aged (A)	N (J/A)	df	T or $\chi^2$	p
<b>Excitability</b>						
Adaptation ratio	1.34 $\pm$ 0.59	0.546 $\pm$ 0.07	10/9	9.263	-1.327	.216
Discontinuation rate	see N(J)	see N(A)	22	1	0.013	.908
Last current (pA)	241 $\pm$ 38.0	232 $\pm$ 35.2	11/11	20	-0.175	.863
50 pA step (Hz)	0.0 $\pm$ 0.0	0.0 $\pm$ 0.0	11/11			
100 pA step (Hz)	9.1 $\pm$ 2.65	3.7 $\pm$ 2.21	10/11	19	-1.568	.133
150 pA step (Hz)	16.6 $\pm$ 4.23	4.67 $\pm$ 3.05	9/9	16	-2.279	.037 *
200 pA step (Hz)	27.0 $\pm$ 4.14	4.10 $\pm$ 3.06	6/7	11	-4.525	.000 ***
250 pA step (Hz)	35.2 $\pm$ 2.5	8.5 $\pm$ 4.21	6/4	8	-5.844	.000 ***
300 pA step (Hz)	37.2 $\pm$ 3.38	12.0 $\pm$ 6.43	5/3	6	-3.871	.008 **
350 pA step (Hz)	37.5 $\pm$ 4.57	16.7 $\pm$ 6.98	4/3	5	-2.616	.047 *
400 pA step (Hz)	35.0 & 52.0	29.0 $\pm$ 2.08	2/3	3	-2.107	.126
DB (%exist)	27.3 (n = 3)	18.2 (n = 2)	11/11			
DB current (nA)	0.317 $\pm$ 0.08	0.25 & 0.35	3/2	3	-0.146	.893
DB duration (ms)**	200 $\pm$ 50	400 & 350	3/2	3	2.605	.080 †

Data represented as M  $\pm$  SEM. Two-sample T-test, unless otherwise stated. †  $p < 0.1$ , \*  $p < 0.05$ , \*\*  $p < 0.01$ , \*\*\*  $p < 0.001$ .

Discontinuation rate: Degree of the cell's drop out from the assessment for excitability by incrementing (50 pA) 1 s current stimulations. Last current: The amplitude of the last current amplitude with which the excitability could be assessed. DB: Depolarization block. DB current: Amplitude of the direct current necessary for the first induction of DB.

**Table 6.1.11: Effects of the cells' dorso-ventral location within the hippocampus on their intrinsic electrophysiological properties during the superfusion with ACSF+SB.**

The table summarizes the comparison of intrinsic electrophysiological properties between CA1 pyramidal neurons obtained either from dorsal or the ventral half of the hippocampus.

	Dorsal (D)	Ventral (V)	N (D/V)	df	T or $\chi^2$	p
<b>Passive properties</b>						
RMP (mV)	-63.9 ± 0.43	-63.3 ± 0.36	58/101	157	1.016	.311
-70 mV R <sub>in</sub> (MΩ)	112 ± 4.83	111 ± 3.27	55/88	141	-0.249	.803
-65 mV R <sub>in</sub> (MΩ)	167 ± 12.15	156 ± 7.08	33/57	88	-0.847	.399
-60 mV R <sub>in</sub> (MΩ)	229 ± 16.22	230 ± 10.16	29/55	82	0.088	.930
<b>Hyperpolarization activated current</b>						
Sag (-10 mV step)	0.233 ± 0.01	0.239 ± 0.01	55/89	142	0.562	.575
Sag (-15 mV step)	0.237 ± 0.01	0.252 ± 0.01	55/89	142	1.640	.103
Sag (-20 mV step)	0.246 ± 0.01	0.250 ± 0.01	55/89	142	0.381	.704
<b>Action potential properties</b>						
Threshold (mV)	-45.5 ± 0.91	-45.8 ± 0.71	53/87	138	-0.258	.796
Amplitude (mV)	74.0 ± 1.33	73.1 ± 1.06	53/87	138	-0.518	.606
Rising slope (mV/ms)	275 ± 11.58	253 ± 8.48	53/87	138	-1.598	.112
falling slope (mV/ms)	-64.3 ± 2.12	-62.1 ± 1.59	53/87	138	0.834	.405
1/2 width (ms)	1.18 ± 0.03	1.19 ± 0.02	53/87	138	0.467	.641
1/3 width (ms)	1.45 ± 0.04	1.48 ± 0.03	53/87	138	0.484	.629
fAHP (mV)	-5.05 ± 0.760	-2.94 ± 0.66	53/87	138	2.043	.043 *
firing type (%regular)	92.1 (n = 58)	74.1 (n = 60)	63/81	1	7.751	.005 **
<b>Post-burst properties</b>						
AHP (%exist)	100 (n = 31)	100 (n = 44)	31/44			
AHP duration (s)	0.325 ± 0.11	0.640 ± 0.11	31/44	73	1.949	.055 †
AHP area (mV*s)	-0.199 ± 0.07	-0.416 ± 0.07	31/44	73	-2.085	.041 *
mAHP latency (ms)	28.6 ± 1.53	34.2 ± 2.23	31/44	70.618	2.086	.041 *
mAHP peak (mV)	-1.25 ± 0.11	-1.88 ± 0.11	31/44	73	-3.949	.000 ***
AHP decay τ (ms)	67.9 ± 11.5	112 ± 20.7	31/44	64.808	1.866	.067 †
sAHP at 0.5 s (mV)	0.193 ± 0.07	-0.228 ± 0.07	31/44	73	-4.346	.000 ***
sAHP at 1 s (mV)	0.139 ± 0.09	-0.171 ± 0.06	31/44	73	-3.121	.003 **
<b>Excitability</b>						
Adaptation ratio	2.282 ± 0.24	3.039 ± 0.35	52/66	109.786	1.759	.081 †
50 pA step (Hz)	0.382 ± 0.27	0.146 ± 0.11	55/89	72.559	-0.814	.418
100 pA step (Hz)	5.76 ± 1.06	3.20 ± 0.66	55/89	142	-2.167	.032 *
150 pA step (Hz)	14.46 ± 1.68	10.90 ± 1.00	55/89	91.726	-1.822	.072 †
200 pA step (Hz)	22.9 ± 1.79	19.7 ± 1.04	55/89	90.176	-1.573	.119
250 pA step (Hz)	30.0 ± 1.69	26.4 ± 1.04	55/89	94.426	-1.832	.070 †
300 pA step (Hz)	35.2 ± 1.57	31.1 ± 1.04	55/89	142	-2.297	.023 *
350 pA step (Hz)	38.8 ± 1.54	35.0 ± 1.05	53/87	138	-2.113	.036 *
400 pA step (Hz)	41.3 ± 1.60	37.8 ± 1.06	49/83	130	-1.932	.056 †

Data represented as M ± SEM. Two-sample T-test, unless otherwise stated. † p < 0.1, \* p < 0.05, \*\* p < 0.01, \*\*\* p < 0.001.

RMP: resting membrane potential. R<sub>in</sub>: input resistance at the specified holding membrane potential. Sag: Sag ratio induced by a hyperpolarizing voltage step as specified. rising slope: the peak of the rising slope. falling slope: the peak of the falling slope 1/2 width: Full width of the action potential at one half of its amplitude. 1/3 width: Full width of the action potential at one third of its amplitude. AHP: afterhyperpolarization. fAHP: fast AHP. mAHP: medium AHP. sAHP: slow AHP.

**Table 6.1.12: Gradual effects of the cells' dorso-ventral location within the hippocampus on their intrinsic electrophysiological properties during the superfusion with ACSF+SB.**

The table summarizes linear regressions of intrinsic electrophysiological properties against the dorso-ventral location of CA1 pyramidal neurons.

	N	R <sup>2</sup>	p	Slope of the linear fit
<b>Passive properties</b>				
RMP (mV)	159	.026	.041 *	0.597 mV/mm
-70 mV R <sub>in</sub> (MΩ)	143	.000	.968	
-65 mV R <sub>in</sub> (MΩ)	90	.003	.594	
-60 mV R <sub>in</sub> (MΩ)	84	.006	.478	
<b>Hyperpolarization activated current</b>				
Sag (-10 mV step)	144	.000	.853	
Sag (-15 mV step)	144	.003	.537	
Sag (-20 mV step)	144	.001	.717	
<b>Action potential properties</b>				
Threshold (mV)	140	.025	.060 †	+1.12 mV/mm
Amplitude (mV)	140	.013	.173	
Rising slope (mV/ms)	140	.024	.065 †	-13.6 mVs <sup>-1</sup> /mm
falling slope (mV/ms)	140	.005	.423	
1/2 width (ms)	140	.001	.721	
1/3 width (ms)	140	.001	.790	
fAHP (mV)	140	.000	.987	
firing type (%regular)	81.9 (118/144)	.038	.072 †	binomial logistic regression
<b>Post-burst properties</b>				
AHP (%exist)	100 (75/75)			
AHP duration (s)	75	.015	.299	
AHP area (mV*s)	75	.018	.250	
mAHP latency (ms)	75	.052	.049 *	+3.28 ms/mm
mAHP peak (mV)	75	.097	.006 **	-0.262 mV/mm
AHP decay τ (ms)	75	.143	.102	
sAHP at 0.5 s (mV)	75	.143	.001 **	-0.196
sAHP at 1 s (mV)	75	.056	.041 *	-0.120 mV/mm
<b>Excitability</b>				
Adaptation ratio	118	.001	.801	
50 pA step (Hz)	144	.008	.292	
100 pA step (Hz)	144	.054	.005 **	-1.71 Hz/mm
150 pA step (Hz)	144	.039	.018 *	-2.24 Hz/mm
200 pA step (Hz)	144	.021	.082 †	-1.74 Hz/mm
250 pA step (Hz)	144	.023	.068 †	-1.78 Hz/mm
300 pA step (Hz)	144	.030	.039 *	-1.95 Hz/mm
350 pA step (Hz)	140	.025	.063 †	-1.77 Hz/mm
400 pA step (Hz)	132	.028	.055 †	-1.91 Hz/mm

Linear regression, unless otherwise stated. † p < 0.1, \* p < 0.05, \*\* p < 0.01, \*\*\* p < 0.001.

RMP: resting membrane potential. R<sub>in</sub>: input resistance at the specified holding membrane potential. Sag: Sag ratio induced by a hyperpolarizing voltage step as specified. rising slope: the peak of the rising slope. falling slope: the peak of the falling slope 1/2 width: Full width of the action potential at one half of its amplitude. 1/3 width: Full width of the action potential at one third of its amplitude. AHP: afterhyperpolarization. fAHP: fast AHP. mAHP: medium AHP. sAHP: slow AHP.

**Table 6.1.13: Effects of the cells' dorso-ventral location within the hippocampus on their intrinsic electrophysiological properties during the bath application of 10  $\mu$ M Cch.**

The table summarizes the comparison of intrinsic electrophysiological properties between CA1 pyramidal neurons obtained either from dorsal or the ventral half of the hippocampus.

	Dorsal (D)	Ventral (V)	N (D/V)	df	T or $\chi^2$	p
<b>Passive properties</b>						
RMP (% silent)	36.7 (n = 11)	38.5 (n = 15)	30/39	1	0.023	.879
RMP (mV)	-64.4 $\pm$ 1.4	-63.5 $\pm$ 0.86	10/16	24	0.572	.573
-70 mV R <sub>in</sub> (M $\Omega$ )	98.7 $\pm$ 7.53	114 $\pm$ 6.41	26/40	64	1.501	.138
-65 mV R <sub>in</sub> (M $\Omega$ )	128 $\pm$ 11.23	120 $\pm$ 7.07	19/26	43	-0.571	.571
-60 mV R <sub>in</sub> (M $\Omega$ )	182 $\pm$ 17.66	199 $\pm$ 13.98	16/20	34	0.777	.442
<b>Hyperpolarization activated current</b>						
Sag (-10 mV step)	0.242 $\pm$ 0.01	0.25 $\pm$ 0.01	27/40	65	0.669	.506
Sag (-15 mV step)	0.256 $\pm$ 0.01	0.267 $\pm$ 0.01	27/40	65	0.925	.359
Sag (-20 mV step)	0.259 $\pm$ 0.01	0.274 $\pm$ 0.01	27/40	65	1.201	.234
<b>Action potential properties</b>						
Threshold (mV)	-43.5 $\pm$ 1.20	-45.4 $\pm$ 0.89	28/40	66	-1.305	.196
Amplitude (mV)	68.3 $\pm$ 2.43	69.4 $\pm$ 1.68	28/40	66	0.399	.691
Rising slope (mV/ms)	248 $\pm$ 17.8	244 $\pm$ 10.9	18/40	66	-0.218	.828
falling slope (mV/ms)	-59.6 $\pm$ 2.77	-64.1 $\pm$ 1.92	28/40	66	-1.398	.167
1/2 width (ms)	1.17 $\pm$ 0.04	1.11 $\pm$ 0.02	28/40	42.978	-1.292	.203
1/3 width (ms)	1.46 $\pm$ 0.06	1.37 $\pm$ 0.03	28/40	41.321	-1.505	.140
fAHP (mV)	-3.69 $\pm$ 0.93	-3.00 $\pm$ 0.75	28/40	66	0.579	.565
firing type (%regular)	89.7 (n = 26)	94.6 (n = 35)	29/37		0.567	.452
<b>Post-burst properties</b>						
AHP (%exist)	(n = 3)	(n = 8)	11/17			
AHP duration (s)	0.038 $\pm$ 0.02	0.06 $\pm$ 0	3/8	9	1.74	.116
AHP area (mV*s)	-0.013 $\pm$ 0.01	-0.026 $\pm$ 0.01	3/8	9	-1.063	.315
mAHP latency (ms)	21.3 $\pm$ 10.1	27.3 $\pm$ 2.47	3/8	9	0.871	.406
mAHP peak (mV)	-0.361 $\pm$ 0.19	-0.64 $\pm$ 0.11	3/8	9	-1.264	.238
AHP decay $\tau$ (ms)	11.7 $\pm$ 8.71	22.3 $\pm$ 2.57	3/8	9	1.633	.137
sAHP at 0.5 s (mV)	1.85 $\pm$ 0.45	2.29 $\pm$ 0.25	3/8	9	0.888	.397
sAHP at 1 s (mV)	2.22 $\pm$ 0.32	2.64 $\pm$ 0.33	3/8	9	0.72	.490
V <sub>m</sub> at peak (mV)	0.60 $\pm$ 0.25	0.14 $\pm$ 0.23	11/17	26	-1.29	.208
V <sub>m</sub> at 200 ms (mV)	1.58 $\pm$ 0.17	1.23 $\pm$ 0.14	11/17	26	-1.565	.130
V <sub>m</sub> at 500 ms (mV)	2.42 $\pm$ 0.26	2.50 $\pm$ 0.19	11/17	26	0.257	.799
V <sub>m</sub> at 1 s (mV)	2.48 $\pm$ 0.26	2.88 $\pm$ 0.26	11/17	26	1.051	.303

Data represented as M  $\pm$  SEM. Two-sample T-test, unless otherwise stated. † p < 0.1, \* p < 0.05, \*\* p < 0.01, \*\*\* p < 0.001.

RMP: resting membrane potential. R<sub>in</sub>: input resistance at the specified holding membrane potential. Sag: Sag ratio induced by a hyperpolarizing voltage step as specified. rising slope: the peak of the rising slope. falling slope: the peak of the falling slope. 1/2 width: Full width of the action potential at one half of its amplitude. 1/3 width: Full width of the action potential at one third of its amplitude. AHP: afterhyperpolarization. fAHP: Fast AHP. mAHP: Medium AHP. sAHP: Slow AHP. V<sub>m</sub> at: Membrane potential at the specified time after a burst of five action potentials, irrespective of the occurrence of an AHP.

**Continuation of Table 6.1.13:**

	Dorsal (D)	Ventral (V)	N (D/V)	df	T or $\chi^2$	p
<b>Excitability</b>						
Adaptation ratio	0.914 $\pm$ 0.150	1.11 $\pm$ 0.330	23/35	47.321	0.532	.597
Discontinuation rate	see N(D)	see N(V)	67	1	0.930	.335
Last current (pA)	252 $\pm$ 22.3	225 $\pm$ 17.6	27/40	65	-0.953	.344
50 pA step (Hz)	0.333 $\pm$ 0.333	0.400 $\pm$ 0.49	27/40	64.974	0.128	.899
100 pA step (Hz)	5.81 $\pm$ 2.24	7.66 $\pm$ 1.59	26/38	62	0.694	.490
150 pA step (Hz)	17.1 $\pm$ 2.63	18.0 $\pm$ 2.09	25/32	55	0.287	.775
200 pA step (Hz)	25.8 $\pm$ 3.38	27.4 $\pm$ 1.91	15/22	35	0.433	.668
250 pA step (Hz)	29.2 $\pm$ 3.70	32.7 $\pm$ 1.43	14/19	16.911	0.889	.387
300 pA step (Hz)	31.1 $\pm$ 3.40	35.2 $\pm$ 1.36	13/14	15.892	1.131	.275
350 pA step (Hz)	31.5 $\pm$ 2.70	35.4 $\pm$ 1.74	10/10	18	1.215	.240
400 pA step (Hz)	33.2 $\pm$ 2.97	38.4 $\pm$ 2.28	6/8	12	1.418	.182
DB (%exist)	34.5 (n = 10)	18.4 (n = 7)	29/38	1	2.241	.134
DB current (nA)	0.265 $\pm$ 0.03	0.157 $\pm$ 0.01	10/7	11.944	-3.227	.007 **
DB duration (ms)	305 $\pm$ 69.7	307 $\pm$ 63.1	10/7	15	0.022	.983
postDB (%exist)	20.7 (n = 6)	7.9 (n = 3)	10/7	1	0.486	.486

Data represented as M  $\pm$  SEM. Two-sample T-test, unless otherwise stated. † p < 0.1, \* p < 0.05, \*\* p < 0.01, \*\*\* p < 0.001.

Discontinuation rate: Degree of the cell's drop out from the assessment for excitability by incrementing (50 pA) 1 s current stimulations. Last current: The amplitude of the last current amplitude with which the excitability could be assessed. DB: Depolarization block. DB current: Amplitude of the direct current necessary for the first induction of DB.

Amongst all the comparisons, merely the current amplitude needed for the induction of depolarization block was significantly higher in neurons from the dorsal (n = 10, 265  $\pm$  30 pA), compared to the ventral (n = 7, 157  $\pm$  10 pA) half of the hippocampus (p = 0.007). However, this finding was in contrast to the higher excitability of dorsally located neurons in ACSF+SB. Furthermore, this result was obtained from a limited sample size, and it was not supported by other measures of excitability. Consequently, this observation may be regarded as type II error due to multiple comparisons.

The lack of significant results in the two-sample comparison may be explained by the dorsal half of the hippocampus being tangent to the ventral half of the hippocampus. However, significantly linear changes along the full extent of the dorso-ventral axis could not be detected either (Tab. 6.1.14)

**Table 6.1.14: Gradual effects of the cells' dorso-ventral location within the hippocampus on their intrinsic electrophysiological properties during the bath application of 10  $\mu$ M Cch.**

The table summarizes the comparison of intrinsic electrophysiological properties between CA1 pyramidal neurons obtained either from dorsal or the ventral half of the hippocampus.

	N	R <sup>2</sup>	p	Slope of the linear fit
<b>Passive properties</b>				
RMP (%silent)*	37.7 (26/69)	.013	.411	binomial logistic regression
RMP (mV)	26	.005	.727	
-70 mV R <sub>in</sub> (M $\Omega$ )	66	.043	.097	† +7.7 M $\Omega$ /mm
-65 mV R <sub>in</sub> (M $\Omega$ )	45	.025	.302	
-60 mV R <sub>in</sub> (M $\Omega$ )	36	.012	.529	
<b>Hyperpolarization activated current</b>				
Sag (-10 mV step)	67	.008	.479	
Sag (-15 mV step)	67	.001	.781	
Sag (-20 mV step)	67	.013	.357	
<b>Action potential properties</b>				
Threshold (mV)	68	.000	.869	
Amplitude (mV)	68	.000	.881	
rising slope (mV/ms)	68	.001	.767	
falling slope (mV/ms)	68	.023	.221	
1/2 width (ms)	68	.029	.164	
1/3 width (ms)	68	.039	.107	
fAHP (mV)	68	.005	.568	
firing type (%regular)	91.0 (61/67)	The six cells showing burst firing were recorded at 1.9, 2.3, 2.9, 3.8, 3.9 and 4.8 mm		
<b>Post-burst properties</b>				
AHP (%exist)*	39.3 (11/28)	.118	.131	binomial logistic regression
AHP duration (s)	11	.172	.204	
AHP area (mV*s)	11	.044	.537	
mAHP latency (ms)	11	.003	.866	
mAHP peak (mV)	11	.065	.449	
mAHP decay $\tau$ (ms)	11	.188	.183	
sAHP at 0.5 s (mV)	11	.025	.643	
sAHP at 1 s (mV)	11	.013	.739	
V <sub>m</sub> at peak (mV)	28	.056	.224	
V <sub>m</sub> at 200 ms (mV)	28	.078	.151	
V <sub>m</sub> at 500 ms (mV)	28	.000	.954	
V <sub>m</sub> at 1 s (mV)	28	.021	.462	

Linear regression, unless otherwise stated. †  $p < 0.1$ , \*  $p < 0.05$ , \*\*  $p < 0.01$ , \*\*\*  $p < 0.001$ .

RMP: resting membrane potential. R<sub>in</sub>: input resistance at the specified holding membrane potential. Sag: Sag ratio induced by a hyperpolarizing voltage step as specified. rising slope: the peak of the rising slope. falling slope: the peak of the falling slope 1/2 width: Full width of the action potential at one half of its amplitude. 1/3 width: Full width of the action potential at one third of its amplitude. AHP: afterhyperpolarization. fAHP: Fast AHP. mAHP: Medium AHP. sAHP: Slow AHP. V<sub>m</sub> at: Membrane potential at the specified time after a burst of five action potentials, irrespective of the occurrence of an AHP.

**Continuation of Table 6.1.14:**

	N	R <sup>2</sup>	p	Slope of the linear fit
<b>Excitability</b>				
Adaptation ratio	59	.006	.549	
Last current (pA)	67	.046	.083	† -22 pA/mm
50 pA step (Hz)	67	.004	.595	
100 pA step (Hz)	64	.004	.599	
150 pA step (Hz)	57	.000	.981	
200 pA step (Hz)	37	.001	.849	
250 pA step (Hz)	33	.008	.617	
300 pA step (Hz)	27	.020	.482	
350 pA step (Hz)	20	.010	.677	
400 pA step (Hz)	14	.117	.231	
DB (%exist)*	25.4 (17/67)	.025	.286	binomial logistic regression
DB current (nA)	17	.147	.129	
DB duration (ms)	17	.006	.775	

Linear regression, unless otherwise stated. †  $p < 0.1$ , \*  $p < 0.05$ , \*\*  $p < 0.01$ , \*\*\*  $p < 0.001$ .

DB: Depolarization block. DB current: Amplitude of the direct current necessary for the first induction of DB.



**Table 6.1.15: Effects of the cells' proximo-distal location within the CA1 area on their intrinsic electrophysiological properties during the superfusion with ACSF+SB.**

The table summarizes the comparison of intrinsic electrophysiological properties between pyramidal neurons obtained either from the most proximal or the most distal third of the CA1 area.

	Proximal(P)	Distal(D)	N (P/D)	df	T or $\chi^2$	p
<b>Passive properties</b>						
RMP (mV)	-63.6 ± 0.47	-63.7 ± 0.53	55/50	103	-0.136	.892
-70 mV R <sub>in</sub> (MΩ)	119 ± 4.75	102 ± 4.50	53/48	99	-2.565	.012 *
-65 mV R <sub>in</sub> (MΩ)	187 ± 11.2	137 ± 8.61	33/29	60	-3.408	.001 **
-60 mV R <sub>in</sub> (MΩ)	261 ± 10.5	206 ± 16.0	30/29	48.698	-2.842	.007 **
<b>Hyperpolarization activated current</b>						
Sag (-10 mV step)	0.249 ± 0.01	0.233 ± 0.01	53/48	99	-1.399	.165
Sag (-15 mV step)	0.257 ± 0.01	0.247 ± 0.01	53/48	99	-0.935	.352
Sag (-20 mV step)	0.265 ± 0.01	0.245 ± 0.01	53/48	99	-1.893	.061 †
<b>Action potential properties</b>						
Threshold (mV)	-46.1 ± 0.86	-44.9 ± 1.07	53/45	96	0.900	.371
Amplitude (mV)	74.4 ± 1.47	73.3 ± 1.18	53/45	94.289	-0.615	.540
Rising slope (mV/ms)	281 ± 12.7	250 ± 9.78	53/45	93.210	-1.944	.055 †
falling slope (mV/ms)	-64.6 ± 2.03	-62.2 ± 2.05	53/45	96	0.840	.403
1/2 width (ms)	1.17 ± 0.03	1.16 ± 0.04	53/45	96	-0.102	.919
1/3 width (ms)	1.44 ± 0.03	1.45 ± 0.05	53/45	96	0.343	.732
fAHP (mV)	-4.76 ± 0.78	-2.86 ± 0.96	53/45	96	1.556	.123
firing type (%regular)	88.7 (n = 47)	70.8 (n = 34)	53/48	1	5.051	.025 *
<b>Post-burst properties</b>						
AHP (%exist)	96.9 (n = 31)	100 (23)	32/23		Fisher-Yates test	.582
AHP duration (s)	0.432 ± 0.13	0.508 ± 0.10	31/23	51.256	0.463	.646
AHP area (mV*s)	-0.275 ± 0.08	-0.324 ± 0.08	31/23	52	-0.431	.669
mAHP latency (ms)	32.3 ± 2.17	30.6 ± 2.08	31/23	52	-0.569	.572
mAHP peak (mV)	-1.50 ± 0.11	-1.73 ± 0.15	31/23	52	-1.303	.198
AHP decay τ (ms)	69.3 ± 7.01	105 ± 24.4	31/23	25.656	1.394	.175
sAHP at 0.5 s (mV)	-0.03 ± 0.08	-0.151 ± 0.10	31/23	52	-0.990	.327
sAHP at 1 s (mV)	-0.75 ± 0.09	-0.058 ± 0.07	31/23	52	0.148	.883
<b>Excitability</b>						
Adaptation ratio	2.28 ± 0.28	2.78 ± 0.45	47/34	79	0.987	.327
50 pA step (Hz)	0.40 ± 0.28	0.0 ± 0.0	53/48	52.000	-1.426	.160
100 pA step (Hz)	5.57 ± 1.04	2.27 ± 0.75	53/48	92.251	-2.570	.012 *
150 pA step (Hz)	16.3 ± 1.28	7.52 ± 1.32	53/48	99	-4.753	.000 ***
200 pA step (Hz)	25.5 ± 1.23	15.5 ± 1.56	53/48	99	-5.079	.000 ***
250 pA step (Hz)	31.9 ± 1.20	22.4 ± 1.50	53/48	99	-5.008	.000 ***
300 pA step (Hz)	36.4 ± 1.21	27.8 ± 1.36	53/48	99	-4.751	.000 ***
350 pA step (Hz)	40.0 ± 1.26	31.6 ± 1.27	52/46	96	-4.681	.000 ***
400 pA step (Hz)	42.4 ± 1.30	34.7 ± 1.25	47/44	89	-4.283	.000 ***

Data represented as M ± SEM. Two-sample T-test, unless otherwise stated. † p < 0.1, \* p < 0.05, \*\* p < 0.01, \*\*\* p < 0.001.

RMP: resting membrane potential. R<sub>in</sub>: input resistance at the specified holding membrane potential. Sag: Sag ratio induced by a hyperpolarizing voltage step as specified. rising slope: the peak of the rising slope. falling slope: the peak of the falling slope 1/2 width: Full width of the action potential at one half of its amplitude. 1/3 width: Full width of the action potential at one third of its amplitude. AHP: afterhyperpolarization. fAHP: fast AHP. mAHP: medium AHP. sAHP: slow AHP.

**Table 6.1.16: Gradual effects of the cells' proximo-distal location within the CA1 area on their intrinsic electrophysiological properties during the superfusion with ACSF+SB.**

The table summarizes linear regressions of intrinsic electrophysiological properties against the proximo-distal location of CA1 pyramidal neurons.

	N	R <sup>2</sup>	p	Slope of the linear fit
<b>Passive properties</b>				
RMP (mV)	151	.000	.825	
-70 mV R <sub>in</sub> (MΩ)	142	.073	.001 **	-17.0 MΩ/50%
-65 mV R <sub>in</sub> (MΩ)	88	.151	.000 ***	-45.1 MΩ/50%
-60 mV R <sub>in</sub> (MΩ)	82	.095	.005 **	-47.2 MΩ/50%
<b>Hyperpolarization activated current</b>				
Sag (-10 mV step)	143	.009	.267	
Sag (-15 mV step)	143	.001	.701	
Sag (-20 mV step)	143	.013	.167	
<b>Action potential properties</b>				
Threshold (mV)	139	.005	.393	
Amplitude (mV)	139	.002	.596	
Rising slope (mV/ms)	139	.027	.052 †	-25.9 mVs <sup>-1</sup> /50%
falling slope (mV/ms)	139	.006	.357	
1/2 width (ms)	139	.000	.920	
1/3 width (ms)	139	.001	.743	
fAHP (mV)	139	.022	.081 †	+1.7 mV/50%
firing type (%regular)	81.8 (117/143)	.092	.006 **	binomial logistic regression
<b>Post-burst properties</b>				
AHP exist <sup>†</sup>	100 (75/75)			
AHP duration (s)	75	.000	.857	
AHP area (mV*s)	75	.000	.882	
mAHP latency (ms)	75	.004	.585	
mAHP peak (mV)	75	.021	.213	
AHP decay τ (ms)	75	.028	.149	
sAHP at 0.5 s (mV)	75	.008	.437	
sAHP at 1 s (mV)	75	.002	.720	
<b>Excitability</b>				
Adaptation ratio	117	.029	.067 †	+0.85 AU/50%
50 pA step (Hz)	143	.009	.253	
100 pA step (Hz)	143	.041	.015 *	-2.7 Hz/50%
150 pA step (Hz)	143	.121	.000 ***	-2.9 Hz/50%
200 pA step (Hz)	143	.150	.000 ***	-8.4 Hz/50%
250 pA step (Hz)	143	.151	.000 ***	-8.3 Hz/50%
300 pA step (Hz)	143	.136	.000 ***	-7.6 Hz/50%
350 pA step (Hz)	139	.135	.000 ***	-7.4 Hz/50%
400 pA step (Hz)	131	.124	.000 ***	-7.1 Hz/50%

Linear regression, unless otherwise stated. † p < 0.1, \* p < 0.05, \*\* p < 0.01, \*\*\* p < 0.001.

RMP: resting membrane potential. R<sub>in</sub>: input resistance at the specified holding membrane potential. Sag: Sag ratio induced by a hyperpolarizing voltage step as specified. rising slope: the peak of the rising slope. falling slope: the peak of the falling slope 1/2 width: Full width of the action potential at one half of its amplitude. 1/3 width: Full width of the action potential at one third of its amplitude. AHP: afterhyperpolarization. fAHP: fast AHP. mAHP: medium AHP. sAHP: slow AHP.

**Table 6.1.17: Effects of the cells' proximo-distal location within the CA1 area on their intrinsic electrophysiological properties during the bath application of 10  $\mu$ M carbachol.** The table summarizes the comparison of intrinsic electrophysiological properties between pyramidal neurons obtained either from the most proximal or the most distal third of the CA1 area.

	Proximal (P)	Distal (D)	N (P/D)	df	T or $\chi^2$	p
<b>Passive properties</b>						
RMP (%silent)	32.1 (n = 9)	36.0 (n = 9)	28/25	1	0.088	.767
RMP (mV)	-64.8 $\pm$ 1.47	-63.4 $\pm$ 1.01	9/9	16	0.768	.454
-70 mV R <sub>in</sub> (M $\Omega$ )	109 $\pm$ 5.68	96.5 $\pm$ 9.22	26/24	38.651	-1.193	.240
-65 mV R <sub>in</sub> (M $\Omega$ )	118 $\pm$ 7.42	121 $\pm$ 12.9	19/14	31	0.262	.795
-60 mV R <sub>in</sub> (M $\Omega$ )	205 $\pm$ 12.4	169 $\pm$ 20.4	17/10	25	-1.613	.119
<b>Hyperpolarization activated current</b>						
Sag (-10 mV step)	0.260 $\pm$ 0.01	0.247 $\pm$ 0.01	27/24	49	-0.887	.379
Sag (-15 mV step)	0.271 $\pm$ 0.01	0.263 $\pm$ 0.01	27/24	49	-0.640	.525
Sag (-20 mV step)	0.282 $\pm$ 0.01	0.262 $\pm$ 0.01	27/24	49	-1.582	.120
<b>Action potential properties</b>						
Threshold (mV)	-45.4 $\pm$ 1.15	-44.5 $\pm$ .123	27/25	50	0.552	.583
Amplitude (mV)	70.3 $\pm$ 2.30	10.0 $\pm$ 2.17	27/25	50	-0.067	.947
Rising slope (mV/ms)	261 $\pm$ 15.8	245 $\pm$ 13.9	27/25	50	-0.740	.463
falling slope (mV/ms)	-63.9 $\pm$ 2.44	-60.7 $\pm$ 2.61	27/25	50	0.904	.371
1/2 width (ms)	1.11 $\pm$ 0.03	1.16 $\pm$ 0.04	27/25	50	0.937	.353
1/3 width (ms)	1.36 $\pm$ 0.04	1.45 $\pm$ 0.06	27/25	50	1.300	.199
fAHP (mV)	-4.05 $\pm$ 0.85	-1.80 $\pm$ 0.91	27/25	50	1.815	.075 $\dagger$
firing type (%regular)	100 (n = 26)	83.3 (n = 20)	26/24		Fisher-Yates test	.046 $\dagger$
<b>Post-burst properties</b>						
AHP (%exist)	40.0 (n = 6)	55.6 (n = 5)	15/9			
AHP duration (s)	0.05 $\pm$ 0.01	0.06 $\pm$ 0.01	6/5	9	0.723	.488
AHP area (mV*s)	-0.018 $\pm$ 0.01	-0.027 $\pm$ 0.01	6/5	9	-0.849	.418
mAHP latency (ms)	20.3 $\pm$ 3.62	32.1 $\pm$ 3.60	6/5	9	2.297	.047 $\dagger$
mAHP peak (mV)	-0.494 $\pm$ 0.11	-0.647 $\pm$ 0.19	6/5	9	-0.738	.479
AHP decay $\tau$ (ms) <sup>+</sup>	19.4 $\pm$ 4.69	19.4 $\pm$ 4.53	6/5	9	-0.004	.997
sAHP at 0.5 s (mV) <sup>+</sup>	1.87 $\pm$ 0.31	2.5 $\pm$ 0.24	6/5	9	1.634	.137
sAHP at 1 s (mV) <sup>+</sup>	2.232 $\pm$ 0.33	2.88 $\pm$ 0.37	6/5	9	1.307	.224
V <sub>m</sub> at peak (mV)	0.308 $\pm$ 0.22	-0.079 $\pm$ 0.29	15/9	22	-1.072	.295
V <sub>m</sub> at 200 ms (mV)	1.39 $\pm$ 0.16	1.16 $\pm$ 0.18	15/9	22	-0.980	.374
V <sub>m</sub> at 500 ms (mV)	2.36 $\pm$ 0.24	2.55 $\pm$ 0.24	15/9	22	0.521	.608
V <sub>m</sub> at 1 s (mV)	2.52 $\pm$ 0.28	3.01 $\pm$ 0.32	15/9	22	1.114	.277

Data represented as M  $\pm$  SEM. Two-sample T-test, unless otherwise stated.  $\dagger$   $p < 0.1$ , \*  $p < 0.05$ , \*\*  $p < 0.01$ , \*\*\*  $p < 0.001$ .

RMP: resting membrane potential. R<sub>in</sub>: input resistance at the specified holding membrane potential. Sag: Sag ratio induced by a hyperpolarizing voltage step as specified. rising slope: the peak of the rising slope. falling slope: the peak of the falling slope. 1/2 width: Full width of the action potential at one half of its amplitude. 1/3 width: Full width of the action potential at one third of its amplitude. AHP: afterhyperpolarization. fAHP: Fast AHP. mAHP: Medium AHP. sAHP: Slow AHP. V<sub>m</sub> at: Membrane potential at the specified time after a burst of five action potentials, irrespective of the occurrence of an AHP.

**Continuation of Table 6.1.17:**

	Proximal (P)	Distal (D)	N (P/D)	df	T or $\chi^2$	p
<b>Excitability</b>						
Adaptation ratio	0.67 $\pm$ 0.16	1.19 $\pm$ 0.32	26/19	26.891	1.457	.157
Discontinuation rate	see N(P)	see N(D)		1	7.676	.006
Last current (pA)	194 $\pm$ 17	271 $\pm$ 24	27/24	49	2.666	.010 $\dagger$
50 pA step (Hz) <sup>++</sup>	0.0 $\pm$ 0.0	1.04 $\pm$ 0.75	27/24	23.000	1.388	.178
100 pA step (Hz) <sup>++</sup>	8.35 $\pm$ 2.09	5.35 $\pm$ 1.99	26/23	47	-1.031	.308
150 pA step (Hz) <sup>++</sup>	21.2 $\pm$ 2.52	13.0 $\pm$ 2.53	22/21	31	-2.293	.027 $\dagger$
200 pA step (Hz) <sup>++</sup>	34.3 $\pm$ 1.60	22.2 $\pm$ 3.01	11/17	23.343	-3.529	.002 $\dagger$
250 pA step (Hz) <sup>++</sup>	37.6 $\pm$ 1.43	28.1 $\pm$ 3.14	9/16	20.266	-2.733	.013 $\dagger$
300 pA step (Hz) <sup>++</sup>	39.9 $\pm$ 1.53	29.5 $\pm$ 3.04	7/13	16.723	-3.031	.008 $\dagger$
350 pA step (Hz) <sup>++</sup>	40.0 $\pm$ 2.00	31.3 $\pm$ 2.00	2/12	12	-1.711	.113
400 pA step (Hz) <sup>++</sup>	39.0	34.4 $\pm$ 2.13	1/7			
DB (%exist)	40.7 (n = 11)	16.7 (n = 4)	27/24	1	3.547	.060 $\dagger$
DB current (nA)	0.218 $\pm$ 0.02	0.263 $\pm$ 0.07	11/4	13	0.796	.440
DB duration (ms)	305 $\pm$ 64.5	225 $\pm$ 66.1	11/4	13	-0.688	.504

Data represented as M  $\pm$  SEM. Two-sample T-test, unless otherwise stated.  $\dagger$   $p < 0.1$ , \*  $p < 0.05$ , \*\*  $p < 0.01$ , \*\*\*  $p < 0.001$ .

Discontinuation rate: Degree of the cell's drop out from the assessment for excitability by incrementing (50 pA) 1 s current stimulations. Last current: The amplitude of the last current amplitude with which the excitability could be assessed. DB: Depolarization block. DB current: Amplitude of the direct current necessary for the first induction of DB.

**Table 6.1.18: Gradual effects of the cells' proximo-distal location within the CA1 area on their intrinsic electrophysiological properties during the bath application of 10  $\mu$ M carbachol.**

The table summarizes linear regressions of intrinsic electrophysiological properties against the proximo-distal location of CA1 pyramidal neurons.

	N	R <sup>2</sup>	p	Slope of the linear fit
<b>Passive properties</b>				
RMP silent	38.2 (26/68)	.004	.654	binomial logistic regression
RMP (mV)	26	.047	.288	
-70 mV R <sub>in</sub> (M $\Omega$ )	65	.042	.103	
-65 mV R <sub>in</sub> (M $\Omega$ )	44	.001	.852	
-60 mV R <sub>in</sub> (M $\Omega$ )	35	.075	.112	
<b>Hyperpolarization activated current</b>				
Sag (-10 mV step)	66	.003	.685	
Sag (-15 mV step)	66	.002	.713	
Sag (-20 mV step)	66	.017	.293	

Linear regression, unless otherwise stated.  $\dagger$   $p < 0.1$ , \*  $p < 0.05$ , \*\*  $p < 0.01$ , \*\*\*  $p < 0.001$ .

RMP: resting membrane potential. R<sub>in</sub>: input resistance at the specified holding membrane potential. Sag: Sag ratio induced by a hyperpolarizing voltage step as specified.

Continuation of Table 6.1.18:

	N	R <sup>2</sup>	p	Slope of the linear fit
<b>Action potential properties</b>				
Threshold (mV)	67	.006	.526	
Amplitude (mV)	67	.000	.980	
rising slope (mV/ms)	67	.006	.543	
falling slope (mV/ms)	67	.013	.362	
1/2 width (ms)	67	.010	.412	
1/3 width (ms)	67	.022	.228	
fAHP (mV)	67	.058	.050 †	+2.1 mV/50%
firing type regular	90.9 (60/66)	The six cells showing burst firing were recorded at 28, 59, 70, 80, 86, and 95%		
<b>Post-burst properties</b>				
AHP exist*	39.3 (11/28)	.008	.691	binomial logistic regression
AHP duration (s)	11	.030	.611	
AHP area (mV*s)	11	.082	.392	
mAHP latency (ms)	11	.303	.079 †	7.5 ms/50%
mAHP peak (mV)	11	.072	.425	
AHP decay $\tau$ (ms)	11	.000	.989	
sAHP at 0.5 s (mV)	11	.237	.129	
sAHP at 1 s (mV)	11	.147	.245	
V <sub>m</sub> at peak (mV)	28	.013	.566	
V <sub>m</sub> at 200 ms (mV)	28	.005	.717	
V <sub>m</sub> at 500 ms (mV)	28	.022	.454	
V <sub>m</sub> at 1 s (mV)	28	.067	.184	
<b>Excitability</b>				
Adaptation ratio	58	.017	.322	
Last current (pA)	66	.107	.007 **	+65 pA/50%
50 pA step (Hz)	66	.038	.115	
100 pA step (Hz)	63	.028	.193	
150 pA step (Hz)	56	.087	.027 *	-6.6 Hz/50%
200 pA step (Hz)	36	.268	.001 **	-10.5 Hz/50%
250 pA step (Hz)	32	.137	.037 *	-7.3 Hz/50%
300 pA step (Hz)	26	.212	.018 *	-8.3 Hz/50%
350 pA step (Hz)	19	.218	.044 *	-8.4 Hz/50%
400 pA step (Hz)	13	.148	.195	
DB exist*	25.8 (17/66)	.080	.064 †	binomial logistic regression
DB current (nA)	17	0.47	.405	
DB duration (ms)	17	.004	.810	

Linear regression, unless otherwise stated. †  $p < 0.1$ , \*  $p < 0.05$ , \*\*  $p < 0.01$ , \*\*\*  $p < 0.001$ .

rising slope: the peak of the rising slope. falling slope: the peak of the falling slope 1/2 width: Full width of the action potential at one half of its amplitude. 1/3 width: Full width of the action potential at one third of its amplitude. AHP: afterhyperpolarization. fAHP: Fast AHP. mAHP: Medium AHP. sAHP: Slow AHP. V<sub>m</sub> at: Membrane potential at the specified time after a burst of five action potentials, irrespective of the occurrence of an AHP. Last current: The amplitude of the last current amplitude with which the excitability could be assessed. DB: Depolarization block. DB current: Amplitude of the direct current necessary for the first induction of DB.

Table 6.1.19 Correlation analysis of the post-stimulus plateau potential against inter-cellular variability.

The table summarizes linear regressions of the post-stimulus plateau potential (during 10-20 s after the stimulus offset, PP<sub>fix</sub>) of cells exhibiting persistent firing in the presence of 10  $\mu$ M Cch against the animals' age, the cells' location within CA1 and the cells' intrinsic electrophysiological properties in the presence of 10  $\mu$ M Cch.

	N	R <sup>2</sup>	p	slope of the linear fit
<b>Maturation</b>				
Age (postnatal days)	39	.004	.688	
<b>Anatomical location</b>				
Dorso-ventral axis (mm)	39	.023	.352	
Proximo-distal axis (%)	38	.014	.476	
<b>Passive properties</b>				
RMP (% silent)**	38.5 (15/39)	silent RMP: 14.8 $\pm$ 0.96 mV, non-silent RMP: 13.6 $\pm$ 0.91 mV Two-sample T-test: T <sub>(37)</sub> = -0.862, p = 0.395		
RMP (mV)	15	.057	.391	
-70 mV Rin (M $\Omega$ )	37	.032	.287	
-65 mV Rin (M $\Omega$ )	22	.050	.316	
-60 mV Rin (M $\Omega$ )	17	.038	.456	
<b>Hyperpolarization activated current</b>				
Sag (-10 mV step)	37	.014	.479	
Sag (-15 mV step)	37	.024	.357	
Sag (-20 mV step)	37	.096	.062 †	+2.9 mV PP <sub>fix</sub> / 0.1 AU sag ratio
<b>Action potential properties</b>				
threshold (mV)	39	.157	.013 *	+0.26 mV PP <sub>fix</sub> / mV thresh. depol.
amplitude (mV)	39	.019	.405	
rising slope (mV/ms)	39	.034	.263	
falling slope (mV/ms)	39	.000	.945	
1/2 width (ms)	39	.020	.395	
1/3 width (ms)	39	.014	.472	
fAHP (mV)	39	.046	.188	
firing type (%regular)	91.7 (33/36)			

Linear regression, unless otherwise stated. †  $p < 0.1$ , \*  $p < 0.05$ , \*\*  $p < 0.01$ , \*\*\*  $p < 0.001$ .

RMP: resting membrane potential. Rin: input resistance at the specified holding membrane potential. Sag: Sag ratio induced by a hyperpolarizing voltage step as specified. rising slope: the peak of the rising slope. falling slope: the peak of the falling slope 1/2 width: Full width of the action potential at one half of its amplitude. 1/3 width: Full width of the action potential at one third of its amplitude. AHP: afterhyperpolarization. fAHP: Fast AHP.

Continuation of Table 6.1.19:

	N	R <sup>2</sup>	<i>p</i>	slope of the linear fit
<b>Post-burst properties</b>				
AHP exist <sup>++</sup>	45.5 (5/11)			AHP existent: 12.0 ± 1.87 mV, AHP absent: 16.45 ± 1.77 mV Two-sample T-test: $T_9 = 1.723, p = 0.119$
AHP duration (s)	5			
AHP area (mV*s)	5			
mAHP latency (ms)	5			
mAHP peak (mV)	5			
AHP decay $\tau$ (ms)	5			
sAHP at 0.5 s (mV)	5			
sAHP at 1 s (mV)	5			
V <sub>m</sub> at peak	11	.571	.007	** +3.55 mV PP <sub>fix</sub> / mV peak amplitude
V <sub>m</sub> at 200 ms	11	.131	.274	
V <sub>m</sub> at 500 ms	11	.058	.475	
V <sub>m</sub> at 1 s	11	.002	.908	
<b>Excitability</b>				
Adaptation ratio	56	.009	.485	
Last current (pA)	64	.0192	.000	*** -1.5 mV PP <sub>fix</sub> / 100 pA current step
0.05 nA step (Hz)	64	.003	.654	
0.10 nA step (Hz)	63	.001	.794	
0.15 nA step (Hz)	57	.005	.608	
0.20 nA step (Hz)	50	.026	.264	
0.25 nA step (Hz)	43	.046	.167	
0.30 nA step (Hz)	35	.030	.319	
0.35 nA step (Hz)	29	.028	.382	
0.40 nA step (Hz)	24	.067	.223	

Linear regression, unless otherwise stated. †  $p < 0.1$ , \*  $p < 0.05$ , \*\*  $p < 0.01$ , \*\*\*  $p < 0.001$ .

AHP: Afterhyperpolarization. mAHP: Medium AHP. sAHP: Slow AHP. V<sub>m</sub> at: Membrane potential at the specified time after a burst of five action potentials, irrespective of the occurrence of an AHP. Last current: The amplitude of the last current amplitude with which the excitability could be assessed.

To allow for the assessment of the post-burst properties, the sample was extended by including cells that exhibited persistent firing while having been superfused with 5 or 20  $\mu$ M Cch.

Table 6.1.19a Correlation of PP<sub>fix</sub> with the post-burst membrane potential

	N	R <sup>2</sup>	<i>p</i>	slope of the linear fit
<b>Post-burst properties</b>				
AHP exist	38.5 (15/26)			AHP existent: 12.5 ± 0.84 mV, AHP absent: 16.0 ± 1.01 mV Two-sample T-test: $T_{24} = 2.616, p = 0.015$
AHP duration (s)	15	.013	.684	
AHP area (mV*s)	15	.006	.785	
mAHP latency (ms)	15	.008	.757	
mAHP peak (mV)	15	.000	.992	
AHP decay $\tau$ (ms)	15	.038	.489	
sAHP at 0.5 s (mV)	15	.021	.608	
sAHP at 1 s (mV)	15	.036	.500	
V <sub>m</sub> at peak	26	.277	.006	** +1.6 mV PP <sub>fix</sub> / mV peak depol.
V <sub>m</sub> at 200 ms	26	.110	.099	† +1.3 mV PP <sub>fix</sub> / mV depolarization
V <sub>m</sub> at 500 ms	26	.174	.034	* +1.5 mV PP <sub>fix</sub> / mV depolarization
V <sub>m</sub> at 1 s	26	.117	.087	† +0.95 mV PP <sub>fix</sub> / mV depolarization

Linear regression, †  $p < 0.1$ , \*  $p < 0.05$ , \*\*  $p < 0.01$ , \*\*\*  $p < 0.001$ .

AHP: Afterhyperpolarization. mAHP: Medium AHP. sAHP: Slow AHP. V<sub>m</sub> at: Membrane potential at the specified time after a burst of five action potentials, irrespective of the occurrence of an AHP.

**Table 6.1.20: Correlation analysis of the post-stimulus firing frequency against inter-cellular variability.**

The table summarizes linear regressions of the post-stimulus firing frequency (during 10-20 s after the stimulus offset,  $FF_{fix}$ ) of cells exhibiting persistent firing in the presence of 10  $\mu$ M Cch against the animals' age, the cells' location within CA1 and the cells' intrinsic electrophysiological properties in the presence of 10  $\mu$ M Cch.

	N	R <sup>2</sup>	p	slope of the linear fit
<b>Maturation</b>				
Age (postnatal days)	39	.035	.256	
<b>Anatomical location</b>				
Dorso-ventral axis (mm)	39	.075	.092	† -0.90 Hz $FF_{fix}$ / mm
Proximo-distal axis (%)	38	.095	.060	† -2.2 Hz $FF_{fix}$ / 50%
<b>Passive properties</b>				
RMP (%silent)++	38.5 (15/39)	silent RMP: 12.0 $\pm$ 0.86 Hz, non-silent RMP: 11.7 $\pm$ 0.82 Hz Two-sample T-test: $T_{(37)} = -0.472$ , $p = 0.806$		
RMP (mV)	15	.221	.077	† -0.54 Hz $FF_{fix}$ / mV RMP depol.
-70 mV Rin (M $\Omega$ )	37	.008	.089	† +0.24 Hz $FF_{fix}$ / 10 M $\Omega$
-65 mV Rin (M $\Omega$ )	22	.071	.232	
-60 mV Rin (M $\Omega$ )	17	.029	.511	
<b>Hyperpolarization activated current</b>				
Sag (-10 mV step)	37	.043	.219	
Sag (-15 mV step)	37	.047	.197	
Sag (-20 mV step)	37	.013	.500	
<b>Action potential properties</b>				
threshold (mV)	39	.425	.000	*** -0.38 Hz $FF_{fix}$ / mV thresh. depol.
amplitude (mV)	39	.017	.431	
rising slope (mV/ms)	39	.011	.531	
falling slope (mV/ms)	39	.174	.008	** -2.3 Hz $FF_{fix}$ / 20 mV/ms flattening
1/2 width (ms)	39	.116	.034	* -6.3 Hz $FF_{fix}$ / ms width increase
1/3 width (ms)	39	.154	.013	* -5.6 Hz $FF_{fix}$ / ms width increase
fAHP (mV)	39	.53	.159	
firing type (%regular)	91.7 (33/36)			

Linear regression, unless otherwise stated. †  $p < 0.1$ , \*  $p < 0.05$ , \*\*  $p < 0.01$ , \*\*\*  $p < 0.001$ .

RMP: resting membrane potential. Rin: input resistance at the specified holding membrane potential. rising slope: the peak of the rising slope. falling slope: the peak of the falling slope 1/2 width: Full width of the action potential at one half of its amplitude. 1/3 width: Full width of the action potential at one third of its amplitude. AHP: afterhyperpolarization. fAHP: Fast AHP.

**Continuation of Table 6.1.20:**

	N	R <sup>2</sup>	p	slope of the linear fit
<b>Post-burst properties</b>				
AHP (%exist)	45.5 (5/11)	AHP exist: 12.5 $\pm$ 1.91 Hz, AHP absent: 10.12 $\pm$ 1.14 Hz Two-sample T-test: $T_{(9)} = -1.099$ , $p = 0.300$		
AHP duration (s)	5			
AHP area (mV*s)	5			
mAHP latency (ms)	5			
mAHP peak (mV)	5			
AHP decay $\tau$ (ms)	5			
sAHP at 0.5 s (mV)	5			
sAHP at 1 s (mV)	5			
V <sub>m</sub> at peak	11	.440	.026	* -2.4 Hz $FF_{fix}$ / mV peak amplitude
V <sub>m</sub> at 200 ms	11	.014	.725	
V <sub>m</sub> at 500 ms	11	.001	.935	
V <sub>m</sub> at 1 s	11	.081	.398	

Linear regression, unless otherwise stated. †  $p < 0.1$ , \*  $p < 0.05$ , \*\*  $p < 0.01$ , \*\*\*  $p < 0.001$ .

AHP: afterhyperpolarization. mAHP: Medium AHP. sAHP: Slow AHP. V<sub>m</sub> at: Membrane potential at the specified time after a burst of five action potentials, irrespective of the occurrence of an AHP.

To allow for the assessment of the post-burst properties, the sample was extended by including cells that exhibited persistent firing while having been superfused with 5 or 20  $\mu$ M Cch.

**Table 6.1.20a: Correlation of  $FF_{fix}$  with the post-burst membrane potential**

	N	R <sup>2</sup>	p	slope of the linear fit
<b>Post-burst properties</b>				
AHP exist++	38.5 (15/26)	AHP exist: 10.6 $\pm$ 1.03 Hz, AHP absent: 9.8 $\pm$ 0.84 Hz Two-sample T-test: $T_{(24)} = -0.583$ , $p = 0.565$		
AHP duration (s)	15	.154	.148	
AHP area (mV*s)	15	.041	.468	
mAHP latency (ms)	15	.255	.055	† -0.16 Hz $FF_{fix}$ / ms prolongation
mAHP peak (mV)	15	.021	.610	
AHP decay $\tau$ (ms)	15	.044	.455	
sAHP at 0.5 s (mV)	15	.291	.038	* +2.1 Hz $FF_{fix}$ / mV depolarization
sAHP at 1 s (mV)	15	.293	.037	* +1.9 Hz $FF_{fix}$ / mV depolarization.
V <sub>m</sub> at peak	26	.035	.360	
V <sub>m</sub> at 200 ms	26	.019	.505	
V <sub>m</sub> at 500 ms	26	.040	.330	
V <sub>m</sub> at 1 s	26	.038	.343	

Linear regression. †  $p < 0.1$ , \*  $p < 0.05$ , \*\*  $p < 0.01$ , \*\*\*  $p < 0.001$ .

AHP: Afterhyperpolarization. mAHP: Medium AHP. sAHP: Slow AHP. V<sub>m</sub> at: Membrane potential at the specified time after a burst of five action potentials, irrespective of the occurrence of an AHP.

Continuation of Table 6.1.20:

	N	R <sup>2</sup>	p	slope of the linear fit
<b>Excitability</b>				
Adaptation ratio	33	.003	.748	
Last current (pA)	37	.005	.679	
0.05 nA step (Hz)	37	.076	.098	† not meaningful (1 cell spiking)
0.10 nA step (Hz)	36	.141	.024	* +0.12 Hz FF <sub>ex</sub> / Hz in I-F relationship
0.15 nA step (Hz)	32	.140	.035	* +0.12 Hz FF <sub>ex</sub> / Hz in I-F relationship
0.20 nA step (Hz)	27	.109	.093	† +0.13 Hz FF <sub>ex</sub> / Hz in I-F relationship
0.25 nA step (Hz)	23	.123	.101	
0.30 nA step (Hz)	20	.260	.022	* +0.23 Hz FF <sub>ex</sub> / Hz in I-F relationship
0.35 nA step (Hz)	16	.155	.131	
0.40 nA step (Hz)	12	.198	.147	
DB (%exist)	5.13 (2/39)			
DB current (nA)	2			
DB duration (ms)	2			

Linear regression. †  $p < 0.1$ , \*  $p < 0.05$ , \*\*  $p < 0.01$ , \*\*\*  $p < 0.001$ .

Last current: The amplitude of the last current amplitude with which the excitability could be assessed.

**Table 6.1.21: Correlation analysis of the depolarization block duration against inter-cellular variability.**

The table summarizes linear regressions of the duration of the depolarization block throughout the post-stimulus interval of cells exhibiting depolarization block in the presence of 10  $\mu$ M Cch against the animals' age, the cells' location within CA1 and the cells' intrinsic electrophysiological properties in the presence of 10  $\mu$ M Cch.

	N	R <sup>2</sup>	p	slope of the linear fit
<b>Maturation</b>				
Age (postnatal days)	30	.070	.158	
<b>Anatomical location</b>				
Dorso-ventral axis (mm)	30	.013	.553	
Proximo-distal axis (%)	30	.024	.411	
<b>Passive properties</b>				
RMP (%silent)**	36.7 (11/30)			silent RMP: 10.1 $\pm$ 3.02 s, non-silent RMP: 15.0 $\pm$ 2.31 s Two-sample T-test: $T_{(28)} = -1.289$ , $p = 0.208$
RMP (mV)	11	.043	.542	
-70 mV Rin (M $\Omega$ )	29	.032	.355	
-65 mV Rin (M $\Omega$ )	23	.008	.677	
-60 mV Rin (M $\Omega$ )	19	.006	.752	

Linear regression, unless otherwise stated. †  $p < 0.1$ , \*  $p < 0.05$ , \*\*  $p < 0.01$ , \*\*\*  $p < 0.001$ .

RMP: resting membrane potential. Rin: input resistance at the specified holding membrane potential.

Continuation of Table 6.1.21:

	N	R <sup>2</sup>	p	slope of the linear fit
<b>Hyperpolarization activated current</b>				
Sag (-10 mV step)	30	.104	.082	
Sag (-15 mV step)	30	.223	.008	** +8.8 s DB duration / 0.1 AU sag ratio
Sag (-20 mV step)	30	.282	.003	** +9.4 s DB duration / 0.1 AU sag ratio
<b>Action potential properties</b>				
threshold (mV)	29	.023	.565	
amplitude (mV)	29	.027	.397	
rising slope (mV/ms)	29	.013	.563	
falling slope (mV/ms)	29	.089	.116	
1/2 width (ms)	29	.038	.309	
1/3 width (ms)	29	.054	.226	
fAHP (mV)	29	.000	.963	
firing type (%regular)	93.3 (28/30)			Regular spiking cells: 13.4 $\pm$ 1.91 s (range: 0 - 30 Hz) The two bursting cells had a DB duration of 0 and 21.8 s
<b>Post-burst properties</b>				
AHP (%exist)	35.5 (6/17)			AHP exist: 13.7 $\pm$ 3.01 s, AHP absent: 12.6 $\pm$ 2.85 s Two-sample T-test: $T_{(15)} = -0.248$ , $p = 0.808$
AHP duration (s)	6			
AHP area (mV*s)	6			
mAHP latency (ms)	6			
mAHP peak (mV)	6			
AHP decay $\tau$ (ms)	6			
sAHP at 0.5 s (mV)	6			
sAHP at 1 s (mV)	6			
V <sub>m</sub> at peak	17	.000	.996	
V <sub>m</sub> at 200 ms	17	.001	.897	
V <sub>m</sub> at 500 ms	17	.117	.180	
V <sub>m</sub> at 1 s	17	.245	.043	* -5.1 s DB dur / mV post-burst depol.
<b>Excitability</b>				
Adaptation ratio	26	.043	.307	
Last current (pA)	30	.029	.371	
0.05 nA step (Hz)	30	.026	.399	
0.10 nA step (Hz)	28	.004	.763	
0.15 nA step (Hz)	25	.006	.706	
0.20 nA step (Hz)	10	.071	.455	
0.25 nA step (Hz)	10	.063	.486	
0.30 nA step (Hz)	7			
0.35 nA step (Hz)	4			
0.40 nA step (Hz)	2			
DB (%exist)	50% (15/30)			DB in IV: 13.5 $\pm$ 2.71 s, no DB in IV: 12.9 $\pm$ 2.63 s Two-sample T-test: $T_{(28)} = -0.170$ , $p = 0.867$
DB current (nA)	15	.204	.091	† +5.9 s DB dur after 2 s, 100 pA step per 100 pA step increment in IV
DB duration (ms)	15	.433	.008	** -4.5 s DB dur after 2s, 100 pA step per 100 ms DB lengthening in IV

Linear regression, unless otherwise stated. †  $p < 0.1$ , \*  $p < 0.05$ , \*\*  $p < 0.01$ , \*\*\*  $p < 0.001$ .

rising slope: the peak of the rising slope. falling slope: the peak of the falling slope 1/2 width: Full width of the action potential at one half of its amplitude. 1/3 width: Full width of the action potential at one third of its amplitude. AHP: afterhyperpolarization. fAHP: Fast AHP. mAHP: Medium AHP. sAHP: Slow AHP. V<sub>m</sub> at: Membrane potential at the specified time after a burst of five action potentials, irrespective of the occurrence of an AHP. Last current: The amplitude of the last current amplitude with which the excitability could be assessed.

To allow for the assessment of the depolarization block duration, the sample was extended by including cells that exhibited depolarization block while having been superfused with 5 or 20  $\mu\text{M}$  Cch.

**Table 6.1.21a Correlation of DB duration with the post-burst membrane potential**

	N	R <sup>2</sup>	p	slope of the linear fit
<b>Post-burst properties</b>				
AHP duration (s)	7			
AHP area (mV*s)	7			
mAHP latency (ms)	7			
mAHP peak (mV)	7			
AHP decay $\tau$ (ms)	7			
sAHP at 0.5 s (mV)	7			
sAHP at 1 s (mV)	7			
V <sub>m</sub> at peak	26	.000	.923	
V <sub>m</sub> at 200 ms	26	.001	.873	
V <sub>m</sub> at 500 ms	26	.054	.252	
V <sub>m</sub> at 1 s	26	.116	.088	† -3.4 s DB duration / mV depolarization

Linear regression, unless otherwise stated. †  $p < 0.1$ , \*  $p < 0.05$ , \*\*  $p < 0.01$ , \*\*\*  $p < 0.001$ .

AHP: afterhyperpolarization. mAHP: Medium AHP. sAHP: Slow AHP. V<sub>m</sub> at: Membrane potential at the specified time after a burst of five action potentials, irrespective of the occurrence of an AHP.

**Table 6.1.22: Comparison of cellular properties between cells expressing persistent firing or depolarization block.**

The table summarizes two-sample T-test the animals' age, the cells' location within CA1 and the cells' intrinsic electrophysiological properties in the presence of 5, 10, or 20  $\mu\text{M}$  Cch of cells that expressed either persistent firing or depolarization block in response to a 2 s, 100 pA square pulse.

	Persistent firing (PF)	Depolarization block (DB)	N (PF/DB)	df	T or $\chi^2$	p
<b>Maturation</b>						
Age (postnatal days)	17.0 $\pm$ 0.27	17.4 $\pm$ 0.29	67/68	133	1.036	.302
<b>Anatomical location</b>						
Dorso-ventral (mm)	3.27 $\pm$ 0.12	3.35 $\pm$ 0.11	67/68	133	0.488	.626
Proximo-distal (%)	58.9 $\pm$ 3.20	37.9 $\pm$ 2.86	66/68	132	-5.043	.000 ***
<b>Passive properties</b>						
RMP (%silent)	28.4 (n = 19)	25.0 (n = 17)	67/68	1	0.195	.659
RMP (mV)	-63.0 $\pm$ 0.70	-62.5 $\pm$ 1.19	19/17	34	0.315	.755
-70 mV Rin (M $\Omega$ )	103 $\pm$ 5.23	106 $\pm$ 3.7	64/65	113.777	0.546	.586
-65 mV Rin (M $\Omega$ )	125 $\pm$ 6.02	126 $\pm$ 6.92	42/39	79	0.155	.878
-60 mV Rin (M $\Omega$ )	197 $\pm$ 13.45	191 $\pm$ 11.71	31/30	59	-0.323	.748
<b>Hyperpolarization activated current</b>						
Sag (-10 mV step)	0.252 $\pm$ 0.01	0.254 $\pm$ 0.01	64/66	128	0.255	.799
Sag (-15 mV step)	0.266 $\pm$ 0.01	0.267 $\pm$ 0.01	64/66	128	0.139	.890
Sag (-20 mV step)	0.275 $\pm$ 0.01	0.274 $\pm$ 0.01	64/66	128	-0.079	.937
<b>Action potential properties</b>						
threshold (mV)	-44.5 $\pm$ 0.76	-44.8 $\pm$ 0.72	67/67	132	-0.253	.801
amplitude (mV)	69.2 $\pm$ 1.32	73.2 $\pm$ 1.36	67/67	132	2.116	.036 *
rising slope (mV/ms)	243 $\pm$ 9.14	283 $\pm$ 10.8	67/67	132	2.877	.005 **
falling slope (mV/ms)	-62.8 $\pm$ 1.55	-64.8 $\pm$ 1.68	67/67	132	-0.882	.379
1/2 width (ms)	1.12 $\pm$ 0.02	1.09 $\pm$ 0.02	67/67	132	-0.998	.320
1/3 width (ms)	1.39 $\pm$ 0.03	1.35 $\pm$ 0.03	67/67	132	-1.002	.318
fAHP (mV)	-2.77 $\pm$ 0.66	-4.28 $\pm$ 0.59	67/67	132	-1.707	.090 †
firing type (%regular)	87.5 (n = 56)	98.4 (n = 63)	64/64	1	0.626	.429
<b>Post-burst properties</b>						
AHP (%exist)	57.7 (n = 15)	26.9 (n = 7)	26/26	1	5.042	.025 *
AHP duration (s)	0.078 $\pm$ 0.01	0.058 $\pm$ 0.01	15/7	20	-1.226	.235
AHP area (mV*s)	-0.035 $\pm$ 0.01	-0.032 $\pm$ 0.01	15/7	20	0.216	.831
mAHP latency (ms)	33.0 $\pm$ 3.18	23.4 $\pm$ 4.29	15/7	20	-1.749	.096 †
mAHP peak (mV)	-0.649 $\pm$ 0.09	-0.712 $\pm$ 0.22	15/7	20	-0.317	.756
AHP decay $\tau$ (ms)	30.4 $\pm$ 6.48	22.3 $\pm$ 5.00	15/7	20	-0.801	.432
sAHP at 0.5 s (mV)	2.24 $\pm$ 0.27	1.64 $\pm$ 0.26	15/7	20	-1.388	.180
sAHP at 1 s (mV)	2.68 $\pm$ 0.30	1.82 $\pm$ 0.22	15/7	20	-1.839	.081 †
V <sub>m</sub> at peak (mV)	0.166 $\pm$ 0.24	0.365 $\pm$ 0.18	26/26	50	0.678	.501
V <sub>m</sub> at 200 ms (mV)	1.22 $\pm$ 0.19	1.40 $\pm$ 0.13	26/26	50	0.753	.455
V <sub>m</sub> at 500 ms (mV)	2.49 $\pm$ 0.21	2.30 $\pm$ 0.17	26/26	50	-0.718	.476
V <sub>m</sub> at 1 s (mV)	3.03 $\pm$ 0.26	2.39 $\pm$ 0.20	26/26	50	-1.958	.056 †

Data represented as M  $\pm$  SEM. Two-sample T-test. †  $p < 0.1$ , \*  $p < 0.05$ , \*\*  $p < 0.01$ , \*\*\*  $p < 0.001$ .

RMP: resting membrane potential. R<sub>in</sub>: input resistance at the specified holding membrane potential. Sag: Sag ratio induced by a hyperpolarizing voltage step as specified. rising slope: the peak of the rising slope. falling slope: the peak of the falling slope 1/2 width: Full width of the action potential at one half of its amplitude. 1/3 width: Full width of the action potential at one third of its amplitude. AHP: afterhyperpolarization. fAHP: Fast AHP. mAHP: Medium AHP. sAHP: Slow AHP. V<sub>m</sub> at: Membrane potential at the specified time after a burst of five action potentials, irrespective of the occurrence of an AHP.

Continuation of Table 6.1.22:

	Persistent firing (PF)	Depolarization block (DB)	N (PF/DB)	df	T or $\chi^2$	p
<b>Excitability</b>						
Adaptation ratio	1.05 ± 0.13	0.716 ± 0.18	56/60	107.839	-1.486	.140
Discontinuation rate	see N(PF)	see N(DB)	129	1	27.015	.000 ***
Last current (pA)	224 ± 16	256 ± 25	42/25	65	1.129	.263
0.05 nA step (Hz)	0.250 ± 0.25	0.154 ± 0.14	64/65	98.7197	-0.336	.738
0.10 nA step (Hz)	7.27 ± 1.32	7.85 ± 1.27	63/60	121	0.316	.752
0.15 nA step (Hz)	16.4 ± 1.46	19.7 ± 1.98	57/46	101	1.365	.175
0.20 nA step (Hz)	25.7 ± 1.21	26.8 ± 2.91	50/20	25.8477	0.333	.742
0.25 nA step (Hz)	30.8 ± 1.12	31.2 ± 3.02	43/16	19.2888	0.109	.915
0.30 nA step (Hz)	32.6 ± 1.32	36.2 ± 3.19	35/10	43	1.198	.238
0.35 nA step (Hz)	33.7 ± 1.22	38.0 ± 4.44	29/7	6.933	0.936	.381
0.40 nA step (Hz)	34.8 ± 1.22	42.8 ± 5.49	24/5	4.4018	1.417	.223
DB (%exist)	4.7 (n = 3)	64.6 (n = 42)	64/65	1	50.986	.000 ***
DB current (pA)	367 ± 20	219 ± 10	3/42	43	-2.814	.007 **
DB duration (ms)	417 ± 205	280 ± 25	3/42	2.061	-0.663	.574

Data represented as M ± SEM. Two-sample T-test, unless otherwise stated. †  $p < 0.1$ , \*  $p < 0.05$ , \*\*  $p < 0.01$ , \*\*\*  $p < 0.001$ .

Discontinuation rate: Degree of the cell's drop out from the assessment for excitability by incrementing (50 pA) 1 s current stimulations. Last current: The amplitude of the last current amplitude with which the excitability could be assessed. DB: Depolarization block. DB current: Amplitude of the direct current necessary for the first induction of DB.

## References

- Benardo, L.S., and Prince, D.A. (1982). Cholinergic excitation of mammalian hippocampal pyramidal cells. *Brain research* 249, 315–331.
- Champagne, F.A., Francis, D.D., Mar, A., and Meaney, M.J. (2003). Variations in maternal care in the rat as a mediating influence for the effects of environment on development. *Physiology & Behavior* 79, 359–371.
- Clark, A.S. (2002). Chronic Administration of Anabolic Steroids Disrupts Pubertal Onset and Estrous Cyclicity in Rats. *Biology of Reproduction* 68, 465–471.
- Cole, A.E., and Nicoll, R.A. (1983). Acetylcholine mediates a slow synaptic potential in hippocampal pyramidal cells. *Science (New York, N.Y.)* 221, 1299–1301.
- Hönigsperger, C., Marosi, M., Murphy, R., and Storm, J.F. (2014). Dorsoventral differences in Kv7/M-current and its impact on resonance, temporal summation and excitability in rat hippocampal pyramidal cells. *The Journal of physiology*.
- Liu, D., Dionio, J., Day, J.C., Francis, D.D., and Meaney, M.J. (2000). Maternal care, hippocampal synaptogenesis and cognitive development in rats. *Nature neuroscience* 3, 799–806.
- Maccaferri, G., Mangoni, M., Lazzari, A., and DiFrancesco, D. (1993). Properties of the hyperpolarization-activated current in rat hippocampal CA1 pyramidal cells. *Journal of neurophysiology* 69, 2129–2136.
- Moore, C.L., and Morelli, G.A. (1979). Mother rats interact differently with male and female offspring. *Journal of comparative and physiological psychology* 93, 677–684.

Moriyama, C., Galic, M.A., Mychasiuk, R., Pittman, Q.J., Perrot, T.S., Currie, R.W., and Esser, M.J. (2013). Prenatal transport stress, postnatal maternal behavior, and offspring sex differentially affect seizure susceptibility in young rats. *Epilepsy & behavior : E&B* 29, 19–27.

Stanko, J.P., Enoch, R.R., Rayner, J.L., Davis, C.C., Wolf, D.C., Malarkey, D.E., and Fenton, S.E. (2010). Effects of prenatal exposure to a low dose atrazine metabolite mixture on pubertal timing and prostate development of male Long-Evans rats. *Reproductive toxicology (Elmsford, N.Y.)* 30, 540–549.

Surges, R., Freiman, T.M., and Feuerstein, T.J. (2004). Input resistance is voltage dependent due to activation of Ih channels in rat CA1 pyramidal cells. *Journal of neuroscience research* 76, 475–480.



## 6.2 Curriculum Vitae

### PERSONAL INFORMATION

Name	Knauer, Beate
Date of birth:	25.08.1984,
Place of birth	Freiberg, Germany
Work address	Ruhr-Universität Bochum Mercator Research Group 1 Universitätsstraße 150 GA 04/146 44801 Bochum, Germany
E-mail address	beate.knauer@rub.de

### EDUCATION

Oct 2011 – present	<b>PhD Candidate</b> , <i>International Graduate School of Neuroscience, Ruhr-University Bochum</i> , Working title: Persistent firing and depolarization block in CA1 pyramidal neurons
Oct 2009 – Oct 2011	<b>Master of Science</b> , Psychology, focus: Cognitive Neuroscience, <i>Ruhr-University Bochum</i> , Intrinsic Persistent Firing of Pyramidal Neurons in the CA1 Region of the Rat Hippocampus,
Oct 2006 – Sep 2009	<b>Bachelor of Science</b> , Psychology, <i>Ruhr-University Bochum</i> , Mental Time Travel as a Function of a Unilateral Lesion of Medial Thalamus Nuclei
1996-2003	<b>Secondary School</b> : Greifenstein-Gymnasium Thum, Germany Major: Biology and Mathematics
1995-1996	<b>Grammar school</b> : Schule des Friedens, Ehrenfriedersdorf, Germany
1991-1995	<b>Elementary school</b> : Grundschule Ehrenfriedersdorf, Germany

RESEARCH EXPERIENCE

- Sept 2010 – present     Conducting *in vitro* electrophysiology using whole cell patch clamp in acute slices of the rat temporal lobe
- Mar 2010 – Sep 2011     Participated in the development, verification and validation of psychosocial screening instruments related to chronic pain in an institute for health promotion and health services research
- Mar – Apr 2010             Worked with cell cultures and conducted whole cell patch clamp on astrocytes during a seven-week internship in the neuroanatomical laboratory of the medical faculty at Ruhr-University Bochum
- Oct 2008–June 2010     Supported data collection and being an independent rater of narratives from an event generation task in humans (Weiler et al. (2011) J Cogn Neurosci 23: 3037-51.)
- Mar – April 2009          Assisted social stress experiments with tree shrews,  
Executed clicker-training with common marmosets,  
Participated in developing, conducting and scoring an object recognition task for rats during a seven-week internship in the German Primate Center, Göttingen
- Jan – Oct 2005 Internship in a seal center (Seehundstation Friedrichskoog e.V.)  
Conducted environmental education  
Fed harbor seal pups and carried out basic veterinary examinations  
Observed behavioral training and non-invasive acoustic experiments on adult harbor seals on a daily basis

GRANTS, AWARDS AND EXERCISE OF AN OFFICE

- Oct 2014 - Jan 2015     Stipend of the Wilhelm and Günter Esser Foundation
- 2014                          PhD student representative in the Executive Board of the Research School PLUS (RS+) at Ruhr-University Bochum
- Dec 2013                     Invited talk during the annual graduation day of the International Graduate School of Neuroscience (IGSN) at Ruhr-University Bochum
- Nov 2013                     funding from RS+ and from IGSN to attend SfN 2013
- Oct 2013                     funding from RS+ for participating in a workshop
- 2013                          Deputy of the PhD student representative in the Executive Board of the RS+ at Ruhr-University Bochum
- Oct 2011– Sep 2014     PhD-Stipend of the IGSN including yearly appraisal resulting in re-approval

FURTHER EDUCATION AND SOFT SKILLS

May 2013 – present	Supervising a master student
Oct 2013	One-week workshop "Analysis and Models in Neurophysiology"
Feb 2013	Five-day perforated patch clamp instructions by Dr. Antonio Reboreda
Aug 2012	Three-day workshop "Basic Scientific Presentation for Doctoral Fellows"
SS 2012	Seminar: Programming in MATLAB
Nov 2011	Three-day workshop "Getting Research Published"
SS 2011 and WS 2011/12	Course accredited by the Federation of European Laboratory Animal Science Associations (FELASA) for the education and training of persons carrying out animal experiments (Category B)

INTERNATIONAL EXPERIENCE

WS 2007/08	One semester abroad in Blagoevgrad, Bulgaria
May – Aug 2006	Voluntary service near Kumasi, Ghana Supported the teaching and taught in an elementary school
Oct 2003 – Nov 2004	Au Pair in the Lehigh Valley, Pennsylvania, USA

## 6.3 List of publications

### PEER REVIEWED JOURNALS

**Knauer, B.**, Yoshida, M. Switching between persistent firing and depolarization block during cholinergic stimulation in rat CA1 pyramidal neurons. In preparation.

**Knauer, B.**; Jochems, A.; Valero-Aracama, M.J.; Yoshida, M. (2013). Long-lasting intrinsic persistent firing in rat CA1 pyramidal cells: A possible mechanism for active maintenance of memory. *Hippocampus*. 23(9): 820-31.

Yoshida, M.; **Knauer, B.**; Jochems, A. (2012). Cholinergic modulation of the CAN current may adjust neural dynamics for active memory maintenance, spatial navigation and time-compressed replay. *Front Neural Circuits*. 6:10

### POSTER PRESENTATIONS

**Knauer, B.**; Yoshida, M. Switching between cholinergic-dependent mnemonic and epileptiform responses in individual hippocampal CA1 pyramidal neurons in acute rat brain slice preparations. Neuroscience 2014 Abstract # 507.15. Washington, DC: Society for Neuroscience, 2014.

**Knauer, B.**; Yoshida, M. Switching between persistent firing and epileptiform activity in individual rat CA1 pyramidal neurons during cholinergic stimulation. FENS 2014 Abstract # 0924.

**Knauer, B.**; Yoshida, M. Two response modes of rat hippocampal CA1 pyramids during cholinergic excitation, *Neurovisionen 9* (Cologne), 83. 2013.

Jochems, A.; **Knauer, B.**; Yoshida, M. Intrinsic persistent firing in hippocampal CA1 and CA3 pyramidal cells. Neuroscience 2012 Abstracts # 812.15. New Orleans, Louisiana: Society for Neuroscience, 2012. Online.

**Knauer, B.**; Jochems, A.; Valero-Aracama M.J.; Yoshida, M. Cholinergic-dependent intrinsic persistent firing of *in vitro* rat CA1 pyramidal neurons - a possible mechanism for short-term retention of information. FENS 2012 Abstract # 1890.

## 6.4 Acknowledgements

I would like to thank...

**Jun.-Prof. Dr. Motoharu Yoshida** for having allowed me to conduct my PhD project within his Neural Dynamics Lab (NDL) and for having been a highly influential role model in every respect.

**Prof. Dr. Stefan Herlitze** for being my second supervisor during the first two years of my PhD and in particular for his time spent critically reading and commenting both my PhD proposal as well as my PhD progress report.

**Prof. Dr. Denise Manahan-Vaughan** for having offered to be my second supervisor for the remaining time after December 2013 and thereby for offering me inspiring insights into closely related but still different fields of research. I kindly thank for allowing me the continued use of the *in vitro* set up, for her interest in my work and her advice regarding my time after RUB.

**Prof. Dr. Ulf Eysel** for allowing me to use the *in vitro* set up, for his enjoyable participation in the happy hours at MRG1, for his endeavor in supporting me to find a promising post-doctoral position.

**María Jesus Valero Aracama** for having been a energetic, fun, stimulating and supportive colleague. I am indebted to her not only for her intellectual and emotional but also her hands on support when it really mattered.

**Aurore Malet Karas** for providing insights into very different fields of research and for sharing her enthusiasm and joyfulness and strong mind.

**Kati Reip** for being a warm and welcoming colleague, for her typing effort and for providing me an opportunity to grow with my tasks.

All members of the Mercator Research Group 1, especially my office mates **Carolin Chwiesko, Erika Atutxa, Nozomu Nakamura, Vanessa Lux** and **Zachery Beer**.

All members of the Biopsychology lab, especially **Sarah Starosta** and **Nils Kasties** for allowing me little getaways down to GAFO 05 and the mensa.

**Ursula Heiler** und **Giesela Stephan** for being empathic, supportive, cheerful and always proficient.

**Dr. David Reser** for having faith in my abilities and for offering a perspective for the time after my PhD project.

**Dr. Douglas Fraser** and **Dr. Chao Tai** for their patience in answering my repeated inquiries regarding their publications on the plateau potential in CA1 pyramidal neurons.

**Dr. Michael X Zuh** for momentarily influencing my project by the e-mail support on the potential peculiarities of ML204.

**Dr. Yoe Marylka Uusisaari** for her very detailed e-mail support regarding the slice preparation of brains from aged animals

**Dr. Kerstin Hill** for her e-mail advice on riluzole.

**The Vanderbilt University Medical Center** for the kind donation of 502 mg ML204.

**The International Graduate School of Neuroscience** for intellectual and financial support and for offering a motivating and multifaceted research environment.

**All members of the Research School and Research School PLUS** for offering an amazing wealth of high quality support all around the issues that make up the PLUS, like soft skills courses, stipend guidance and so forth. I owe them a thank for the interesting Ex-Board-meetings which kept me going throughout 2014.

**The Faculty of Psychology at the Ruhr University** for having provided me with an excellent training.

**Anne Klepp, Aurore Malet Karas, Erika Atutxa, María Jesus Valero Aracama and Motoharu Yoshida** for their helpful comments on various sections of the manuscript.

**My mother, my sister and my brother** for having supported me in any respect that was possible on that long distance. I want to thank them for their considerateness and sympathy, as well as for always having conceded the space and time to me that I needed. I am thankful for the encouraging phone calls we had and for their cheerful visits to Bochum.

**My father.**

**The 304 rats** (287 juveniles, 2 adults, 15 aged) who were always brave, at times adventurous or charming and who unintentionally made this work possible.